A Multiscale Examination of Surface Flow Convergence in the Mohawk and Hudson Valleys

Abstract of

A thesis presented to the Faculty

of the University at Albany, State University of New York

in partial fulfillment of the requirements

for the degree of

Master of Science

College of Arts & Sciences

Department of Earth and Atmospheric Sciences

Michael E. Augustyniak
2008

Abstract

Forecasters have surmised that the unique terrain found in eastern New York and western New England plays a pivotal role in modulating various weather phenomena in the region. Several studies have examined the interplay between low-level channeled airflow within the Mohawk and Hudson River valleys, the surrounding hilly terrain (i.e., the Adirondack, Catskill, Green, and Berkshire Mountains), and the overall effect on warm-season severe weather events. To date, however, the impact on cold-season weather events of low-level flow channeling in eastern New York and western New England has gone largely unmentioned in the peer-reviewed literature.

The goal of this study is to examine, on the synoptic and mesoscale, the occurrence of a low-level convergence zone, which forms during the cold season from time to time, where the Mohawk and Hudson valleys intersect. Known to pose a challenge to local forecasters and referred to colloquially as the "Mohawk–Hudson convergence zone" (MHC), the development of the convergence zone generally does not lead to high-impact weather; however, convergence-related precipitation can wreak havoc if it occurs with little or no warning or at peak travel times. Such was the case on 27 November 2002, when a localized area of light-to-moderate snow persisted over eastern New York and western New England for several hours following the conclusion of synoptic-scale snowfall from an "Alberta Clipper." The nascent interest generated following that event led to a total of seven observational studies of MHC events, all of which occurred between November 2002 and January 2008.

Several noteworthy similarities were observed from case to case, all of which control the physical processes necessary to generate a MHC event. These include: (1) a

positive north–south (west–east) sea-level pressure difference along the Hudson (Mohawk) Valley, which drives the confluent flow; (2) an absence of strong cold air advection, which precludes strong subsidence and drying of the boundary layer; and (3) a statically stable atmospheric stratification, which prevents downward transport of higher-speed air aloft to the surface that would tend to reduce or eliminate the local terrain-induced surface wind signature.

The empirical nature of this study led to the development of a conceptual model of MHC in the form of a composite map containing the synoptic and mesoscale weather features present during an event. These features include: (1) an intensifying surface cyclone over the western Atlantic Ocean, which moves east and/or south of 40°N, 70°W; (2) a trough of surface low pressure, which extends westward from the low center along the New York–Pennsylvania border; (3) a geopotential-height trough at 300 hPa, which places eastern New York and western New England under the left-entrance region of a jet streak, an area that favors sinking air. Furthermore, sea-level isobars are generally arranged in the shape of a reverse-S, with higher pressures located to the north (west) of Poughkeepsie, New York (Pittsfield, Massachusetts).

Finally, an effort is made to increase the predictability of future MHC events through the use of an operational forecasting scheme. To this end, a decision tree for forecasters is developed and presented in this study.

A Multiscale Examination of Surface Flow Convergence in the Mohawk and Hudson Valleys

A thesis presented to the Faculty

of the University at Albany, State University of New York

in partial fulfillment of the requirements

for the degree of

Master of Science

College of Arts & Sciences

Department of Earth and Atmospheric Sciences

Michael E. Augustyniak
2008

Acknowledgements

I am deeply indebted to my advisor Lance Bosart, the person who first helped me to realize that pursuing an advanced degree in the atmospheric sciences was a goal within my reach. Since our fateful first conversation, eight years, three bosses, two presidents and (seemingly) one lifetime have passed by, but Lance has maintained his support and faith in me and, through his, I have sustained mine. Without Lance's wisdom, advice, and understanding of my job's erratic schedule, you would not be reading this now. Likewise, my thanks go to Dan Keyser for being a second reader of this thesis, as well as for his guidance and review of my proof-of-concept paper on Mohawk–Hudson convergence.

My deepest gratitude extends to the rest of the faculty and staff in the Department of Earth and Atmospheric Sciences. I am proud of the degrees that you have helped me to earn and I believe in the unparalleled excellence of the Atmospheric Science program at the University at Albany. In particular I wish to thank Mike Landin, whose enthusiasm for the weather is contagious, and whose tour of the Map Room in the early 1990s helped to make my choice for undergraduate schooling an easy one.

I am grateful for the funding made available to me by the Collaborative Science, Technology, and Applied Research (CSTAR) Program, through grant #NA04NWS4680005 and #NA07NWS4680001. This joint-research initiative between the Department of Earth and Atmospheric Sciences at the University at Albany, and the Albany office of the National Weather Service, provided a unique and beneficial framework for an exchange of ideas. Special thanks are extended to Gene Auciello,

Hugh W. Johnson, IV, Kenneth LaPenta, Thomas Wasula, and Warren Snyder for their consideration over the years.

The company, advice and assistance provided by my officemates and classmates through the years have been invaluable, and for them I am deeply grateful. There is no finer group of people with which to have long discussions on quasi-geostrophic theory, differential equations and, especially, atmospheric chemistry. A special thanks to all of those who helped me to conquer innumerable computing problems, including Kevin Tyle, David Knight and Alan Srock. And, lastly, thank you for all that you have done to make me feel like part of the family, despite having such an unforgiving schedule. Friendships forged in class begot friendships for life, and mine will forever be a little richer and a little funnier because of Josh and Mary Beth Darr, Dave and Danielle Groenert, Scott Runyon, Matt Novak and Dan Lipper. Tom Galarneau deserves a special mention as a kindred spirit, as we both survived last-name butcherings on a weekly basis, delivered by a certain physics professor.

Finally, this thesis is dedicated to Mom, Dad, Nanny, and the friends who have taken this academic journey with me. Thank you for the sacrifices you've made on my behalf, for being here to share in the celebration of my triumphs, and for urging me on towards the finish line when I wanted to give up. You all have my deepest appreciation for your encouragement and support and I am lucky to have you all in my life. This degree is as much yours as it is mine. You can borrow it on Tuesdays, if you like.

Table of Contents

List of Tables

List of Figures

positive pressure differences indicate higher pressures to the north (west). (a) For all observations; (b) for observations taken during the "beginning" of MHC events, where the solid blue line indicates the best-fit linear regression between north-south and west-east pressure difference pairs; (c) as in (b), but for the "middle" of MHC events; (d) as in (b), but for the "end" of MHC events. Data source: University at Albany archive; supplemental data from the Historical Weather Data Archives of the National Severe Storms Laboratory (NSSL) in Norman, Oklahoma.

Figure 3.6: Scatterplot graph of SLP differences between KGFL and KPOU (KSYR and KPSF) during the January 2007 MHC case study, where positive pressure differences indicate higher pressures to the north (west). Data source: University at Albany archive; supplemental data from the Historical Weather Data Archives of the National Severe Storms Laboratory (NSSL) in Norman, Oklahoma.

Figure 3.7: Sea level pressure (solid black lines every 4 hPa) with high- (low-) pressure centers labeled by a blue "H" (red "L"), and 1000–500-hPa thickness (dashed green lines every 6 dam) at (a) 0600, (b) 1200, and (c) 1800 UTC 27 November 2002, and at (d) 0000 UTC 28 November 2002. (Data source: 0-h gridded, initialized 1.0° NCEP GFS analyses).

Figure 3.8: 850-hPa geopotential height (solid black lines, every 3 dam), temperatures (solid colored lines, every 3°C), and winds (m s^{-1}, with pennant, full barb, and half barb denoting 25, 5, and 2.5 m s^{-1}, respectively) at (a) 0600, (b) 1200, and (c) 1800 UTC 27 November 2002, and at (d) 0000 UTC 28 November 2002. (Data source: 0-h gridded, initialized 1.0° NCEP GFS analyses).

Figure 3.9: 700-hPa geopotential height (solid black lines, every 3 dam), relative humidity (shaded beginning at 70% according to the scale), vertical motion [solid red (blue) contours show ascent (descent), every 2×10^{-3} hPa s^{-1}], and winds (m s^{-1}, with pennant, full barb, and half barb denoting 25, 5, and 2.5 m s^{-1}, respectively) at (a) 0600, (b) 1200, and (c) 1800 UTC 27 November 2002, and at (d) 0000 UTC 28 November 2002. (Data source: 0-hour gridded, initialized 1.0° NCEP GFS analyses).

Figure 3.10: Sea level pressure (solid black lines every 4 hPa), 700-hPa vertical motion (ascent shaded beginning at -2×10^{-3} hPa s^{-1} according to the scale), and 1000–500-hPa thickness (dashed green lines every 6 dam) at (a) 0600, (b) 1200, and (c) 1800 UTC 27 November 2002, and at (d) 0000 UTC 28 November 2002. (Data source: 0-hour gridded, initialized 1.0° NCEP GFS analyses).

Figure 3.11: Sea level pressure (solid black lines every 4 hPa), 700-hPa geostrophic relative vorticity (shaded beginning at 4×10^{-5} s^{-1} according to the scale), and 1000–500-hPa thickness (dashed green lines every 6 dam) at (a) 0600, (b) 1200, and (c) 1800 UTC 27 November 2002, and at (d) 0000 UTC 28 November 2002. (Data source: 0-hour gridded, initialized 1.0° NCEP GFS analyses).

Figure 3.33: As in Fig. 3.16, except for 0600 UTC 29 January 2007.

Figure 3.34: As in Fig. 3.17, except from 2000 UTC 28 January to 1200 UTC 29 January 2007 for (a) KSYR, (b) KGFL, (c) KALB and (d) KPOU.

Figure 3.35: As in Fig. 3.18, except from 2200 UTC 28 January to 1400 UTC 29 January 2007 for KSYR, KGFL, KALB, KPOU, and KSPF. (Data source: University at Albany DEAS archives).

Figure 3.36: As in Fig. 3.19, except for 1200 UTC 29 January 2007.

Figure 3.37: As in Fig. 3.21, except for 0000 (green line and barbs), 0600 (black line and barbs), and 1200 UTC 29 January 2007 (red line and barbs).

Figure 3.38: As in Fig. 3.22, except for 0000 (green line and barbs), 0600 (black line and barbs), and 1200 UTC 29 January 2007 (red line and barbs).

Figure 3.39: in Fig. 3.23, except from GOES-12 at 0845 UTC 29 January 2007.

Figure 3.40: As in Fig. 3.15, except for (a) 1803, (b) 2101, (c) 2358 UTC 16 December 2002, (d) 0302, (e) 0603, and (f) 0900 UTC 17 December 2002.

Figure 3.41: As in Fig. 3.7, except for (a) 0000, (b) 0600, (c) 1200, (d) 1800 UTC 16 December 2002, (e) 0000, and (f) 0600 UTC 17 December 2002.

Figure 3.42: As in Fig. 3.10, except for (a) 0000, (b) 0600, (c) 1200, (d) 1800 UTC 16 December 2002, (e) 0000, and (f) 0600 UTC 17 December 2002.

Figure 3.43: As in Fig. 3.13, except for (a) 0000, (b) 0600, (c) 1200, (d) 1800 UTC 16 December 2002, (e) 0000, and (f) 0600 UTC 17 December 2002.

Figure 3.44: Regional surface analysis for eastern New York and New England at 0300 UTC 17 December 2002. Isobars (solid) every 4 hPa. Isotherms (dashed) every 4°C. Temperature (°C) is plotted above visibility at several stations; missing station data have been omitted. (Data source: the University at Albany DEAS archives, with supplemental data provided by the Historical Weather Data Archives of NSSL).

Figure 3.45: As in Fig. 3.17, except from 1800 UTC 16 December to 0600 UTC 17 December 2002. (Data source: the University at Albany DEAS archives, with supplemental data provided by the Historical Weather Data Archives of NSSL).

Figure 3.46: As in Fig. 3.18, except from 1800 UTC 16 December to 0800 UTC 17 December 2002).

1. Introduction

1.1 General Purpose

This thesis presents a multiscale examination of low-level flow channeling in the Mohawk and Hudson River valleys of New York State. Insight into how synoptic and mesoscale flow patterns interact with the region's topography to drive low-level flow convergence (known colloquially as Mohawk–Hudson convergence and, hereafter, as MHC) is obtained by examining several detailed case studies. Case-to-case similarities prior to and during MHC events are described in an effort to develop an operational forecasting strategy.

The remainder of this chapter will provide a literature review of pressure-gradient-driven flow channeling, with an emphasis on orographic channeling of low-level flow. An examination of orographically induced low-level convergence zones is included, such as the Puget Sound convergence zone, the Snake River Plain convergence zone, and the Denver Cyclone. Several existing studies of how orographic features in eastern New York and western New England impact the local climatology will also be presented. This chapter ends with a discussion of the scientific goals and organizational structure of this thesis.

1.2 Review of Available Literature Discussing Orographically Modified Flows

The literature review begins by discussing the basic conditions which favor orographically altered valley wind flows and the means by which they are produced. Examples of the influence that low-level flow channeling within a valley has on the precipitation distribution are introduced next. Finally, existing research on how the

Mohawk and Hudson valleys influence the weather of eastern New York and western New England, specifically during the warm season, is highlighted.

1.2.1 The Basics of Low-Level Flow Channeling Within a Valley

Flow channeling occurs when orographic features, such as breaks in mountain barriers or valleys through hilly terrain, act to change the local wind direction or speed. Oftentimes this phenomenon reveals itself as a recurring area of surface wind observations that differ systematically from surrounding observations, and which occur only under certain specific synoptic conditions.

Intuitively, one might imagine that only highly exaggerated terrain or deep valleys would effectively channel winds, but Gross and Wippermann (1987) prove otherwise in their examination of channeling in Germany's upper Rhine valley. The authors indicate that the broad and flat valley, which has a width of only 35 km and is flanked by mountains on each side that rise only about 500 m, is nevertheless an effective flow channeling mechanism (Fig. 1.1a; Gross and Wippermann 1987). The Hudson valley of New York, which is approximately 45 km wide and is flanked by terrain that rises no more than 750 m above the valley floor (a measurement known hereafter as "local relief"), is similar in scale to the upper Rhine valley and would therefore likely be an effective flow-channeling mechanism (Fig. 1.2). The hourglass shape of the Mohawk valley, which comprises two broad plains (one located near Rome, NY; the other near Albany, NY) funneling into a relatively narrow (approximately 15-km wide) section, and local relief similar to that of the Hudson valley, also points to the Mohawk's effectiveness for flow channeling, following Gross and Wippermann (Fig. 1.2).

In their treatment of the relatively broad and shallow Tennessee valley (Fig. 1.1c) Whiteman and Doran (1993) examined four mechanisms that can produce valley winds that differ from the overlying winds found above the valley. The first process, thermal forcing, produces strong day-to-night shifts in wind direction within the valley and is not prone to occur in shallow valleys (Whiteman and Doran 1993). As both the Hudson and Mohawk valleys are characterized as shallow in the framework of Gross and Wippermann (1987), and as no discernable diurnal wind signature appears with respect to them, thermal forcing is not expected to affect winds within these valleys to any great extent. The downward transport of horizontal momentum from above a valley is the second process that can influence winds within a valley, according to Whiteman and Doran (1993). This process generates in-valley winds that are of a similar direction as the overlying, ambient flow. In most instances where MHC is occurring, it will be shown that a low- to mid-level temperature inversion is present and that surface winds within the valleys tend to be light (less than 8 m s^{-1}), indicating that downward momentum transfer is relatively unimportant. Winds within a valley can oppose the direction of the ambient flow if the third process presented by Whiteman and Doran (1993), known as "forced channeling," is at work. This process directs the perpendicular (relative to the valley) component of the overlying geostrophically balanced winds into the valley, in a direction that is parallel to the valley axis. Occasional but sudden changes in direction can occur when overlying geostrophic winds become more- or less-normal to the valley sidewalls. Wind directions prior to, during, and following MHC events, conversely, shift subtly and gradually, indicating that forced channeling likely plays little or no role. Finally, Whiteman and Doran (1993) assert that valley winds can arise from the geostrophic

pressure gradient that is aligned along the valley's axis. This final process is called "pressure-driven channeling." Gross and Wippermann (1987) also addressed this phenomenon, stating that pressure-driven channeling is produced when a column of air passes across a valley and expands vertically, becoming subgeostrophic and turning left, referenced to the direction of the large-scale pressure gradient (Fig. 1.3). In this way, only the along-valley component of the large-scale pressure gradient is effective in driving the winds within a valley (Gross and Wippermann 1987). Whiteman and Doran (1993) argue that it is the pressure gradient directed along the valley alone that affects valley winds, and that air is not necessarily required to expand into the valley from above, stating that:

> "Pressure-driven channeling is expected to be a dominant mechanism in valleys under conditions where the influence of the downward momentum transport and thermal wind mechanisms are minimized. This occurs for shallow, but well-channeled, linear valleys in a climatological regime with light to moderate geostrophic above-valley winds and slightly or moderately stable atmospheres."

The authors go on to state that "[t]o date, the pressure-driven channeling mechanism has been documented for Germany's Rhine Valley and in the Tennessee Valley" (Whiteman and Doran 1993). The Mohawk and Hudson valleys are also shallow, well-channeled, linear valleys, and it will be shown that all MHC cases examined occur in light to moderate geostrophic flow regimes, with a high overall static stability in the lower troposphere. It follows, then, that pressure-driven channeling may be a dominant force in the formation of MHC.

Kossmann and Sturman (2003) continue the discussion of pressure-driven channeling, asserting that the wind speed generated within a valley is proportional to the pressure gradient force (PGF) that acts along the valley axis. They note that a greater

frequency of channeling events is seen in the presence of more stable atmospheric stratifications, which act to decouple winds within a valley from the ridge-level winds and limit downward mixing of momentum from above (Kossmann and Sturman 2003).

Kossmann and Sturman (2003) also dissect pressure-driven channeling within a curved or bent valley, where the angle between the synoptic-scale pressure gradient vector and the valley axis will differ from one valley segment to another. The Mohawk and Hudson valleys, while themselves linear in nature, intersect near Albany, NY (KALB), at an approximate 100° angle, which may generate effects similar to those caused by a valley bend. Following Kossmann and Sturman (2003), and given this valley configuration and the typical background PGF associated with MHC, Fig. 1.4h mostly closely approximates how the valleys and the effects of pressure-driven channeling interact. In this configuration, the along-valley PGF is of the same sign in both valleys but of greater magnitude along the Mohawk valley, resulting in convergence at the valley bend and associated upward vertical motion. This bent-valley effect could contribute to the surface convergence that gives rise to MHC, although it is likely not the primary cause. Kossmann and Sturman (2003) go on to say that inertial effects, owing to differing wind speeds in each segment of a bent valley, can displace the convergence zone away from the valley bend and in the direction of the stronger wind speed. In the case of MHC, precipitation is rarely centered directly over the intersection of the Mohawk and Hudson valleys, and its actual location may be modulated by the aforementioned inertial effects.

1.2.2 Effects of Low-Level Flow Channeling on Precipitation

The orographic channeling of low-level winds can impact the precipitation distribution in several ways. In some cases, channeled flow can modify the temperature profile of the atmosphere enough to locally change the phase of falling precipitation. Orographic channeling of low-level flow may also lead to zones of convergence, which can in turn generate areas of mesoscale precipitation. The Puget Sound of Washington State, the area surrounding Denver, Colorado, and the Snake River Plain of eastern Idaho are among the areas that experience precipitation from these convergence zones.

1.2.2.1 PUGET SOUND CONVERGENCE ZONE

Chien and Mass (1997) introduce the Puget Sound convergence (PSCZ) as "probably the most important topographically induced mesoscale phenomenon affecting the Puget Sound lowlands." In a given year, the PSCZ occurs dozens of times and has a significant impact on the climatology of the region (Chien and Mass 1997). Whitney et al. (1993) indicate that "the PSCZ can be strong enough to produce thunderstorms with brief heavy rain, snow, ice pellets or hail," and that, during the cold season, can produce over 100 cm of snow per event, necessitating winter storm warnings. While MHC does not appear to have a discernable effect on the climate of eastern New York and western New England, its evolution does share some similarities with the PSCZ and its impacts on the public can be significant several days per year.

A conceptual model of the PSCZ, presented by Mass (1981), illustrates the way in which the Cascade Mountains, Strait of Juan de Fuca, and Chehalis Gap act to direct northwest low-level flow off of the Pacific Ocean and over the Puget Sound, forming a

convergence zone, and creating enhanced precipitation around Seattle and Everett (Fig. 1.5). These conditions (and the resulting convergence zone) are shown by Mass (1981) to be most likely during the late spring and early summer months due to the wind climatology of the region. Chien and Mass (1997) also note that PSCZ events tend to develop directly following a cold frontal passage. This postfrontal environment is also characteristic of MHC development, which also shows a strong seasonal dependence.

Utilizing sets of case studies selected at random, Mass (1981) finds that the PSCZ develops only through a narrow subset of coastal surface wind directions, as measured at several representative sites (Fig. 1.6). Winds are generally of light or moderate speeds (approximately 2.5–7.5 m s^{-1}), and several calm readings are reported in the area of surface convergence during PSCZ events (Mass 1981). A similarly narrow range of surface wind directions are present at bellwether sites during MHC and wind speeds are generally light to moderate as well, as shown in Table I.

A case and subsequent modeling study of a PSCZ even that occurred on 26 May 1992 is presented by Chien and Mass (1997) and provides insight into what drives the PSCZ phenomenon. Initially, surface winds in the convergence zone were quite weak (and, at times, calm), and throughout the entire event analyzed wind speeds were 5 m s^{-1} or less (Fig. 2, not shown; Chien and Mass 1997). These light-to-moderate wind speeds are characteristic of those present during MHC events as well.

Chien and Mass (1997) found that the PSCZ could be modeled successfully by the Pennsylvania State University–National Center for Atmospheric Research Mesoscale Model (PSU–NCAR MM5), and determined that both the Olympic and Cascade Mountains are critical to the formation of the convergence zone (Fig. 1.7). These terrain

features act to steer the onshore flow so that this flow splits and then converges over the central Puget Sound; without these features and the split flow, the PSCZ does not form (Chien and Mass 1997). Furthermore, the modeling of this event corroborates what Mass (1981) had found previously through examining vertical wind profiles; namely, the winds responsible for PSCZ formation are relatively shallow with a depth generally less than 1.2 km. It should be noted that the winds responsible for producing MHC are even shallower, on the order of 0.5 km in depth.

Additional model results indicate that, during its strongest phase, the PSCZ produces maximum vertical motions centered at approximately 850 hPa (Chien and Mass 1997; Figs. 1.8 and 1.9). It will be shown that maximum vertical motions associated with MHC tend to be centered lower in the atmosphere (around 925 hPa) and are weaker, even during the peak of events.

Modeling conducted by Chien and Mass (1997) also reveals the important role that latent heat release plays in regard to the formation and strength of the PSCZ. Latent heat released by condensation in the rising air acts to destabilize the lower troposphere, creating a positive-feedback mechanism in which convection and accompanying low-level convergence strengthens. The removal of latent heating from the model simulations of the 26 May 1992 case still allowed the PSCZ to form, but in a weakened state. Without latent heat effects, "low-level wind convergence near the central [Puget] sound is attenuated compared to the control run; in addition, there is lighter and more widespread precipitation over the Puget Sound" due to greater stability, which limits vertical development (Chien and Mass 1997). It will be shown that, with precipitable water (PWAT) values between 3.8 and 7.6 mm and high static stability present in all

cases, MHC lacks the contribution of latent heat release. This key difference likely explains the shallow nature of ascent and precipitation associated with MHC, and plays a substantial role in limiting its overall climatological impact.

Mass (1981) experimented with forecasting the PSCZ through examining synoptic-scale weather features. The experiments resulted in a successful prediction of the PSCZ 22 out of 23 times, but also indicated several "false alarm" events which did not actually occur (Mass 1981; Fig 1.10). Overall, Mass (1981) found that the PSCZ is inherently predictable, given accurate forecasts of surface wind speed and direction. Building on this finding, Whitney et al. (1993) conclude that "it is possible to make a reasonably skillful medium-range forecast of the occurrence of a PSCZ." To that end, a methodology and decision tree for forecasting the PSCZ was devised (Fig. 1.11), and was put into operational use by the Seattle Forecast Office of the National Weather Service. Whitney et al. (1993) highlight the important role that coastal surface wind direction plays in allowing the PSCZ to form by making it the first criterion of the decision tree. When the direction and speed of surface winds at Hoquium, Washington (KHQM), fall into a predetermined range, a PSCZ event is likely within several hours. Furthermore, the likelihood of PSCZ formation increases as the initially larger west-to-east sea-level pressure (SLP) difference becomes similar in magnitude to the north-to-south SLP. Such a rotation of the SLP gradient permits a generally southwest and west-southwest surface flow to develop over western Washington State. As this southwest and west-southwest flow develops it can sometimes bifurcate around the Olympic Peninsula, with one part of the flow moving down the Strait of Juan de Fuca and turning southward across Puget Sound and the other part of the flow moving across the Puget Sound lowlands and

turning northward across Puget Sound. Where the northerly and southerly air streams in Puget Sound converge marks the location of the PSCZ.

Whitney et al. (1993) conclude that the only factors controlling lead time for PSCZ forecasts are the accuracy of model simulations and forecaster confidence. Like the PSCZ, MHC is a mesoscale phenomenon driven by synoptic-scale features and likely has a high degree of predictability in the medium- to short-range.

1.2.2.2 Snake River Plain Convergence Zone

Andretta and Hazen (1998) describe the Snake River Plain convergence zone (SRPCZ) as a periodic feature that forms in the Snake River Plain (SRP) of eastern Idaho under northwest synoptic flow at mid and low levels. Fig. 1.12 reveals that the SRP is approximately 100 km wide and features local height relief of 1700 m with respect to the bounding mountains to the northwest, and 400 m with respect to the bounding mountains to the southeast (Andretta and Hazen 1998). The valley-to-ridgeline height difference to the southeast is somewhat similar to that of the Mohawk or Hudson valleys but, overall, local relief is much greater in the case of the SRP.

Steenburgh and Blazek (2001) highlight the effectiveness of the SRP in channeling low-level flow through their study of a cold front that was distorted by the topography of the region. Fig. 1.13 shows the progression of the cold front through the SRP and an accompanying frontal bulge, which developed as the cold front was locally accelerated within the SRP. The acceleration is attributed by Steenburgh and Blazek (2001) to an isolated wind maximum that developed directly behind the cold front within the plain. The authors go on to explain that the development of this wind maximum is a

direct result of the highly ageostrophic flow field that developed within the channeled terrain.

Andretta and Hazen (1998) present a case study of a SRPCZ event that took place on 26 November 1995 and was preceded by the passage of a surface cold front. This front brought an end to synoptic-scale precipitation and was associated with a 40 m decrease in the 1000–500 hPa thickness over 6 h, indicating cold advection. Behind the front, the rise in SLP pressure averaged 4 hPa as the pressure gradient in the area tightened significantly. Geopotential height rises and a tightening of the geopotential height gradient accompanied weak cyclonic flow at 850 and 700 hPa. Also, the static stability of the lower troposphere decreased, with lapse rates increasing from 5.7 to 7.0°C km^{-1} over 7 h. Aside from the presence of low-level cold advection, which is characteristic of MHC, there are few similarities between the synoptic patterns associated with MHC and SRPCZ. Steady, rising, and falling SLP trends are all observed during MHC events, and neutral or falling heights are observed at 850 and 700 hPa. In many cases, cyclonic curvature of the 850- and 700-hPa geopotential height contours is present during MHC events, but such curvature is not always pronounced.

Using the Weather Surveillance Radar-1988 Doppler (WSR-88D) located in Springfield, Idaho (SFX; see Fig. 1.12 for location), and various surface observation sites, Andretta and Hazen (1998) diagnose mesoscale wind patterns throughout the SRPCZ event of 26 November 1995. At the onset, the lowest tilt of the radar (at a 0.5° elevation above horizontal, or slightly above the 850-hPa level given the elevation of the radar site) reveals the presence of 16–21 m s^{-1} winds as well as a band of moderate-to-heavy snow (24–44 dBZ) over the region. Surface winds [as indicated by mesoscale

observation network (mesonet) sites] of 5–15 m s^{-1} are also present. A convergent wind signature seen over the upper SRP in the lowest 1 km of the atmosphere on the radar's Vertical Azimuth Display (VAD; not shown) is attributed to the SRPCZ, and a zone of low-level convergence. This zone and an attendant area of precipitation associated with 35–45 dBZ radar reflectivities propagate down-valley at approximately 5–10 m s^{-1}. Maximum snowfall totals from the SRPCZ event ranged from approximately 10.2 to 15.3 cm. Qualitative similarities between the MHC and the SRPCZ exist, including the vertical stratification of winds, the relatively shallow atmospheric depth of convergence, and the propagation of convergence zone, but quantitative differences also exist. These differences include wind speeds, both at the surface and aloft (which are generally half as great during MHC events), depth of convergence (again, half as great during MHC events), and precipitation intensity (which generally does not exceed 30 dBZ in cases of MHC).

1.2.2.3 Denver Cyclone

In their seminal paper, Szoke et al. (1984) describe the formation of a narrow line of surface convergence and cyclonic turning of low-level winds in the vicinity of Denver, Colorado, which they dubbed the Denver convergence–vorticity zone (see Fig. 1.14). Also known as the Denver Cyclone (DC) in several subsequent papers (e.g., Wilczak and Glendening 1988; Wilczak and Christian 1990), Szoke et al. (1984) came upon the phenomenon while investigating the 3 June 1981 tornado outbreak in the Denver area, the worst tornadic outbreak for the region to date at that time. Identifying the presence of the convergence–vorticity zone more than 5 h before the tornado outbreak, Szoke et al.

(1984) note its importance in the development of severe weather that day, and acknowledged the role that this mesoscale feature may have played in tornado spin-up. The authors briefly examine two seasons (May–August of 1981–82) of severe weather occurrences in the Denver area, finding a correlation between a convergence–vorticity zone regime and the occurrence of severe weather. Namely, they find that during the period of study 14 out of the 23 reported tornadoes (61%) occurred in the presence of a convergence–vorticity zone (which may or may not include a closed circulation), or in the presence of south to southeasterly surface flow.

The topography of the north-to-south oriented Rocky Mountain Front Range features significantly more local relief than that of eastern New York and western New England, with peak elevations of more than 3700 m in northeastern Colorado and a 2000 m rise occurring in less than 20 km (Wilczak and Glendening 1988; Fig. 1, not shown). The DC itself occurs in the lee of the Front Range, bounded by two west-to-east oriented ridges: the Cheyenne Ridge to the north and the Palmer Ridge to the south.

Case studies of two different DC events provide insight into its life cycle and manifestation. In their treatment of the DC event of 1 August 1985, Wilczak and Glendening (1988) show that the gyre develops following the passage of a surface cold front, in an air mass that becomes more stably stratified with time. A southeasterly surface return flow sets up several days later, allowing a well-mixed boundary layer to grow slowly out of a stable layer, which was initially present from the surface to a height of about 1 km above ground level. The authors also find falling pressures in the vicinity of the mature gyre. In most instances of MHC, which also tend to follow the arrival of a

cooler and more stably stratified airmass, surface pressures tend to be nearly steady or rising during the mature phase.

A case study by Wilczak and Christian (1990) of a DC occurrence, which began on 25 June 1987 and persisted in a quasi-steady-state fashion for 30 h, indicates that this feature developed in the presence of a stable nocturnal inversion layer (their Fig. 4, not shown). Beginning under weak upper-level synoptic forcing as a shallow, near-surface phenomenon (as revealed in wind reports gathered from observation towers and wind profilers), the mixed layer and vortex both grew in depth over the next several hours to a height at which a strong inversion layer existed, i.e., 700 hPa. As ground level in the vicinity of Denver occurs at approximately 850 hPa, this height indicates that the DC occurred only in the lowest 150 hPa of the atmosphere, the depth of which is similar to MHC. It will be shown that the discernable wind and model-diagnosed vertical-motion signatures associated with MHC generally occur only in the lowest 75 hPa of the atmosphere.

Wilczak and Christian (1990) also examined how the presence of the DC may have assisted in the formation of severe thunderstorms during the 25 June 1987 episode. The close inspection by these authors of radar data showed weak cells (reflectivities less than 25 dBZ) forming over the mountains to the west of Denver, which dissipated as they drifted eastward. Some of these dissipating elevated cells passed over part of the convergence zone associated with the DC and reached 40 dBZ in intensity within an hour doing so, while the strongest cells reached 70 dBZ, split, and produced hail up to 4.5 cm in diameter. From the timing of the supercells' formation, the authors infer that the dissipating elevated cells may have triggered convection along the convergence zone as

they passed overhead. This inference suggests a mechanism by which existing precipitation can be enhanced by the presence of a convergence zone, a mechanism that will be discussed later in reference to MHC.

Through their mixed-layer modeling of the 1 August 1985 DC episode, Wilczak and Glendening (1988) conclude that "baroclinicity is of paramount importance in the formation of the Denver Cyclone." Conversely, close inspection of multiple MHC events indicate that baroclinicity is not a factor in the formation of MHC. Furthermore, the presence of large amounts of baroclinicity may, in fact, inhibit MHC from forming, as the stronger forcing generally associated with baroclinic regimes would tend to overpower the weaker pressure-driven forcing which accompanies MHC.

1.2.2.4 LONGMONT ANTICYCLONE

The Longmont Anticyclone (LA) is introduced by Wesley et al. (1995) as a counterpart of the Denver Cyclone, stating "[t]he Longmont Anticyclone [is] a region of low-level anticyclonic turning and convergence," which forms when northerly flow along the Front Range of the Rocky Mountains interacts with the complex local terrain (Fig. 1.15). The LA forms in a post frontal environment (similar to the phenomena previously discussed above, including MHC), as a gusty, partially isallobaric wind develops in response to rapid surface pressure rises over Wyoming. The low-level northerly flow turns anticyclonically and decelerates in the lee of the Cheyenne Ridge (the axis of which is seen just north of the Colorado–Wyoming border in Fig. 1.15), and the resulting convergence can generate precipitation. The ensuing precipitation can have a significant impact on local snowfall distributions, despite the shallow, anticyclonic nature of the air

mass (Wesley et al. 1995). The authors also note that preexisting precipitation that enters the area can be enhanced by an ongoing LA, an effect that will be further examined with regard to MHC.

In their case study of the LA event of 16 January 1991, Wesley et al. (1995) documented a synoptic environment which is strikingly similar to that of MHC events The synoptic environment included: 1) the lack of any jet streak dynamics; 2) the presence of a large-scale 500 hPa trough with northwest flow and slowly falling geopotential heights; 3) the lack of robust vorticity advection; 4) weak low-level cold advection following the passage of a weak surface cold front; 5) a period of calm surface winds in the area of convergence; and 6) low-level winds generally weaker than 10 m s^{-1} during the event. As determined by vertical thermodynamic and wind profiles taken in the region at the onset of the 16 January 1991 LA event (not shown), the atmosphere was moist from the surface to 500 hPa and featured a shallow, ground-based stable layer, above which dry-adiabatic lapse rates existed to 690 hPa. It should be noted that the Appendix of Wesley et al. (1995) addresses the unusual nature of saturated atmospheric conditions coexisting with dry-adiabatic lapse rates, and the way in which riming on humidity sensors may have caused inaccurate measurements. Ultimately, though, the authors conclude that relative humidities above 75% were present in the 800–600 hPa layer. At the peak of the LA, a moist and conditionally unstable layer was found in the lowest 130 hPa of the atmosphere, with a layer of greater static stability (and moist-adiabatic lapse rates) above. The stabilization of the lower troposphere, warming of cloud top temperatures (CTTs), and drying in the low and midlevels of the atmosphere coincided with the end of the LA event. The thermodynamic profile presented by Wesley

et al. (1995) indicates that the atmosphere was supportive of convection throughout much of the LA event, a contrast to the stably stratified atmosphere common to MHC cases. The vertical wind profiles also speak to the shallow nature of the LA (another characteristic shared by MHC), with Wesley et al. (1995) detecting the wind signature associated with the LA in a layer only 500 m deep.

Radar loops of the precipitation intensity associated with the LA event of 16 January 1991 indicate that intensification of weaker echoes occurred as they moved from north-to-south through the convergence zone domain (Wesley et al. 1995). Radar reflectivity values as high as 30 dBZ were noted as snowbands drifted across the area where the LA was present, with heavy snow and wind gusts to 9 m s^{-1} reported as one such band passed the Denver observation site. Snowfall amounts totaled 6–9 cm just south of the LA region (over and west of DEN and BOU, Fig. 1.15), and was attributed by Wesley et al. (1995) to convergence. It will be shown that the amount of snow that falls during typical MHC events, and the corresponding radar reflectivities, are on the order of what fell during the LA event discussed by Wesley et al. (1995).

1.2.2.5 Cold-Air Damming in the Appalachian Mountains

Citing Richwein (1980), Bell and Bosart (1988) define cold-air damming (CAD) as "[t]he phenomenon of cold air becoming entrenched along the slopes of mountain ranges..." Utilizing archived surface weather charts, Bell and Bosart (1988) developed a monthly climatology of CAD events along the eastern slopes of the Appalachian Mountains, and found that the phenomenon occurs year round (Fig. 1.16). Closer inspection of the data, however, reveals a seasonal signature in the frequency of

occurrence, with 67% of all damming events and 68% of all damming days taking place from October to April (Bell and Bosart 1988). The tendency for CAD to occur during the cold season is similar to the seasonality observed with respect to MHC.

A case study of the CAD event of 21–23 March 1985 presented by Bell and Bosart (1988) also presents a conceptual model of how CAD develops along the eastern slopes of the Appalachians (Fig. 1.17). Prior to this damming event, Bell and Bosart (1988) note "classic precursor conditions" (not shown), including the relative positions of two 500 hPa troughs. The subsidence which results from the passage of the first 500-hPa trough is able to drive a surface anticyclone into the region (following the passage of a surface cold front) well before the arrival of a surface cyclone associated with the second, southern 500-hPa trough. In this way, down-gradient surface flow is able to drive cold air southward along the eastern slopes of the Appalachians before the southern trough can induce coastal surface cyclogenesis and its associated warm-air advection (Bell and Bosart 1998). The notion of an identifiable synoptic-scale pattern heralding the onset of a mesoscale phenomenon will be shown to be applicable to cases of MHC as well.

As synoptic-scale warm-air advection (WAA) at 850 hPa begins in the region and cold-air advection (CAA) at the surface continues, Bell and Bosart (1988) indicate the development and eventual strengthening of a sloping inversion at the top of the surface cold pool. In this fashion, a positive-feedback mechanism ensues, in which the strengthening inversion renders the cold pool increasingly stable. This mechanism differs fundamentally from the processes that drive MHC, which occurs within an inherently transient synoptic regime. Conversely, the shallowness of CAD and its attendant dome of low-level cold air, which Bell and Bosart (1988) indicate develops below 850 hPa and

is therefore not evident on mandatory-level constant pressure charts, is similar to the shallow nature of MHC, which, too, is not directly evident on such charts. Indeed, CAD is most readily apparent from the surface to 930 hPa, a level at which Bell and Bosart (1988) indicate that winds are "clearly orographically influenced," as evidenced by a substantial northeasterly bias in wind direction as compared to overlying flow. The winds at the 930-hPa level (with speeds ranging from 12 to 17 m s^{-1}) are referred to by Bell and Bosart (1988) as the low-level wind maximum (LLWM), which the authors state is accelerated by an unbalanced along-mountain component of the pressure-gradient force. Air flowing toward the mountains is partially blocked and slows down, resulting in a weakening of the Coriolis force and the creation of an unbalanced pressure gradient force with resulting down-gradient mountain-parallel flow. The CAD signature weakens when the mountain-parallel component of the low-level flow decreases, allowing the cold dome to disperse and expand toward the coast. The CAD signature is eliminated when the mountain-perpendicular component of the flow becomes directed away from the mountains. Thus, while low-level wind speeds and pressure gradients exceed those seen in cases of MHC (see Table I), both CAD and MHC are pressure-gradient-driven channeling phenomena.

1.2.2.6 Saint Lawrence River Valley

Close to the Mohawk and Hudson River valleys of eastern New York State is the St. Lawrence River valley, shown in Fig. 1.1b as the broad area of low elevation that emanates northeastward from the eastern shores of Lake Ontario. Roebber and Gyakum (2003) discuss the role that the St. Lawrence valley played in the development of a long-

duration catastrophic ice storm that brought more than 100 mm of freezing rain to parts of northern New York and New England in the United States, and Quebec, Ontario, and New Brunswick in Canada from 5–9 January 1998. This icing event developed under the influence of a strong high pressure system situated off the eastern seaboard of the United States (a Bermuda high), which delivered moisture-rich air (PWAT values 2.5 times greater than the climatological average) and light-to-moderate rains to the region concurrent with the arrival of shallow, low-level cold air. This cold air was initially introduced by the passage of a surface cold front, and an extended period of cold surface flow into the region ensued as a strong surface high developed over north-central Quebec. Five analogous events, occurring over a 34 year period, were examined by Roebber and Gyakum (2003), who indicate that even "the best analog produced maximum precipitation amounts less than 50% of the 1998 event."

Pointing to surface wind observations from Montreal and Ottawa (not shown) as evidence of pressure-driven channeling within the St. Lawrence Valley, Roebber and Gyakum (2003) hypothesize that this effect was "crucial" in determining the type of precipitation at times during the event. Fig. 7 (not shown) from Roebber and Gyakum (2003) also provides evidence of orographic flow channeling based on data collected by the McGill University wind profiler (located in Montreal), showing a discontinuity between near-surface winds (easterlies and northeasterlies) and overlying winds (southwesterlies). While more pronounced in the case of the 1998 ice storm, low-level wind signatures which are decoupled from the overlying synoptic-scale flow are also evident in cases of MHC.

Roebber and Gyakum (2003) attribute maximum precipitation amounts from the 1998 ice storm to the presence of a deformation zone in the vicinity of the St. Lawrence Valley and frontogenetical forcing. Frontogenesis was locally enhanced by persistent down-valley transport of cold air driven by pressure-gradient-driven flow channeling, which had the effect of controlling not only precipitation intensity (an effect also seen in cases of MHC), but also precipitation type in the region. Indeed, model (MM5) simulations conducted by Roebber and Gyakum (2003; not shown) indicate that little or no freezing rain would have occurred at Burlington, Vermont, had flow channeling not occurred. Pressure-gradient-driven channeling, responsible for keeping the surface-based freezing line from retreating northward despite the surrounding synoptic-scale conditions, was found by Roebber and Gyakum (2003) to play a vital role in sustaining the long-duration icing event. The inherent difficulty in forecasting mesoscale features prevented forecasters at the time of this event from properly identifying its magnitude; however, as the presence and effect of orographic channeling is tied to the synoptic-scale pressure field, Roebber and Gyakum (2003) "speculate that the intrinsic predictability of such events may be relatively high."

1.2.3 Effects of the Mohawk and Hudson River Valleys on Overlying Synoptic Flows

Several previous studies have examined the impacts of complex terrain on the weather of eastern New York and western New England. As of this writing, there are no existing references in the refereed literature on how the Mohawk and Hudson valleys may influence cold season weather regimes in the region. There are, however, recent refereed publications that address the influence of these valleys on warm-season severe

weather within the region, including Wasula et al. (2002), LaPenta et al. (2005), and Bosart et al. (2006). Reviews of these publications follow, in an effort to assess the flow-channeling properties of the Mohawk and Hudson valleys.

Wasula et al. (2002) addressed the climatology of severe weather (wind, hail and tornado reports) over eastern New York and western New England in relation to terrain influences (for an overview of the terrain, see Figs. 1.1d, 1.2). Surface wind roses were generated for hourly observations of wind direction between March 1993 and March 1997 at Albany, NY (ALB), and from July 1995 through May 1997 at Utica, NY (UCA). These wind roses are presented in Fig. 1.18, showing a tri- and bimodal wind distribution at ALB and UCA, respectively. At ALB, the three dominant wind directions (in terms of frequency of occurrence) are south, north, and west-northwest, and at UCA are west-northwest and east-southeast. Noting that these wind directions at ALB (UCA) align well with the axes of the Mohawk and Hudson (Mohawk) River valleys, Wasula et al. (2002) conclude that "near and just above the surface the terrain funneling is an important effect." Additional wind roses (not shown), constructed from atmospheric sounding data at 850, 700, and 500 hPa, indicate an increased tendency for severe weather reports to occur south of the Mohawk Valley into the Catskills and Berkshires on severe weather days with northwest flow, and a preference for severe weather reports to occur from the Mohawk valley northward into the southern Adirondacks on southwest-flow severe weather days.

LaPenta et al. (2005) present a multiscale examination of the Mechanicville, NY, tornado of 31 May 1998, finding that the Hudson River valley may have locally enhanced the already favorable tornadic environment present that day. The authors find the

presence of southerly near-surface flow within the Hudson valley at the same time south-southwest flow was observed to the west of the valley. Such an in-valley flow may have increased the northward transport of heat and moisture (refer to LaPenta et al. 2005, Fig. 24; not shown).

Bosart et al. (2006) examined how the complex terrain of eastern New York and western New England influenced the development of the 1995 Great Barrington, MA (GBR), tornado and its parent mesocyclone. The authors found a pattern of marked rotational intensification as the mesocyclone moved from the high terrain located west of the Hudson River valley into the valley itself, followed by a marked weakening as the mesocyclone continued eastward over the mountains of western Massachusetts. Bosart et al. (2006) conclude that "the most important factor in the observed intensification of the GBR mesocyclone and ensuing tornadogenesis was the existence of a terrain-channeled low-level (0–1 km) southerly flow in the Hudson [v]alley...." As compared to the background environment, this flow channeling produces a more clockwise-turned hodograph at low levels and lengthens the hodograph (i.e. increases the shear) overall.

1.3 Goals and Thesis Synopsis

The ultimate goal of this research is to determine how the topography of eastern New York and western New England interacts with overlying synoptic-scale conditions to generate a zone of low-level convergence and mesoscale precipitation in the vicinity of Albany, NY. Building on previous research which shows the Mohawk and Hudson River valleys to be effective agents for channeling of low-level flow (i.e., Wasula et al. 2002;

LaPenta et al. 2005; and Bosart et al. 2006), the impacts on MHC of pressure-gradient-driven channeling in these valleys will be addressed in this study.

In an effort to determine empirically the processes that drive MHC, several case studies were completed. Two such cases (27 November 2002 and 29 January 2007) are considered "benchmark" cases, and are presented in greater detail. Four other cases (16–17 December 2002, 23 January 2003, 17 January 2005, and 3 March 2006) are presented as supporting cases and are described in lesser detail. These cases were analyzed individually and in the aggregate to determine similarities and differences between them. A seventh case of interest occurred on 2 January 2008, just prior to the completion of this thesis. Sufficient time was not available to undertake an in-depth analysis of the January 2008 event, but an overview of it is included here for completeness.

The physical processes necessary to generate a MHC event will be discussed, including positive north–south (west–east) SLP differences along the Hudson (Mohawk) valley that drive the convergent flow, an absence of strong CAA, which precludes strong subsidence and drying of the boundary layer, and statically stable atmospheric stratification, which prevents downward momentum transfer that could damp out the convergent wind signature. A discussion of the synoptic-scale features that contribute to the aforementioned mesoscale environment will also be presented.

Finally, an effort is made to increase the predictive skill of future MHC events through the use of an operational forecasting scheme. To this end, a conceptual model detailing the interplay during MHC events of upper-air and surface weather features and orography is presented, and a decision tree for forecasters is developed.

1.4 Organization of the Thesis

Chapter 2 addresses the acquisition of observational and model data sources used to develop MHC case studies. The parameters used to describe and those used to make comparisons between each case study comprises an explanation of methodology. Statistical results of these comparisons and an objective analysis and description of each of the seven case studies are presented in Chapter 3. Chapter 4 contains an overview of the findings gained from the case studies, which will be presented in light of the reviewed literature and also with respect to MHC formation and forecasting. A conceptual model of MHC and a decision tree to aid in operational forecasting of this phenomenon also is presented in Chapter 4. Lastly, Chapter 5 includes the conclusion of this thesis as well as suggested avenues of exploration for future researchers.

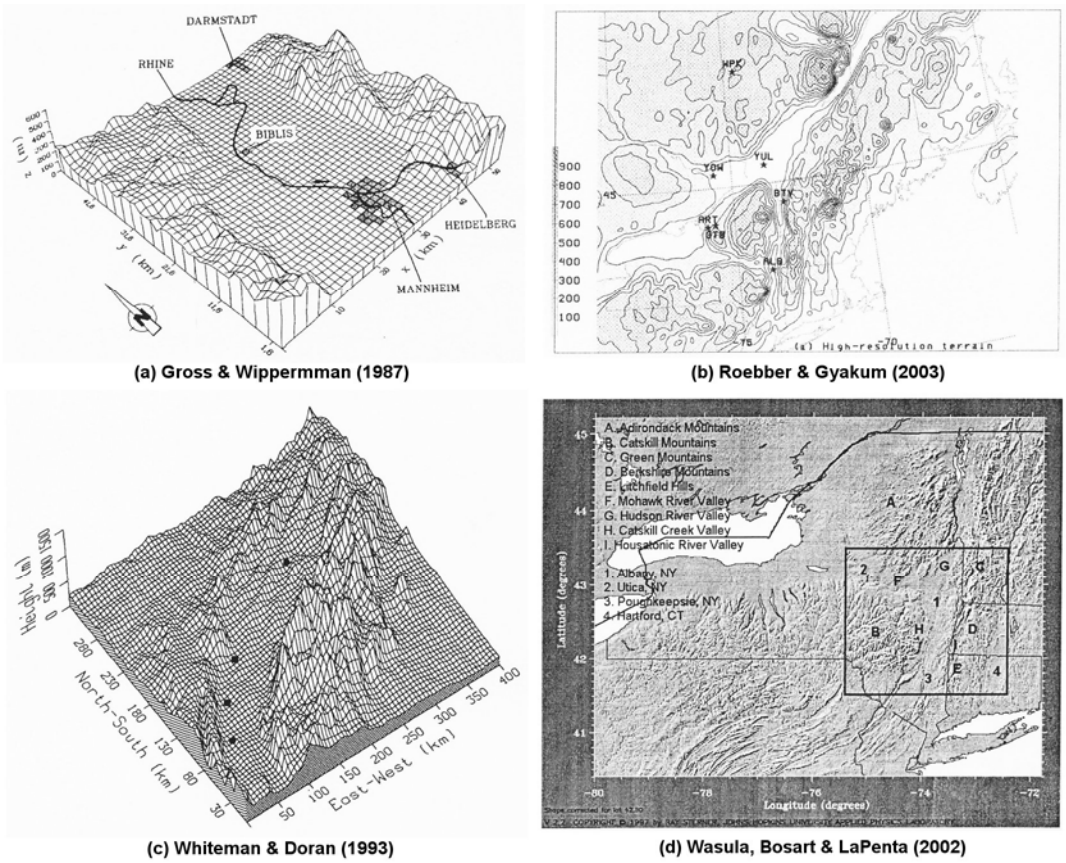

Figure 1.1: Topographic features of selected flow-channeling case studies. (a) The northern part of the upper Rhine valley. (Source: Fig. 2 from Gross and Wippermann 1987). (b) Fifth-generation Pennsylvania State University–National Center for Atmospheric Research Mesoscale Model (PSU–NCAR MM5) 9 km resolution topography (contours and shading) of the northeastern U.S. and southeastern Canada. Contour interval is 100 m, beginning at 100 m, with progressively darker shading for higher elevations. (Source: Fig. 2a from Roebber and Gyakum 2003). (c) Topography of the Tennessee Valley, with the locations of four observation towers indicated. (Source: Fig. 2 from Whiteman and Doran 1993). (d) Terrain map of New York and New England with important terrain and political features labeled. (Source: Fig. 1 from Wasula et al. 2002).

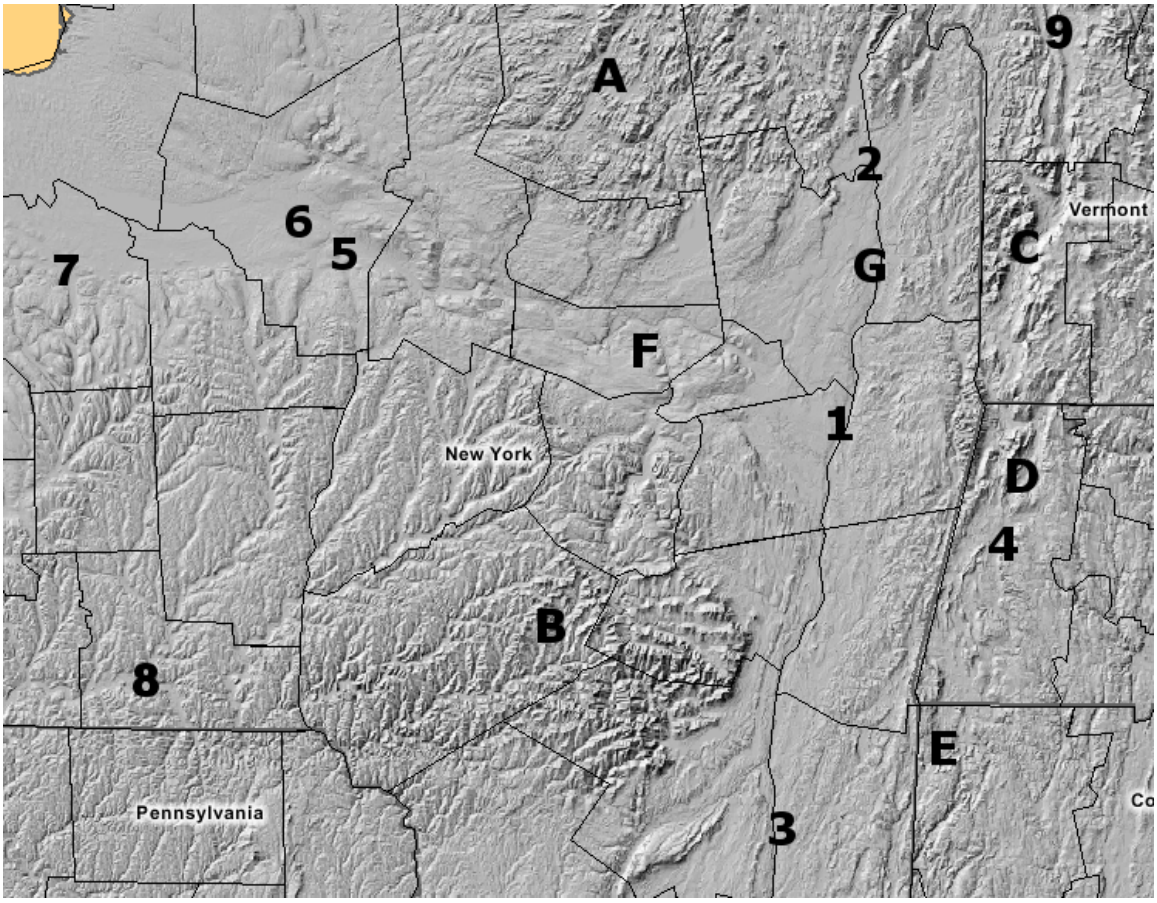

Figure 1.2: Terrain map of Mohawk–Hudson Convergence (MHC) domain in New York and western New England, with important terrain and political features labeled: (1) Albany, NY (KALB), (2) Glens Falls, NY (KGFL), (3) Poughkeepsie, NY (KPOU), (4) Pittsfield, MA (KPSF), (5) Utica, NY (KUCA), (6) Rome, NY (KRME), (7) Syracuse, NY (KSYR), (8) Binghamton, NY (KBGM), (9) Rutland, VT (KRUT), (A) Adirondack Mountains, (B) Catskill Mountains, (C) Green Mountains, (D) Berkshire Mountains, (E) Litchfield Hills, (F) Mohawk River valley, (G) Hudson River valley.

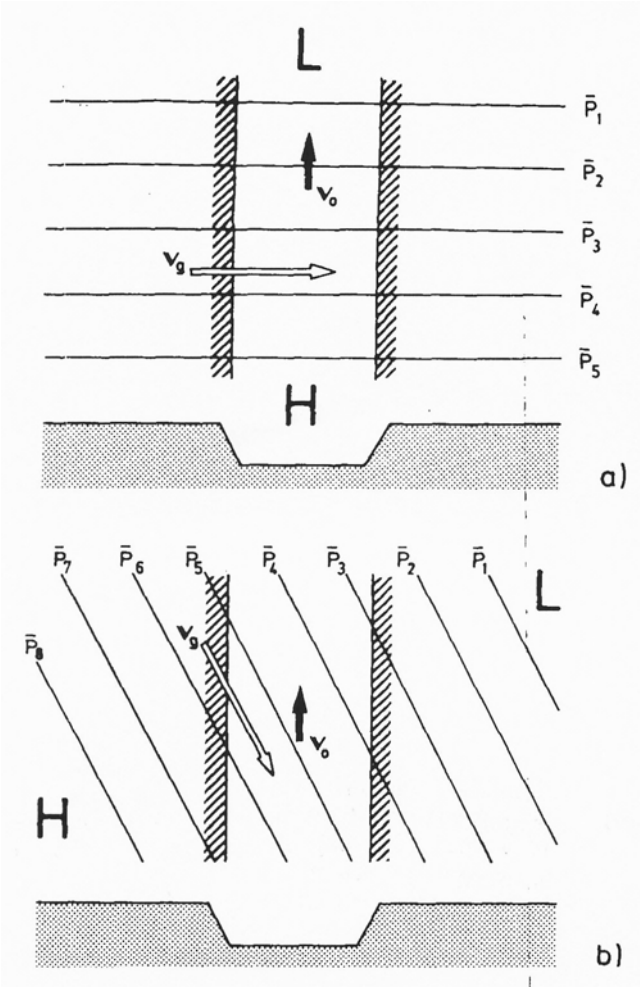

Figure 1.3: Schematic from Gross and Wippermann (1987; originally Fig. 1) showing channeling (**v**, black arrow) for (a) a geostrophic wind perpendicular to the valley, above, and (b) a counter-current, below.

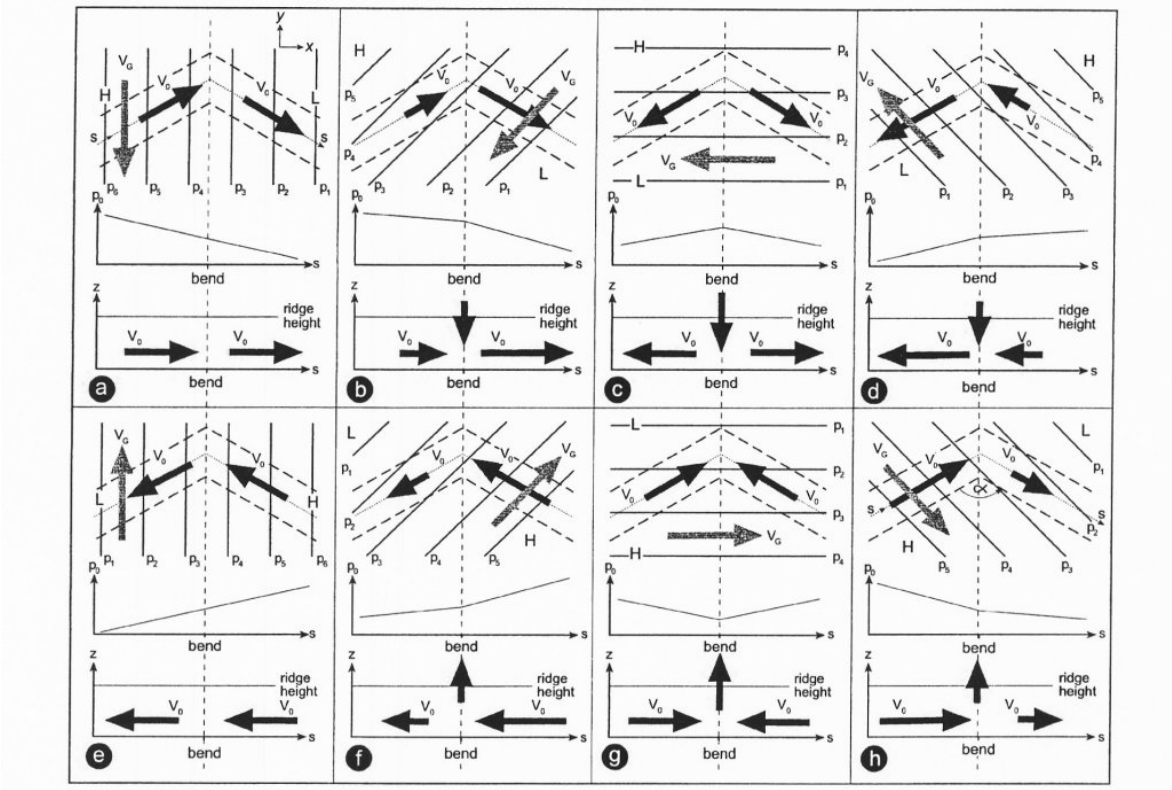

Figure 1.4: Plan and cross-section representations of pressure-driven channeling in a bent valley from Kossman and Sturman (2003; originally Fig. 3). Here, the angle formed by the valley bend (α) is 120°, with geostrophic wind directions from (a) north, (b) northeast, (c) east, (d) southeast, (e) south, (f) southwest, (g) west, (h) northwest; *s* indicates the along-valley direction. For Mohawk-Hudson convergence, α equals approximately 100°, and schematic (h) most closely represents the attendant synoptic conditions.

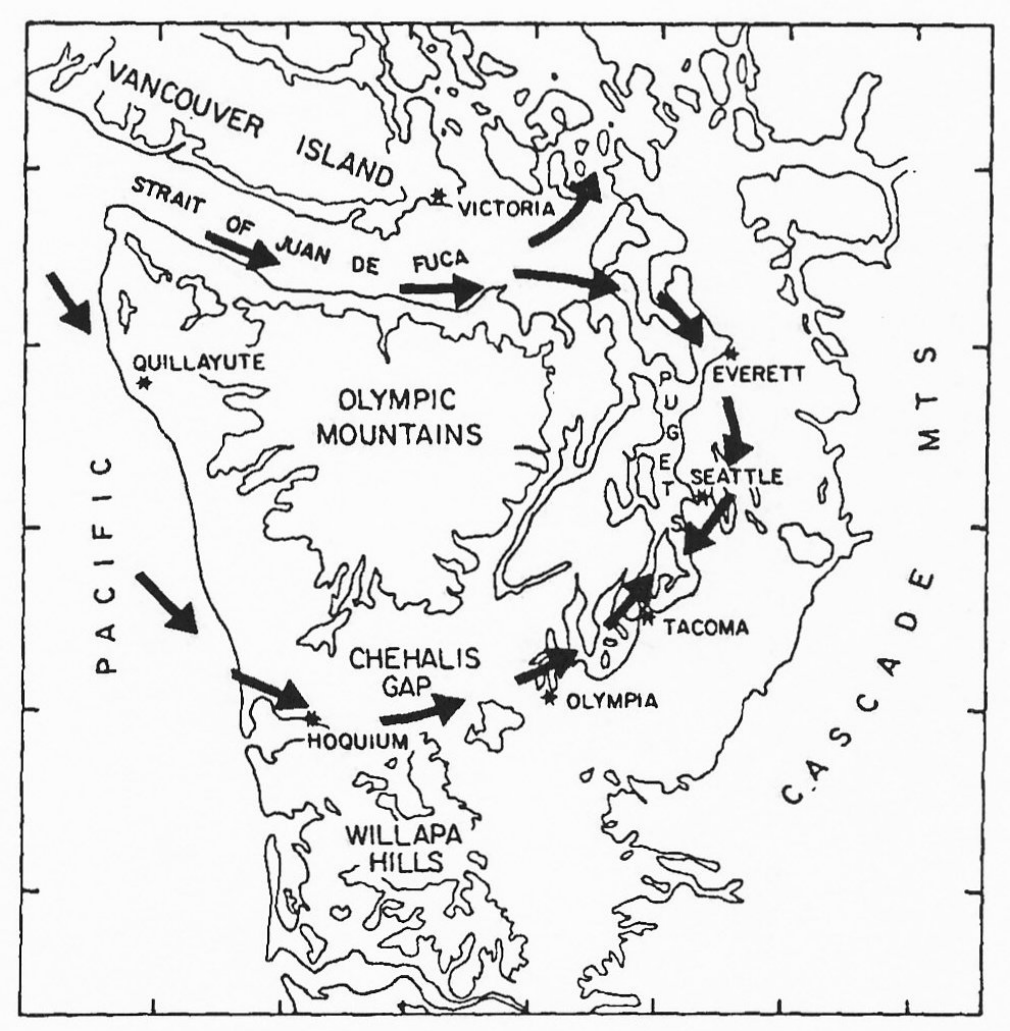

Figure 1.5: Major cities and geographical features of western Washington State. Thin, solid lines indicate elevation, every 300 m. The arrows represent typical surface winds during a Puget Sound convergence event. (Source: Fig. 2 from Mass 1981).

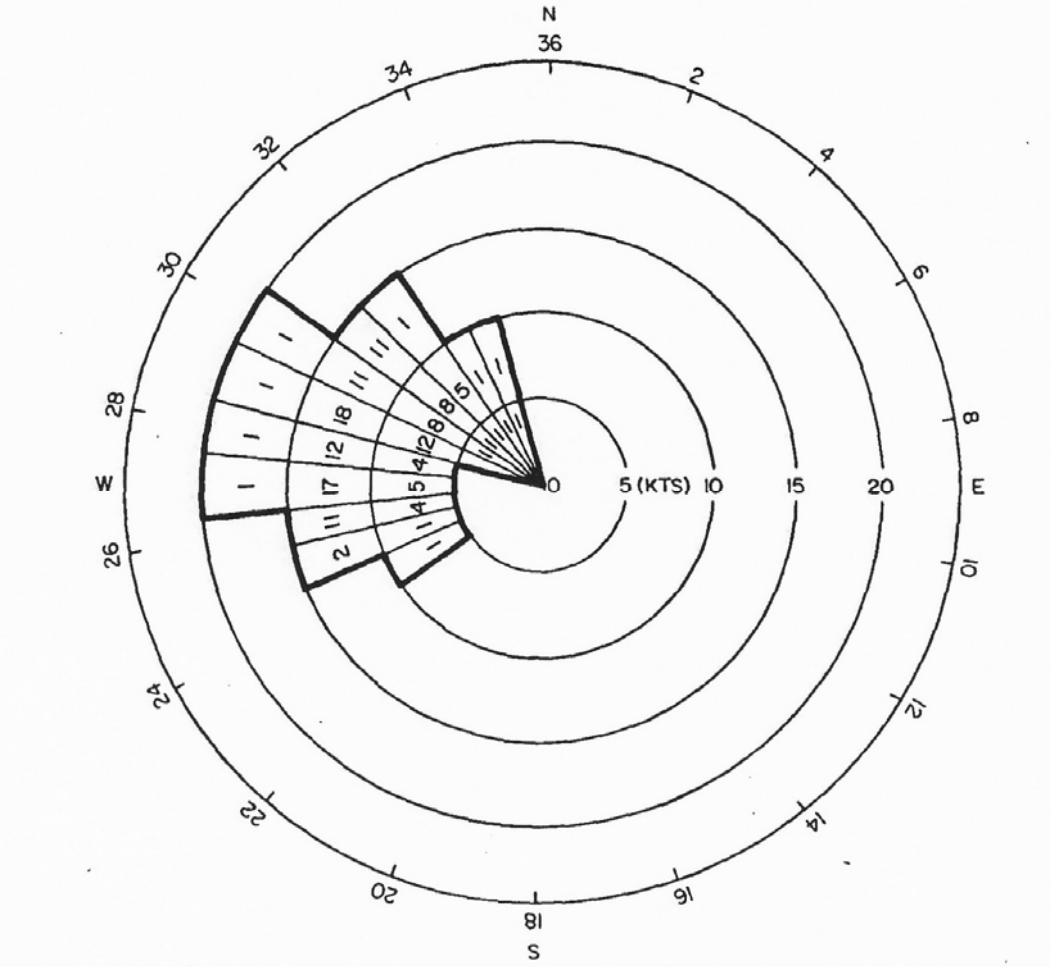

Figure 1.6: Polar representation of the surface wind speed and direction at Hoquium, Washington (KHQM), during 10 Puget Sound convergence events. (Source: Fig. 4 from Mass 1981).

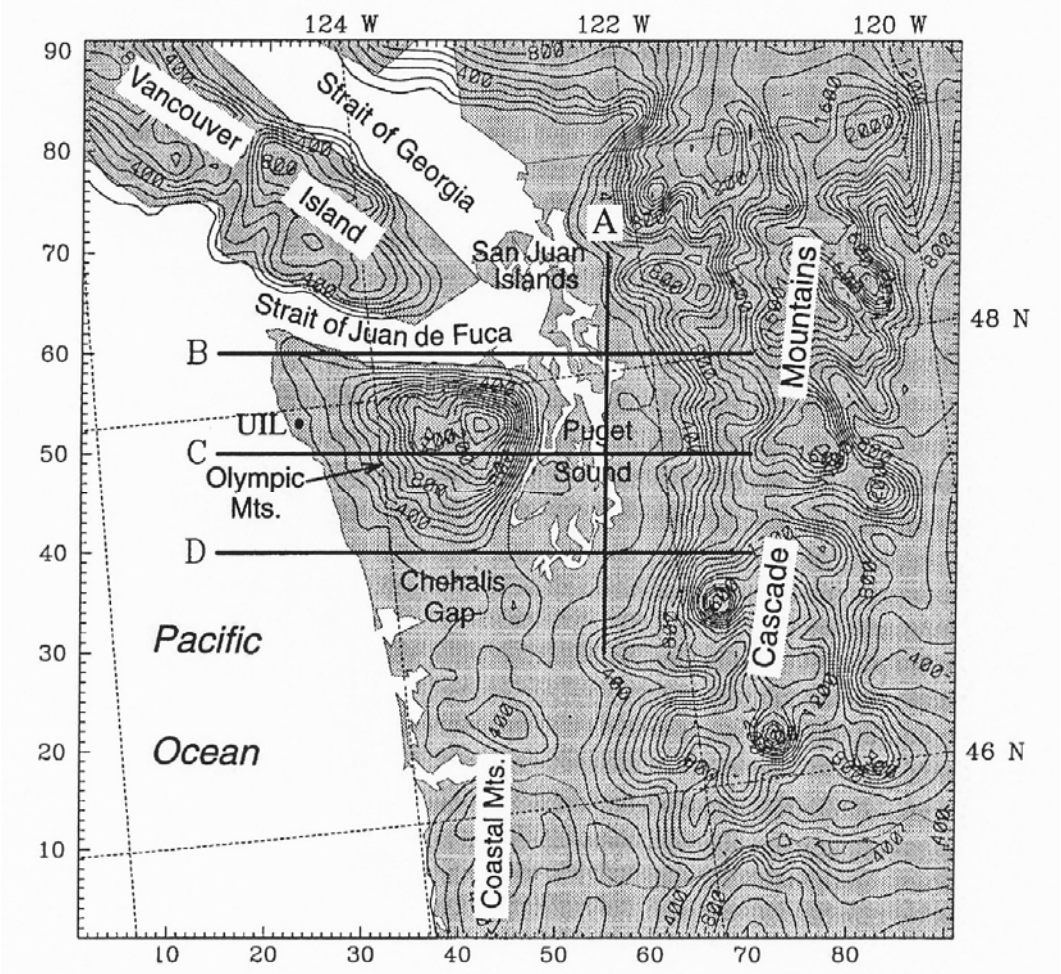

Figure 1.7: Terrain height (contour interval of 100 m) for the control experiment using a PSU–NCAR MM5 model simulation. The heavy black lines (labeled A–D) indicate the position of cross sections that are referenced in section 1.2.2.1. (Source: Fig. 1 from Chien and Mass 1997.

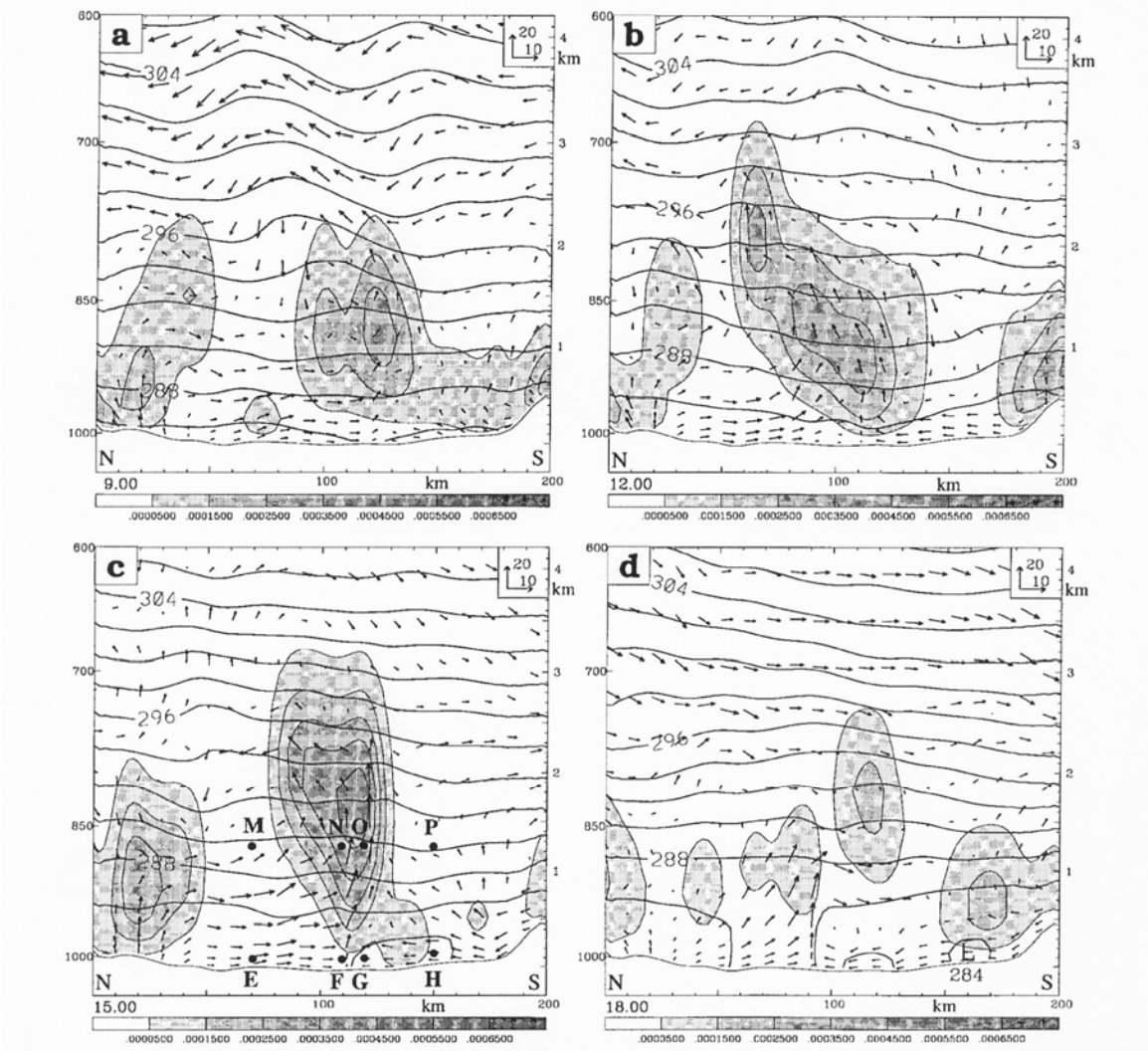

Figure 1.8: North–south cross sections along line A in Fig. 1.7 at (a) 0900, (b) 1200, (c) 1500, and (d) 1800 UTC 26 May 1992 for the control simulation. Thick solid lines are isentropes at a 2-K interval. Wind vectors represent flow within the cross section. Wind vector scales are shown at the upper-right corner of each plot (horizontal wind, m s^{-1}; vertical velocity, μb s^{-1}). Shaded areas denote cloud water mixing ratio. (Source: Fig. 6 from Chien and Mass 1997).

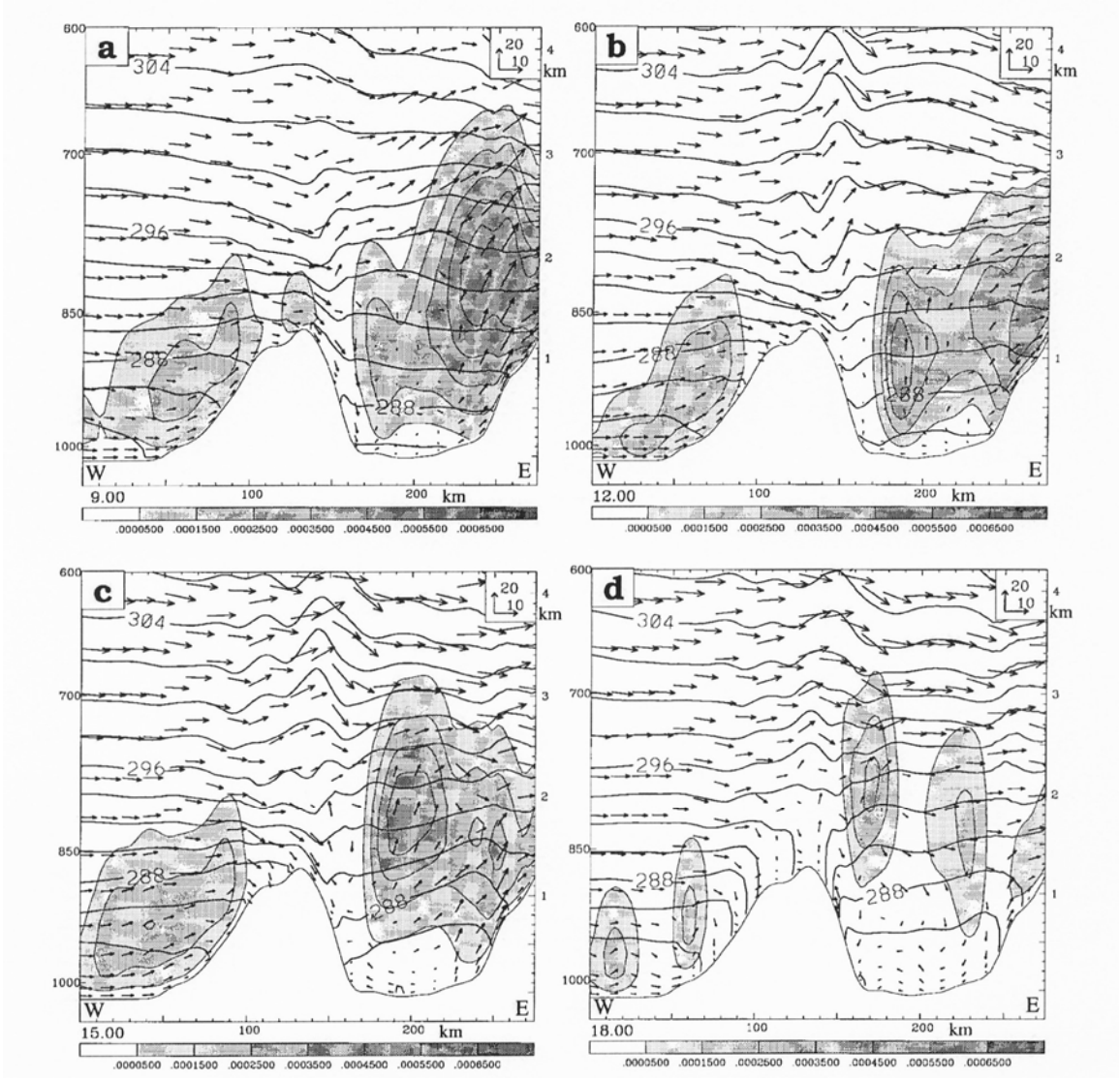

Figure 1.9: West–east cross sections along line C in Fig. 1.7 at (a) 0900, (b) 1200, (c) 1500, and (d) 1800 UTC 26 May 1992. Presented fields and contour conventions are the same as for Fig. 1.8. (Source: Fig. 7 from Chien and Mass 1997).

Month	Number of CZ events	Number of predicted CZ events	Number of correct predictions
January	0	3	0
February	2	3	2
April	9	11	9
May	12	13	11
Total	23	30	22

Figure 1.10: Results of an experiment to determine the feasibility of forecasting [Puget Sound] convergence zone (CZ) events. (Source: Table 1 from Mass 1981).

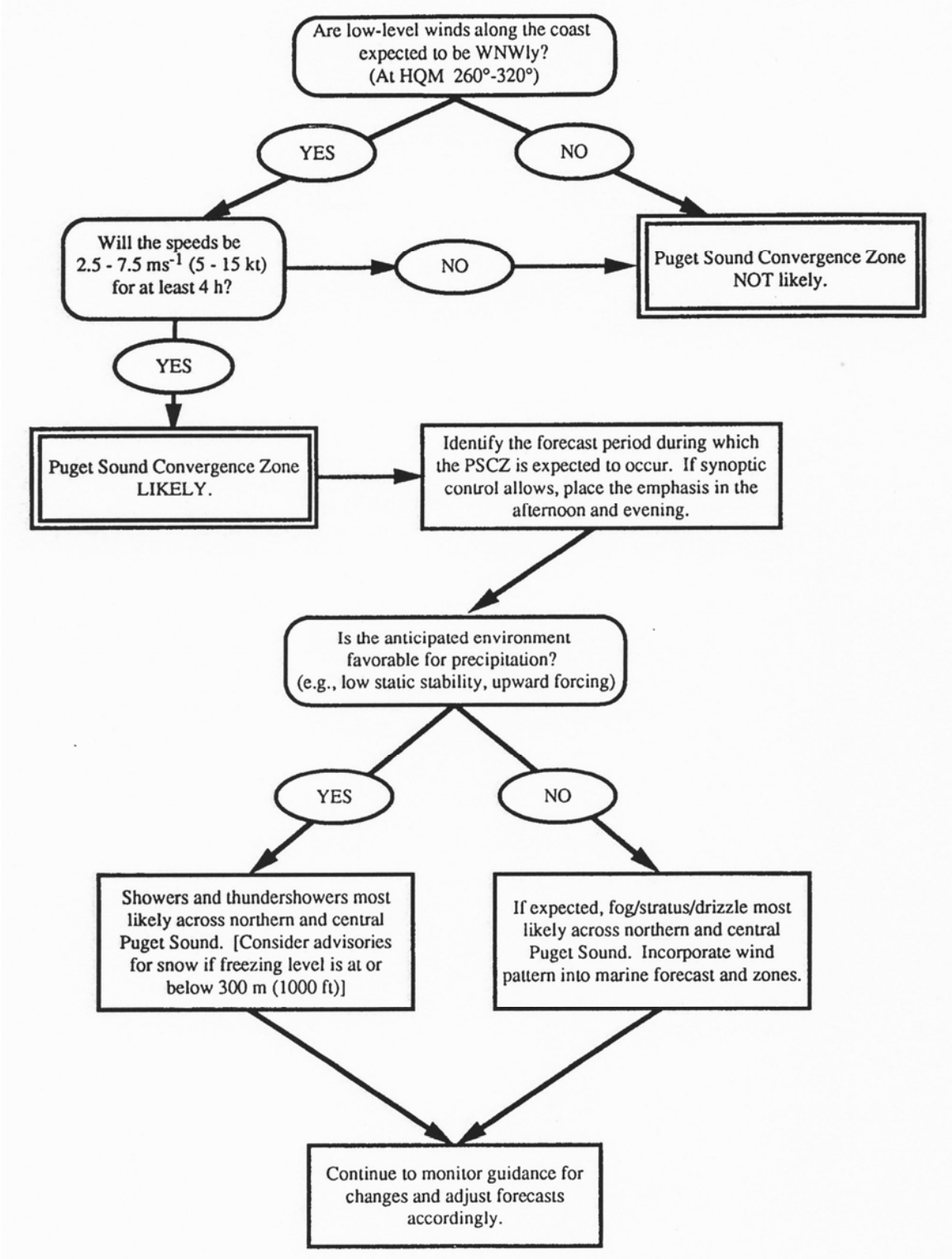

Figure 1.11: Decision tree for forecasting the Puget Sound convergence (PSCZ). (Source: Fig. 2 from Whitney et al. 1993).

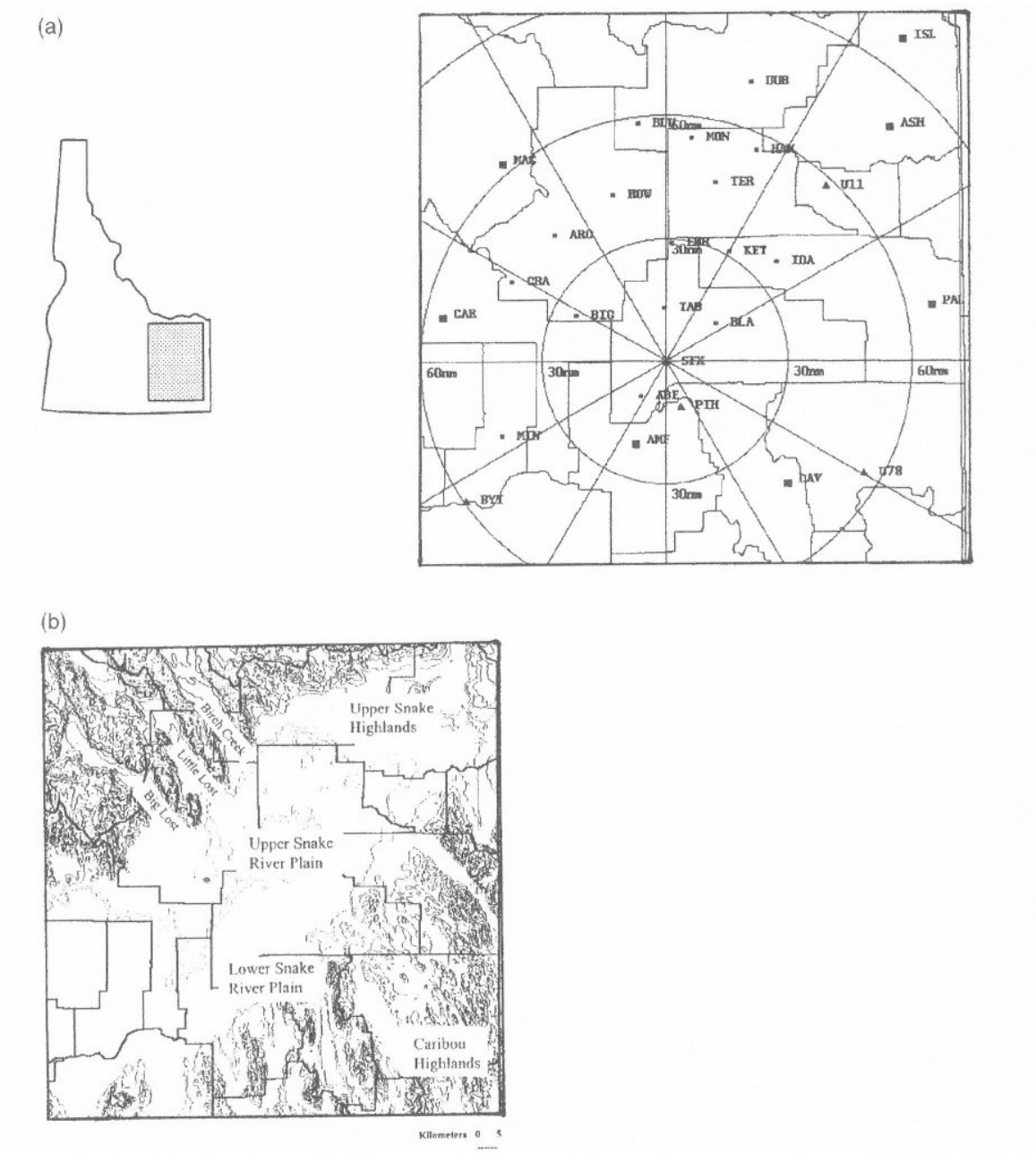

Figure 1.12: (a) Important political features of eastern Idaho, showing the location of mesonet sites (small squares), NWS METAR stations (triangles), city locations (large squares), the Springfield, ID (SFX), Weather Surveillance Radar–1988 Doppler (WSR-88D) (diamond) and range rings (nautical miles). (b) Topographic map of eastern Idaho and geographical references. (Source: Fig. 1 from Andretta and Hazen 1998).

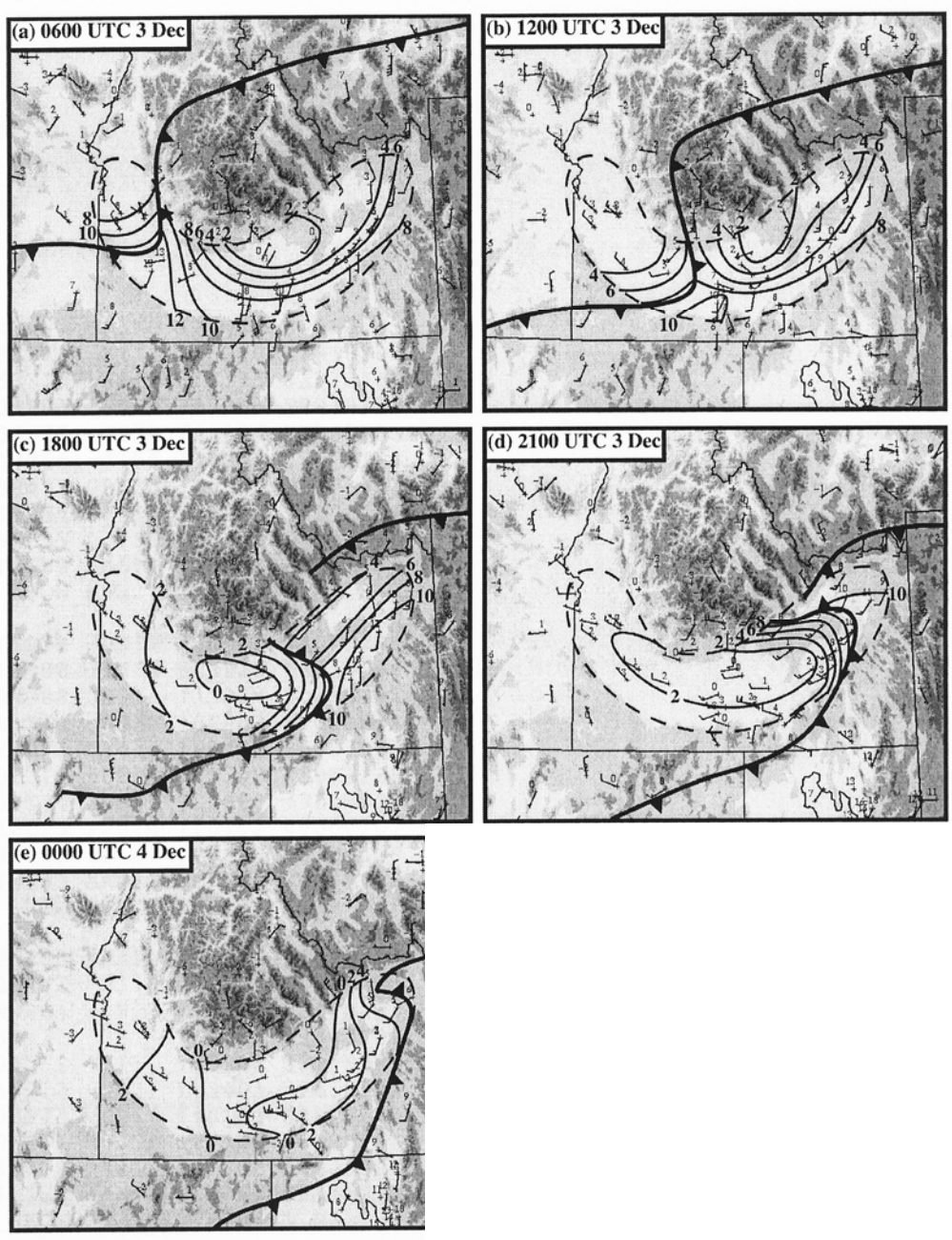

Figure 1.13: Mesoscale frontal analyses (conventional frontal symbols) and low-level isotherms (every 2°C) within the region identified by a dashed line (the Snake River Plain of Idaho) at (a) 0600 UTC 3 Dec, (b) 1200 UTC 3 Dec, (c) 1800 UTC 3 Dec, (d) 2100 UTC 3 Dec, and (e) 0000 UTC 4 Dec 1988. Station plots of wind (full and half barb denote 5 and 2.5 m s^{-1}, respectively) and temperature (°C, upper left). Shading corresponds to terrain. (Source: Fig. 7 from Steenburgh and Blazek 2001).

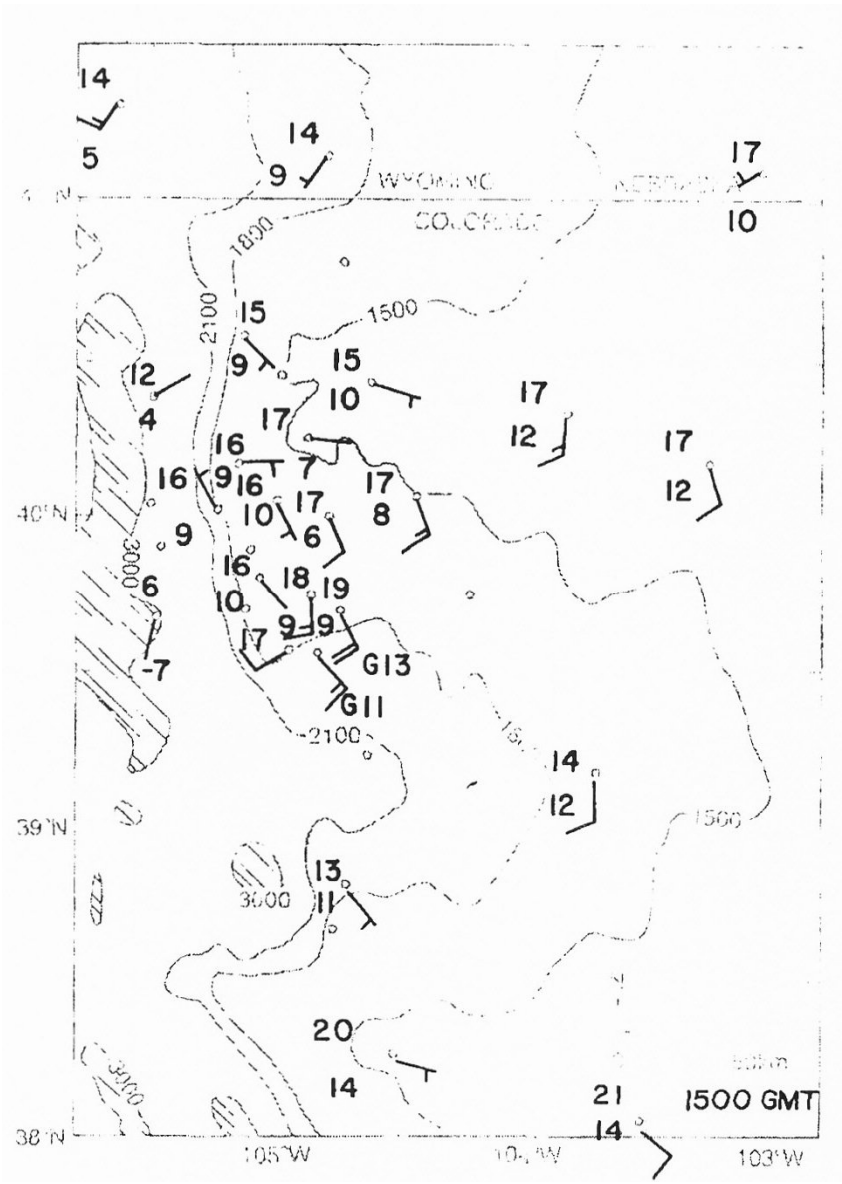

Figure 1.14: Surface plot at 1500 UTC 3 June 1981 of winds associated with the Denver convergence–vorticity zone. Temperature and dewpoint are in °C, full wind barb is 5 m s^{-1}, and G indicates gust speeds in m s^{-1}. Map background shows contours (m) of elevation (hatched above 3000 m). (Source: Fig. 7 from Szoke et al. 1984).

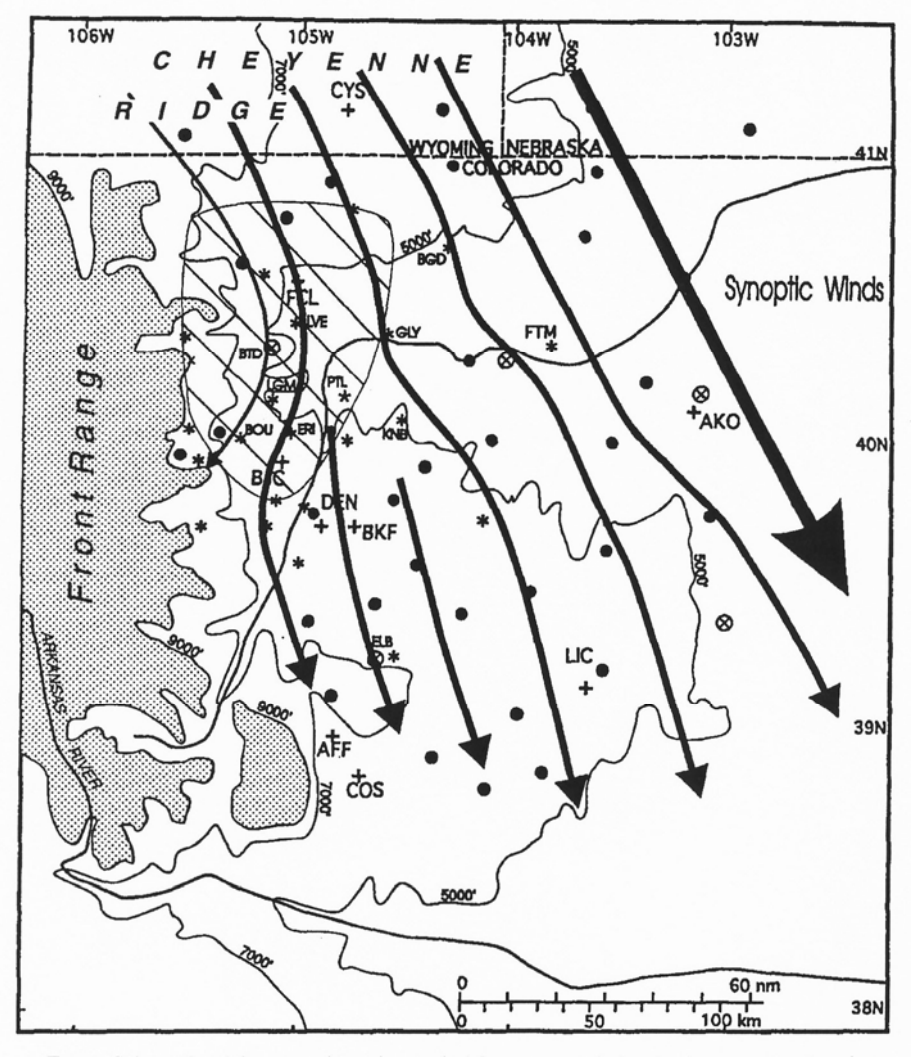

Figure 1.15: Schematic of the general low-level wind flow present during the Longmont anticyclone (LA) event of 16 January 1991. Solid contours indicate elevation, and shading indicates elevations above 2.75 km. Hatching indicates the region of anticyclonic turning and convergence. Several observation sites are labeled with their three-letter identifiers, including CYS: Cheyenne; FCL: Fort Collins; DEN: Denver; COS: Colorado Springs; LIC: Limon; BOU: Boulder; LGM: Longmont. (Source: Fig. 1 from Wesley et al. 1995).

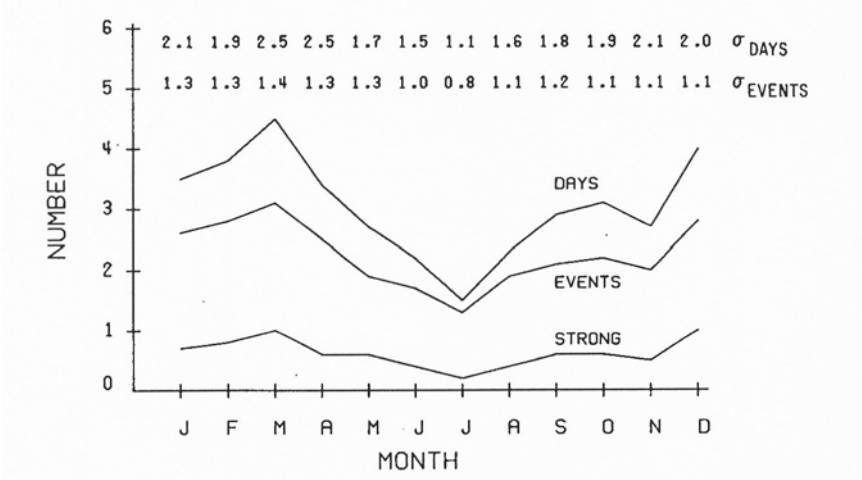

Figure 1.16: A monthly cold-air damming climatology for the eastern Appalachian Mountains spanning 50 years of data. The mean number of actual events is shown by the middle curve. The mean number of days per month in which the eastern Appalachian region is under the influence of damming episodes is shown by the top curve. The mean monthly number of strong damming events is shown by the bottom curve. The bottom (top) horizontal set of numbers above the climatology curves indicates the monthly standard deviation of the number of damming events (the number of days in which eastern Appalachian region is under the influence of damming episodes). (Source: Fig. 3 from Bell and Bosart 1988).

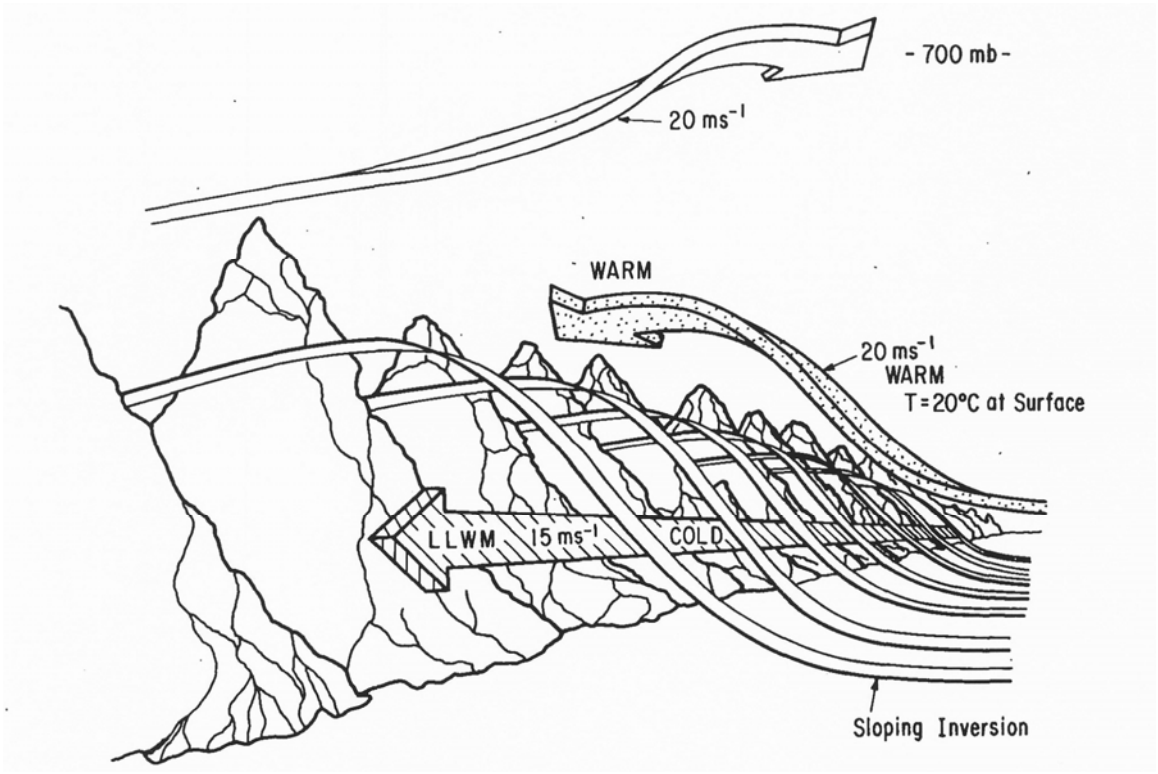

Figure 1.17: Conceptual model of cold-air damming (CAD) as it existed at 1200 UTC 22 March 1985. Note the strong low-level wind maximum (LLWM) within the cold dome, the easterly (or southeasterly) flow just above the cold dome associated with strong warm advection into the warm air above the dome, the sloping inversion of the cold dome top, and the southerly and southwesterly winds above 700 hPa associated with the advancing short-wave trough west of the Appalachian Mountains. (Source: Fig. 22 from Bell and Bosart 1988).

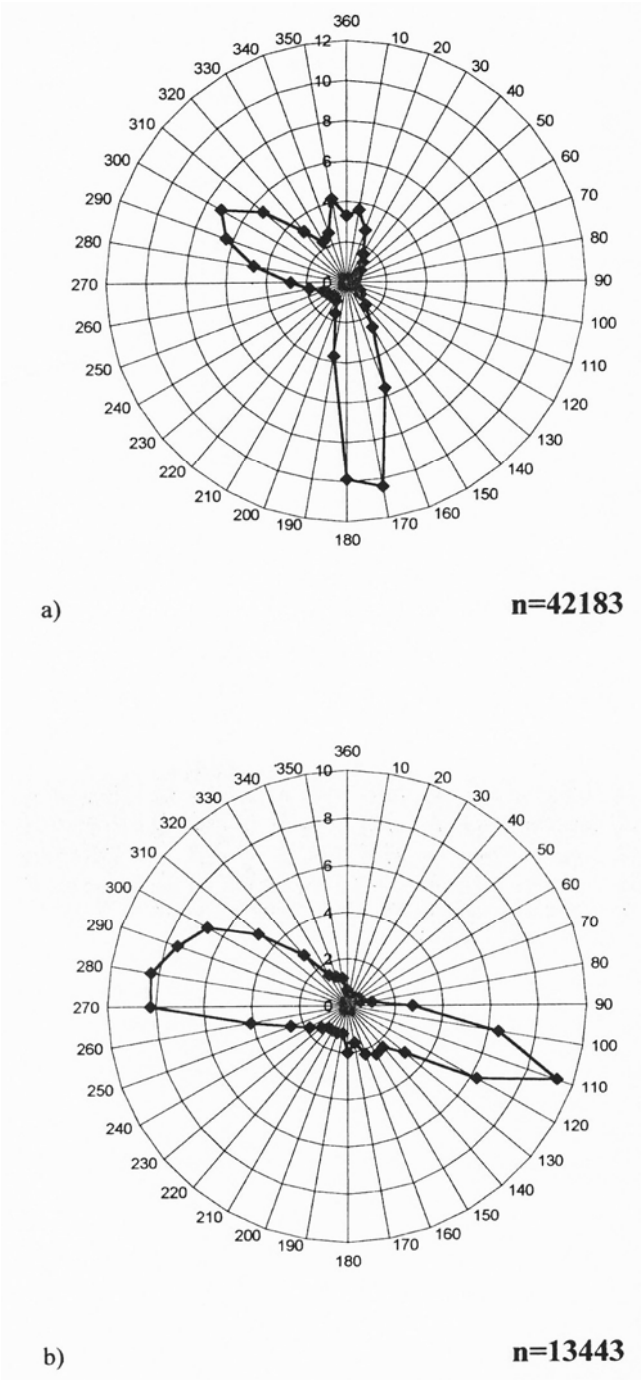

Figure 1.18: Surface wind roses for (a) ALB and (b) UCA for March 1993–March 1997 and July 1995–May 1997, respectively. Azimuthal axis represents wind direction (°), and radial axis represents wind speed (m s^{-1}). (Source: Fig. 4 from Wasula et al. 2002).

2. Data and Methodology

2.1 Data Sources

The main dataset used to construct a broad overview of synoptic-scale weather features present during each case study is from the gridded 1.0° National Centers for Environmental Prediction (NCEP) Global Forecast System (GFS) initialized analyses. Vertical motion and temperature advection profiles are derived from the three-hourly initialized analyses of the 32 km NCEP North American Regional Reanalysis (NARR; Mesinger et al. 2006). These data were chosen in favor of the greater spatial, temporal, and vertical resolutions they provide (as compared to GFS data), in an effort to better capture the subtle synoptic and mesoscale features associated with MHC.

Standard radiosonde data were obtained from the archives of the University at Albany Department of Earth and Atmospheric Sciences (DEAS) and from the archives of Ohio State University. Zero-hour gridded, initialized 1.0° NCEP GFS analyses were used to compensate for missing radiosonde data during the December 2002 case study. Time–height wind profile data for Schenectady, NY, were obtained from the National Oceanic and Atmospheric Administration (NOAA) National Profiler Network (NPN) archive [http://www.profiler.noaa.gov/].

Standard regional surface data, comprising observations from Automated Surface Observing System (ASOS) sites, and buoy and ship observations, were retrieved from the archives of the University at Albany DEAS. In the few instances where hourly surface observation data were missing from this data set (e.g., on 28 November 2002, 17 December 2002, and 24 January 2003), supplementary data were obtained from the

Historical Weather Data Archives of the National Severe Storms Laboratory (NSSL) in Norman, Oklahoma [http://data.nssl.noaa.gov].

Satellite imagery was obtained from the Comprehensive Large Array-data Stewardship System (CLASS) at NOAA [http://www.class.noaa.gov/]. The 2-km composite NOWrad radar imagery [marketed by Weather Services International Corporation (WSI)] was obtained from the archives of the Mesoscale and Microscale Meteorology (MMM) Division of the National Center for Atmospheric Research (NCAR) [http://locust.mmm.ucar.edu/imagearchive1/WSI/]. Imagery from the East Berne, NY (KENX), Weather Surveillance Radar-1988 Doppler (WSR-88D) was obtained from the National Climatic Data Center (NCDC) archive [http://hurricane.ncdc.noaa.gov/pls/plhas/has.dsselect].

Public forecasts and area forecast discussions for the November 2002 MHC event, issued by the Albany office (KALY) of the National Weather Service (NWS), were retrieved from the archives of the University at Albany DEAS. Context for the overall societal impact of the November 2002 MHC event was provided through a storm summary compiled by the meteorologists at television station WRGB-TV, located in Schenectady, NY, which is available online [http://www.cbs6albany.com/sections/weather/historical/daily/]. Monthly climatological precipitable water values for the Albany, NY, area were obtained from the website of the Rapid City, South Dakota, NWS Forecast Office [http://www.crh.noaa.gov/unr/?n=pw]. Topographic maps of the MHC domain and surrounding areas were generated using graphical information systems (GIS) data obtained through the Environmental Systems

Research Institute, Incorporated (ESRI) Geography Network [http://geographynetwork.com/].

2.2 Methodology

As no published research regarding MHC exists, case studies of the phenomenon were conducted. A thorough synoptic and mesoscale analysis was completed for six cases, spanning November 2002 to January 2007. A more cursory analysis of a seventh case (January 2008), which occurred while this thesis was being written, is included for completeness.

Each case was investigated to determine whether synoptic-scale forcing mechanisms were responsible for generating convergence episodes. The parameters examined include frontal forcing, static stability, jet streak dynamics, temperature advection in the lower troposphere, advection of 500 hPa geostrophic absolute vorticity, and advection of 700 hPa relative vorticity by the thermal wind over the 1000–500 hPa layer. Describing, to the first order, the quasi-geostrophic forcing for vertical motion in a synoptic scale system,

$$-\vec{V}_T \bullet \nabla \zeta_{700} \qquad (2.1)$$

denotes the advection of 700 hPa relative vorticity by the thermal wind, where ζ_{700} is the geostrophic relative vorticity. The thermal wind is calculated by subtracting the lower-level (1000-hPa) geostrophic wind from the upper-level (500-hPa) geostrophic wind

$$\vec{V}_T = \vec{V}_{500} - \vec{V}_{1000}, \qquad (2.2)$$

and the definition of geostrophic relative vorticity in the 700 hPa layer is standard, given by

$$\zeta_{700} = \frac{g}{f}\nabla^2 Z_{700}, \qquad (2.3)$$

where Z_{700} represents the geopotential height field at 700 hPa.

An analysis of surface wind direction and SLP was also conducted across the six cases for several sites including Albany, NY (KALB), Glens Falls, NY (KGFL), Utica, NY (KUCA), and Syracuse, NY (KSYR). Surface wind observations, collected hourly while MHC-related precipitation was ongoing, were aggregated and plotted on wind roses, creating a climatology of surface wind direction at each station during MHC events. SLP differences between pairs of stations were also plotted on X–Y plots (scatterplots) in an effort to determine what role pressure-gradient magnitude may play in MHC formation.

3. Results

The results section of this thesis is arranged in three main subsections. Section 3.1 presents the statistical results of composite surface wind and SLP pressure data from the original six case studies (see Table II). Section 3.2 individually highlights and introduces the synoptic and mesoscale configuration of the six original case studies, as well as the seventh, late-addition case study of 2 January 2008. A summary of all seven case studies is presented in section 3.3.

3.1 Statistical Results

3.1.1 Wind Climatology During MHC Events

Hourly observations of surface wind direction were culled from the ASOS sites located in Glens Falls, NY (KGFL), Utica, NY (KUCA), and Albany, NY (KALB), in order to determine the prevailing wind direction at these sites during MHC events (see Fig. 1.2). These sites were used for five of the original six case studies (see Table II for case study dates). By January 2007, however, the ASOS at KUCA had been decommissioned by NOAA and its designated replacement site in Rome, NY (KRME), was not yet fully operational. So, while data from KRME would be an ideal replacement for data from KUCA, winds collected for analysis from the 29 January 2007 case made use instead of KSYR as the westernmost observation point. The wind directions from KUCA and KSYR were aggregated and treated as having come from the same station, as the two stations are both located within the Mohawk River valley and surrounded by similar topography (Fig. 1.2). Thus, wind directions upstream at KSYR are expected to be representative of those at KUCA.

Only observations that were taken during an "ongoing" MHC event were included in the wind climatology, and therefore this climatology is not representative of antecedent conditions. An hourly observation was classified to have occurred during an ongoing MHC event if:

(a) Radar echoes of at least 5 dBZ (KENX, base reflectivity, 0.5° beam elevation) were present near the intersection of the Mohawk and Hudson River valleys at the time of the observation
(b) The echoes did not originate over Lake Ontario, and therefore were not attributable to lake effects
(c) The echoes were discrete and unconnected to any larger area of synoptically forced precipitation

Or, alternatively (and, as will be shown later, less frequently)

(d) A marked enhancement of preexisting radar echoes was observed as the echoes passed through the area where the Mohawk and Hudson River valleys intersect

Hourly reports from the original six case studies which met these criteria were grouped by wind direction, into 10° bins, and counted (see Table III). The total number of reports in each 10° bin was then plotted, according to observation site, onto wind roses, where the azimuthal axis represents wind direction in degrees and the radial axis represents the number of hourly occurrences. A description of the resulting three wind roses follows,

with a comprehensive analysis of wind direction at KALB thereafter, categorized by the time the observation was made relative to the onset of MHC.

3.1.1.1 Wind Climatology at KGFL During MHC Events

Figure 3.1a shows the number of hourly wind reports at KGFL from each direction during ongoing MHC events, while Fig. 3.1b relates each report value to the total number of wind reports at KGFL during ongoing MHC events (a number which varies slightly from station to station, owing to several missing hourly observations which could not be recovered). Figure 3.1a shows a prevailing northeasterly wind direction during MHC events at KGFL. The maximum number of reports from any one bin is seven (from 050°), with 52% of wind reports coming from 040°–070°. A much weaker secondary signal, from the northwest, is also seen, with 16% of wind reports falling between 310° and 340°. It is interesting to note that, while not included in the totals or percentages shown in Figs. 3.1a,b, calm wind reports KGFL numbered six during MHC events, equaling the second-greatest number of reports for any one bin. Calm surface winds were also reported by Chien and Mass (1997) during the 26 May 1992 PSCZ event, and also by Wesley et al. (1995) during the LA event which occurred on 16 January 1991.

3.1.1.2 Wind Climatology at KUCA/KSYR During MHC Events

A strong single-mode surface wind direction signature also exists at KUCA/KSYR. Figure 3.2a shows a sharp maximum at 290° in number of occurrences (11 out of 45 total; see Table III). This one-bin maximum accounts for 24% of all

reports, with 59% of all reports coming from 270°–300° (Fig. 3.2b). This range of wind directions corresponds well with the axis of the Mohawk River valley (see Fig. 1.2). The next-largest grouping of reports is from 320°–350°, with 30% of all reports falling in this range.

3.1.1.3 Wind Climatology at KALB During MHC Events

Differing from the surface wind signatures at KGFL and KUCA/KSYR, the wind direction at KALB during MHC events is shown in Fig. 3.3a to be strongly bimodal. Seven reports, the maximum number in any one bin for KALB, are seen from 020° and 030°, and also from 310°. Figure 3.3b shows that winds from 000°–030° and from 300°–330° account for an overwhelming majority of reports (85%), with winds from the north to north-northeast occurring preferentially over winds from the west-northwest (47% to 38%, respectively). This finding is consistent with the geography that surrounds the observation site, situated at the intersection of the Mohawk valley, which opens to the west-northwest of KALB, and the Hudson valley, which opens to the north (see Fig. 1.2). This finding is also consistent the results of Wasula et al. (2002), who found prevailing wind directions of north, south, and west-northwest at KALB during severe weather events.

3.1.1.4 Wind Climatology at KALB Classified By Relative Observation Time

To determine if either wind mode tends to occur at a particular time relative to the onset of MHC (e.g., whether west-northwest winds occur as the event winds down and as high pressure builds in), each of the 46 hourly surface wind observations taken at KALB

was grouped into three time periods—"beginning," "middle," and "end." Table II contains the starting and ending times for each classification for each case study. These observation-time classifications were made based on radar presentation at the time of the report, and are inherently subjective in nature. While there are likely slight inconsistencies in how individual observations were classified, the aim is simply to generalize how winds evolve during MHC events in a qualitative sense.

3.1.1.4.1 Wind Direction at the "Beginning" of MHC Events

Observations made concurrently with the first appearance of MHC-related precipitation on radar were assigned to the "beginning" classification. Generally, this time period is characterized by a small, discrete area of echoes visible on radar (often in clear-air mode) or, alternately, the first discernable signs of enhanced radar reflectivity as preexisting echoes approach KALB.

Ten such time periods were identified, with wind directions ranging across 90° and reports from the northwest, north, and northeast (see Fig. 3.4a). The highest number of reports from any one bin is 3, from 000°, with 2 reports from 030° (see Table IV). Given the small sample size, a definitive signal is difficult to find, however the reports do skew towards the north and northeasterly directions.

3.1.1.4.2 Wind Direction at the "Middle" of MHC Events

The "middle" classification is characterized by the presence on radar of widespread, discrete echoes, which may fluctuate in intensity. Twenty-five wind

observations were made during the middle of an ongoing MHC event. A stronger bimodal wind direction signature appears during this time period, as shown in Fig. 3.4b. A peak of five wind reports occurs from both 030° and 310°, showing equal preference for north-northeast winds and west-northwest winds at this time. This bimodal nature to the winds may reflect the position of the boundary representing the two low-level flows, e.g., north or south of KALB.

3.1.1.4.3 Wind Direction at the "End" of MHC Events

Observations designated as having been taken at the "end" of an MHC event occur concurrent with a marked decrease in precipitation coverage and intensity (as visible on radar), followed within several hours by the end of MHC-induced precipitation altogether. Precipitation may still be continuing in the area, but it has become clear that its origins are not related to MHC.

Eleven such observations were identified, with wind directions ranging across 120° and reports from the west-northwest, northwest, north and north-northeast (see Fig. 3.4c). As with the "beginning" classification, no dominant wind direction signal is present, but reports are slightly skewed towards the northwest.

It should be noted that at no time during these case studies were winds observed from 90°–270°, going through 180°.

3.1.2 Pressure Differences During MHC Events

Calculations of SLP difference were made between several pairs of observation sites in order to examine the effects that pressure gradient has on MHC. Using the same

hourly ASOS observations employed to develop the wind climatology for ongoing MHC events (see section 3.1.1 for results, and Fig. 1.2 for locations of ASOS sites superimposed on terrain), SLP from KGFL and KPOU (KUCA and KPSF; later KSYR and KPSF) were differenced to determine the pressure gradient from north to south (west to east) across the domain. These pairs of stations were chosen because of the reliability of their reports, their location on the perimeter of the MHC domain, and their nearly-equal spacing (straight-line distance from KUCA to KPSF is 189 km; from KGFL to KPOU is 192 km; KSYR to KPSF is 242 km).

West-to-east SLP differences were plotted against north-to-south differences on X-Y (scatterplot) graphs, one for the case studies which utilize KUCA as the westernmost observation point and one for the case study which utilizes KSYR as the westernmost observation point. A description of these graphs follows, including an examination of SLP difference as a function of observation time relative to the onset of MHC.

3.1.2.1 Pressure Differences During MHC Events, Using KUCA

Figures 3.5a–d compare SLP differences for case studies spanning November 2002–March 2006, inclusive, with KUCA as the westernmost observation point. Irrespective of when the observation was taken, relative to the onset of MHC, Fig. 3.5a shows all north-to-south pressure differences were between 1 hPa and 5 hPa. Similarly, all west-to-east pressure differences were between 4 hPa and 7 hPa, irrespective of observational time. Furthermore, in nearly all cases the west-to-east pressure difference (and, it follows, the pressure gradient) is greater than that in the north-to-south direction;

however no calculable ratio of these two pressure differences (or gradients) exists as a threshold value for MHC formation.

In Fig. 3.5b only pressure-difference pairs observed at the "beginning" of MHC events are considered (for a definition of "beginning" as it relates to this research, see section 3.1.1.4.1). A linear regression (solid line) of west-to-east versus north-to-south pressure differences reveals no strong correlation. It is noted, however, that all north-to-south pressure differences were greater than 2 hPa.

Figure 3.5d shows only those pressure-difference pairs attributed to the "end" of MHC events. Again, a linear regression shows no strong correlation between west-to-east pressure differences and those from north-to-south. All but one pressure difference in the north-to-south direction, however, was below 2.5 hPa, suggesting that the pressure gradient along the Hudson valley tends to be higher at the "beginning" of MHC events, as compared to the "end." A comparable signal is not present in the west-to-east direction.

The worst-fitting linear regression between pressure-difference pairs appears during the "middle" of MHC events, as shown in Fig. 3.5c, where the actual values are distributed randomly.

3.1.2.2 Pressure Differences During MHC Events, Using KSYR

The cessation of hourly observations at KUCA required that KSYR be substituted as the westernmost observation point in the MHC domain for the January 2007 case study. The small sample size of the resulting SLP difference calculations prevents a meaningful pressure gradient analysis along the Mohawk valley; however, it is useful to

note that the north-to-south pressure differences fell within the 1 hPa to 4 hPa parameters developed from previous case studies (see Fig. 3.6).

3.2 Case Studies of MHC Events

In choosing which MHC events to include in this thesis, the overall goal was to select those containing precipitation that was generated entirely by flow channeling within the Mohawk and Hudson River valleys. Situations involving lake effects, upslope flows, and forcing due to the presence of strong synoptic systems were generally ignored, in the interest of researching only those events that were plainly attributable to MHC.

Precipitation produced by MHC generally follows a synoptic-scale storm and, in general, is insignificant in comparison, rarely warranting mention in storm reports or climate summaries. Additionally, a robust archive of historical radar data for the region does not exist prior to the Doppler era. Consequently, it is very difficult to identify historical occurrences of MHC through the perusal of existing data. Thus, a real-time evaluation of potential cases for study was employed for this thesis, but was limited to the period after 1 November 2002. Candidate case studies were initially identified through analysis of KENX radar images. The formation or persistence of "unexplained" radar echoes in the vicinity of KALB was an indicator to examine surface parameters; namely, to look for the presence of surface wind convergence. Events which met these basic criteria were subjected to an in-depth synoptic and mesoscale analysis.

There are, undoubtedly, drawbacks and limitations stemming from the way in which case studies were identified and selected. These include: 1) human error and lack of consistent, around-the-clock vigilance leading to missed MHC events; 2) the exclusion

of events in which the confluent surface wind signature produces no precipitation (so-called "null" cases); 3) the failure to examine all cases in which MHC leads to enhancement of preexisting precipitation, a process which is inherently difficult to identify on radar.

Ultimately six occurrences of MHC were chosen (see Table II), with a seventh added during the writing of this thesis. One of the cases (March 2006) is not a pure MHC event, complicated by a synoptic scale system which was affecting the region, but it was included nevertheless to highlight how MHC can act to enhance preexisting precipitation. Two of the final seven cases (November 2002 and January 2007) are designated as "benchmark" cases because of the strong and persistent MHC signal they reveal, and also because of the large impact they had on the general public. These cases are used as a point of reference by which to compare the remaining five cases.

3.2.1 The Benchmark Case of November 2002

This MHC event occurred on the day prior to Thanksgiving, often the busiest travel day of the year in the United States (U.S.), and provided the original impetus to study this phenomenon. A poor forecast, compounded by inopportune timing, combined to create a high-impact weather event out of very little snowfall.

A fast-moving, moisture-starved surface low pressure system ("Alberta Clipper") brought widespread light-to-moderate snowfall to eastern New York state and western New England during the overnight and pre-dawn hours (local time) of 27 November 2002. The snowfall associated with this low was universally expected by local forecasters to end during the early morning, as detailed in the public "zone" forecast for

the immediate Albany area, released at 0822 UTC on 27 November 2002 by the Albany forecast office of the NWS (KALY):

> "TODAY...SNOW LIKELY EARLY THIS MORNING...THEN CLOUDY WITH A CHANCE OF FLURRIES FROM LATE MORNING ON. NO ACCUMULATION."

A storm summary, written by meteorologists of local television station WRGB-TV (2008) and compiled using a mesoscale network of volunteer observers ("weather watchers"), indicates that approximately 2.5–10.0 cm of snow fell in most areas, due to the Clipper low, "only causing minor inconveniences to morning commuters."

Accumulating snow, however, continued to fall through the afternoon (local time) over a majority of the population centers of eastern New York, and forecast updates came too late for many travelers to adjust their plans accordingly. The NWS forecast was not updated to reflect the presence of a persistent, mesoscale area of MHC-induced precipitation until approximately 1800 UTC, as indicated in the area forecast discussion issued by KALY at 1805 UTC:

> "AN AREA OF LIGHT SNOW HOWERS/FLURRIES HAS FORMED ALONG THE MOHAWK/HUDSON CONVERGENCE ZONE WITH A MOSIT [sic] N/NNW FLOW. WL UPDATE ZONES AND FCST SNOW SHOWERS LIKELY IN THIS REGION WITH UP TO AN INCH OF SNOW POSSIBLE."

Additional snowfall totals from this MHC-induced precipitation ranged from 2.5 to 5.0 cm across the region, as recorded from the weather watchers of WRGB-TV (2008). It was this snowfall that generated scores of minor accidents on the roads of eastern New York, creating a harrowing pre-holiday period for both travelers and forecasters alike.

3.2.1.1 SYNOPTIC SUMMARY

The MHC event of November 2002 formed in the wake of a passing Alberta Clipper low, and Figs. 3.7a–d reveal the evolution of the resultant surface features, with high- (low-) pressure centers labeled by a blue "H" (red "L"). At 0600 UTC 27 November (time and date hereafter denoted as 0600/27) a broad area of high pressure extended from the southern shores of Hudson Bay into the midwestern U.S., and a broad area of low pressure was located from the Canadian Maritime provinces southward along and just off the U.S. East Coast (Fig. 3.7a). Also at that time a west-to-east zone of lower pressure ("inverted trough") extended from the Delmarva Peninsula to southeastern lower Michigan, while a zonally oriented ridge of high pressure ran from central Maine to north of Lake Huron. By 1200/27 (Fig. 3.7b), low pressure off the U.S. eastern seaboard had consolidated, deepening to a 1007-hPa low centered well south of Cape Cod, near 38°N, 71°W. The inverted trough extended northwestward from the low center towards southeastern lower Michigan, crossing northeastern Pennsylvania and into western New York. The high pressure ridge remained located near where it was at 0600/27, and a "reverse-S" shaped SLP pattern over New York and western New England is noted (Fig. 3.7b). As low pressure deepened to 999 hPa and moved northeastward to near 40°N, 65°W by 1800/27, the inverted trough and zonal ridge located over the northeastern U.S. were reflected more weakly compared to 1200/27 (Fig. 3.7c). The orientation of isobars was more meridional, but a slight "reverse-S" shaped curve is still noticeable (Fig. 3.7c). The low pressure system continued to deepen through 0000/28, with a 6-hPa decrease in central pressure in the preceding 6 h, as it accelerated to southeast of Nova Scotia, near 41.5°N, 60.5°W (Fig. 3.7d).

The 850-hPa analysis at 0600/27 (Fig. 3.8a) shows a trough of lower geopotential heights, oriented from northeast-to-southwest, from Maine to the Piedmont of North Carolina, with a cyclonic circulation evident and centered in the vicinity of central Pennsylvania. An attendant zone of enhanced baroclinicity was present, along with weak warm advection, over New York and southern New England. By 1200/27, CAA had begun over eastern New York and western New England though there was little-to-no change in temperatures over the region during the preceding six hours (Fig. 3.8b). The center of cyclonic circulation moved to eastern Long Island as the baroclinic zone and geopotential height trough sharpened, running from south of Nova Scotia to Virginia and North Carolina (Fig. 3.8b). Weak cold advection, driven by 15 m s^{-1} winds, continued over New York and New England, with temperatures falling approximately 3°C (to −12°C) over KALB during the 6 h ending 1800/27 (Fig. 3.8c). The trough and center of circulation continued to move offshore through 1800/27. At 0000/28 (Fig. 3.8d), winds had increased to 15 m s^{-1} in the vicinity of KALB as weak cold advection continued. Also at this time, a closed geopotential height contour had appeared around the center of circulation located southeast of Nova Scotia, which continued to move northeast.

As illustrated by relative humidity (RH) values, the atmosphere at 700 hPa was saturated (with respect to water) over eastern New York and western New England during 0600–1200/27 (Figs. 3.9a,b). At that time, a geopotential height trough was moving from western New York to eastern New York. Moderate ascent of approximately −4.0 to −7.0 μb s^{-1} was present over eastern New York and western New England at 0600/27, and a broad area of weak ascent (−2.0 to −4.0 μb s^{-1}), connected with the developing area of surface low pressure, was located off the mid-Atlantic coast

(Fig. 3.10a). Ascent over the ocean and over central and eastern New England increased to −10.0 to −12.0 μb s^{-1} by 1200/27, and was associated with the deepening surface low located south of Cape Cod (Fig. 3.10b). Also at that time, ascent was weakening over eastern New York and western New England. By 1800/27, as the 700-hPa trough moved east of the region, RH values fell to near 70% over extreme eastern New York and western New England, before falling below 70% at 0000/28 (Figs. 3.9c,d). From 1800/27 to 0000/28 (Figs. 3.10c,d), little or no ascent is diagnosed over eastern New York or western New England, but upward motion does increase dramatically well offshore. Some horizontal advection of cyclonic 700-hPa geostrophic relative vorticity by the 1000–500-hPa thermal wind exists over eastern New York and western New England during 0600–1200/27 (Figs. 3.11a,b), however this advection ends by 1800/27, replaced by neutral or anticyclonic advections from 1800/27 to 0000/28 (Figs. 3.11c, d). The advection of lower 1000–500-hPa thickness values by surface winds implies CAA in the lower and middle troposphere, beginning at 1200/27 and continuing through 0000/28.

At 0600/27 (Fig. 3.12a), a positively tilted 500-hPa geopotential height trough was located over the eastern Great Lakes and western New York, with eastern New York and western New England experiencing advection of cyclonic absolute vorticity (CVA). By 1200/27 (Fig. 3.12b), the trough axis has sharpened a bit and progressed to a line from Montreal, Quebec, to the southern tier (Binghamton area) of New York to southwest Pennsylvania, with advection of anticyclonic absolute vorticity (AVA) just beginning over eastern New York. This AVA continued through 1800/27 (Fig. 3.12c), and by 0000/28 little or no absolute vorticity advection was occurring over eastern New York or western New England (Fig. 3.12d). From 1800/27 to 0000/28, MHC-related precipitation

was occurring in the absence of CVA at 500 hPa. Geopotential heights at 500 hPa increased 2 dam between 1800/27 and 0000/28 over eastern New York and western New England, and a confluent wind signature was evident at that level as well at 0000/28 (Fig. 3.12d).

At 0600/27, the core of a 55 m s^{-1} wind maximum (jet streak) at 300 hPa ran from the Adirondack Park region of upstate New York across southeastern Quebec, placing eastern New York and western New England under rising air in its right-rear quadrant (Fig. 3.13a). This jet streak translated northeastward, to over the Canadian Maritime provinces, by 1200/27, placing eastern New York and western New England under sinking air in its left-rear quadrant (Fig 3.13b). The region remains under the sinking air associated with this jet streak until 0000/28, as a confluent wind signature develops over eastern New York and western New England (Figs. 3.13c,d).

The radar mosaics (NOWrad) for eastern New York and western New England at 0900/27 (Fig. 3.14a) and 1200/27 (Fig. 3.14b) show eastern New York and western New England on the northwestern fringe of a large precipitation shield which runs along the coast of New England southward to New Jersey. Scattered precipitation (snow) associated with lake moisture and lingering upper-air dynamics existed over western New York at these times. Synoptic-scale precipitation had ended across the region by 1500/27 (Fig. 3.14c). The first signs of a discrete area of scattered precipitation echoes appeared at 1800/27 and are highlighted with a red circle on Fig. 3.14d. This precipitation area expands over eastern New York and western New England by 2100/27 (Fig. 3.14e) before contracting by 2345/27 (Fig. 3.14f).

A higher-resolution view of the precipitation is provided by the East Berne, NY (KENX), Weather Surveillance Radar-1988 Doppler (WSR-88D). The departure of the synoptically forced precipitation, from northwest to southeast across eastern New York and western New England is shown on the KENX radar in Figs. 3.15a and 3.15b. By 1400/27 (Fig. 3.15c), only weak radar echoes were left over central Massachusetts and northwest Connecticut. A small area of precipitation (snow flurries) had developed about 45 km west of KALB, over north-central Schoharie county. By 1558/27 (Fig. 3.15d), this small area of precipitation had blossomed into a quasi-linear area of light snow, running approximately parallel to and just of the Hudson River valley. At 1803/27 (Fig. 3.15e), snow had increased both in coverage and intensity across eastern New York, with maximum base reflectivity (0.5° beam tilt) values of 25–28 dBZ centered just northwest of KALB, over Schenectady county. The area of moderate snow persists through 2001/27 (Fig. 3.15f), with some areas of spotty, lighter precipitation developing around it.

3.2.1.2 Mesoscale Summary

Inspection of WSR-88D radar imagery from KENX (see Fig. 3.15) shows that precipitation associated with MHC was near peak intensity and maximum areal coverage across eastern New York at 2001/27. This section will examine the mesoscale weather conditions present in the vicinity of KALB around this time.

Figure 3.16 is a manual surface analysis for eastern New York and much of New England, generated using the 2100/27 ASOS and marine weather reports, which shows a confluent surface wind signature in the vicinity of KALB. Winds KALB at that time

were light from the north-northwest; winds at KUCA were light from the northwest; and light north-northeast winds were reported at KGFL. At the same time, Fig. 3.16 shows northwest winds at a station approximately 60 km to the northeast of KALB (Rutland, Vermont; KRUT), and no other north-northeast wind reports in the region to match those at KGFL. Isobars reveal an inverted surface pressure trough across coastal New England and northeast Pennsylvania, as well as a zonally oriented ridge of high pressure across the Adirondack Mountains of upstate New York. The "reverse-S" isobar pattern seen in Figs. 3.7b,c, is also apparent in Fig. 3.16.

Surface meteograms show confluent surface winds between KUCA and KGFL from 1300 to 2100/27 (Figs. 3.17a,b) and between KUCA and KALB from 1700 to 2000/27 (Fig. 3.17a,c), coincident with reports of moderate snowfall at KALB from 1800 to 2100/27 (Fig. 3.17c).

During the period 1200/27–0000/28, Fig. 3.18 shows that SLP values were higher to the north and west of KALB. The difference in SLP was significantly greater from west-to-east across the region (as seen between KUCA and KPSF in Fig. 3.18) than from north-to-south (KGFL to KPOU) across approximately the same distance. At any given station, SLP values changed relatively little between 1200/27 and 0000/28, with the greatest change during this time period (approximately 3 hPa) occurring at KPOU.

The radiosonde sounding (in skew T–log p format) from Albany, NY (KALY), for 1200/27 (Fig. 3.19a) reveals a saturated layer between the surface and approximately 550 hPa. By 0000/28 (Fig. 3.19b), the top of the moist layer had subsided to approximately 850 hPa, and the height of the temperature inversion had decreased in a similar fashion.

A wind profiler located at Schenectady, NY (KSCH; approximately 15 km northwest of KALB), recorded wind direction and speed in a vertical profile, the data from which are presented with hourly resolution from 1200/27 to 0000/28 in Fig. 3.20. Wind speeds remained at 5 m s^{-1} or less from 950 hPa and below during the period 1300/27–0000/28. The profiler showed a backing wind signature with height, consistent with the horizontal advection of colder air over KSCH. By 2000/27, winds below 950 hPa had decoupled, shown in Fig. 3.20 as the wind direction discontinuity which occurs at approximately that pressure height. The lowest 50 hPa of the atmosphere remained isolated from the atmosphere above through 2100/27. Recoupling of the lower atmosphere to the remainder of the air column above occurred beginning at 2200/27, at which time near-surface northwesterly winds increased.

Zero-hour gridded, initialized data from the NARR were utilized to generate time series plots of horizontal temperature advection over KALB. Figure 3.21 shows CAA was occurring from the bottom to the top of the column at 1800 and 2100/27, and 0000/28. Temperature advection values from 850 hPa and below are modest, with a mean value around $-12°C \times 10^{-5}$ s^{-1}. Vertical velocity values over KALB (also derived from 0-h gridded NARR initializations), are presented in Fig. 3.22. Weak ascent is evident in the lower troposphere at 1800 and 2100/27, with maximum ascent values at 925 hPa of -1.5 μb s^{-1} and -1.0 μb s^{-1}, respectively. Downward motion in the remainder of the atmospheric profile increases both in magnitude and depth between 1800/27 and 0000/28, at which time no upward motion is diagnosed at all (Fig. 3.22).

An infrared image of the northeastern U.S. is presented in Fig. 3.23 from the Geostationary Operational Environmental Satellite-8 (GOES-8) satellite. At 1732/27, the

satellite shows CTTs of approximately −14°C located over KALB. This CTT corresponds to an approximate pressure level of 840 hPa, inferred from the KALY radiosonde soundings from 1200/27 and 0000/28 (see Fig. 3.19).

3.2.2 The Benchmark Case of January 2007

The MHC event of January 2007 began during the nighttime hours (local time) of 28 January 2007, and continued overnight and into the morning hours of 29 January 2007. Its societal impact (on morning drivers), unambiguous synoptic pattern, and its duration make it an ideal benchmark case. It is one of the longer-lived cases included in this thesis (see Table II for dates and times of all included case studies), despite associated snowfall totals that were very light, with only trace–2.5 cm amounts reported in the storm summary provided by WRGB-TV (2008). Nevertheless, this small amount of snow was able to create slippery spots on some roads in eastern New York, causing distress to morning travelers in this area.

3.2.2.1 SYNOPTIC SUMMARY

Precipitation resulting from MHC began as several areas of surface low pressure developed off the U.S. East Coast. Figure 3.24a reveals that an inverted low-pressure trough extended from the southern tier of New York westward to near Minneapolis, Minnesota, prior to the MHC event, at 1200/28. A weak zone of low pressure, as indicated by "baggy" isobars, hinted at the development of a surface low over the Piedmont region of North Carolina. A nearly uniform 1000–500 hPa thickness gradient also existed at that time from the southern shores of Hudson Bay in Canada to coastal

North Carolina. At 1800/28 (Fig. 3.24b), a single, closed isobar had formed around a 999-hPa low, centered several hundred kilometers southeast of Cape Hatteras, North Carolina. The isobars located over New York and New England were arranged in an revere-S shape at this time. Figure 3.24c shows the inverted trough of low pressure pivoting farther south by 0000/29, aligned from southeast Pennsylvania to southeastern lower Michigan, as the low-pressure center located offshore deepened to 993 hPa and moved to near 38°N, 67°W. By 0600/29, this low center had deepened to 988 hPa and was centered at 40°N, 63°W (Fig. 3.24d), the pressure trough located over Pennsylvania had drifted slightly northward at this time, and some weak pressure ridging was oriented along a west-to-east axis over northern New York. Light snow was also detected in the vicinity of KALB on the KENX radar beginning at 0601/29 (Fig. 3.32c), and this precipitation continued through 1203/29 (Fig. 3.32e). As the original ocean low deepened to 987 hPa and moved well southeast of Nova Scotia, a second ocean low, located at approximately 38°N, 67°W, deepened to 988 hPa by 1200/29 (Fig. 3.24e). Slight cyclonic curvature to isobars, which existed over southern New York, indicated that the weak inverted surface trough remained at this time. Weak high pressure had also developed over southern Ontario and Quebec provinces. The second ocean low deepened sharply to 980 hPa by 1800/29 and was centered at 40°N, 60.5°W (Fig. 3.24f). Surface isobars had become more meridional (i.e., "straightened out") over eastern New York and western New England at this time.

The 850-hPa analysis shows that very weak cooling due to CAA occurred over New York from 1200/28 to 0600/29, no more than 3°C during this period (Figs. 3.25a–d). A stronger thermal gradient was located over the Appalachian Mountains, and this

gradient moved slowly offshore during these times, along with areas of increasingly cyclonic circulation. From 0600 to 1200/29, CAA over eastern New York and western New England increased (a temperature change of 5°C over KALB during this period), presumably in response to two areas of offshore geopotential height falls (Figs. 3.25d,e). Winds over eastern New York and western New England, which had been light (around 5 m s^{-1} at previous times), increased to approximately 12.5 m s^{-1} between 0600 and 1200/29 as well (Figs. 3.25d,e).

Beginning at 1200/28 and continuing through 0600/29, weak cyclonic curvature in the 700-hPa geopotential height contours existed over eastern New York and western New England (Figs. 3.26a–d). Small geopotential height falls occurred with the passage of a trough axis from 0000 to 0600/29, with ensuing geopotential height rises from 1200 to 1800/29 (Figs. 3.26e,f). Concurrent with the passage of the height trough, RH values in excess of 70% occurred over eastern New York and western New England (Figs. 3.26c,d), but RH values were below 70% at the other times (3.26a,b,e,f). Model-diagnosed ascent values were −2.0 μb s^{-1} or less over eastern New York and western New England at every time shown in Fig. 3.26. Several areas of moderate to vigorous ascent developed over the western Atlantic Ocean, the first of which was evident south of coastal North Carolina at 1200/28 (Fig. 3.27a), and increased to −20.0 μb s^{-1} as it moved south of Newfoundland by 1200/29 (Figs. 3.28b–e). A second center of strong vertical motion developed from broad areas of weak ascent along the mid-Atlantic coast at 0000/29 (Fig. 3.27c), to an area of ascent greater than −28.0 μb s^{-1} by 1800/29 (Figs. 3.27d–f). This area of upward motion at 700 hPa was collocated with the intense surface low-pressure system centered near 40°N, 60.5°W at this time (Figs. 3.24f, 3.27f).

Horizontal advection of cyclonic 700-hPa geostrophic relative vorticity by the 1000–500-hPa thermal wind was either very weak or neutral during the period from 1200/28 to 0600/29 (Figs. 3.28a–d), with weak anticyclonic vorticity advection over far northern New York from 1200 to 1800/29 (Figs. 3.28e,f).

Neutral or slightly anticyclonic curvature in the 500-hPa geopotential height contours was present over eastern New York and western New England at 1200/28 and 1800/28 as a sharp trough dropped out of the Great Lakes and into the Ohio River valley (Figs. 3.29a–c). The trough dug to the mid-Atlantic seaboard and had acquired a slightly negative tilt by 0600/29 (Fig. 3.29d). At this time, weak CVA was occurring over eastern New York and western New England. By 1200/29 the northern end of the trough axis was situated over KALB, where weak AVA had begun; the southern extent of the trough axis had taken on a negative tilt, extending from the southern New Jersey shore to near 35°N, 70°W (Fig. 3.29e). The trough axis continued to pivot eastward through 1800/29, leaving eastern New York and western New England in northwesterly flow at 500 hPa and with little or no absolute vorticity advection (Fig. 3.29f).

Slight anticyclonic curvature in the 300-hPa geopotential height contours was evident over eastern New York and western New England from 1200 to 1800/28, and this area was also located under the left-rear quadrant of a 55 m s^{-1} jet streak (Figs. 3.30a,b). A 65–75 m s^{-1} jet streak developed over coastal North Carolina by 0000/29 but translated offshore well south of the northeast U.S. by 1200/29 (Figs. 3.29c–e). This configuration of the jet stream left the Northeast under a zone of relatively lighter winds (35–45 m s^{-1}) associated with the northern extent of the trough axis (Figs. 3.30d,e).

NOWrad radar images show that scattered light precipitation developed over eastern New York and western New England between 1800/28 and 0000/29 (Figs. 3.31a, b). This area of precipitation was detached from a larger area of synoptically forced precipitation, which affected the lower Hudson Valley and brushed coastal New England from 0600 to 1500/29 (Figs. 3.31c–e). The discrete area of precipitation over eastern New York and western New England was no longer evident at 1800/29, with lake-effect precipitation apparent in western and central New York (Fig. 3.31f).

The WSR-88D located at KENX showed the last of the synoptically forced precipitation (snow) departing eastern New York by 2300/28 (not shown). By 2359/28 an area of light snow had developed just north and northwest of KGFL (Fig. 3.32a). Through 0601/29 this area of light snow expanded in coverage, with some echoes to 10 dBZ shown in Figs. 3.32b,c. A flare-up of light-to-moderate snow was centered over KALB at 0857/29 (Fig. 3.32d), and precipitation continued, though diminishing in intensity through 1203/29 (Fig. 3.32e). Precipitation had ended in the region by 1500/29, at which time only ground clutter is present on the radar (Fig. 3.32f).

3.2.2.2 Mesoscale Summary

An inverted surface trough and accompanying baroclinic zone seen on the surface analysis for eastern New York and much of New England at 0600/29 (Fig. 3.33) reveals a cold front extending from an offshore low to along the New York–Pennsylvania border. Higher SLP was located across northern New York, oriented along a west-northwest to east-southeast ridge axis. Surface CAA was ongoing in New York and across New England, though surface winds in these areas were quite light, on the order of 2.5 m s^{-1}.

A weakly confluent wind signature was evident between KGFL, KALB (both with some easterly wind component) and KSYR (with a slightly westerly component).

Figure 3.34 contains surface meteograms for bellwether sites, with KSYR substituting for KUCA. The wind direction at KSYR is shown to vary throughout the time series (2000/28–1200/29), from west-northwesterly to more northerly, then back to west-northwesterly (Fig. 3.34a). Winds at KGFL (Fig. 3.34b) were very light during the entire event, with reported wind speeds under 2.5 m s^{-1} and six calm reports during the time series. The wind direction at KGFL was consistently northeast or easterly throughout the event. Several periods of strongly confluent winds occurred between KSYR and KGFL, including 2300/28–0100/29 and 0700–1000/29, with over 100° of difference in wind direction reported during these times (Figs. 3.34a,b). The wind direction at KALB (Fig. 3.34c) remains comparatively constant, from the north and north-northeast throughout the event.

Time series plots of SLP reveal higher values at KSYR compared to KALB and KPSF throughout the entire event (Fig. 3.35). Greater SLP was reported at KGFL than at KALB and KPOU during the event as well; however the relative SLP differences between these stations decreased with time (Fig. 3.35). From 0900 to 1400/29, SLP differences between KGFL and KALB approached zero, and the SLP difference between KGFL and KPOU dropped appreciably after 0700/29 (Fig. 3.35). The overall SLP change at any one station during the time period 0000–1200/29 is approximately 6 to 7 hPa (Fig. 3.35), which is approximately double that seen over the same period of time during the November 2002 case (Fig. 3.18). These greater SLP changes are consistent with the presence of a stronger upper-level storm during the January 2007 MHC event

(see 500-hPa analyses in Figs. 3.12a–d for November 2002; Figs. 3.29a–f for January 2007).

The radiosonde sounding from KALY at 1200/29 (Fig. 3.36) shows a moist layer from approximately 950–750 hPa, with a shallow inversion layer near 900 hPa. There is an indication that surface winds may have decoupled from the rest of the column at this time, as shown by the reported northerly wind at the lowest reported level (Fig. 3.36). Gently backing winds from the surface to approximately 600 hPa indicate a layer of weak CAA (Fig. 3.36).

The vertical profile of horizontal temperature advection over KALB at 0000, 0600, and 1200/29 (shown in Fig. 3.37 and generated using 0-hour gridded, initialized data from the NARR) shows CAA at all times and for all levels below 500 hPa. Advection values below 850 hPa were modest, averaging approximately $-12°C \times 10^{-5}\ s^{-1}$. Vertical motions over KALB (shown in Fig. 3.38 and generated with the same model data used to compute the temperature advection values) were small (approximately +/− 2.0 μb s^{-1}) from the top to the bottom of the column at 0000, 0600, and 1200/29. Weak upward motion below 500 hPa at 0000/29 increased slightly by 0600/29, with a maximum upward motion of −2.0 μb s^{-1} shown in Fig. 3.38 between the surface and approximately 900 hPa. By 1200/29, downward vertical motion is shown at all levels above approximately 900 hPa, with weak upward motion (on the order of −0.3 μb s^{-1}) shown from 900 hPa to the surface.

An infrared image of the northeastern U.S. at 0845/29 is presented in Fig. 3.39 from the Geostationary Operational Environmental Satellite-12 (GOES-12) satellite. Shown are CTTs in the vicinity of KALB of approximately −20°C, which correspond to

an approximate pressure level of 775 hPa, inferred from the 1200/29 radiosonde sounding (see Fig. 3.36).

3.2.3 December 2002 Case Study

This MHC event occurred following the passage of an Alberta Clipper. Accumulating snowfall associated with this Alberta Clipper ended in most areas by mid morning (local time) on 16 December 2002. Patchy areas of light snow due to MHC effects continued in a localized area, however, into the early nighttime hours. Snowfall totals were light overall, with 7.1 cm of snow falling at KALB on 16 December (WRGB-TV, 2008).

3.2.3.1 SYNOPTIC SUMMARY

Radar imagery from the WSR-88D located at KENX are shown in Figs. 3.40a–f. At 1803/16 an expansive area of light and moderate snowfall covered eastern New York and western New England (Fig. 3.40a). The precipitation diminished in both coverage and intensity by 2101/16 and 2358/16, with two distinct areas of snow visible at these times: one over KALB and vicinity and the other over the Catskill Mountains (Figs. 3.40b,c). At 0302/17, as precipitation ended over the Catskills, a discrete area of light precipitation was seen over KALB and vicinity (Fig. 3.40d). Maximum reflectivity values at this time were approximately 13 dBZ. Through 0603/17 this area of precipitation diminished in intensity, ending by 0900/17 (Figs. 3.40e,f).

At the surface, Fig. 3.41a shows that a strong area of low pressure (979 hPa central pressure) was located over Newfoundland at 0000/16, while a weaker low

(1004 hPa central pressure) was located over western Lake Ontario. High pressure centered over southern Hudson Bay at this time changed very little in position and intensity during the following 24 h (Figs. 3.41a–e). As the low over Newfoundland slowly weakened, a low over western New York intensified and moved to southeast of Cape Cod by 1800/16 (Figs. 3.41b–d). Figure 3.41d shows a "reverse-S" pattern to the surface isobars over eastern New York and western New England at 1800/16. The area of low pressure centered southeast of Cape Cod at 1800/16 had tracked over 40°N, 70°W (a benchmark point commonly used for forecasting the track of Nor'easter-type storms), deepening 3 hPa in the preceding 6 h. The low center tracked due east and continued to intensify to a minimum central pressure of 987 hPa by 0600/17 (Figs. 3.41e,f). Increasing surface baroclinicity was associated with this storm as it tracked out of western New York and over the eastern Atlantic Ocean, with a well-developed frontal structure evident by 0000/17 (Fig. 3.41a–e).

At 700 hPa, diffuse, weak model-diagnosed ascent was located over the northeastern U.S. from 0000 to 0600/16 (Figs. 3.42a,b). A stronger and more coherent center of ascent (-6.0 μb s^{-1}) developed over western Massachusetts by 1200/16 as the surface low center moved offshore (Fig. 3.42c). Ascent increased to -16.0 μb s^{-1} in the following 18 h as the surface low deepened and moved southeast of Nova Scotia (Figs. 3.42d–f). During this time, no significant vertical motions were present over eastern New York or over western New England.

Figures 3.43a,b show that eastern New York and western New England were located under an area of diffluent 300-hPa winds from 0000 to 0600/16. This region was also located under the left-front quadrant of a 65 m s^{-1} jet streak at that time, a region

supportive of ascent, as a closed 300-hPa low crossed New York and Pennsylvania at that time. By 1800/16 and continuing through 0600/17, a strongly confluent wind conjunction had moved to a position over eastern New York and western New England (Figs. 3.43c–f). At both 0000 and 0600/17, this region was also under the left-rear quadrant of a weakening 65 m s^{-1} jet streak, a region associated with sinking air (Figs. 3.43e,f).

3.2.3.2 MESOSCALE SUMMARY

A regional view of surface weather features in eastern New York and western New England at 0300/17 is presented in Fig. 3.44 (with missing station data for winds, sky cover, and SLP, all of which were also unavailable for surrounding times). At 0300/17, an inverted surface pressure trough ran from central Connecticut west-northwest to the Catskill Mountains, with a zone of higher pressure located across northern New York.

Surface meteograms show a strongly confluent wind signature between KUCA and KGFL at 2000 and 2100/16 (Figs. 3.45a,b). Several hourly surface wind observations are missing from the KGFL data set from 0100 to 0600/17, making wind signatures difficult to analyze during the aforementioned time period.

An analysis of SLP, presented in Fig. 3.46, shows that the SLP at KUCA was greater than that at KALB and KPSF through the entire period from 1800/16 to 0800/17. Pressures at KGFL were greater than those at KPOU and at KALB during this period as well; however the pressure differences between KALB and KGFL were negligible (less than 1 hPa).

Atmospheric soundings from KALB at 1200/16 and 0000/17 (Figs. 3.47a,b) were generated using GFS-based 0-hour, gridded analysis data, to compensate for missing radiosonde data. A deep saturated layer is seen at 1200/16 from the surface to nearly 500 hPa, with near-moist moist adiabatic lapse rates present from 750 hPa to the surface (Fig. 3.47a). Backing winds present from the surface to approximately 550 hPa indicate CAA was occurring (Fig. 3.47a). By 0000/17, a shallow mixed layer was present from the surface to approximately 900 hPa (Fig. 3.47b) with an isothermal layer present above that level. The moist layer had become shallower, but still extended from the surface to approximately 700 hPa.

Infrared satellite imagery from GOES-8 (Fig. 3.48) at 2345/16 showed the impressive "comma-head" cloud structure associated with the developing low pressure system southeast of Cape Cod, and the lingering low clouds left in its wake over the northeastern U.S. The satellite-diagnosed CTT of approximately −18°C corresponds to a pressure level of 650 hPa, as inferred from the 0000/17 sounding (see Fig. 3.48b).

3.2.4 January 2003 Case Study

Several of the synoptic features that were present in eastern New York and western New England during the MHC event of 23–24 January 2003 are unique among the case studies included in this thesis; namely, the presence of weak WAA driven by northerly winds at 850 hPa, a corresponding surface trough that moved from north-to-south across the region, and an accompanying area of initially light precipitation that increased in areal coverage and intensity as it passed through the MHC domain. Thus, while synoptic-scale forcing was provided by the WAA at 850 hPa and the surface

trough, the January 2003 event is useful in examining how MHC effects might act to enhance preexisting precipitation.

3.2.4.1 Synoptic Summary

Radar imagery from the KENX WSR-88D at 1600/23 showed scattered weak precipitation (snow) echoes from KGFL extending north and west over the southern Adirondacks and upper Hudson valley (Fig. 3.49a). The echoes translated south-southeastward through 1958/23, increasing in coverage and intensity (Figs. 3.49b,c). By 2202/23 (Fig. 3.49d), a large area of enhanced echoes was present from the Hudson Valley in the vicinity of KALB on westward. Maximum reflectivity values of approximately 25 dBZ were detected at this time. Precipitation ended quickly thereafter, with no echoes were present near KALB at 0004/24, and only isolated weak echoes seen well south of KALB at 0159/24 (Figs. 3.49e,f). The total snowfall amount at KALB for this event was 2.0 cm, with up to 2.5 cm of snow reported by the weather watchers of WRGB-TV (2008).

At the surface, an inverted trough was apparent at 1200/23 from central Massachusetts westward to southeastern lower Michigan (Fig. 3.50a). A low-pressure center was also present at this time well off of the South Carolina coast, in an area of strong baroclinicity (Fig. 3.50a). As this surface low advanced northeastward away from the South Carolina coast and deepened to 991 hPa by 1800/23 (Fig. 3.50b), the surface features over the northeastern U.S. remained unchanged from 6 h earlier. A “reverse-S” isobar pattern (Fig. 3.50b) revealed a ridge axis oriented from west-northwest to east-southeast over northern New York, and an inverted surface trough over the southern tier

of the state. Close inspection of surface winds (see Figs. 3.54a–d) and the 1000–500-hPa thickness (see Figs. 3.50a–d) suggests that the surface trough is in response to weak WAA occurring from the north, as a core of exceptionally cold air (diagnosed by 1000–500-hPa thickness values below 500 dam) moves away from the region. Six-hourly analyses of 850-hPa wind and temperature (not shown) indicate that WAA is occurring at 850 hPa over eastern New York and western New England from 1200/23 to 0600/24, with warmer air (initially located poleward of KALB) being transported equatorward over KALB. Compared to 1200/23, surface features over the northeastern U.S. remained essentially unchanged from 1800/23 to 0600/24, as the low pressure center off the East Coast passed well south and east of 40°N, 70°W (Figs. 3.50b–d). This low reached a minimum central pressure of 970 hPa at 0600/24, representing a decrease in central pressure of 21 hPa in the preceding 12 h.

As the surface low deepened explosively over the Gulf Stream region of the western Atlantic Ocean, vertical motions at 700 hPa were quite vigorous. At 1200/23, the maximum ascent value associated with the surface low was −20.0 μb s^{-1}; by 0600/24, −40.0 μb s^{-1} of ascent is shown (Figs. 3.51a,d). These ascent maxima remain well off-shore throughout the MHC event, however, and have no direct impact over eastern New York or western New England. Weak upward motion (−2.0 μb s^{-1}) was seen over parts of New York and western New England at 1200 and 1800/23 (Figs. 3.51a,b). No ascent is shown at 0000 or 0600/24 (Figs. 3.51c,d) over eastern New York and western New England.

A cyclonic shear zone at 300 hPa was located over eastern New York and western New England at 1200 and 1800/23, and the region was also under the influence of the

left-rear quadrant of a 55 m s^{-1} jet streak (Figs. 3.52a,b). As this jet streak moved away from the region, winds at 300 hPa became slightly more confluent by 0000 and 0600/24 (Figs. 3.52c,d).

3.2.4.2 MESOSCALE SUMMARY

In the regional surface analysis shown in Fig. 3.53, an inverted surface trough is evident at 2100/23, running from the southern New England coast west-northwestward into central New York. Higher SLP was located over northern New York, shown as a pressure ridge oriented from west-to-east across the eastern shores of Lake Ontario and into the Adirondacks. Surface CAA is apparent across eastern New York and western New England. A strongly confluent wind signature is seen between KGFL (with an east-northeast wind) and KUCA and KALB (both with northwest winds). The confluence between KUCA and KGFL is also evident from 1800/23 to 0100/24 on the surface meteograms presented in Figs. 3.54a,b. The difference in wind direction between the two stations is as much as 180° during this period.

A meteogram analysis of SLP, shown in Fig. 3.55, indicates higher pressures from 1500/23 to 0600/24 at KUCA as compared to KALB and KPSF. Also, SLP was greater at KGFL than at KALB and KPOU during the MHC event, however the relative difference between KGFL and KALB was quite small (less than 1 hPa) at times. The meteogram reveals decreasing SLP values at all stations prior to 1900/23, and rising SLP values at all stations thereafter. The passage of a surface trough likely occurred at all stations around 1900/23, several hours prior to the appearance on radar of the most intense precipitation echoes (shown in Figs. 3.49c,d).

The radiosonde sounding from KALB at 1200/23 (Fig. 3.56a) showed a moist layer from 850 to 750 hPa. At that time, the mixed layer was shallow, extending only up to approximately 950 hPa, with an isothermal layer present between approximately 950 and 750 hPa. By 0000/24 (Fig. 3.56b), the depth of the moist layer had increased, with moisture present from the surface to approximately 500 hPa. A strong temperature inversion was present at this time from 850 to 750 hPa. A veering wind signature indicated WAA in the column above KALB between approximately 925 and 700 hPa (Fig. 3.56b), consistent with WAA from the north implied by 1000–500 hPa-thickness pattern at 0000/24 shown in Fig. 3.50c.

The exceptionally high and cold cloud tops associated with the deep ocean low, and shown by the GOES-8 satellite image in Fig. 3.57, had reached no farther west than coastal New England at 2045/23. Satellite-derived CTTs over eastern New York and western New England were approximately −22°C at this time, which correspond to lower clouds with tops around 675 hPa, as inferred from the radiosonde sounding over KALB at 0000/24 (Fig. 3.56b).

3.2.5 January 2005 Case Study

3.2.5.1 SYNOPTIC SUMMARY

At 1003 UTC 17 January 2005, a large area of light precipitation covered much of eastern New York and western New England, as shown on the KENX radar in Fig. 3.58a. The precipitation diminished in coverage through 1359/17 (Figs. 3.58b,c), at which time a small area of light precipitation (maximum reflectivities of approximately 15 dB*Z*) was located over and just south of KALB. This area of precipitation remained quasi-

stationary but varied in coverage and intensity through 2001/17, with reflectivities as low as 5 dBZ and as high as 25 dBZ (Figs. 3.58d–f). Total snowfall at KALB on 17 January 2005 was 8.6 cm (WRGB-TV 2008). Weather-watcher reports indicated that areas immediately surrounding KALB in the zone of MHC received 7.6–12.7 cm of snow that day; areas outside of the MHC zone received only a trace–7.6 cm of snow (WRGB-TV 2008). Subtracting the highest weather-watcher snowfall total measured outside of the MHC zone (7.6 cm) from the highest weather-watcher snowfall total measured within the MHC zone (12.7 cm) produces a difference of 5.1 cm. Thus, up to an additional 5.1 cm of snow may have fallen on 17 January 2005 as a direct result of MHC effects.

At the surface, from 0000 to 1200/17 (Figs. 3.59a–c), a quasi-stationary area of high pressure remained over south-central Quebec province. A 1006-hPa low, centered several hundred kilometers due east of Cape Hatteras, North Carolina at 0000/17 (Fig. 3.59a), deepened to 994 hPa and moved northeastward toward Nova Scotia through 1200/17 (Figs. 3.59b,c). This storm passed southeast of the 40°N, 70°W benchmark used in forecasting East Coast snowstorms. Cyclonically curved isobars were present over eastern New York and western New England from 0000 to 1200/17, as seen in Figs. 3.59a–c. An inverted trough was present within this region of cyclonic curvature, and moved from central Pennsylvania and the mid-Atlantic coast at 0000/17 (Fig. 3.59a) to near the Mohawk Valley at 1200/17 (Fig. 3.59c).

At 700 hPa, the storm had a well-defined area of upward vertical motion throughout the period 0000–1200/17 (Figs. 3.60a–c). This area of upward vertical motion was located well offshore, and ascent over eastern New York and western New England was weak (less than -2.0 μb s^{-1}) during the period.

At 0000/17 a 300-hPa jet streak was located over southern Vermont, as seen in Fig. 3.61a. By 0600 and 1200/17, the jet streak had translated away from this area, putting eastern New York and western New England under confluent flow and the left-rear quadrant of the departing jet streak, an area frequently associated with sinking air (Figs. 3.61b,c).

3.2.5.2 MESOSCALE SUMMARY

Examination of surface features across the MHC domain at 1200/17 reveals a familiar configuration (Fig. 3.62). An inverted surface trough ran from coastal New England to the southern tier of New York, with higher pressure and a weak ridge oriented along a west-northwest to east-southeast axis across northern New York. Weak CAA was present at the surface in eastern New York and New England. The wind directions at KGFL and KALB (both with northeast winds) and KUCA (west-northwest winds) at 1200/17 oppose each other at an approximate angle of 110°, indicating strongly confluent flow (Fig. 3.62). Surface meteograms suggest that this strongly confluent wind signature existed between KUCA and KGFL throughout the entire period, from 1000 to 1800/17 (Figs. 3.63a,b). During this period, 100° or more of difference in surface wind direction existed between KUCA and KGFL.

Throughout the event, SLP at KUCA remained higher than at KALB and KPSF, as seen in Fig. 3.64. SLP was also higher at KGFL than at KALB and KPOU, but the relative difference in the former was negligible at times (Fig. 3.64). Overall, the change in SLP at any one station throughout the period was small, on the order of 2 hPa.

A deep moist layer, which extended from the surface to 500 hPa, was shown on the radiosonde sounding from KALY at 1200/17 (Fig. 3.65a). Cold advection was also made evident by a backing wind profile at this time, and was maximized from 800 to 600 hPa. By 0000/18 a unidirectional wind profile from the surface to approximately 650 hPa indicated that CAA had ended, and the stability of the 700–600 hPa layer had increased (Fig. 3.65b). The sounding at this time also indicated that the atmosphere was unsaturated throughout its entire depth.

Satellite-estimated CTTs over eastern New York and western New England (shown in Fig. 3.66) are approximately −28°C at 1145/17. As inferred from the 1200/17 radiosonde sounding (Fig. 3.65a), this value corresponds to cloud tops at approximately 600 hPa.

3.2.6 March 2006 Case Study

An area of surface low pressure passed to the south of New York and New England during the daytime hours (local time) of 2 March 2006, bringing synoptic-scale snowfall to parts of the MHC domain. Accumulating snowfall was reported in areas equatorward of a line which ran through the Mohawk Valley, to KALB, to the border between Vermont and Massachusetts (WRGB-TV, 2008). Approximately 7.6–22.9 cm of snow fell south of that line, as reported by the volunteer weather watchers of WRGB-TV (2008). Precipitation related to MHC developed following the end of this synoptic-level snowfall across eastern New York and western New England into the nighttime hours of 2 March 2006 (local time; 3 March 2006, UTC).

3.2.6.1 SYNOPTIC SUMMARY

The departure of synoptic-scale snowfall from north-to-south across the MHC domain is seen at 0000 and 0202/03 in Figs. 3.67a,b. At 0359/03, a sizeable area of moderate and locally heavy snowfall had developed in the vicinity of KALB, with maximum reflectivity values approaching 25 dBZ (Fig. 3.67c). This snowfall maintained its intensity through 0601/03 (Fig. 3.67d), but decreased in coverage. Snowfall appeared to end completely over the region by 0757/03 (Fig. 3.67e) only to reappear, at a much-diminished intensity, briefly at 0901/03 (Fig. 3.67f).

A surface low (central pressure: 996 hPa) was present at 0000/03 on a baroclinic zone centered over the western Atlantic Ocean, southeast of 40°N, 70°W (Fig. 3.68a). The storm intensified and moved rapidly toward the east-northeast, and began to merge with another low centered over Newfoundland by 1200/03 (Figs. 3.68b,c). The SLP pattern over eastern New York and western New England exhibited an inverted surface trough that ran from central Rhode Island northwestward to approximately KALB at 0000/03 (Fig. 3.68a). This trough pivoted south of KALB by 0600/03, ending up along a line from the southern New England coast to western New York by 1200/03 (Figs. 3.68b,c). Decreasing 1000-500 hPa thickness values were observed across eastern New York and western New England between 0000 and 1200/03, suggesting that CAA was occurring over the region (Figs. 3.68a–c).

Upward vertical motion at 700 hPa (associated with the aforementioned surface low located over the eastern Atlantic Ocean) increased from a maximum of −12.0 μb s^{-1} at 0000/03 to −16.0 μb s^{-1} by 1200/03 (Figs. 3.69a–c). This upward motion remained largely offshore at 0000/03 and completely offshore thereafter. Weak ascent was

diagnosed over eastern New York and western New England at 0000/03 (−2.0 μb s^{-1}), with little or no ascent evident after that time (Figs. 3.69a–c). At 300 hPa, a coupled jet structure existed south and east of KALB at 0000/03 (Fig. 3.70a), with weakly confluent flow over KALB from 0000 to 1200/03 (Figs. 3.70a–c).

3.2.6.2 MESOSCALE SUMMARY

A close inspection of surface weather features over eastern New York and western New England at 0300/03 (Fig. 3.71) shows a "reverse-S" isobar pattern over the region, with a ridge of high pressure oriented along a west-northwest to east-southeast axis over northern New York, and an inverted trough located along the border between New York and Pennsylvania. A strongly confluent wind signature existed at 0300/03 between KGFL and KALB (both with northeast winds) and KUCA (with a northwest wind). Some of the strongest surface winds during any MHC case study were recorded at this time at KGFL, which was experiencing wind speeds of 7.5 m s^{-1}.

The confluent wind signature between KGFL and KUCA is evident on surface meteograms (Figs. 3.72a,b) during the period 0000–0700/03. Winds at KALB gradually shifted from northeast to northwest from 0200 to 1000/03 (Fig. 3.72c). Interestingly, calm winds were reported at KPOU for 9 h during the 12 h period ending 1200/03 (Fig. 3.72d). An analysis of SLP at these stations (Fig. 3.73) shows higher pressures at KUCA than at KALB and KSPF throughout the period from 0000 to 1200/03. Likewise, SLP was higher at KGFL than at KPOU during the period, with less than 1 hPa of pressure difference between KGFL and KALB after 0400/03.

The radiosonde sounding from KALY at 0000/03 (Fig. 3.74a) showed the top of the mixed layer was at approximately 780 hPa, with an inversion/isothermal layer between 780 and 625 hPa. By 1200/03 (Fig. 3.74b), the top of the mixed layer had fallen to approximately 950 hPa, with a strong inversion present between approximately 850 and 800 hPa. A deep moist layer was present at both 0000/03 and 1200/03 (Figs. 3.74a,b). Infrared satellite estimates of CTTs over eastern New York, made by GOES-12, were near −20°C at 0401/03 (Fig. 3.75). Such temperatures corresponded to approximately 575 hPa, as inferred from the KALY radiosonde soundings presented in Figs. 3.74a,b.

3.2.7 January 2008 Case Study

The 2 January 2008 MHC event began as an area of surface low pressure deepened in the Gulf of Maine, a low that earlier had brought brief periods of locally heavy snow to eastern New York and western New England. The MHC event that ensued was remarkable in both duration and intensity. Snowfall associated with MHC began in the region around 0600 UTC and continued until approximately 1800 UTC on 2 January 2008. Snowfall amounts which were attributed to MHC-induced precipitation varied widely (not shown) with 0.8 cm reported officially at KALB, and WRGB-TV (2008) weather watcher reports of 2.5–9.4 cm in various parts of Clifton Park, NY (located approximately 10 km north of KALB), to as much as 12.7 cm in North Colonie, NY (located approximately 3 km east of KALB).

While a detailed analysis of the January 2008 MHC event is not included in this thesis, this event would make an excellent benchmark case for further study. A cursory

examination of the key synoptic (mesoscale) weather features which contributed to the January 2008 MHC event follows in section 3.2.7.1 (3.2.7.2); pressure and wind data from this case are not included in the aggregate analyses discussed in section 3.1.

3.2.7.1 Synoptic Summary

Several discrete areas of moderate-to-heavy snow were evident on the KENX WSR-88D radar at 0757/02 (Fig. 3.76a), indicating the early stages of MHC. By 1004/02, only one large area of moderate-to-heavy (reflectivities up to 25 dBZ) snow remained (Fig. 3.76b). This area of snow consolidated between 1004 and 1357/02 (Figs. 3.76c,d), with maximum reflectivities up to 30 dBZ at 1357/02. From 1604 to 1801/02, precipitation continued in the same general area, however its coverage and intensity lessened (Figs. 3.76e,f).

At the surface at 0600/02 (Fig. 3.77a), a 992-hPa low was moving into the Bay of Fundy, and this low had passed slightly west (i.e., "inside") of 40°N, 70°W. At this time, an inverted trough ran from the low center west-southwestward to near KPOU, and then west across the southern tier of New York and over Lake Erie (Fig. 3.77a). Weak high pressure also lay across central Quebec. At 1200/02 (Fig. 3.77b), the storm had intensified to 989 hPa as it neared Prince Edward Island. The inverted trough had moved slightly southward by 1200/02, and was oriented in a "U"–shape from coastal Massachusetts, to southeastern Pennsylvania, to the shores of Lake Erie in northeast Ohio (Fig. 3.77b). At 1800/02 the surface low had intensified further, to 983 hPa, and had moved to near Newfoundland (Fig. 3.77c). The surface trough is shown at this time (Fig. 3.77c) off the southern New England coast and across southern Pennsylvania.

Surface features and ascent at 700 hPa are shown in Figs. 3.78a–c. Strong ascent (in excess of −16.0 μb s^{-1}) is seen on the north and east sides of the surface low, far from eastern New York and western New England, at 0600 and 1200/02 (Figs. 3.78a,b). Weaker ascent (approximately −2.0 μb s^{-1} or less) was diagnosed with the surface trough, located well south of the eastern New York/western New England region, from 0600 to 1800/02, with little or no ascent seen in the vicinity of KALB (Figs. 3.78a–c).

A core of 75 m s^{-1} winds at 300 hPa was located just southeast of eastern New York and western New England at 0600/02, as shown in Fig. 3.79a. As this core of maximum winds shifted southeastward, an area of confluent winds developed over KALB, seen at 1200 and 1800/02 (Figs. 3.79b,c).

3.2.7.2 Mesoscale Summary

By 2 January 2008, the ASOS at KRME was fully operational as the designated replacement for the ASOS at KUCA. Observations of SLP taken at KRME, however, were widely deemed unreliable by forecasters at this time. Indeed, SLP reductions reported at KRME (Fig. 3.80a) on 2 January 2008 show an approximate 5-hPa bias towards higher pressures than those reported at KSYR (Fig. 3.81a). The SLP reductions at KRME are outliers compared to surrounding stations and are not supported by the overall synoptic pattern. Thus, the wind analyses that follow were conducted using wind data from KRME; however pressure analyses were conducted using SLP data from KSYR.

A confluent wind signature is shown between KRME (Fig. 3.80a) and KGFL (Fig. 3.80b) throughout the MHC event, with the strongest confluence occurring around

1600/02. Surface winds are, overall, stronger in this case than in any other case study. Wind speeds at KRME and KALB consistently range between 5 and 7.5 m s^{-1}, while winds at KGFL are 5 m s^{-1} or less. The highest SLP was located on the western side of the domain during this MHC event, with higher SLP reported at KSYR than at KALB and KPSF from 0600 to 2300/02 (Fig. 3.82). Likewise, higher SLP was located on the northern side of the domain, with SLP at KGFL higher than that at KALB and KPOU from 0700 to 2300/02 (Fig. 3.82). SLP change at any one station from 0800 to 2000/02 is over 10 hPa, with over 20 hPa of change at KALB and KGFL, the largest increase in SLP of any case study.

The radiosonde sounding from KALY at 1200/02 (Fig. 3.83) shows a moist layer between the surface and approximately 750 hPa. A shallow mixed layer extends from the surface to approximately 950 hPa, with an isothermal layer above, to near 700 hPa.

3.3 Summary of Case Studies

Presented in Table V is a summary of the important synoptic and mesoscale parameters at the time of peak precipitation coverage and intensity for each of the six original MHC case studies. As shown in this table, weak CAA (values between −7.0 and -17.9×10^{-5} °C s^{-1}) was present at 925 hPa at the peak of all case studies. Similarly, weak CAA (values between −7.1 and -20.7×10^{-5} °C s^{-1}) were observed at 850 hPa in all but one case. This one exception occurred on 23 January 2003 as a warm front at 850 hPa moved from north-to-south across eastern New York and western New England, bringing WAA and an 850-hPa temperature advection value of 52.2×10^{-5} °C s^{-1} at 2100 UTC. CAA was also observed at 700 hPa in four of the six cases presented in Table V,

except for the January 2003 case (involving the passage of a warm front at 850 hPa) and a near-zero temperature advection value at 0000 UTC 17 December 2002. Advection of geostrophic absolute vorticity at 500 hPa and advection of 700-hPa geostrophic relative vorticity by the thermal wind were weak during the six case studies.

Ascent was maximized in five of the six case studies at 925 hPa, although ascent values were still very weak, between 0.0 and −2.2 μb s^{-1}. A maximum ascent value of −4.0 μb s^{-1} occurred at 700 hPa in the January 2003 case, consistent with the midlevel WAA present during that storm.

Radiosonde soundings show a moist PBL is present during MHC events, with the top of the moist layer located from 825–500 hPa during all cases. Infrared satellite imagery confirms the presence of low-topped clouds, with inferred pressure heights at approximately 840–600 hPa. Despite the moist atmosphere, PWAT values of 3.8–7.1 mm were present, representing 60–90% of the climatological normal values during each case. Regarding convection, the lower troposphere is statically stable during each case with mixed-layer convective available potential energy (MLCAPE) and most-unstable convective available potential energy (MUCAPE) values of zero. Likewise, lifted index (and most-unstable lifted index; MULI) values ranged from +4 to +26°C, well above zero and well within the stable categorization. Surface–2 km shear values were small as well, ranging from 3–10 m s^{-1}.

Subsequent to the completion of the writing of this thesis, an MHC event that occurred from approximately 2300 UTC March 28 to 0600 UTC 29 March 2008 generated 1.5 cm of snowfall at KALB (WRGB-TV 2008). Slippery travel persisted in the vicinity of KALB overnight, and lasted through the early morning hours (local time)

of 29 March 2008. The light snow generated by MHC in this event extended the impacts, in a localized area, of a synoptic-scale storm that had concluded nearly 12 h earlier. While further details of the March 2008 MHC event are not included in this thesis, the evolution of this event is in agreement with the benchmark cases of November 2002 and January 2007 (see sections 3.2.1 and 3.2.2). A detailed study of the March 2008 MHC is suggested for future research.

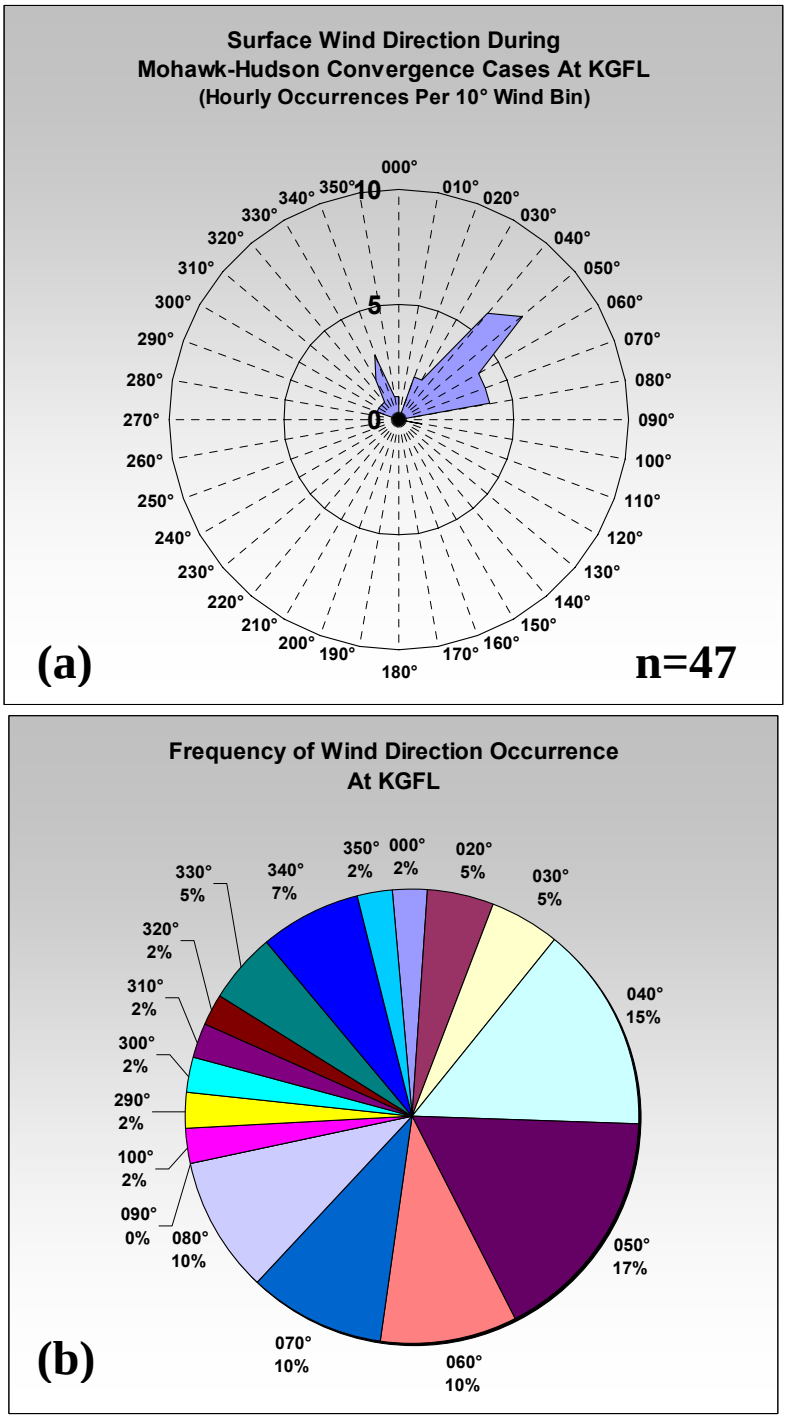

Figure 3.1: (a) Surface wind rose for KGFL during ongoing MHC events studied from November 2002 to January 2007, inclusive. Azimuthal axis represents wind direction in degrees, and radial axis represents number of hourly occurrences. (b) Frequency (in percent) with which each wind direction occurred at KGFL during the aforementioned case studies. Data source: University at Albany archive; supplemental data from the Historical Weather Data Archives of the National Severe Storms Laboratory (NSSL) in Norman, Oklahoma.

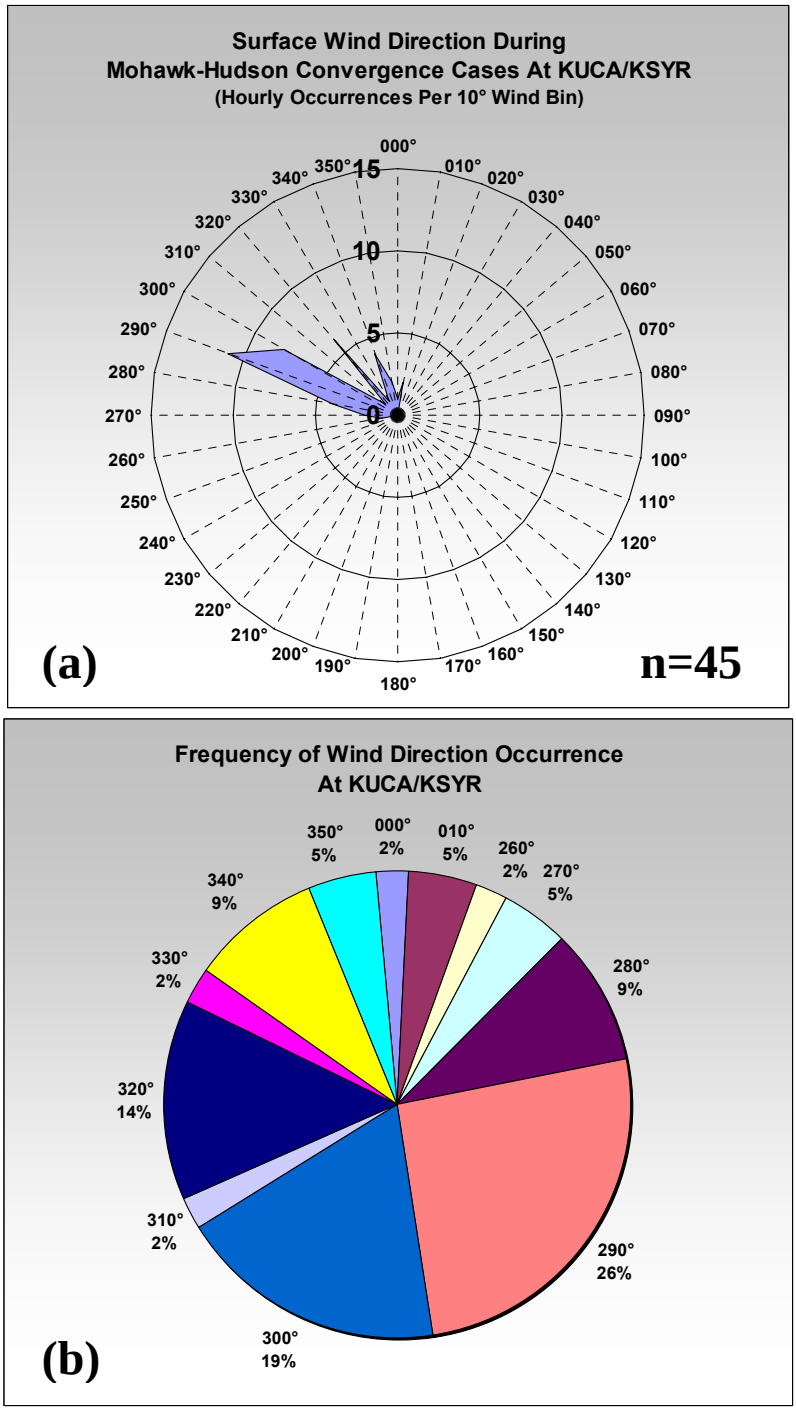

Figure 3.2: (a) Surface wind rose for KUCA (case studies spanning November 2002 – March 2006, inclusive) and KSYR (January 2007 case study) during ongoing MHC events. Azimuthal axis represents wind direction in degrees, and radial axis represents number of hourly occurrences. (b) Frequency (in percent) with which each wind direction occurred at KUCA and KSYR during the aforementioned case studies. Data source: University at Albany archive; supplemental data from the Historical Weather Data Archives of the National Severe Storms Laboratory (NSSL) in Norman, Oklahoma.

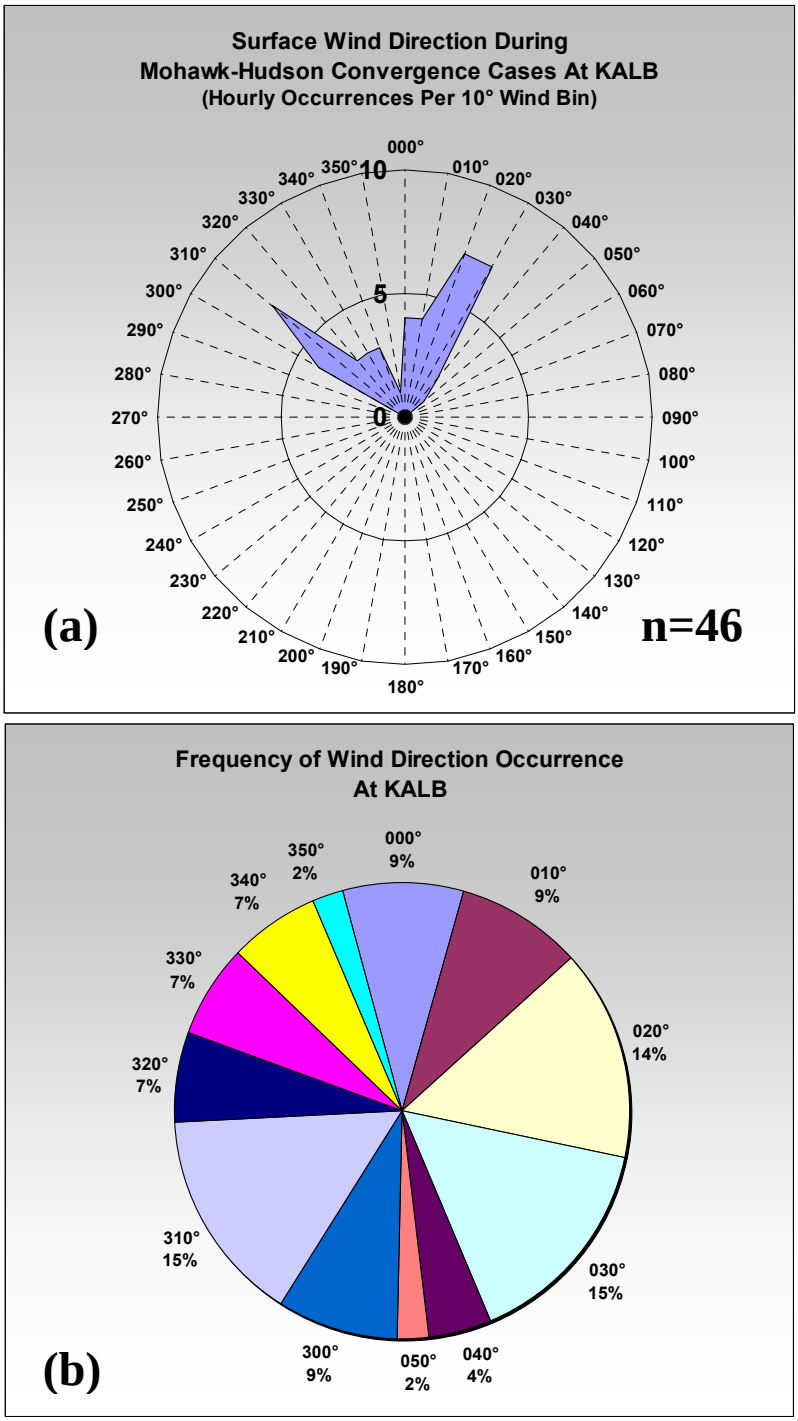

Figure 3.3: As in Fig. 3.1, except for KALB.

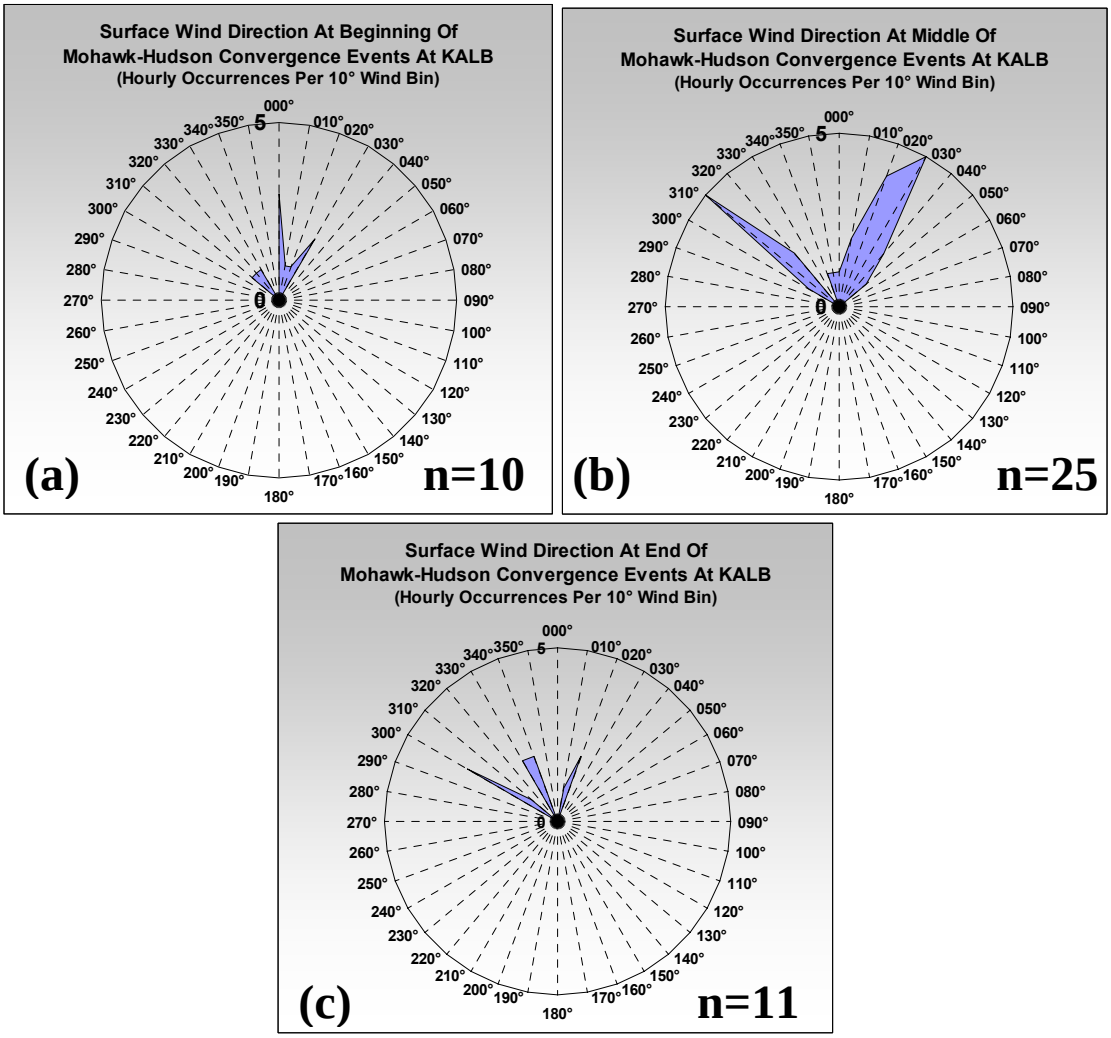

Figure 3.4: Surface wind rose for KALB at (a) beginning, (b) middle, and (c) end of MHC events studied from November 2002 to January 2007, inclusive. Azimuthal axis represents wind direction in degrees, and radial axis represents number of hourly occurrences. Data source: University at Albany archive; supplemental data from the Historical Weather Data Archives of the National Severe Storms Laboratory (NSSL) in Norman, Oklahoma.

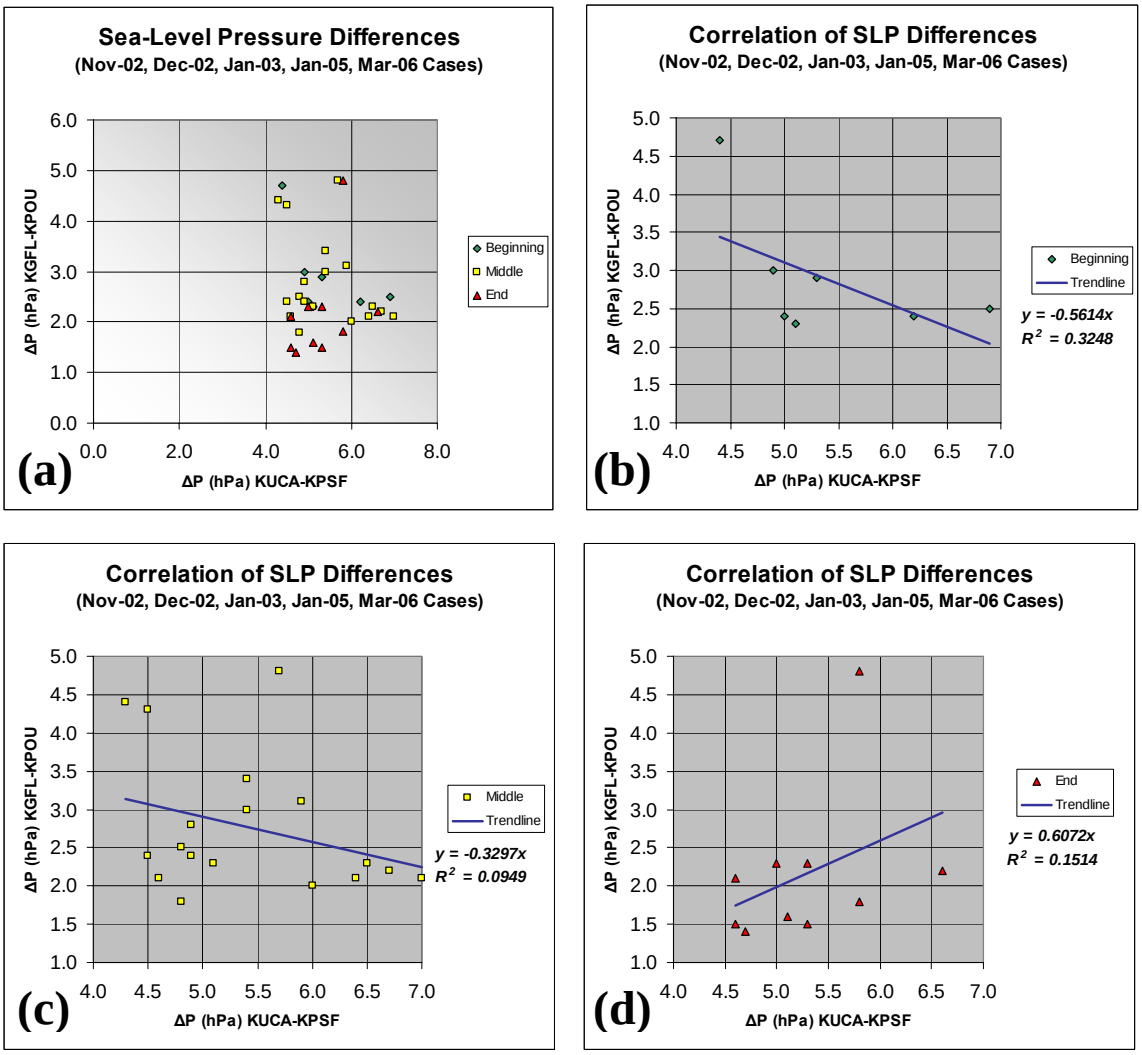

Figure 3.5: Scatterplot graph of SLP differences between KGFL and KPOU (KUCA and KPSF) during MHC case studies from November 2002 to March 2006, inclusive, where positive pressure differences indicate higher pressures to the north (west). (a) For all observations; (b) for observations taken during the "beginning" of MHC events, where the solid blue line indicates the best-fit linear regression between north-south and west-east pressure difference pairs; (c) as in (b), but for the "middle" of MHC events; (d) as in (b), but for the "end" of MHC events. Data source: University at Albany archive; supplemental data from the Historical Weather Data Archives of the National Severe Storms Laboratory (NSSL) in Norman, Oklahoma.

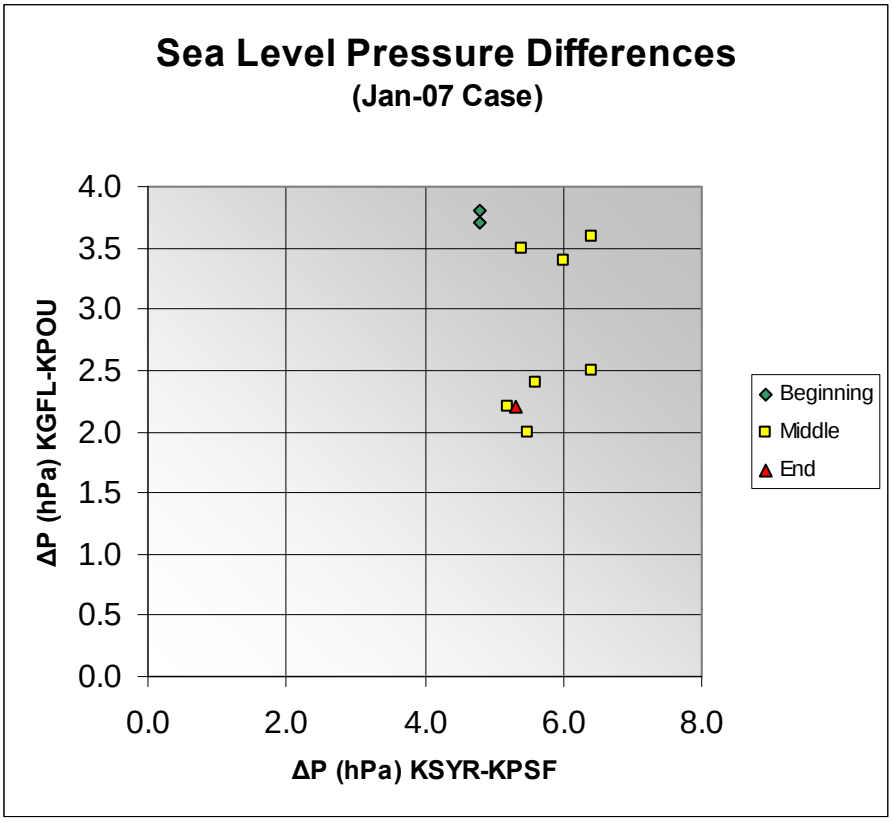

Figure 3.6: Scatterplot graph of SLP differences between KGFL and KPOU (KSYR and KPSF) during the January 2007 MHC case study, where positive pressure differences indicate higher pressures to the north (west). Data source: University at Albany archive; supplemental data from the Historical Weather Data Archives of the National Severe Storms Laboratory (NSSL) in Norman, Oklahoma.

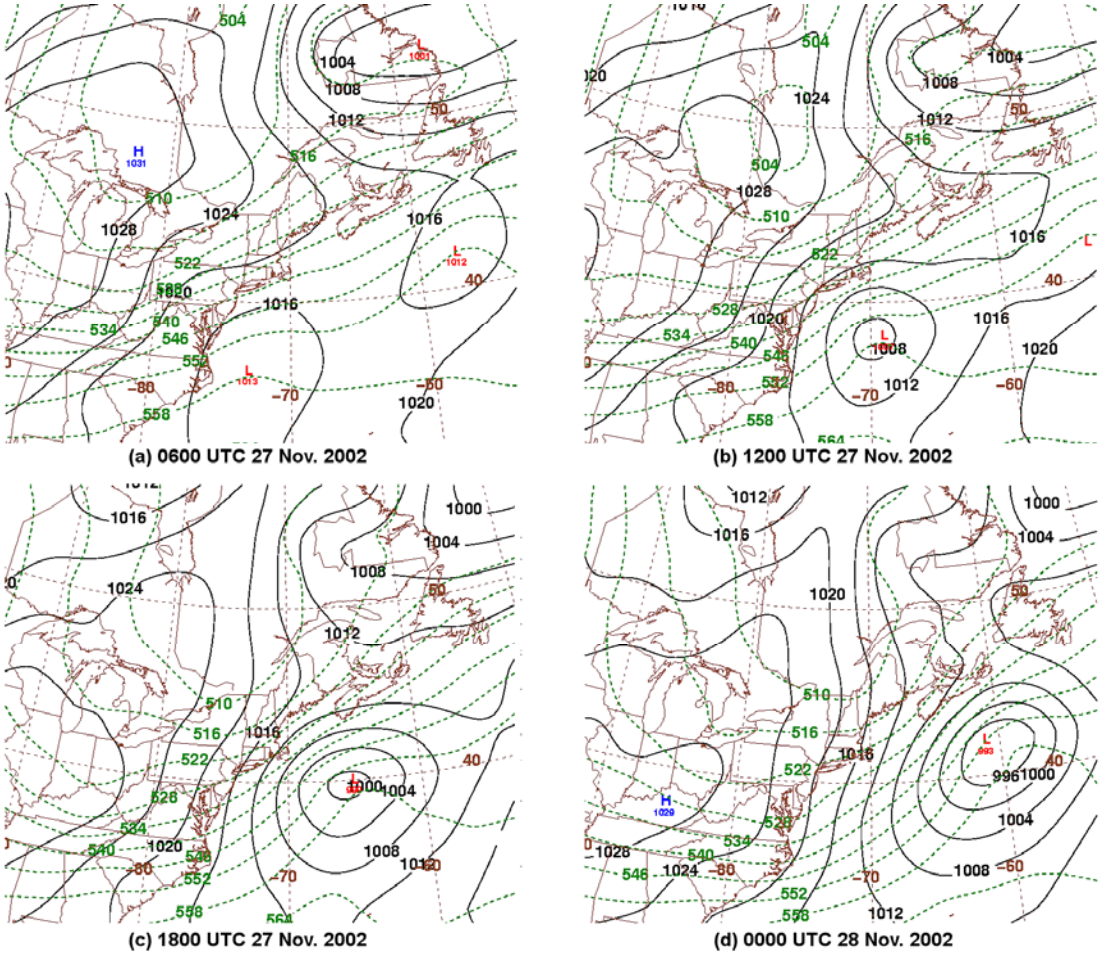

Figure 3.7: Sea level pressure (solid black lines every 4 hPa) with high- (low-) pressure centers labeled by a blue "H" (red "L"), and 1000–500-hPa thickness (dashed green lines every 6 dam) at (a) 0600, (b) 1200, and (c) 1800 UTC 27 November 2002, and at (d) 0000 UTC 28 November 2002. (Data source: 0-h gridded, initialized 1.0° NCEP GFS analyses).

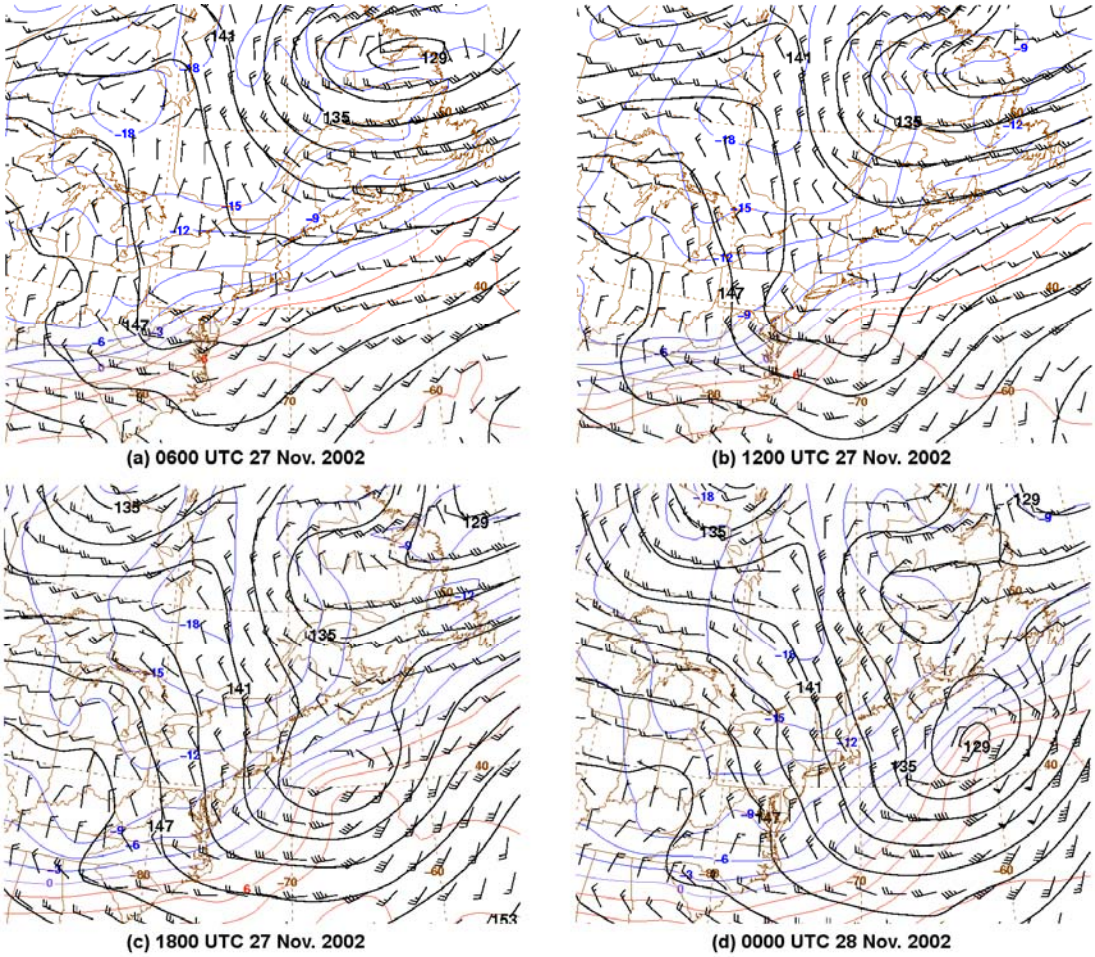

Figure 3.8: 850-hPa geopotential height (solid black lines, every 3 dam), temperatures (solid colored lines, every 3°C), and winds (m s^{-1}, with pennant, full barb, and half barb denoting 25, 5, and 2.5 m s^{-1}, respectively) at (a) 0600, (b) 1200, and (c) 1800 UTC 27 November 2002, and at (d) 0000 UTC 28 November 2002. (Data source: 0-h gridded, initialized 1.0° NCEP GFS analyses).

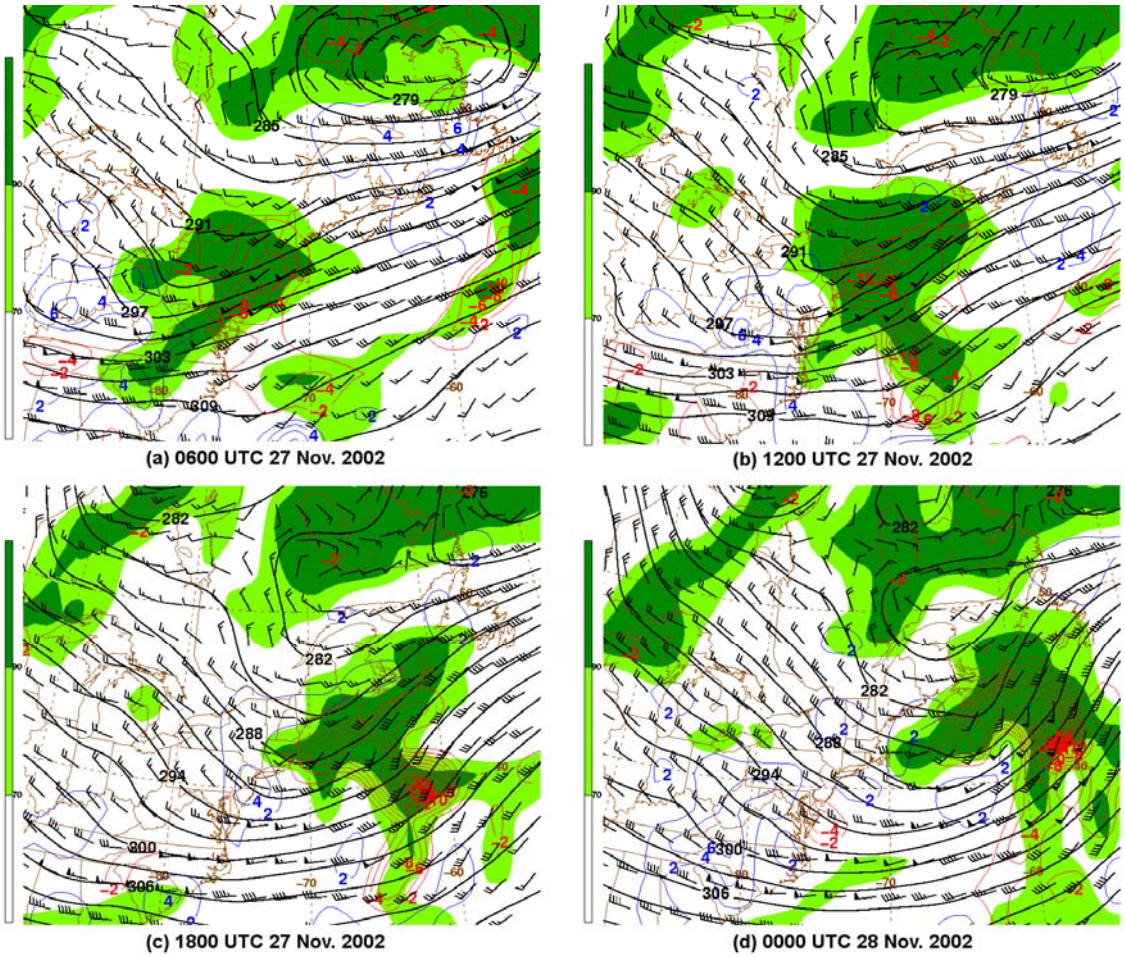

Figure 3.9: 700-hPa geopotential height (solid black lines, every 3 dam), relative humidity (shaded beginning at 70% according to the scale), vertical motion [solid red (blue) contours show ascent (descent), every 2×10^{-3} hPa s^{-1}], and winds (m s^{-1}, with pennant, full barb, and half barb denoting 25, 5, and 2.5 m s^{-1}, respectively) at (a) 0600, (b) 1200, and (c) 1800 UTC 27 November 2002, and at (d) 0000 UTC 28 November 2002. (Data source: 0-hour gridded, initialized 1.0° NCEP GFS analyses).

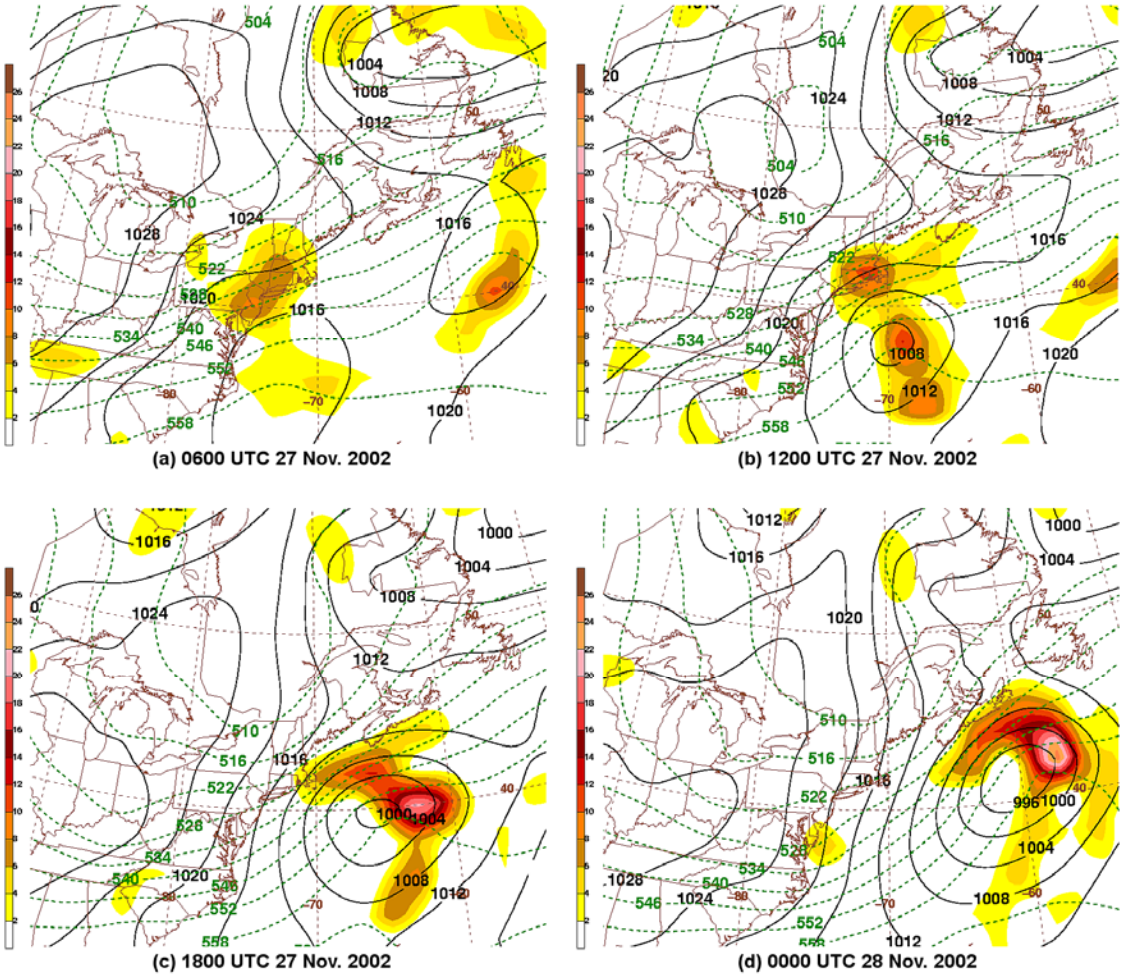

Figure 3.10: Sea level pressure (solid black lines every 4 hPa), 700-hPa vertical motion (ascent shaded beginning at -2×10^{-3} hPa s^{-1} according to the scale), and 1000–500-hPa thickness (dashed green lines every 6 dam) at (a) 0600, (b) 1200, and (c) 1800 UTC 27 November 2002, and at (d) 0000 UTC 28 November 2002. (Data source: 0-hour gridded, initialized 1.0° NCEP GFS analyses).

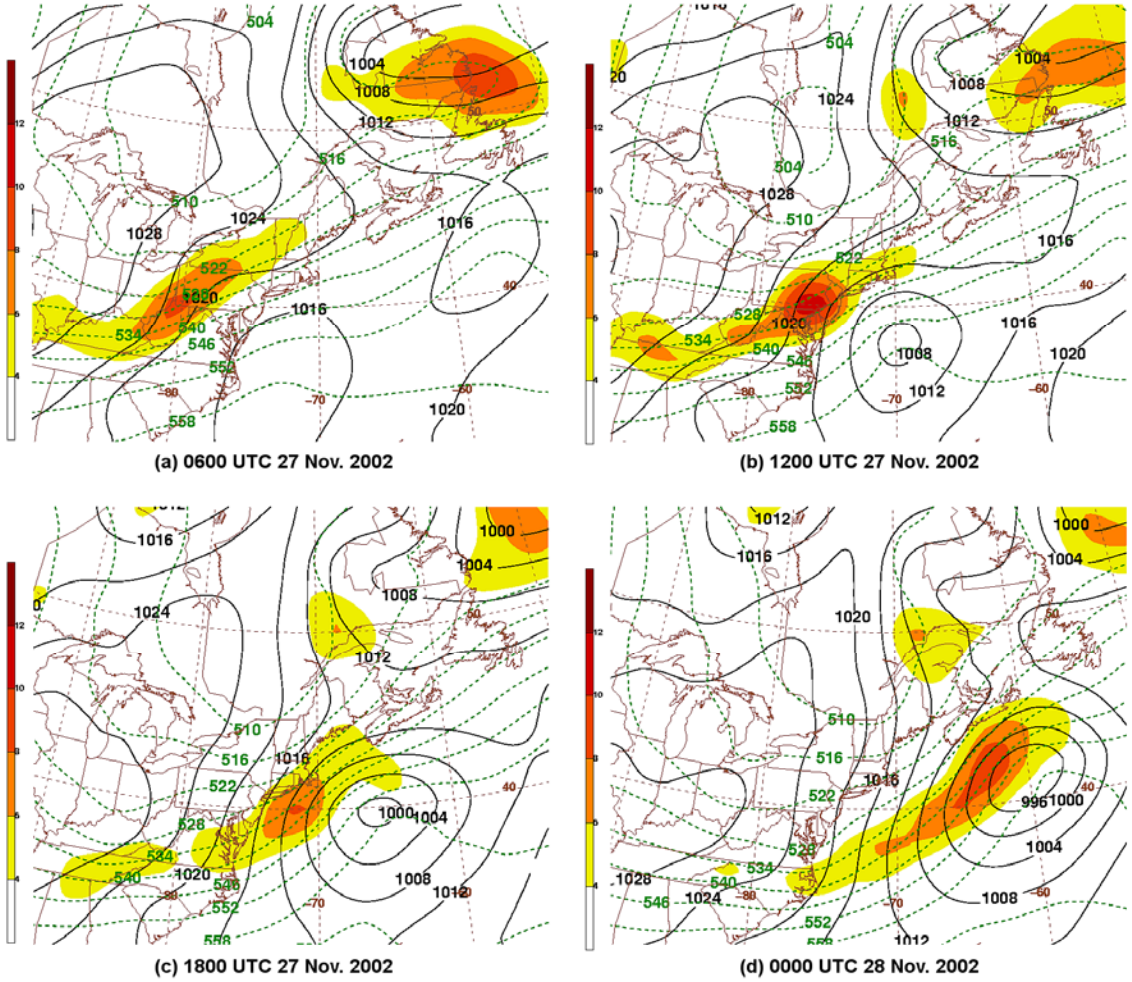

Figure 3.11: Sea level pressure (solid black lines every 4 hPa), 700-hPa geostrophic relative vorticity (shaded beginning at 4×10^{-5} s^{-1} according to the scale), and 1000–500-hPa thickness (dashed green lines every 6 dam) at (a) 0600, (b) 1200, and (c) 1800 UTC 27 November 2002, and at (d) 0000 UTC 28 November 2002. (Data source: 0-hour gridded, initialized 1.0° NCEP GFS analyses).

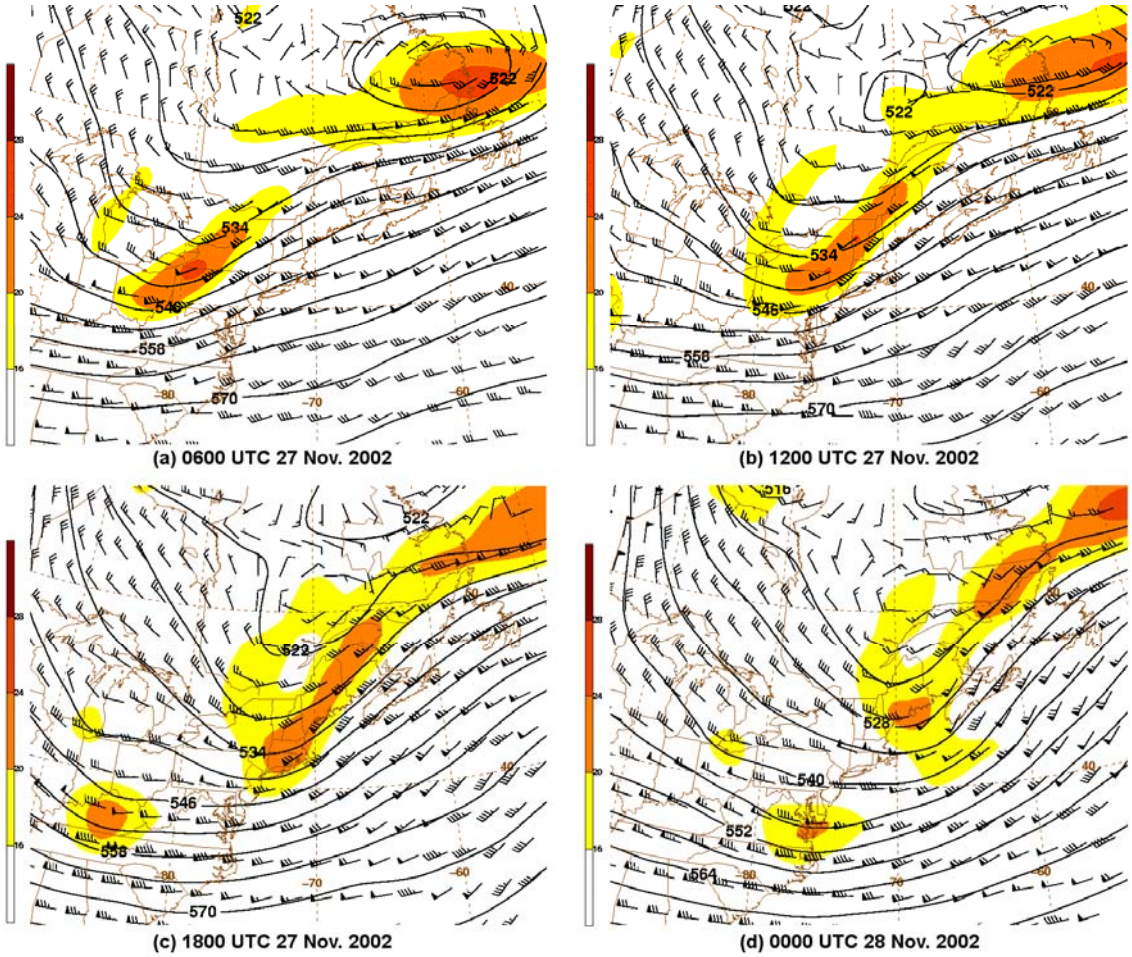

Figure 3.12: 500-hPa geopotential height (solid black lines, every 6 dam), absolute vorticity (shaded beginning at 16×10^{-5} s^{-1} according to the scale), and winds (m s^{-1}, with pennant, full barb, and half barb denoting 25, 5, and 2.5 m s^{-1}, respectively) at (a) 0600, (b) 1200, and (c) 1800 UTC 28 November 2002, and at (d) 0000 UTC 28 November 2002. (Data source: 0-hour gridded, initialized 1.0° NCEP GFS analyses).

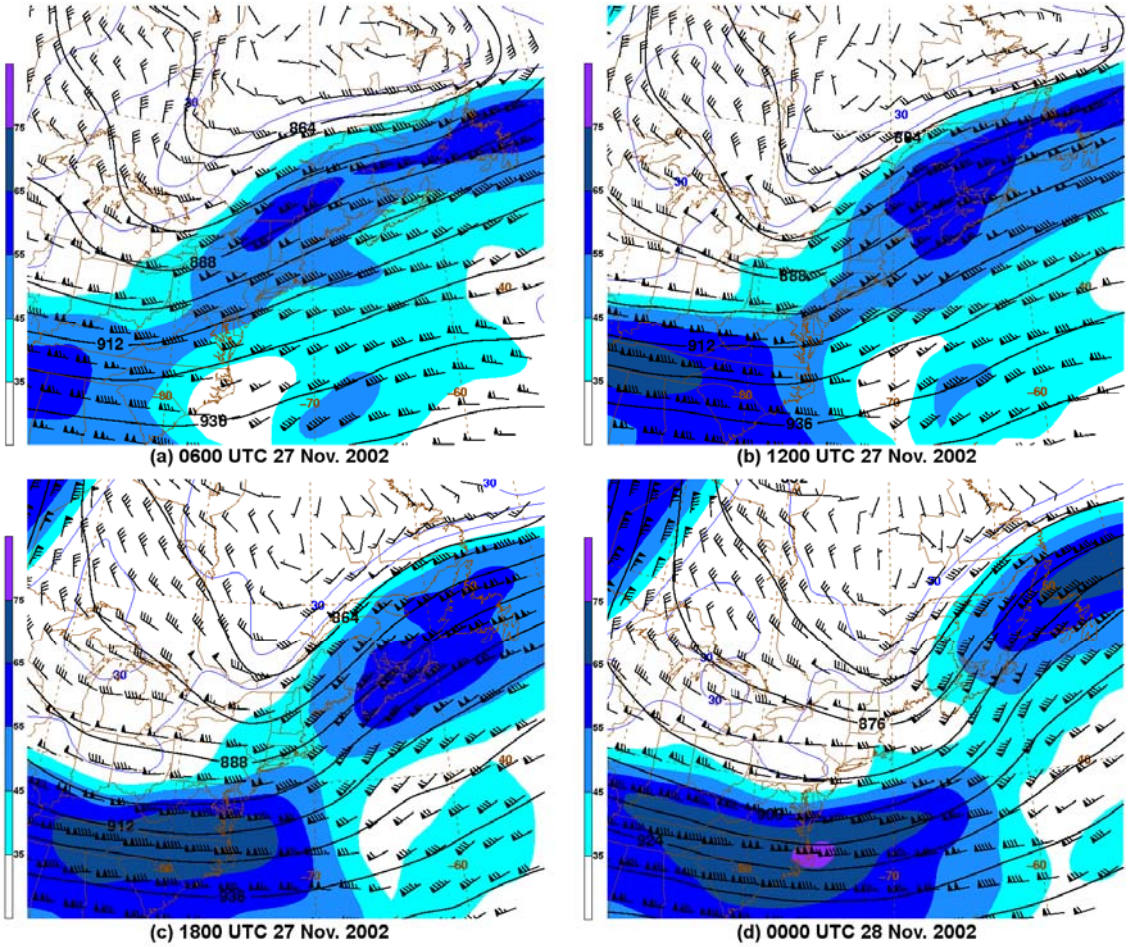

Figure 3.13: 300-hPa geopotential height (solid black lines, every 12 dam), winds (m s^{-1}, with pennant, full barb, and half barb denoting 25, 5, and 2.5 m s^{-1}, respectively), and wind speed (shaded beginning at 35 m s^{-1} according to the scale) at (a) 0600, (b) 1200, and (c) 1800 UTC 27 November 2002, and at (d) 0000 UTC 28 November 2002. (Data source: 0-hour gridded, initialized 1.0° NCEP GFS analyses).

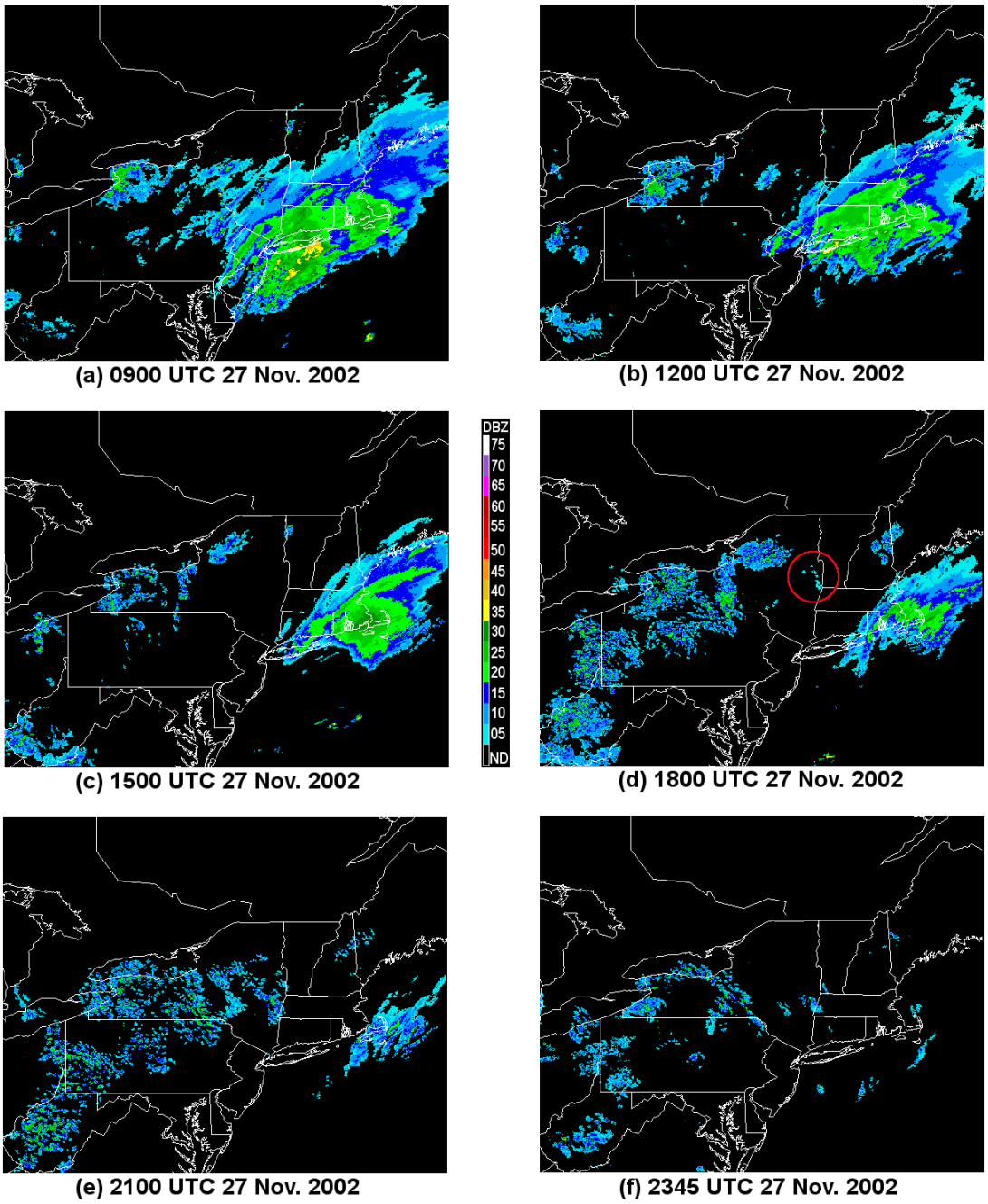

Figure 3.14: Weather Services International (WSI) NOWrad 2 km base reflectivity (dBZ shaded according to scale) mosaic at (a) 0900, (b) 1200, (c) 1500, (d) 1800, (e) 2100, and (f) 2345 UTC 27 November 2002. (Data source: WSI, via MMM/NCAR). Precipitation related to MHC is circled in red.

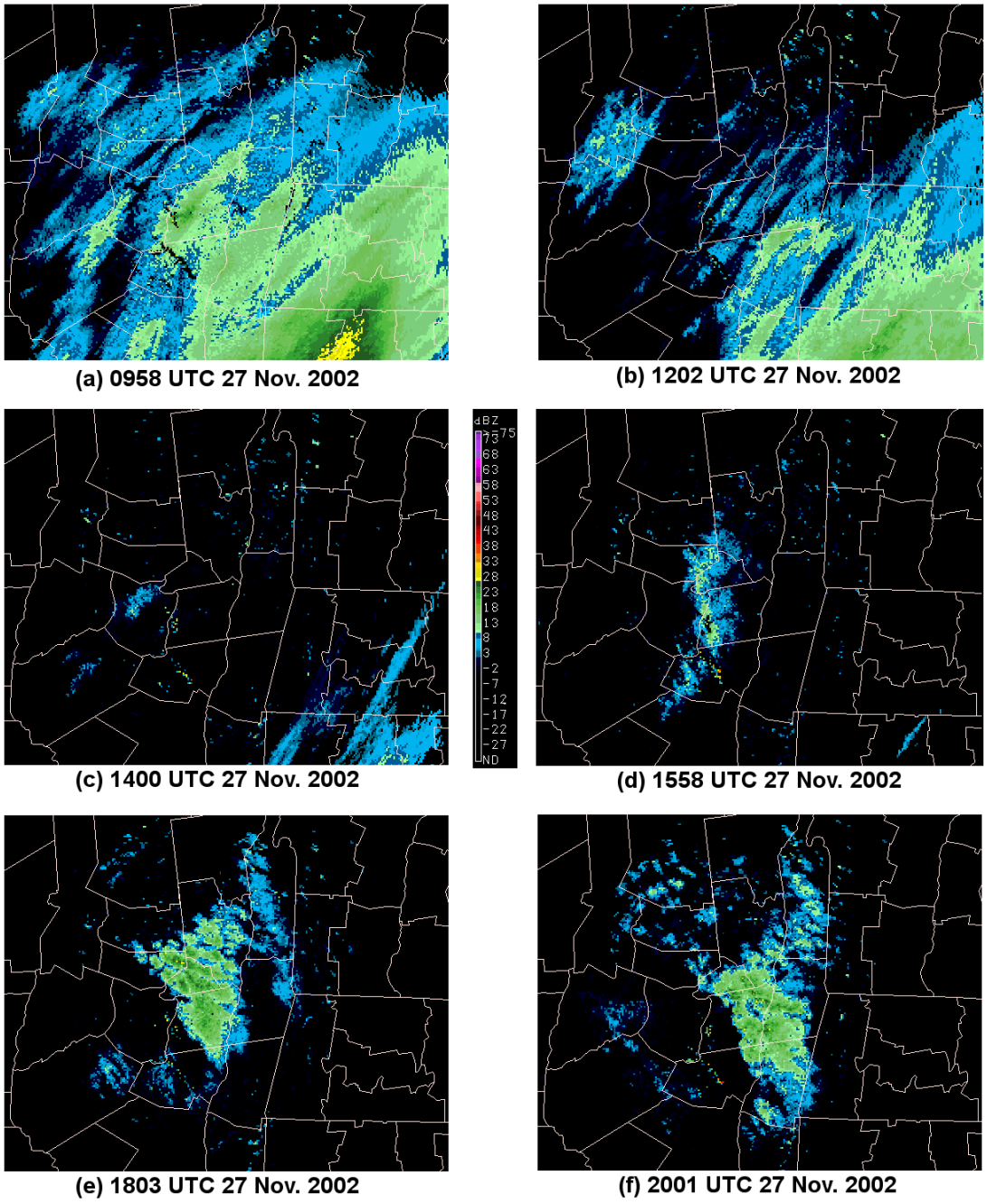

Figure 3.15: KENX 0.5° base reflectivity (dBZ shaded according to scale) at (a) 0958, (b) 1202, (c) 1400, (d) 1558, (e) 1803, and (f) 2001 UTC 27 November 2002. (Data source: NCDC).

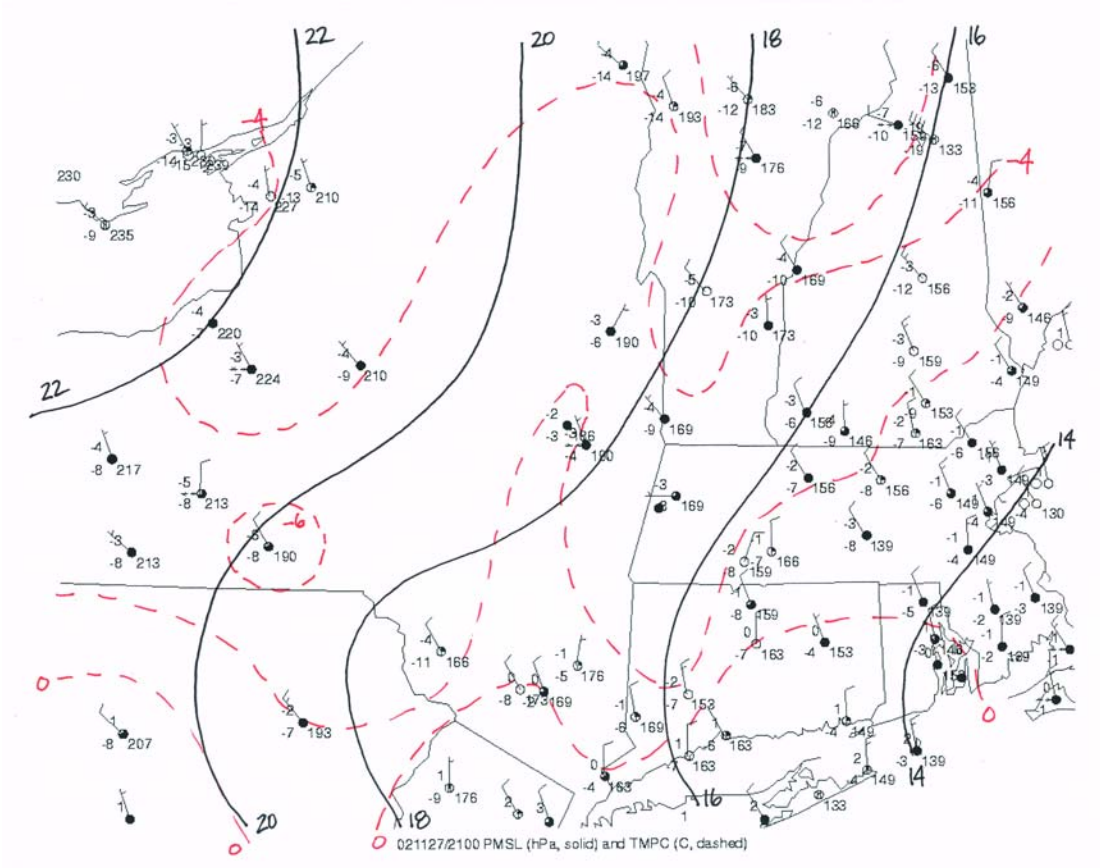

Figure 3.16: Manual regional surface analysis of eastern New York and New England at 2100 UTC 27 November 2002. Isobars (solid) every 2 hPa. Isotherms (dashed red lines) every 2°C. Surface observations are plotted conventionally and show wind speed (m s^{-1}, with full barb, and half barb denoting 5, and 2.5 m s^{-1}, respectively). (Data source: the University at Albany DEAS archives).

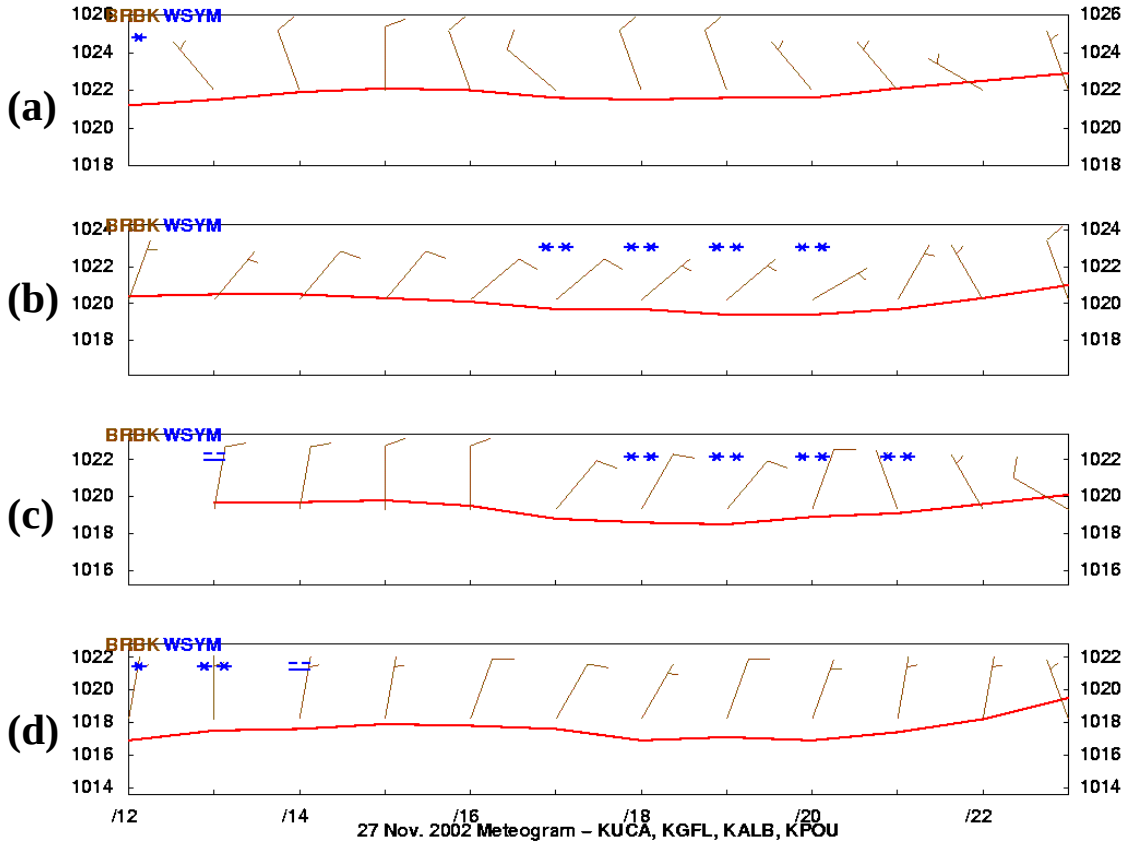

Figure 3.17: Meteograms of surface weather from 1200 to 2300 UTC 27 November 2002 for (a) KUCA, (b) KGFL, (c) KALB, and (d) KPOU. Plotted are sea level pressure (hPa), wind direction and speed (m s^{-1}, with full barb, and half barb denoting 5, and 2.5 m s^{-1}, respectively), and present weather. (Data source: the University at Albany DEAS archives).

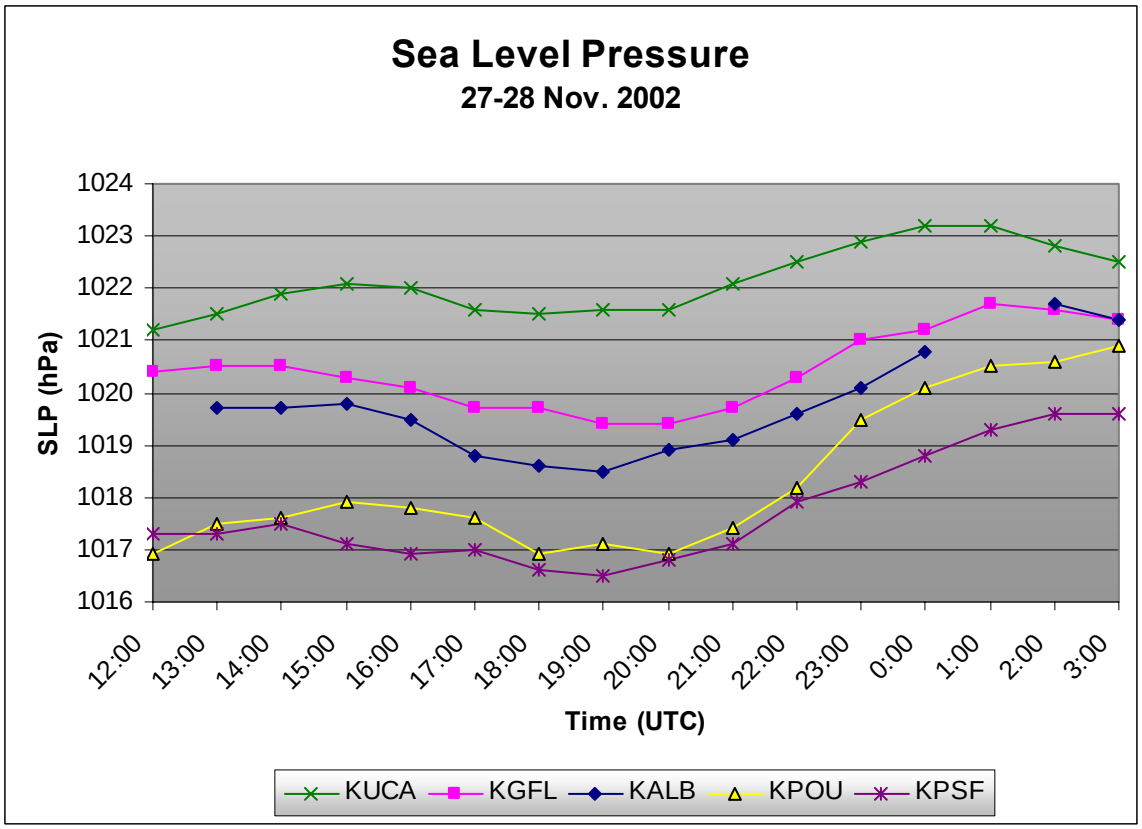

Figure 3.18: Sea level pressure time series (hPa) from 1200 UTC 27 November to 0300 UTC 28 November 2002 for KUCA, KGFL, KALB, KPOU, and KPSF (trace and data point markers according to the legend). (Data source: the University at Albany DEAS archives, with supplemental data provided by the Historical Weather Data Archives of NSSL).

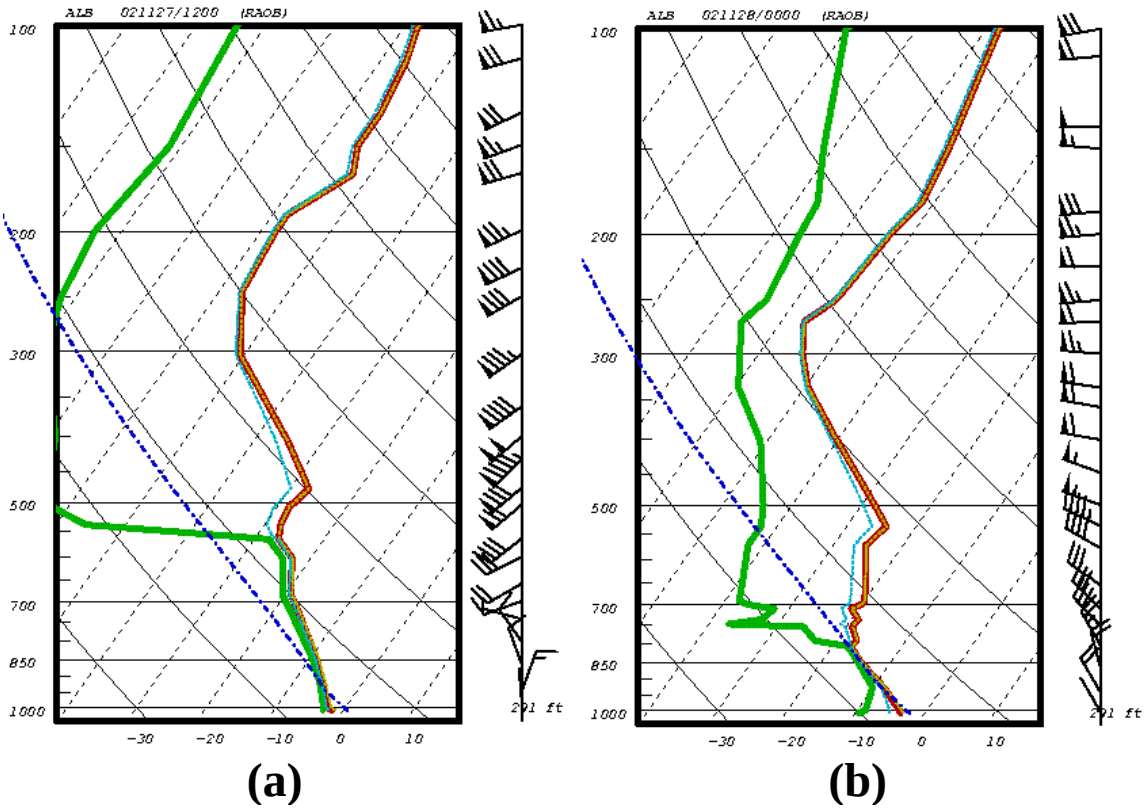

Figure 3.19: Skew *T*–log *p* radiosonde observations at KALY (72518) of air temperature (red line, in °C), dewpoint (green line, in °C), wet-bulb temperature (solid blue line, in °C), and wind (to the right of each sounding; m s^{-1}, with pennant, full barb, and half barb denoting 25, 5, and 2.5 m s^{-1}, respectively) for (a) 1200 UTC 27 November 2002, and (b) 0000 UTC 28 November 2002. (Data source: the University at Albany DEAS archives).

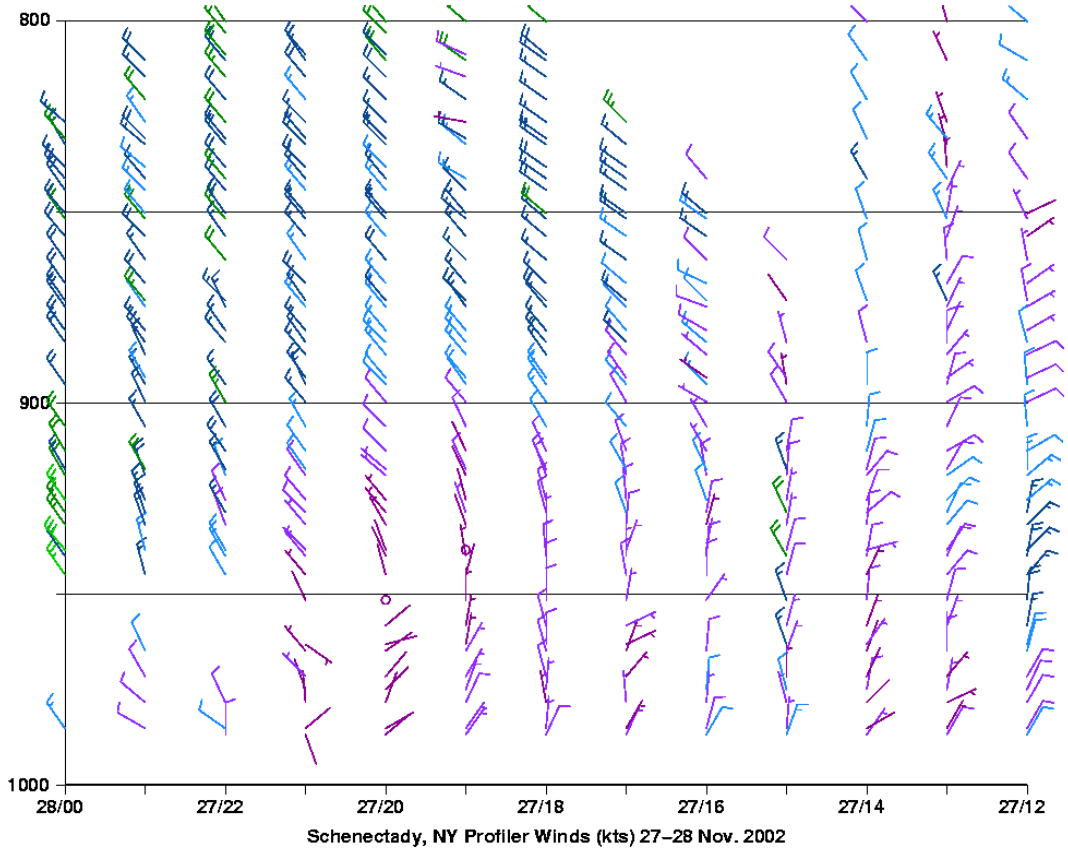

Figure 3.20: Time–height cross section from the Schenectady, NY (KSCH), wind profiler (now defunct; originally part of NPN, established by NOAA). Shown are wind direction and speed (m s^{-1}, with full barb, and half barb denoting 5, and 2.5 m s^{-1}, respectively; barb color proportional to wind speed) from 1200 UTC 27 November to 0000 UTC 28 November 2002. (Data source: NOAA/NPN).

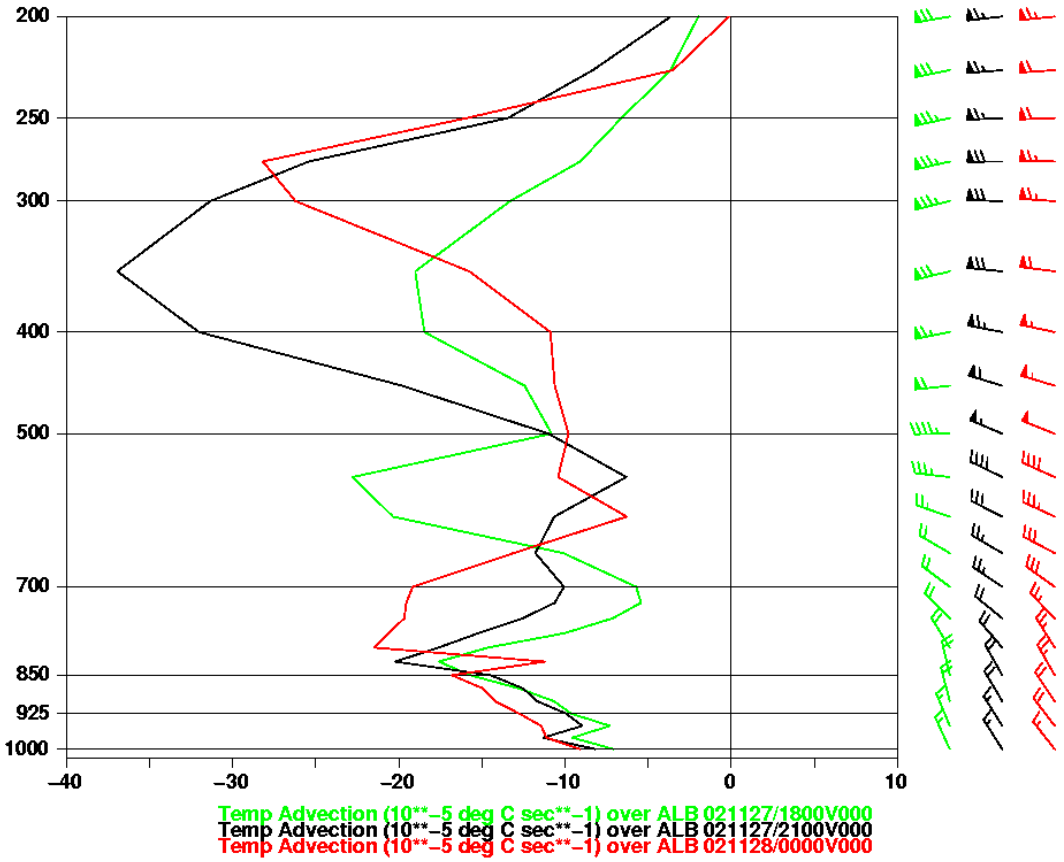

Figure 3.21: Vertical profile (log *p* format) over KALB of horizontal advection of temperature (in 10^{-5} °C s^{-1}) by the wind (m s^{-1}, with pennant, full barb, and half barb denoting 25, 5, and 2.5 m s^{-1}, respectively) at 1800 (green line and barbs), 2100 UTC 27 November 2002 (black line and barbs), and 0000 UTC 28 November 2002 (red line and barbs). (Data source: 0-h gridded, initialized analyses of the 32 km NCEP NARR).

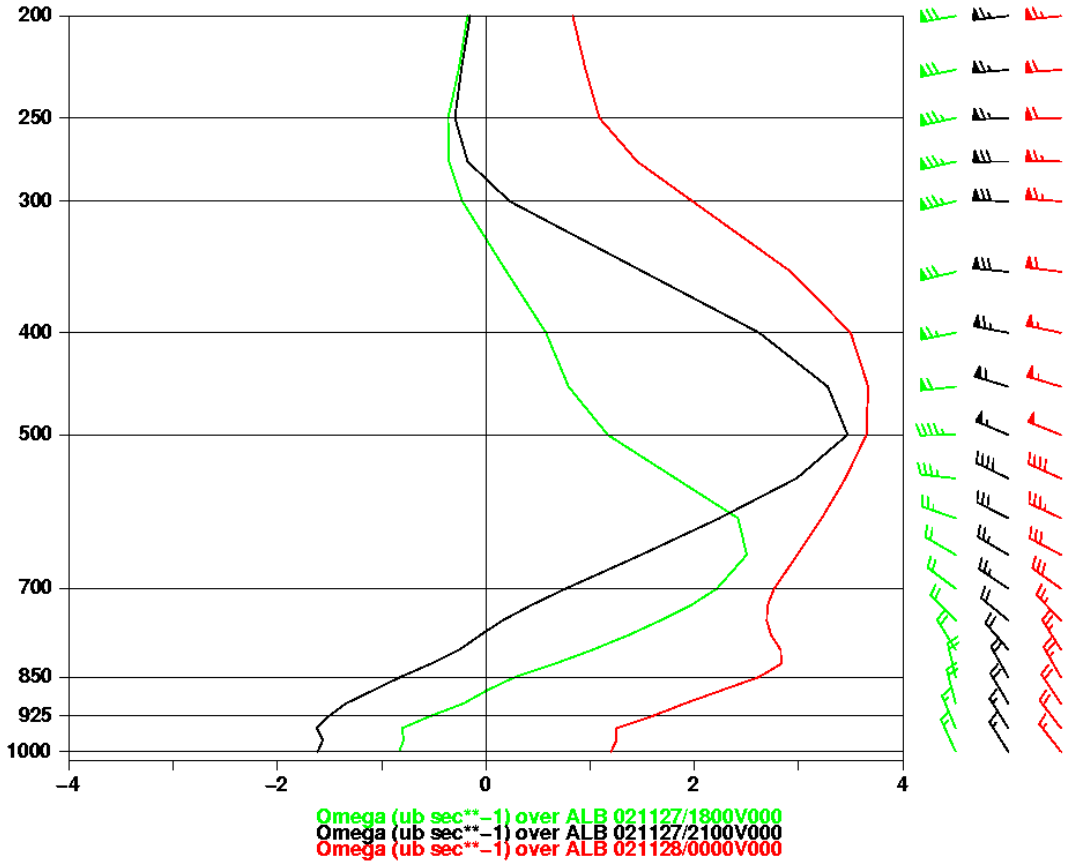

Figure 3.22: As in Fig. 3.21, except for vertical velocity (μb s^{-1}).

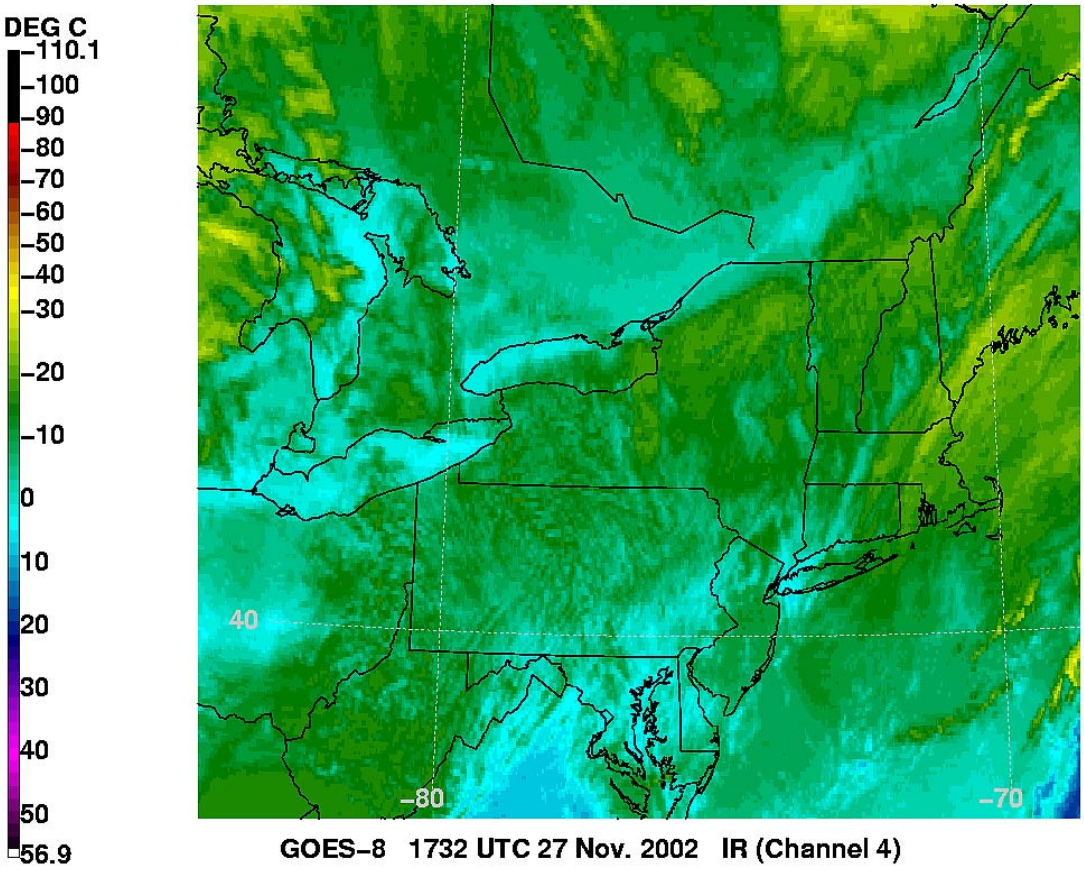

Figure 3.23: Infrared (Channel 4, wavelengths of 10.3–11.5 μm) satellite imagery from the Geostationary Operational Environmental Satellite-8 (GOES-8) at 1732 UTC 27 November 2002. Cloud top temperature (CTT) is shown (in °C shaded according to scale). (Data source: NOAA/CLASS).

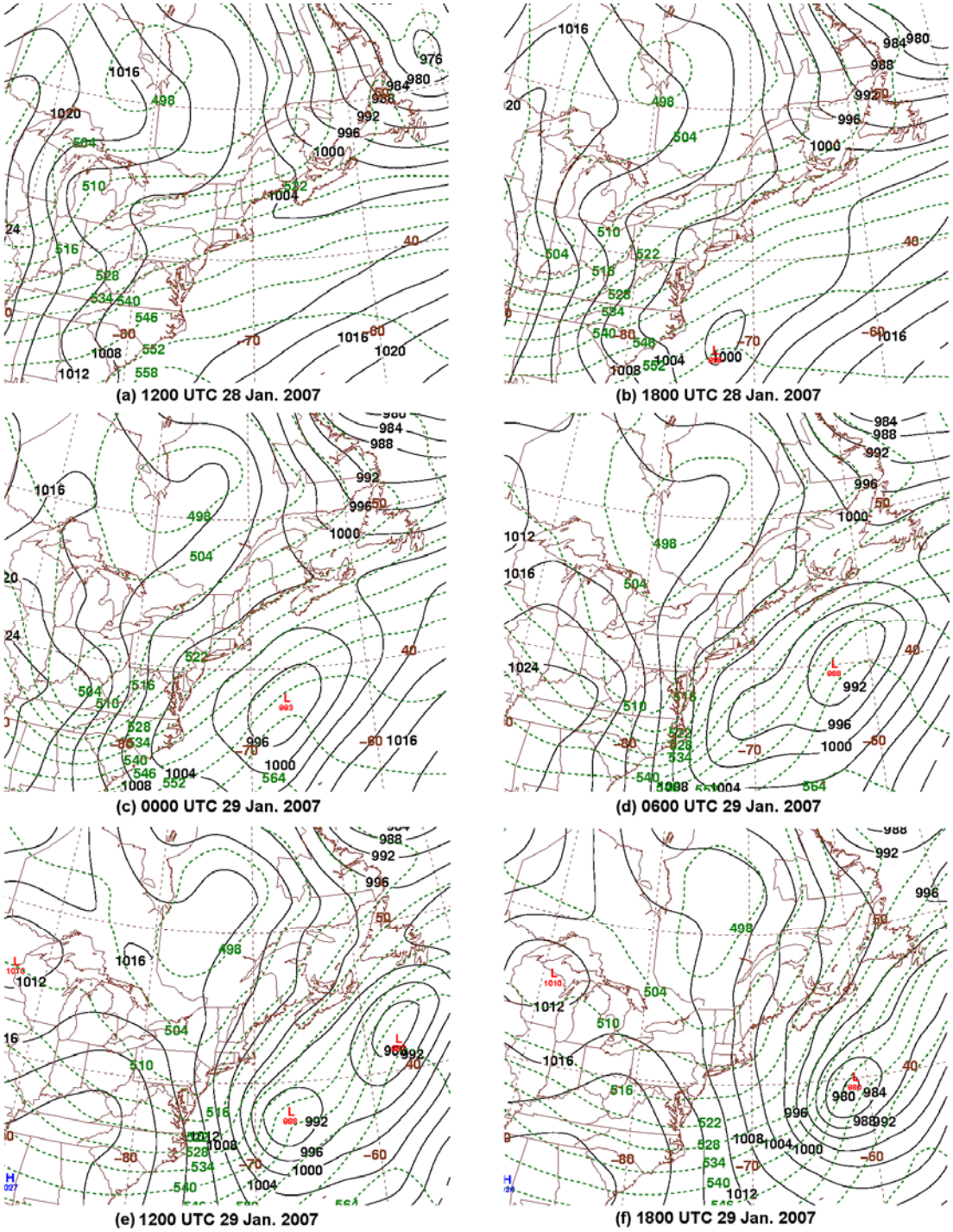

Figure 3.24: As in Fig. 3.7, except for (a) 1200, (b) 1800 UTC 28 January 2007, (c) 0000, (d) 0600, (e) 1200, and (f) 1800 UTC 29 January 2007.

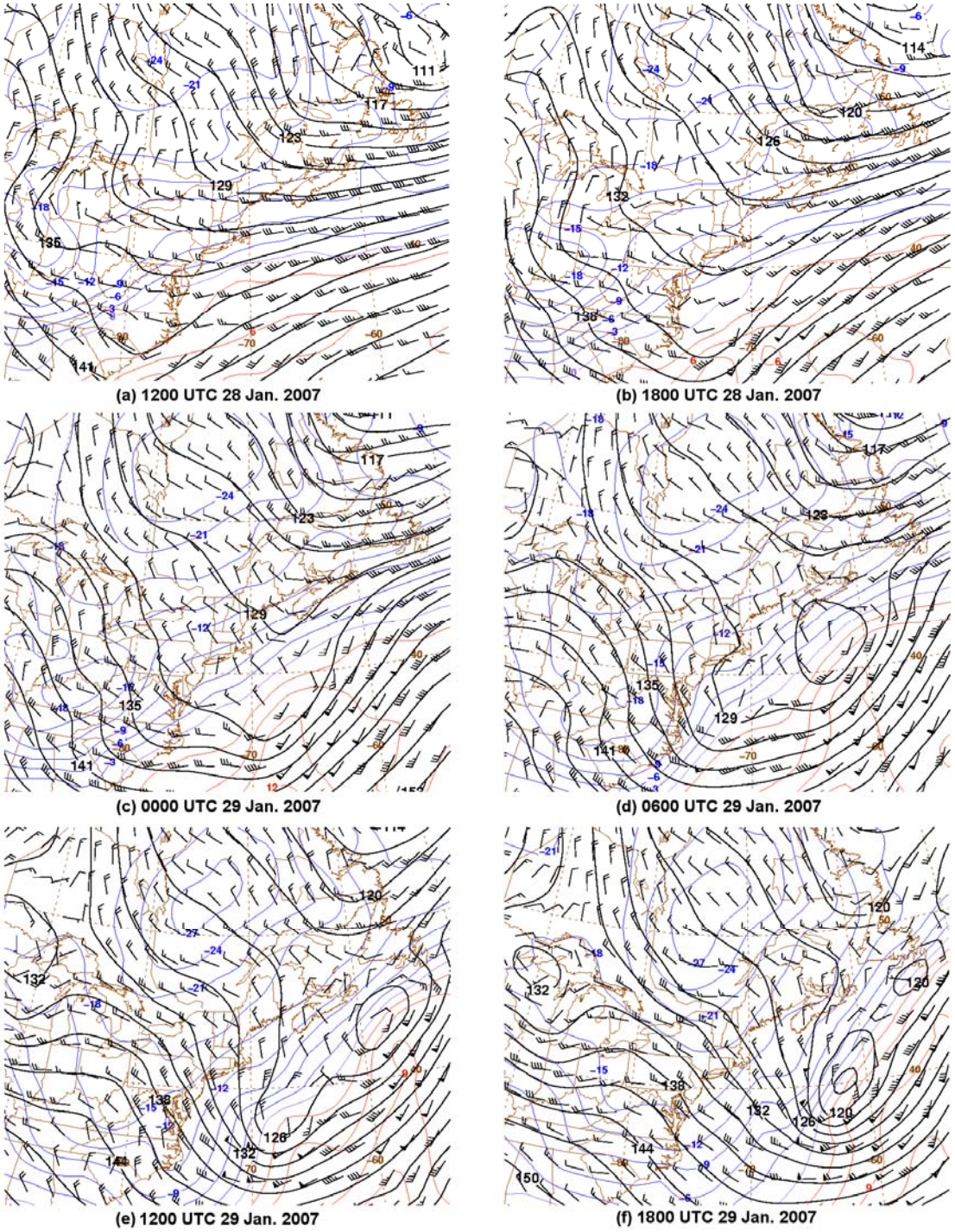

Figure 3.25: As in Fig. 3.8, except for (a) 1200, (b) 1800 UTC 28 January 2007, (c) 0000, (d) 0600, (e) 1200, and (f) 1800 UTC 29 January 2007.

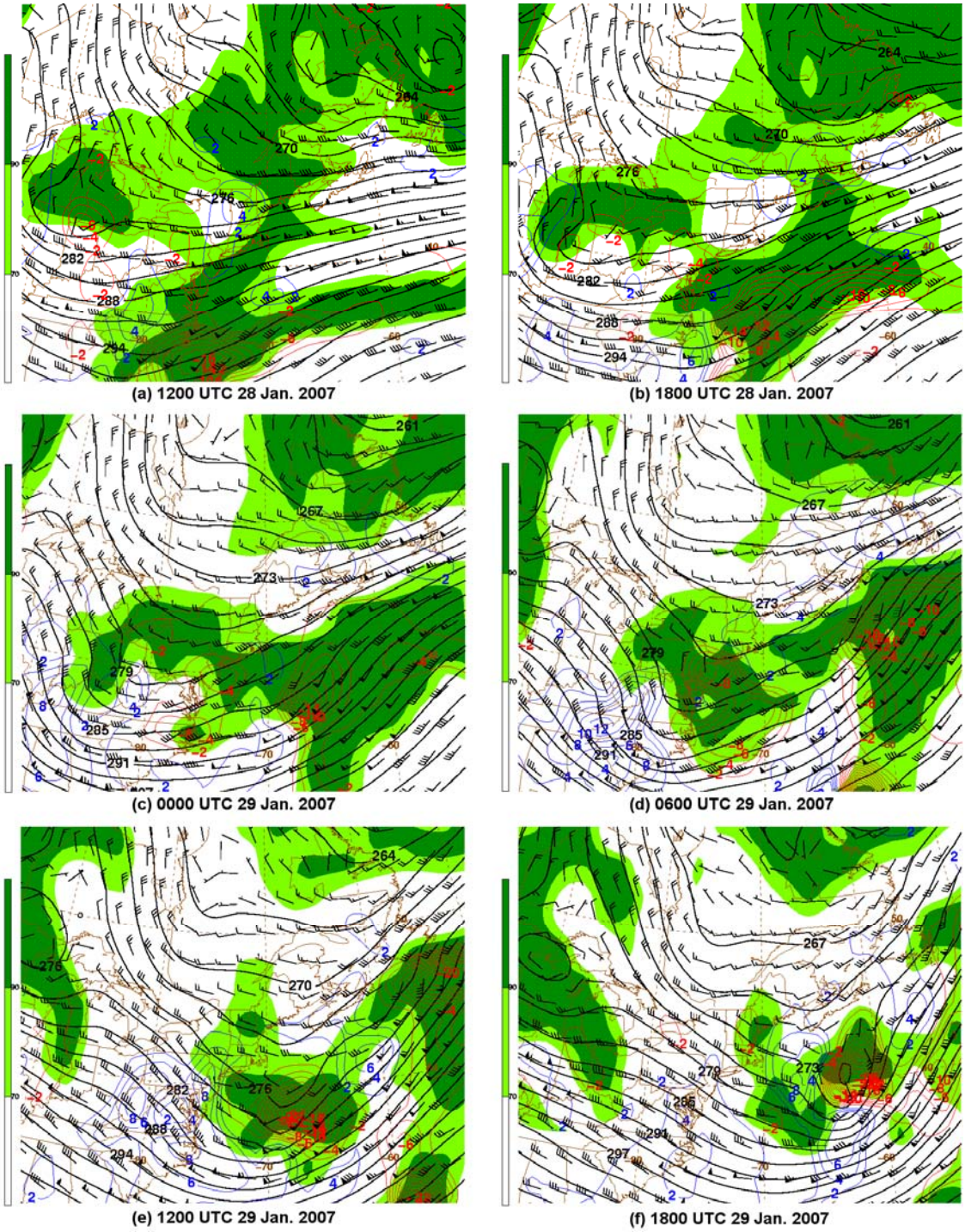

Figure 3.26: As in Fig. 3.9, except for (a) 1200, (b) 1800 UTC 28 January 2007, (c) 0000, (d) 0600, (e) 1200, and (f) 1800 UTC 29 January 2007.

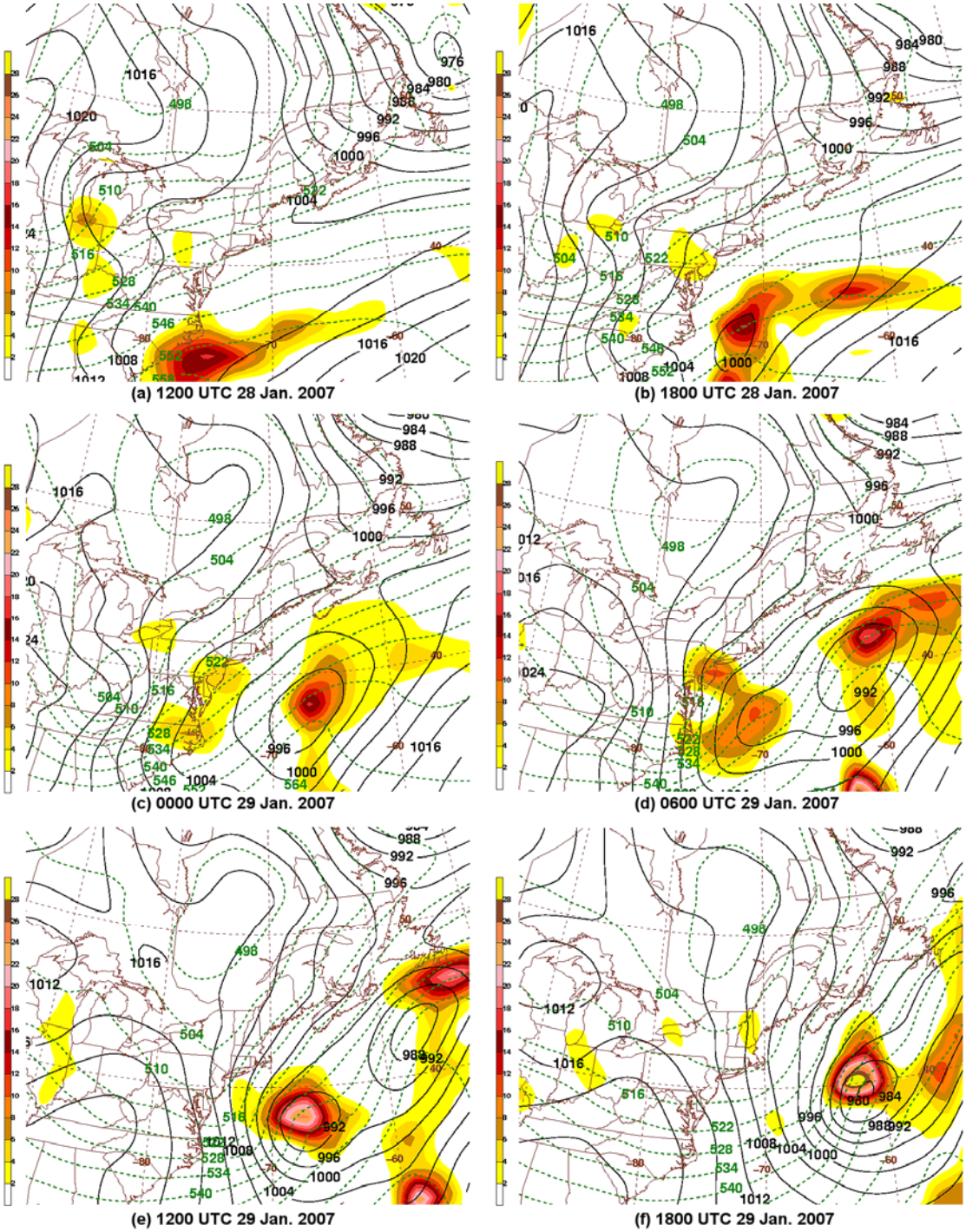

Figure 3.27: As in Fig. 3.10, except for (a) 1200, (b) 1800 UTC 28 January 2007, (c) 0000, (d) 0600, (e) 1200, and (f) 1800 UTC 29 January 2007.

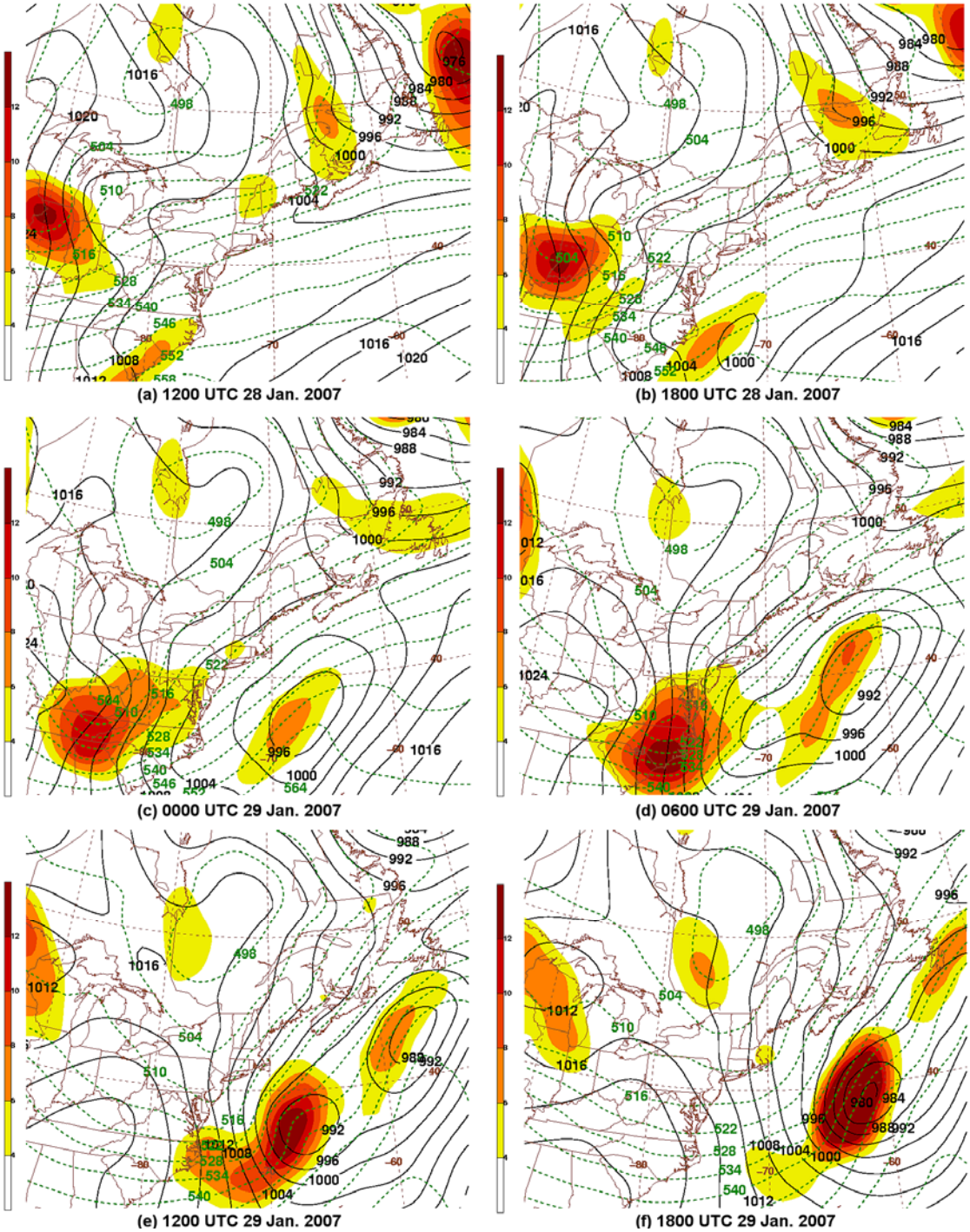

Figure 3.28: As in Fig. 3.11, except for (a) 1200, (b) 1800 UTC 28 January 2007, (c) 0000, (d) 0600, (e) 1200, and (f) 1800 UTC 29 January 2007.

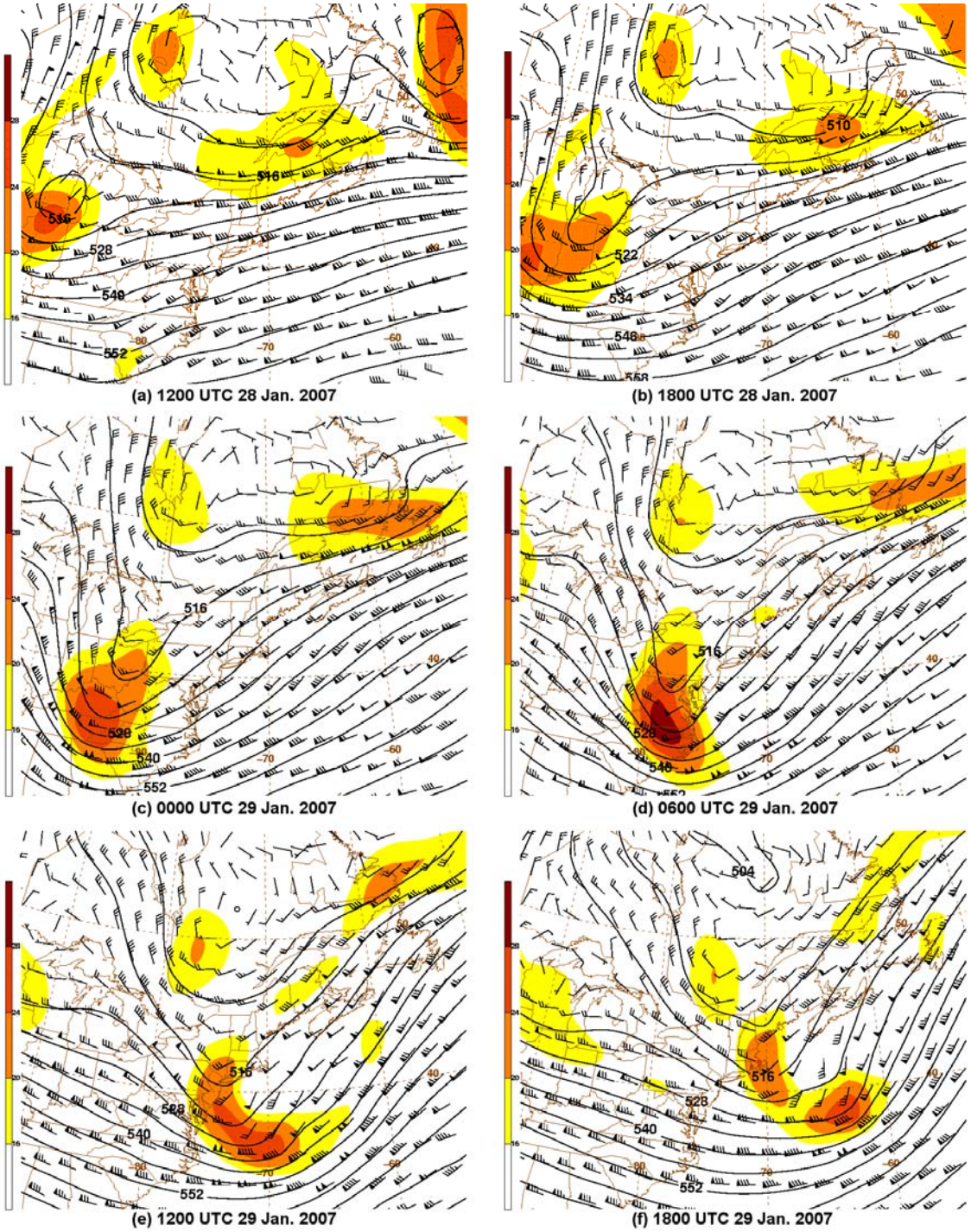

Figure 3.29: As in Fig. 3.12, except for (a) 1200, (b) 1800 UTC 28 January 2007, (c) 0000, (d) 0600, (e) 1200, and (f) 1800 UTC 29 January 2007.

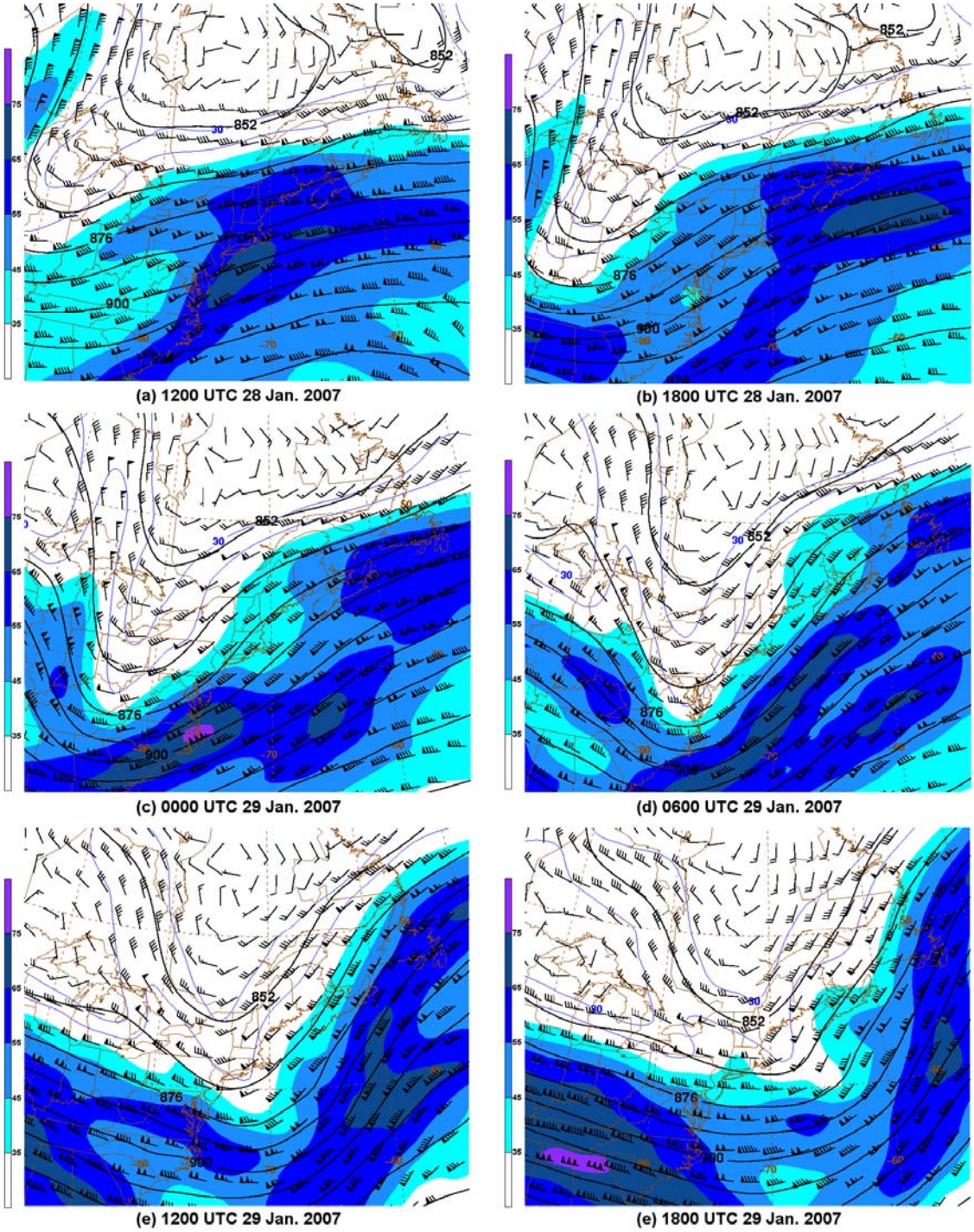

Figure 3.30: As in Fig. 3.13, except for (a) 1200, (b) 1800 UTC 28 January 2007, (c) 0000, (d) 0600, (e) 1200, and (f) 1800 UTC 29 January 2007.

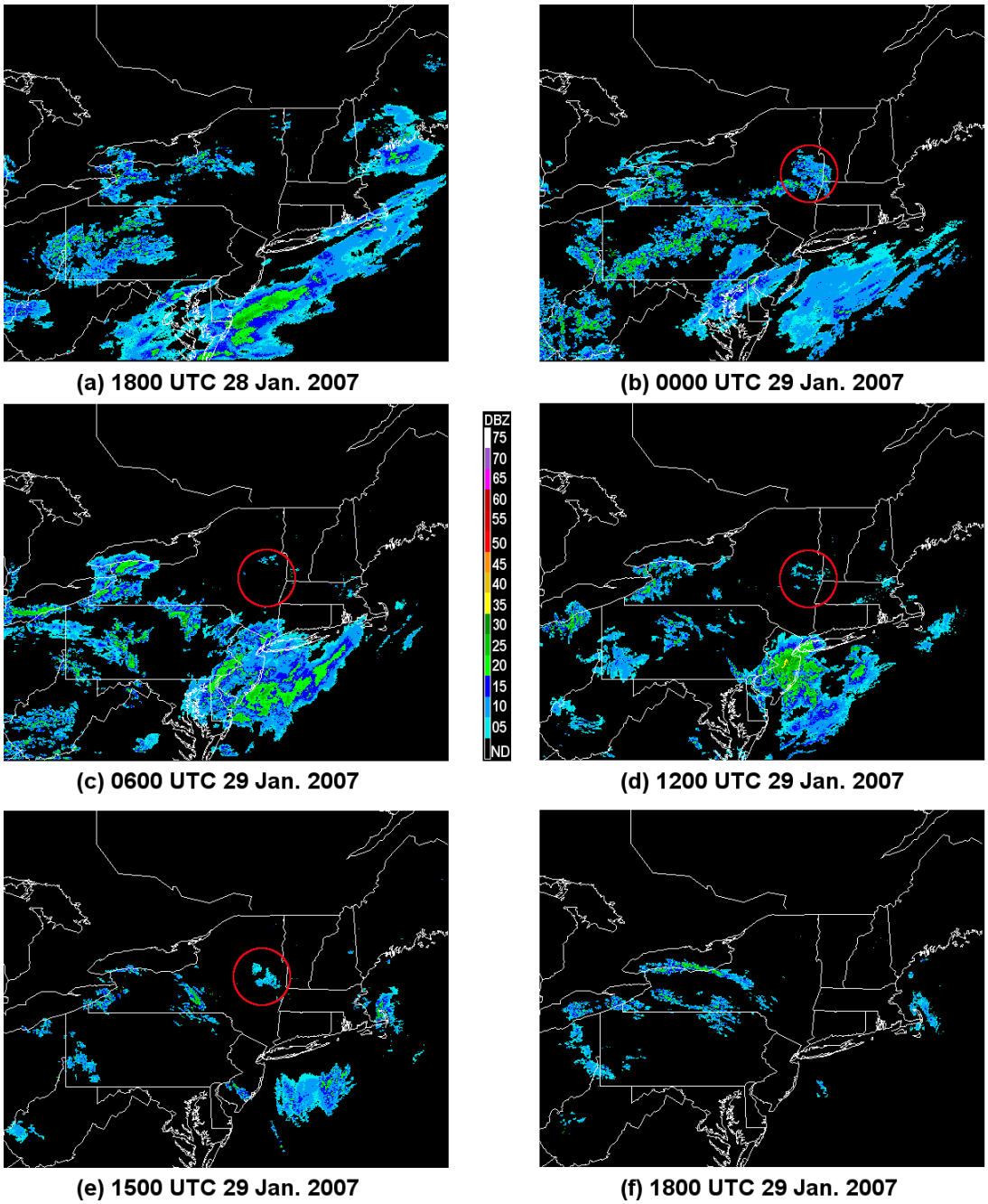

Figure 3.31: As in Fig. 3.14, except for (a) 1800 UTC 28 January 2007, (b) 0000, (c) 0600, (d) 1200, (e) 1500, and (f) 1800 UTC 29 January 2007. Precipitation related to MHC is circled in red.

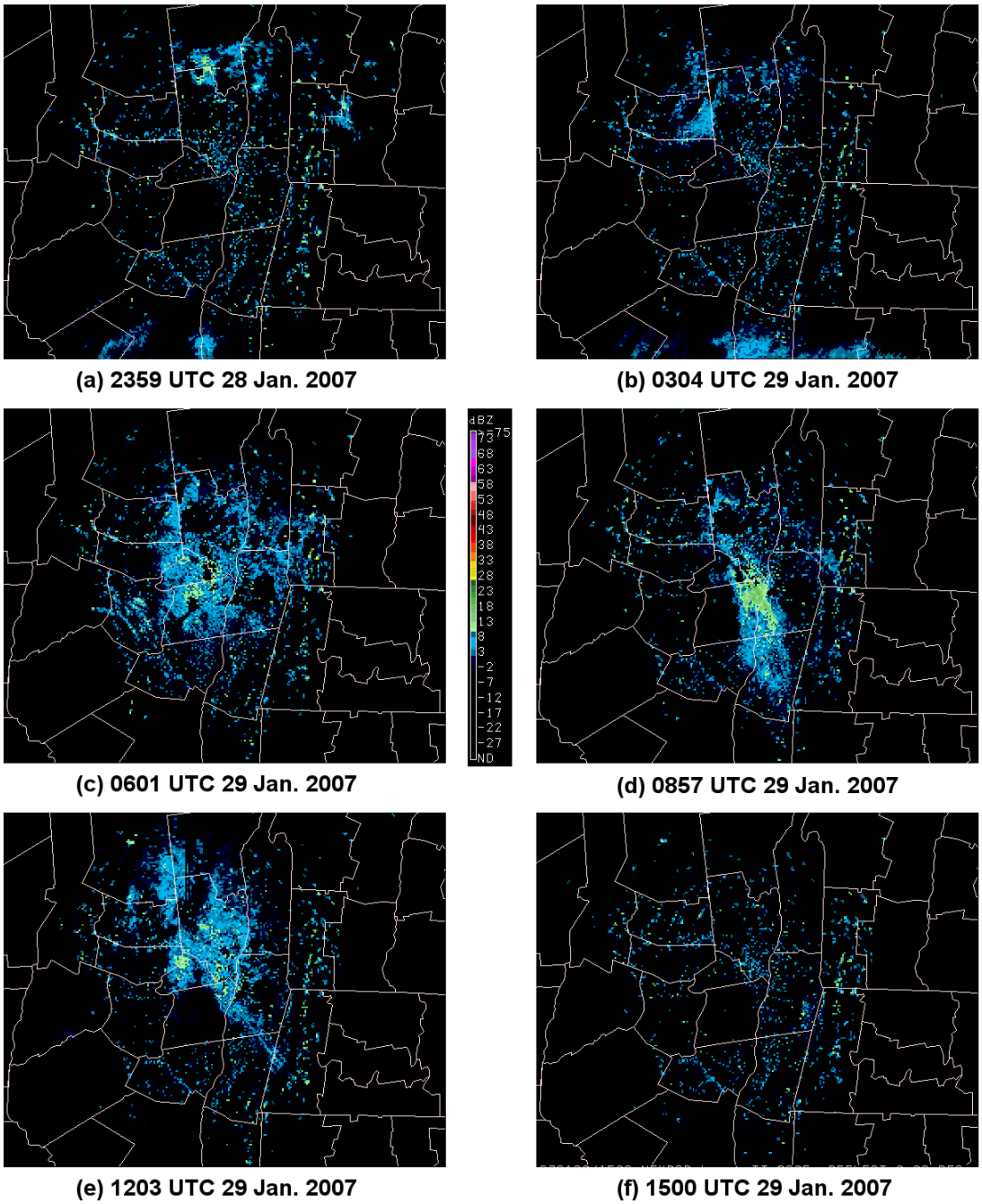

Figure 3.32: As in Fig. 3.15, except for (a) 2359 UTC 28 January 2007, (b) 0304, (c) 0601, (d), 0857, (e) 1203, and (f) 1500 UTC 29 January 2007.

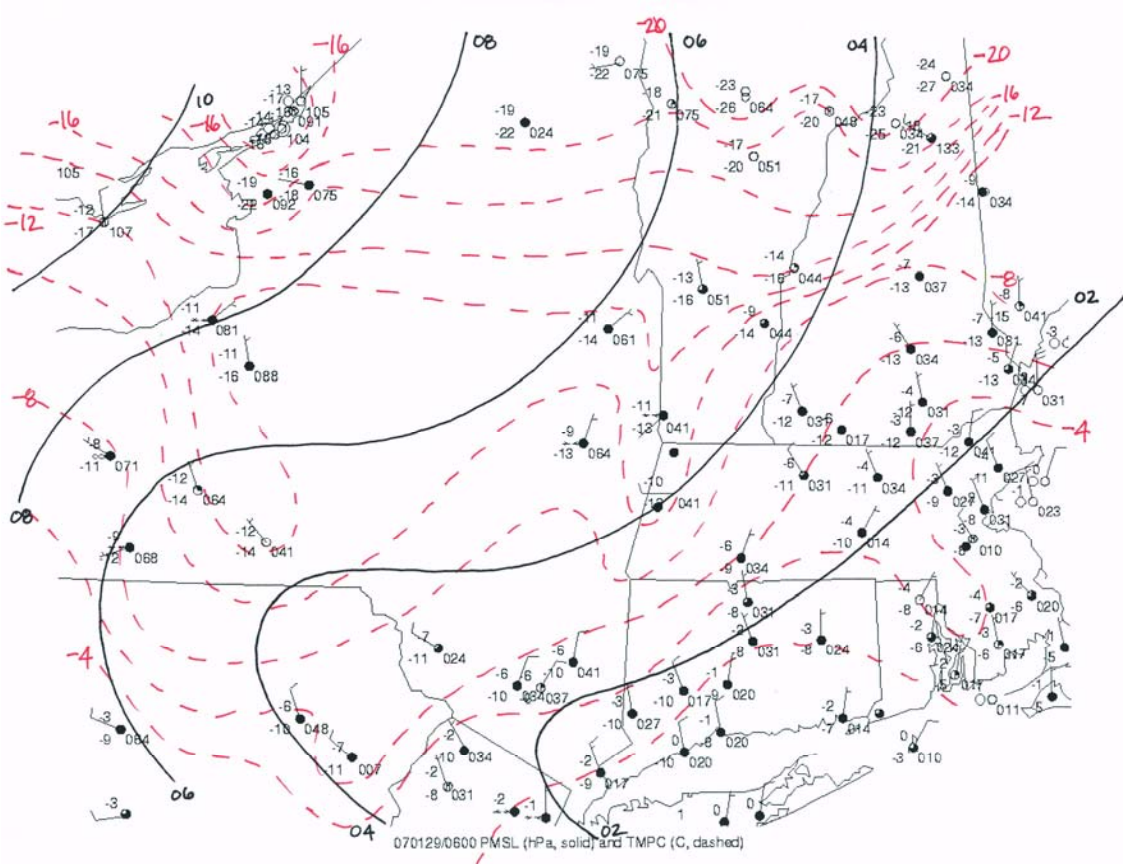

Figure 3.33: As in Fig. 3.16, except for 0600 UTC 29 January 2007.

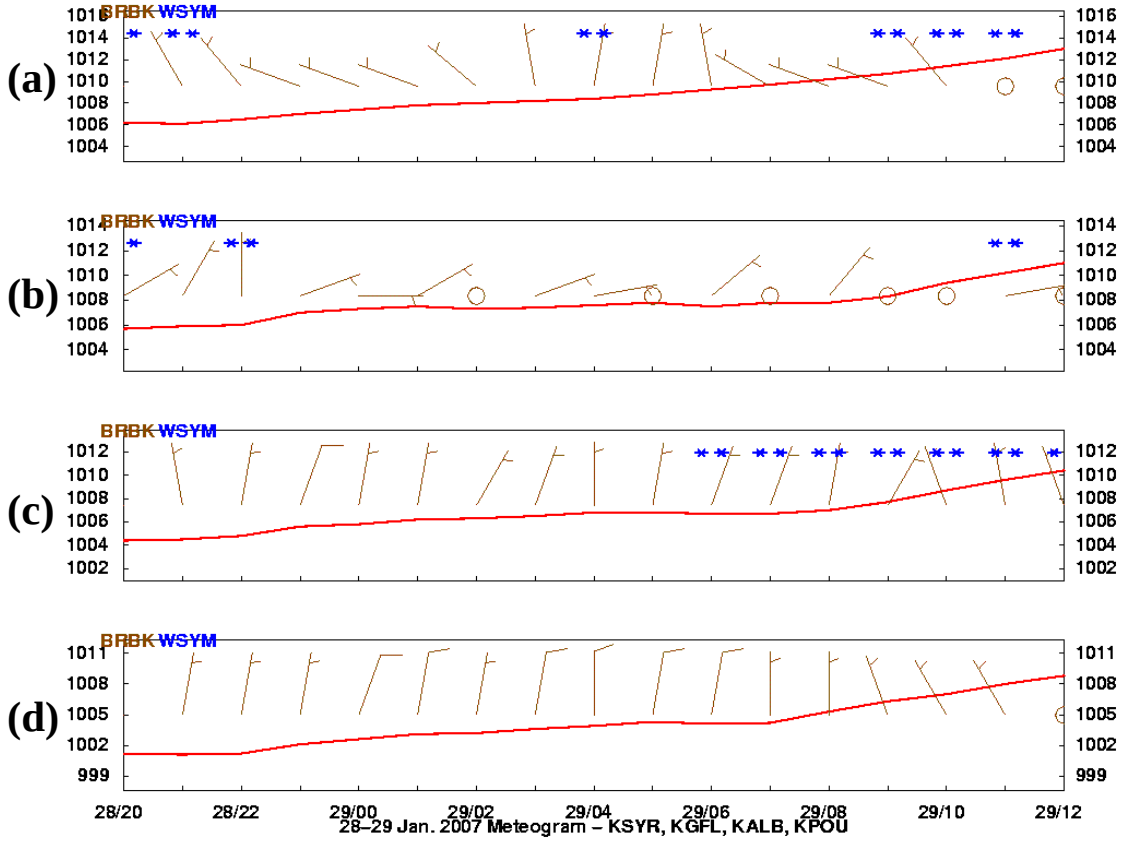

Figure 3.34: As in Fig. 3.17, except from 2000 UTC 28 January to 1200 UTC 29 January 2007 for (a) KSYR, (b) KGFL, (c) KALB and (d) KPOU.

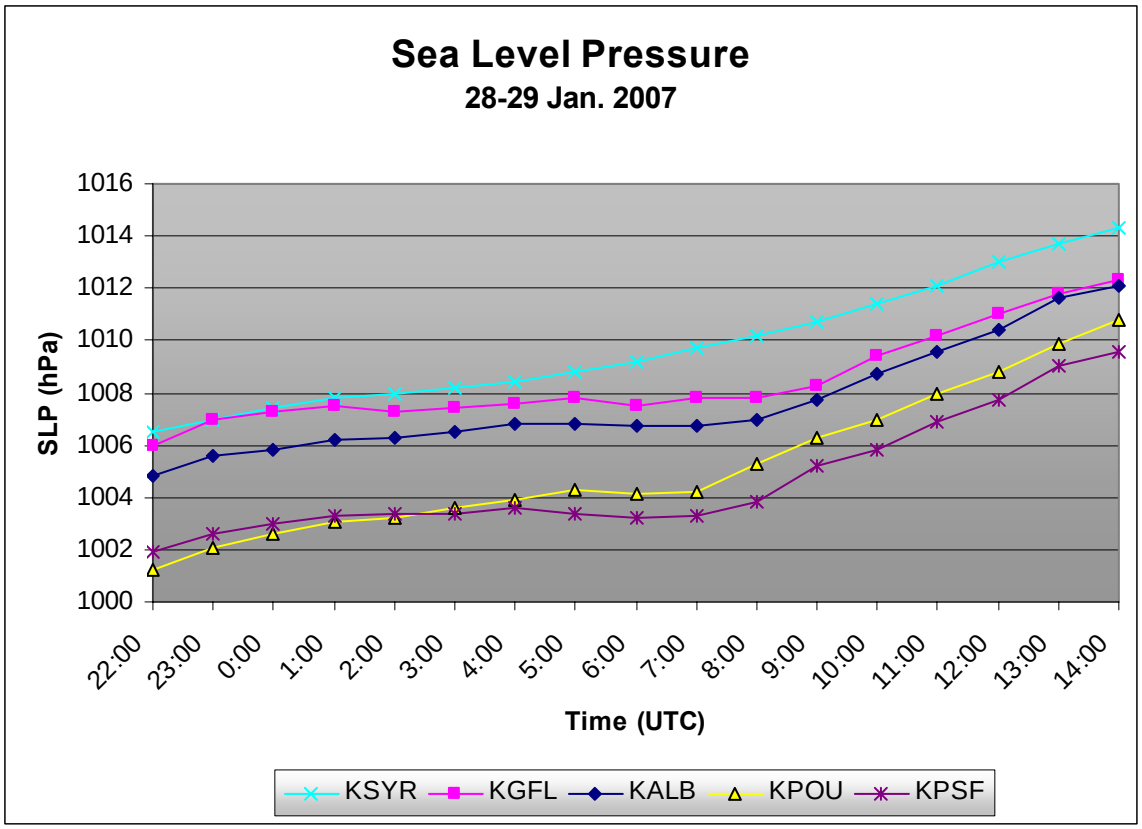

Figure 3.35: As in Fig. 3.18, except from 2200 UTC 28 January to 1400 UTC 29 January 2007 for KSYR, KGFL, KALB, KPOU, and KSPF. (Data source: University at Albany DEAS archives).

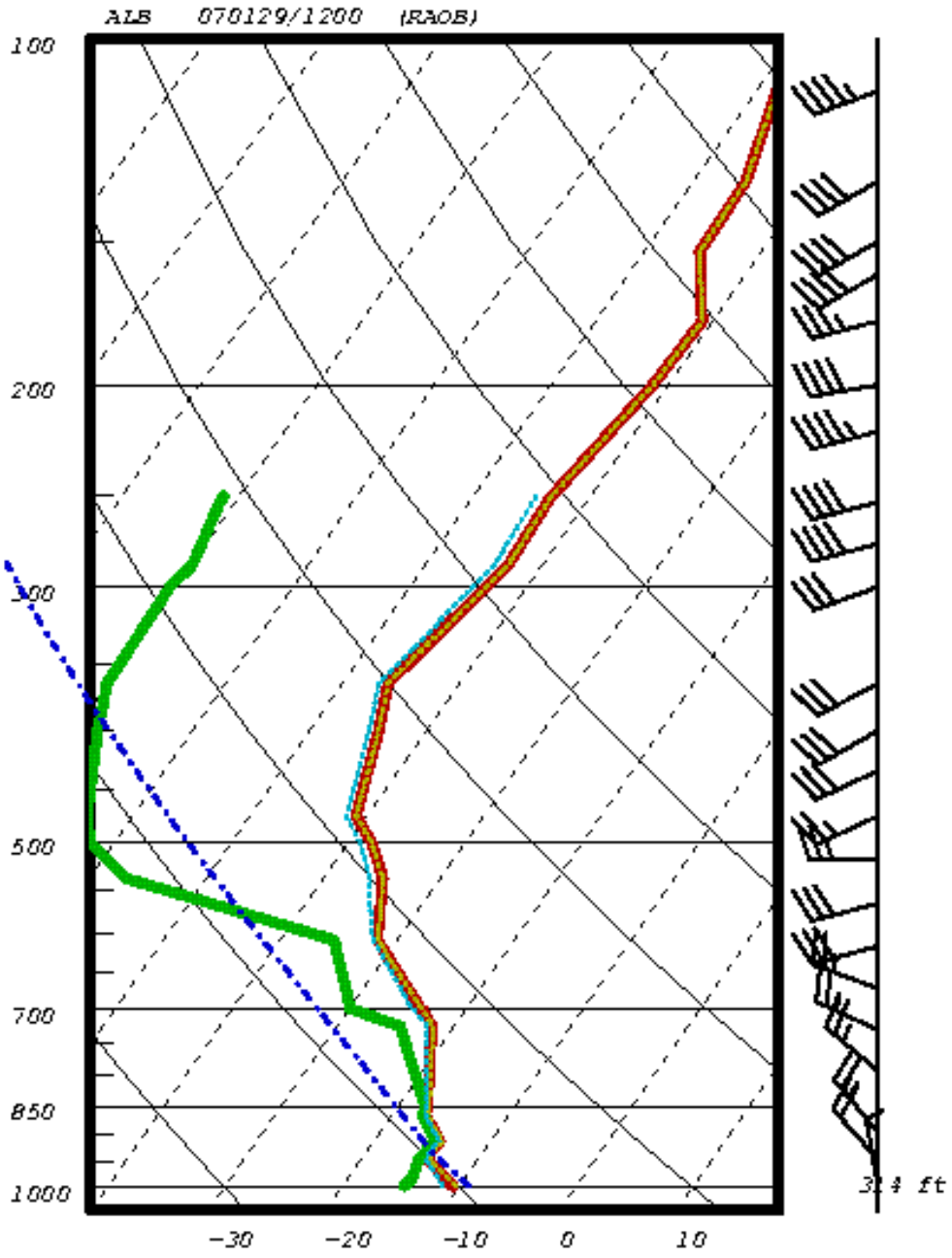

Figure 3.36: As in Fig. 3.19, except for 1200 UTC 29 January 2007.

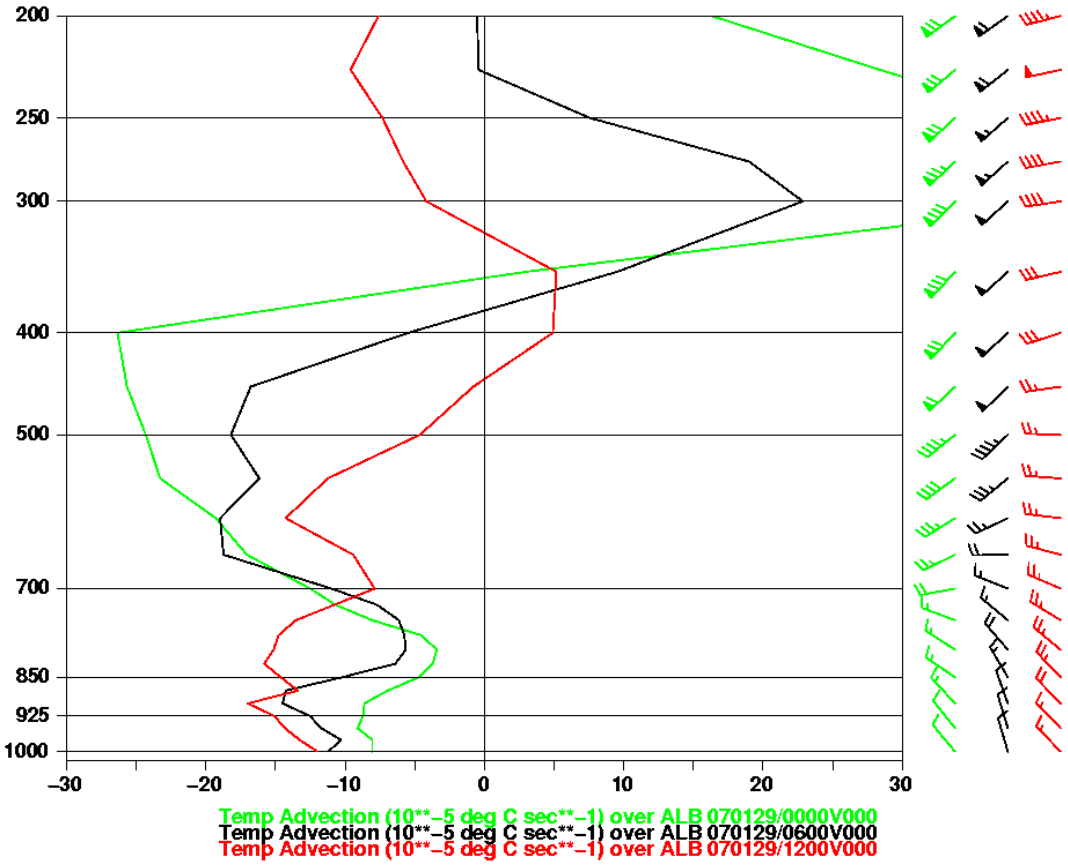

Figure 3.37: As in Fig. 3.21, except for 0000 (green line and barbs), 0600 (black line and barbs), and 1200 UTC 29 January 2007 (red line and barbs).

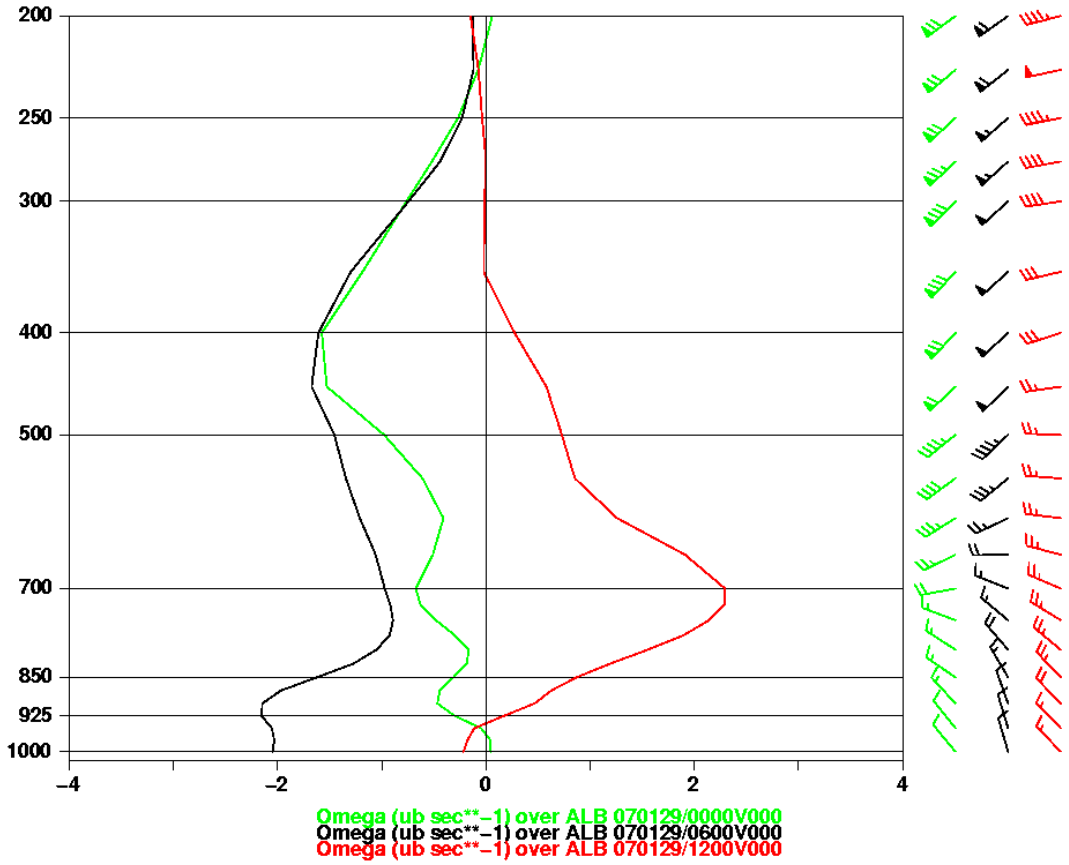

Figure 3.38: As in Fig. 3.22, except for 0000 (green line and barbs), 0600 (black line and barbs), and 1200 UTC 29 January 2007 (red line and barbs).

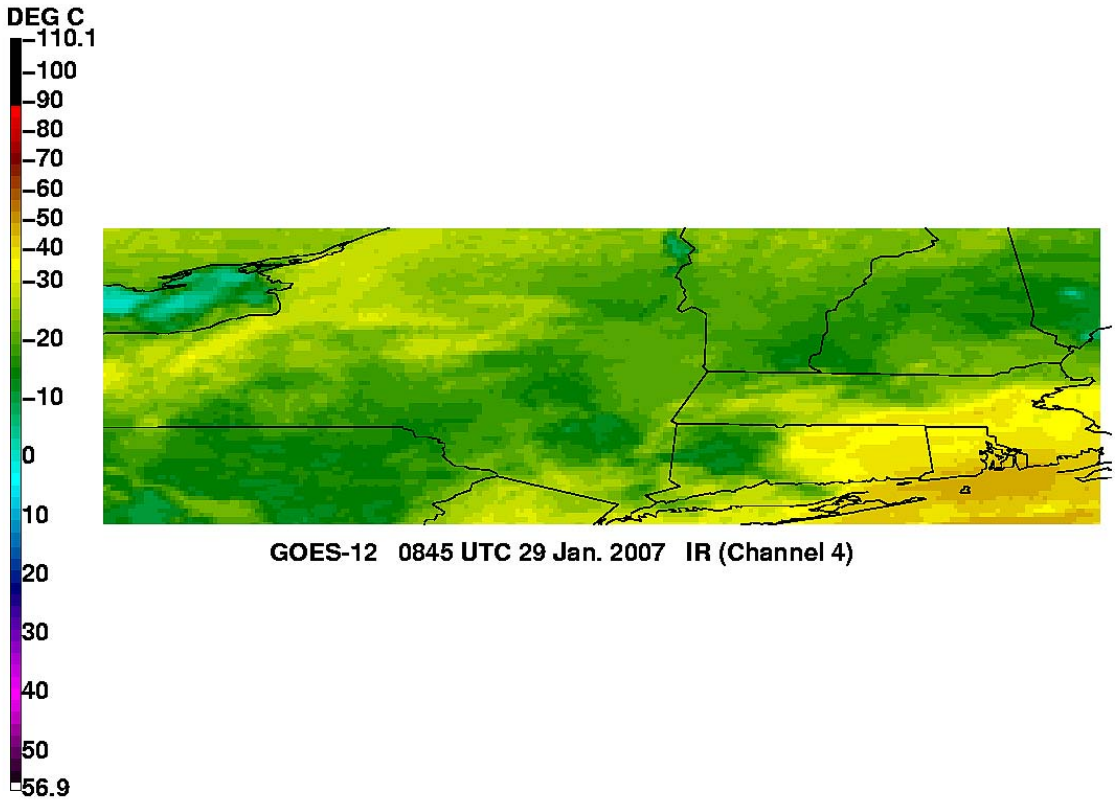

Figure 3.39: As in Fig. 3.23, except from GOES-12 at 0845 UTC 29 January 2007.

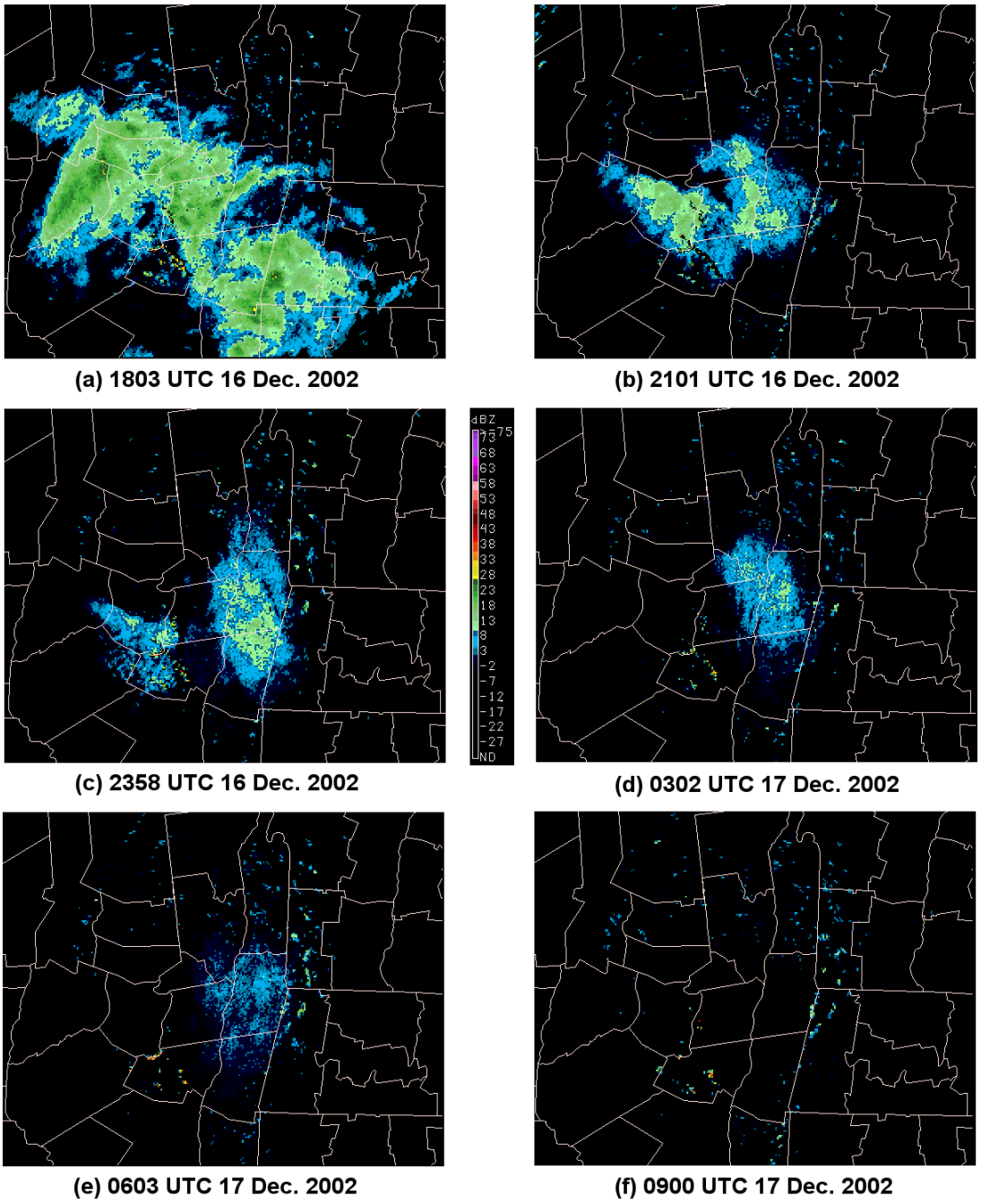

Figure 3.40: As in Fig. 3.15, except for (a) 1803, (b) 2101, (c) 2358 UTC 16 December 2002, (d) 0302, (e) 0603, and (f) 0900 UTC 17 December 2002.

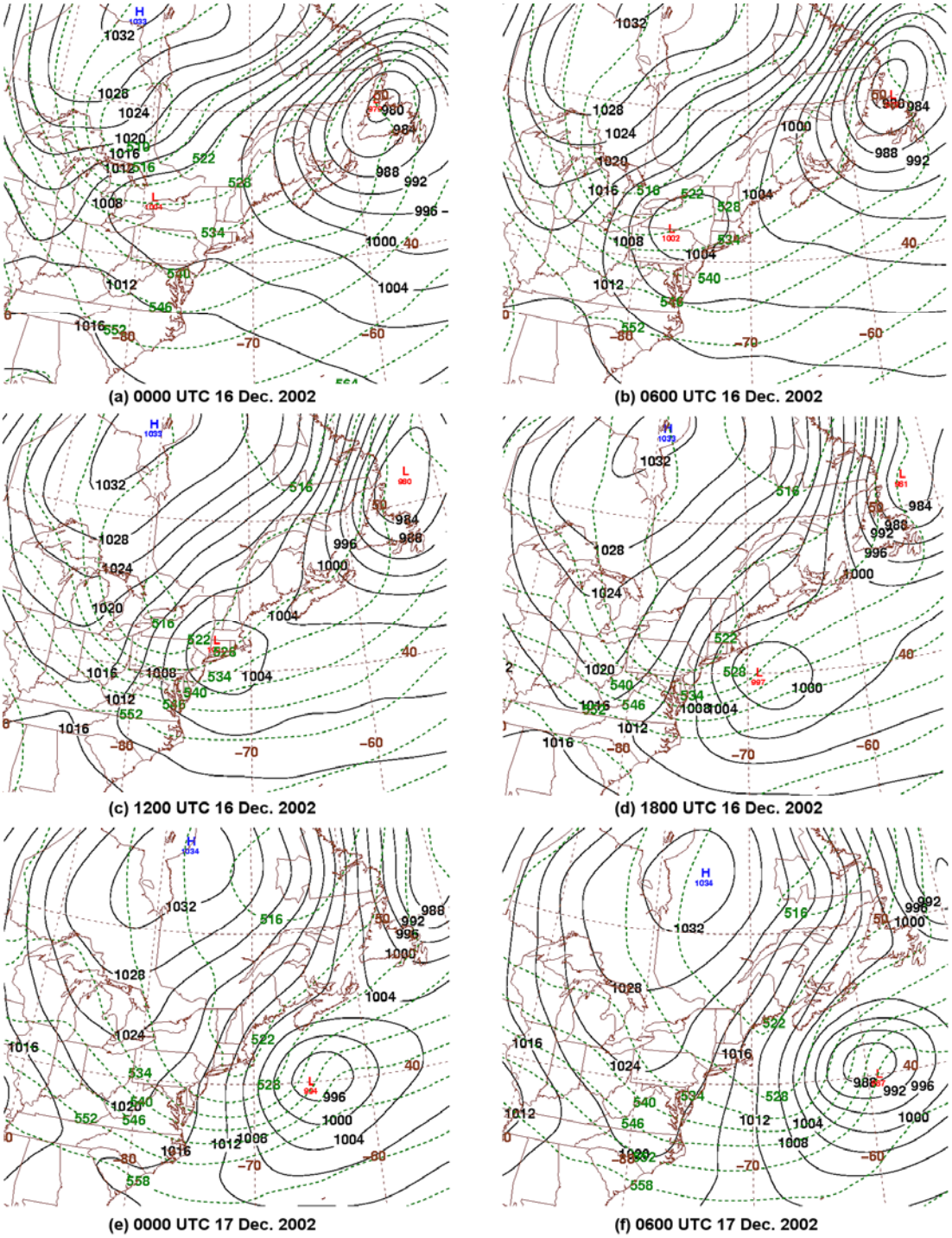

Figure 3.41: As in Fig. 3.7, except for (a) 0000, (b) 0600, (c) 1200, (d) 1800 UTC 16 December 2002, (e) 0000, and (f) 0600 UTC 17 December 2002.

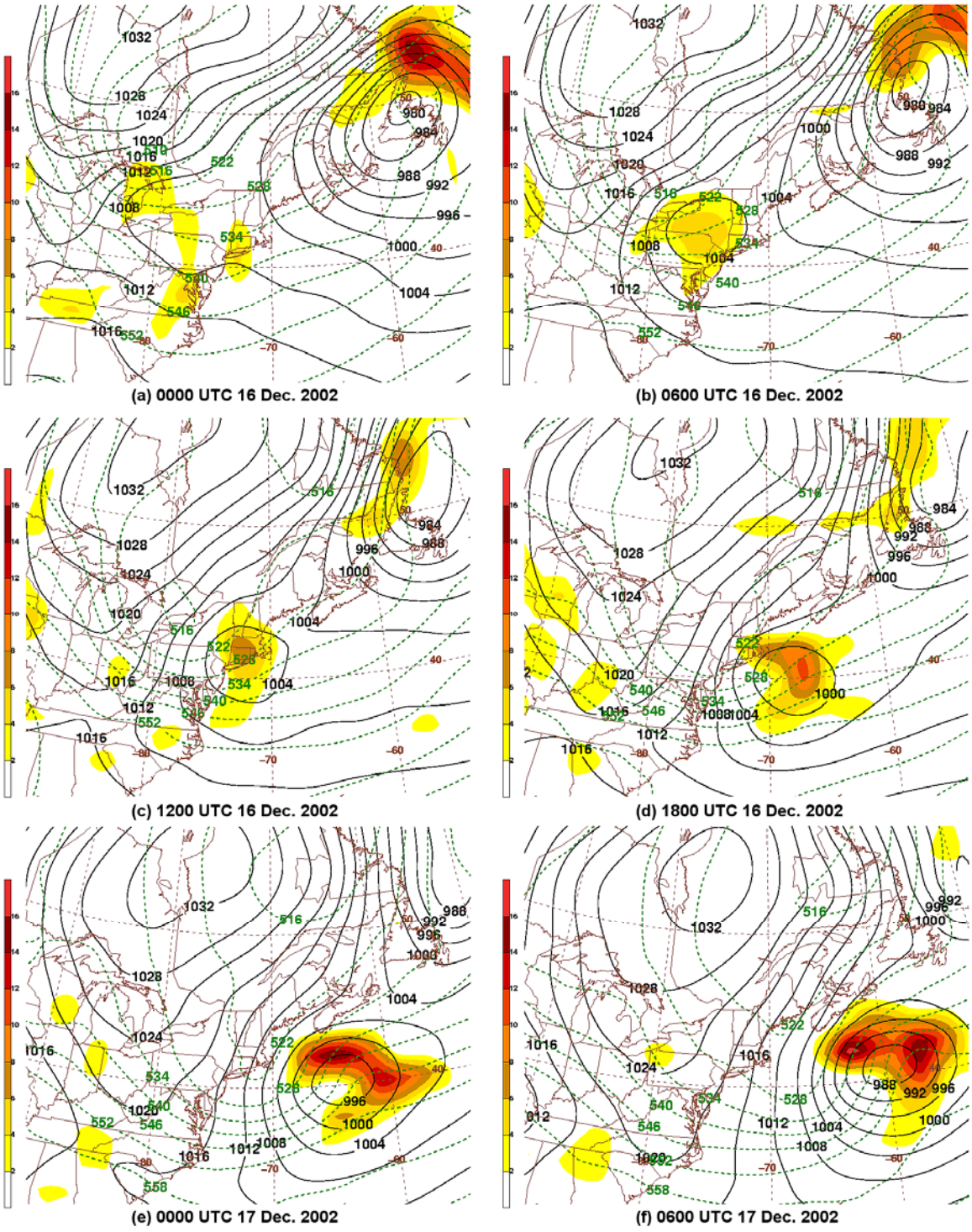

Figure 3.42: As in Fig. 3.10, except for (a) 0000, (b) 0600, (c) 1200, (d) 1800 UTC 16 December 2002, (e) 0000, and (f) 0600 UTC 17 December 2002.

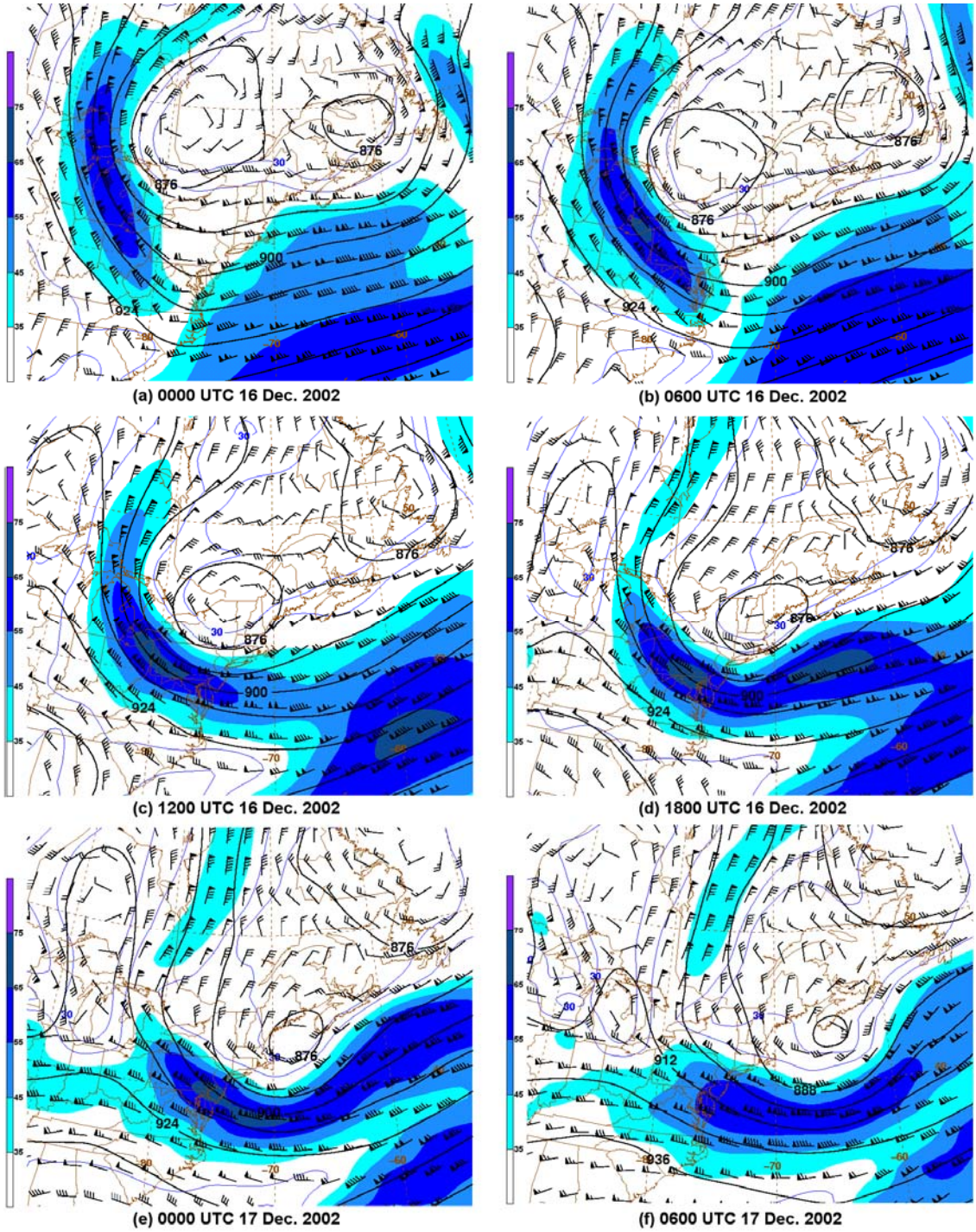

Figure 3.43: As in Fig. 3.13, except for (a) 0000, (b) 0600, (c) 1200, (d) 1800 UTC 16 December 2002, (e) 0000, and (f) 0600 UTC 17 December 2002.

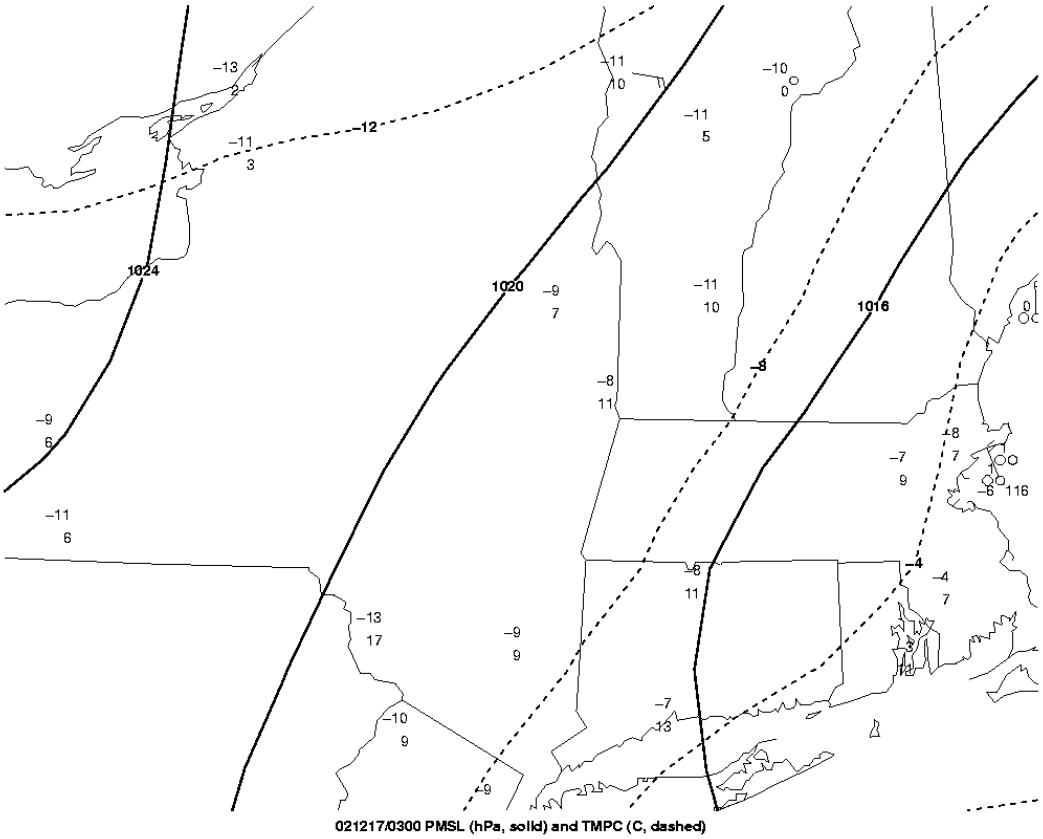

Figure 3.44: Regional surface analysis for eastern New York and New England at 0300 UTC 17 December 2002. Isobars (solid) every 4 hPa. Isotherms (dashed) every 4°C. Temperature (°C) is plotted above visibility at several stations; missing station data have been omitted. (Data source: the University at Albany DEAS archives, with supplemental data provided by the Historical Weather Data Archives of NSSL).

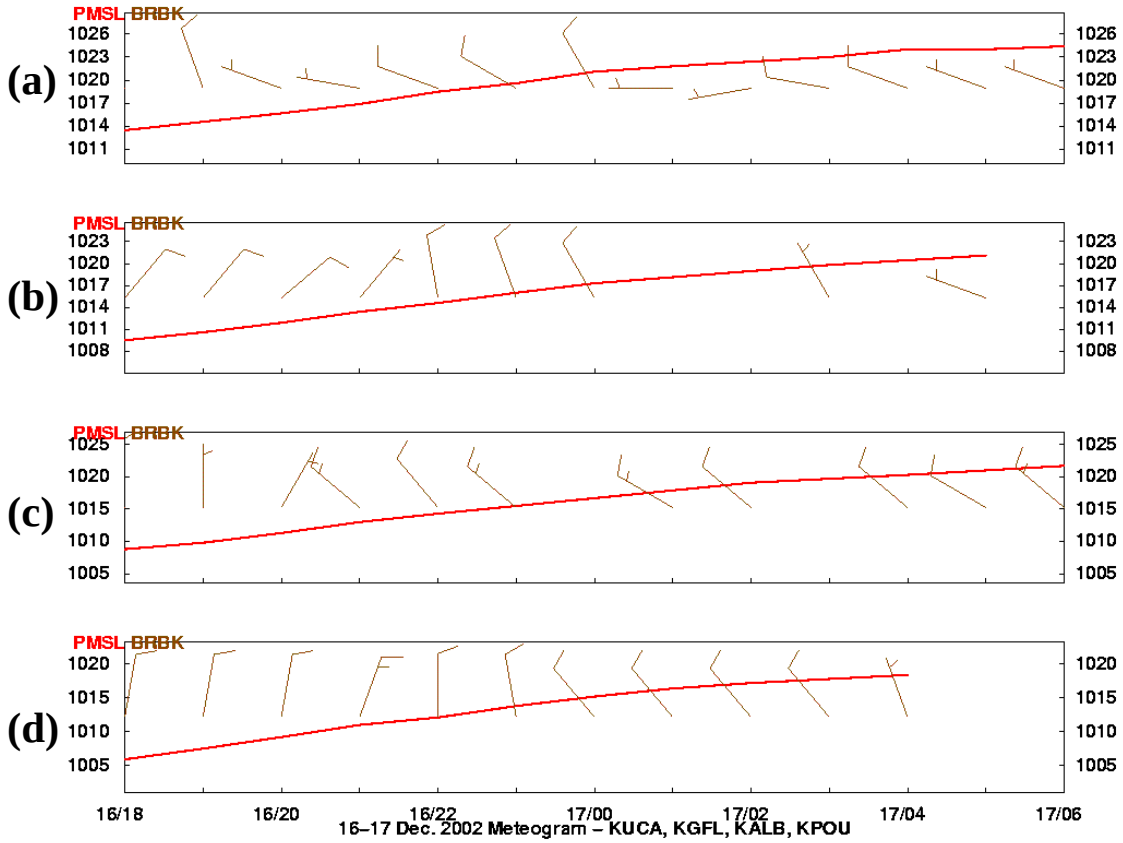

Figure 3.45: As in Fig. 3.17, except from 1800 UTC 16 December to 0600 UTC 17 December 2002. (Data source: the University at Albany DEAS archives, with supplemental data provided by the Historical Weather Data Archives of NSSL).

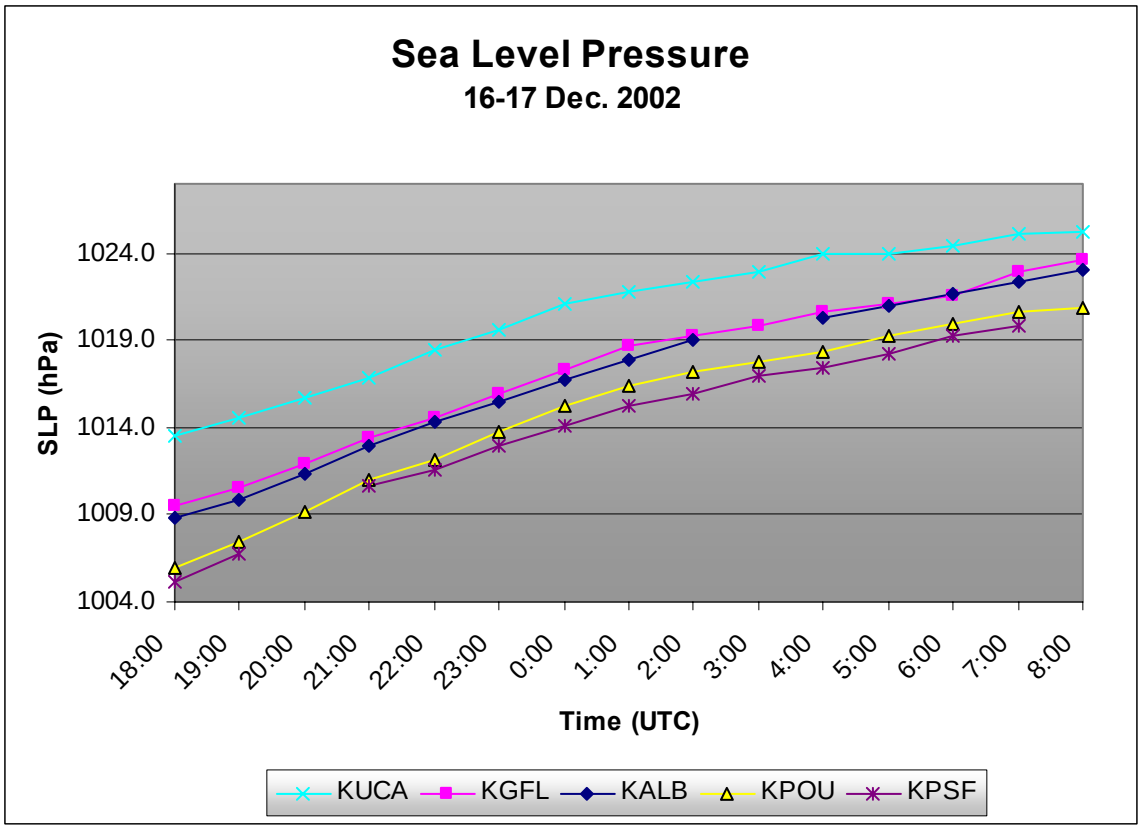

Figure 3.46: As in Fig. 3.18, except from 1800 UTC 16 December to 0800 UTC 17 December 2002).

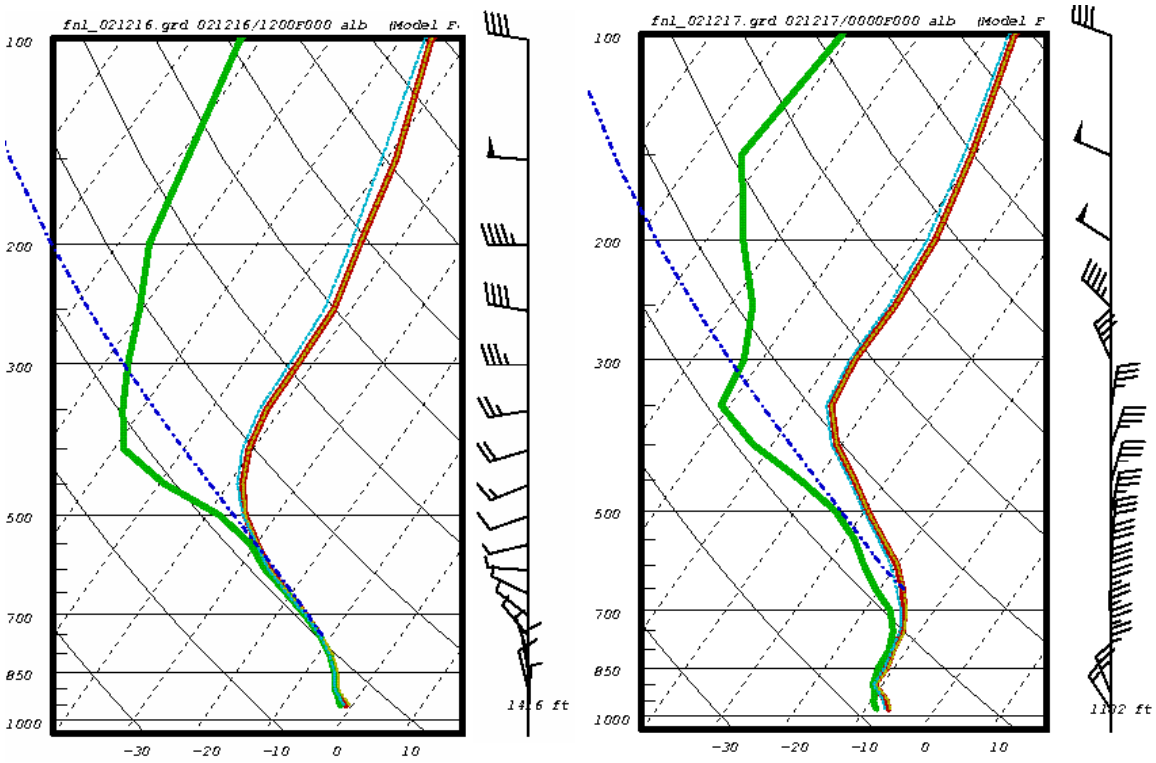

(a) **(b)**

Figure 3.47: As in Fig. 3.19, except for (a) 1200 UTC 16 December 2002 and (b) 0000 UTC 17 December 2002. (Data source: 0-h gridded, initialized 1.0° NCEP GFS analyses).

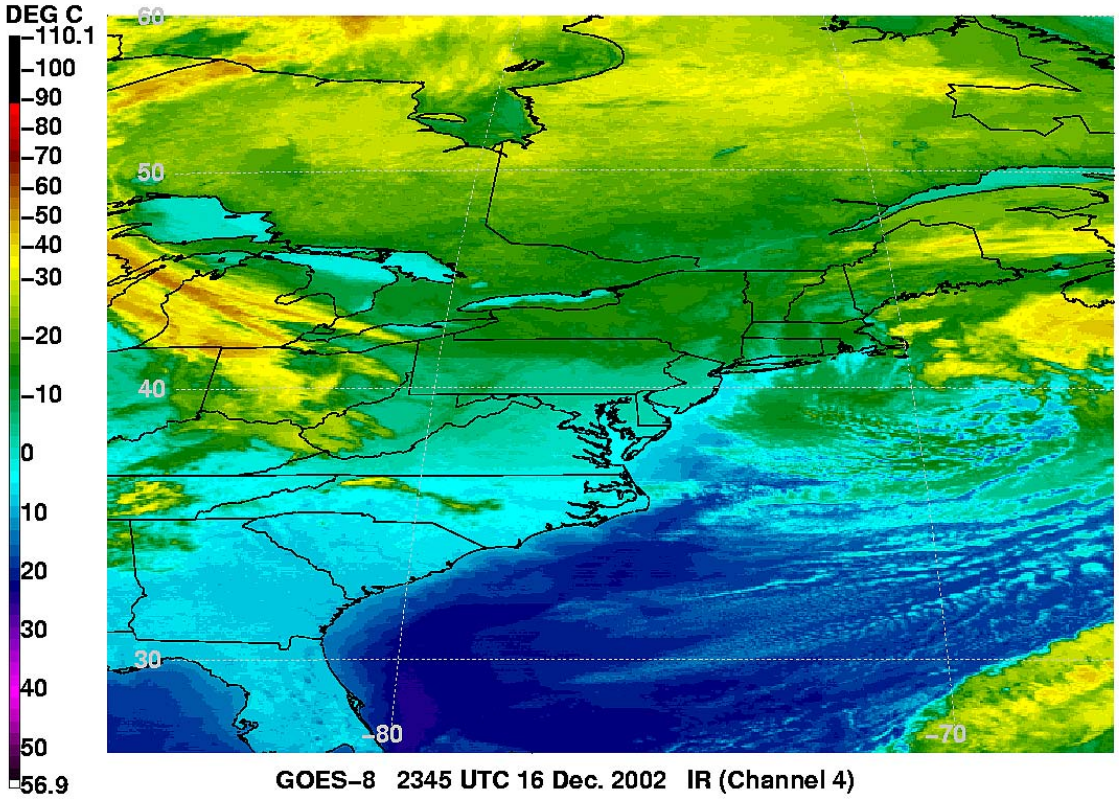

Figure 3.48: As in Fig. 3.23, except for 2345 UTC 16 December 2002.

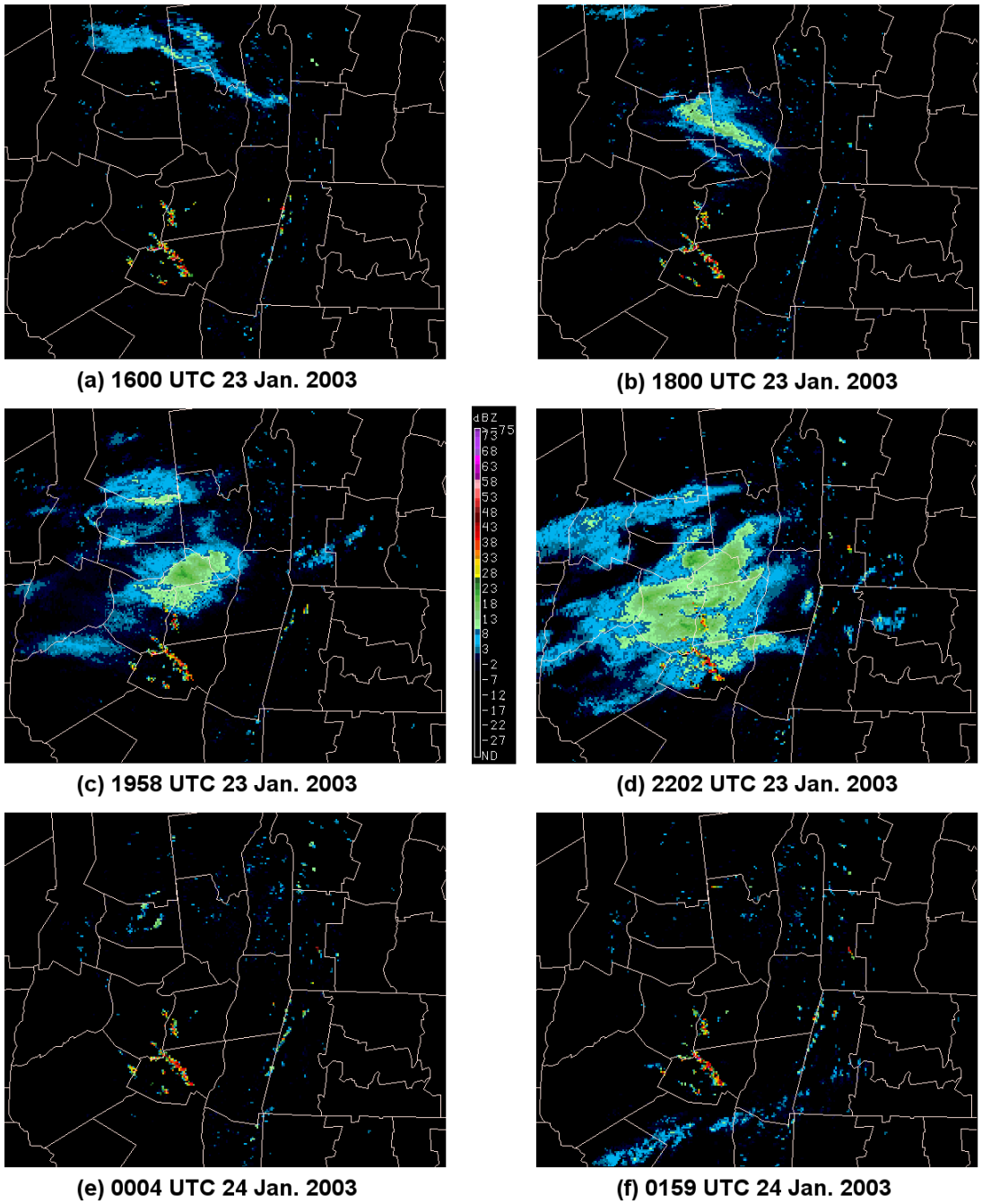

Figure 3.49: As in Fig. 3.15, except for (a) 1600, (b) 1800, (c) 1958, (d) 2202 UTC 23 January 2003, (e) 0004, and (f) 0159 UTC 24 January 2003.

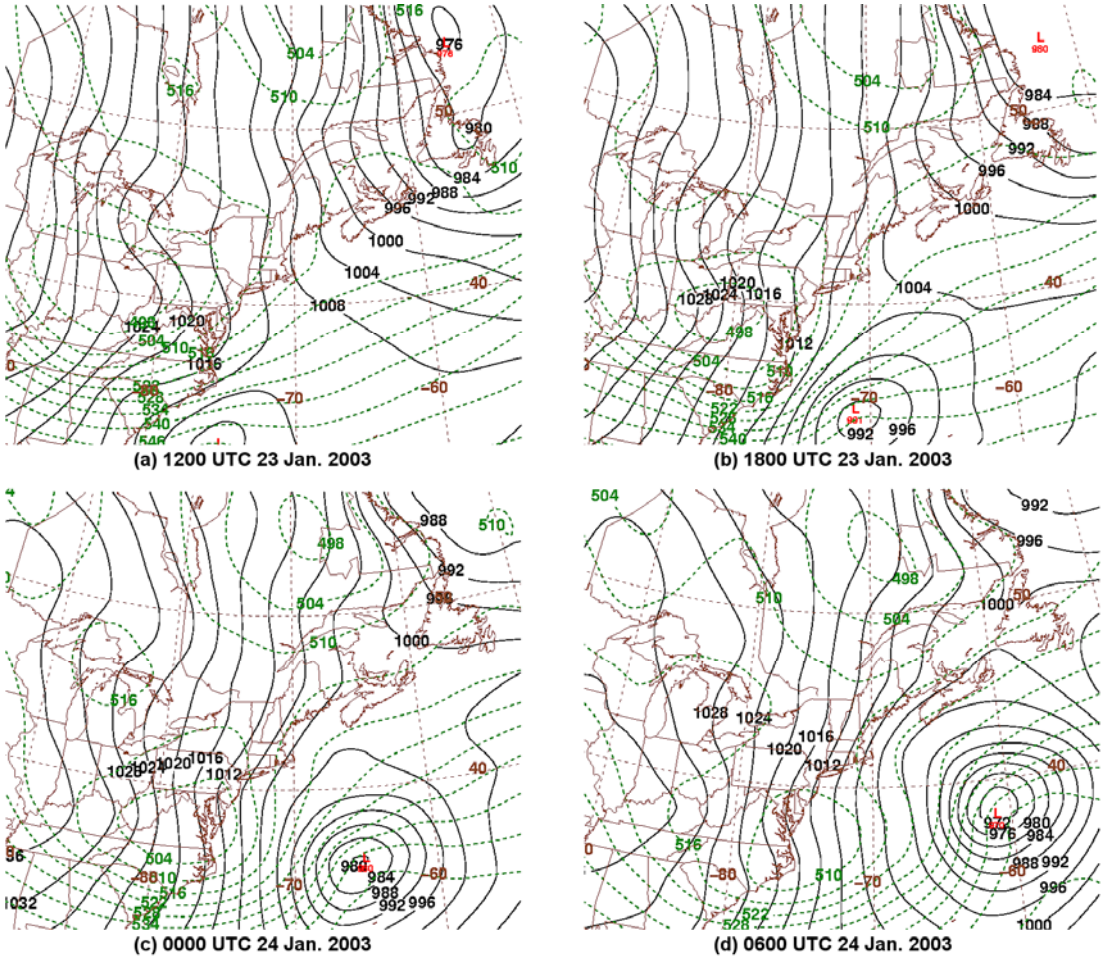

Figure 3.50: As in Fig. 3.7, except for (a) 1200, (b) 1800 UTC 23 January 2003, (c) 0000, and (d) 0600 UTC 24 January 2003.

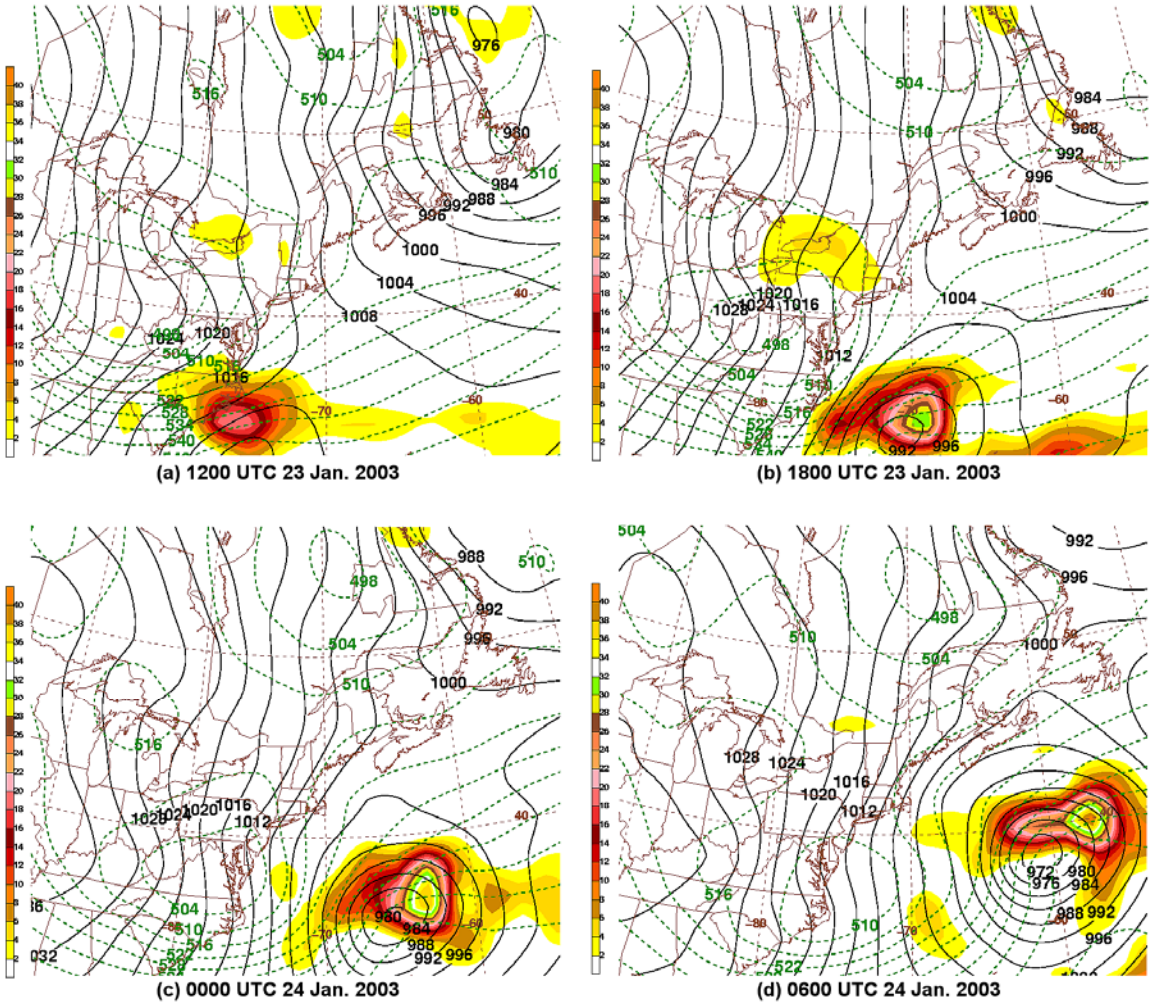

Figure 3.51: As in Fig. 3.10, except for (a) 1200, (b) 1800 UTC 23 January 2003, (c) 0000, and (d) 0600 UTC 24 January 2003.

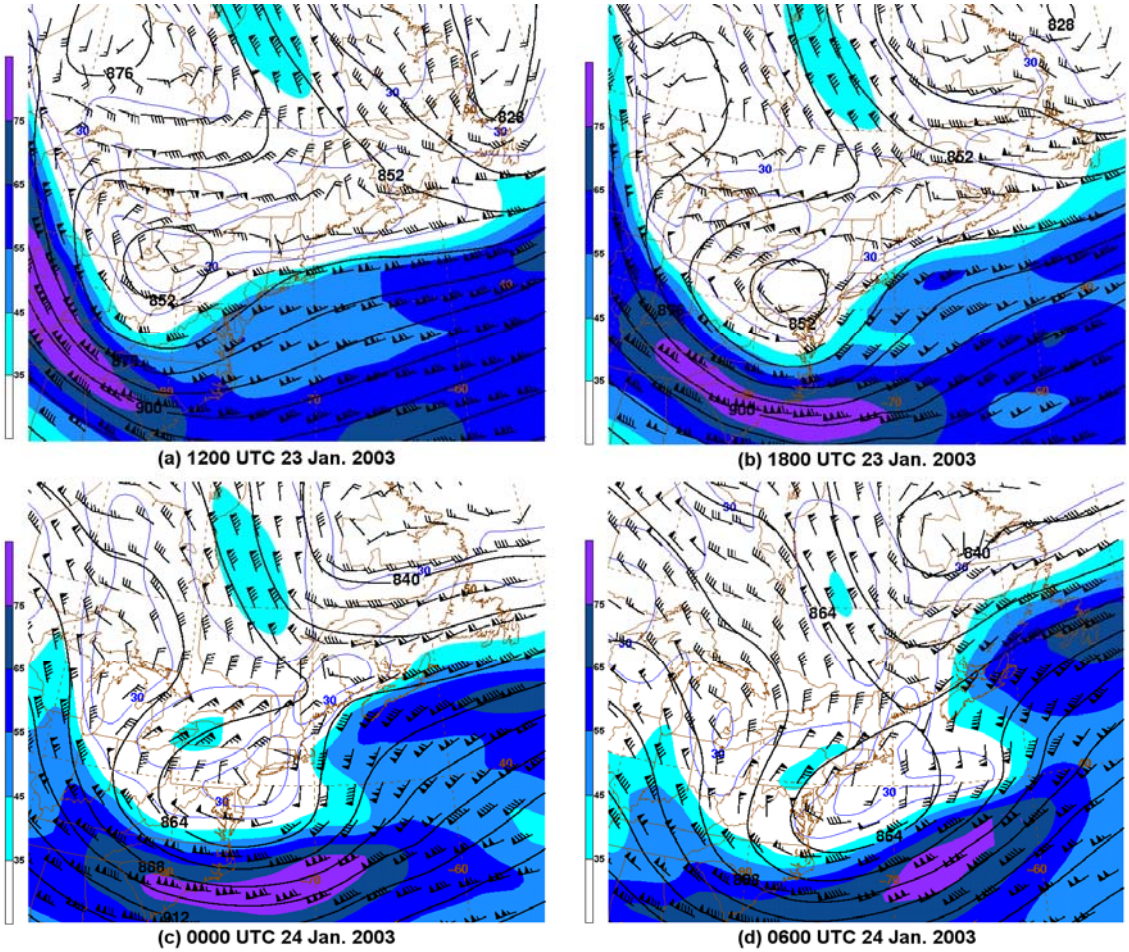

Figure 3.52: As in Fig. 3.13, except for (a) 1200, (b) 1800 UTC 23 January 2003, (c) 0000, and (d) 0600 UTC 24 January 2003.

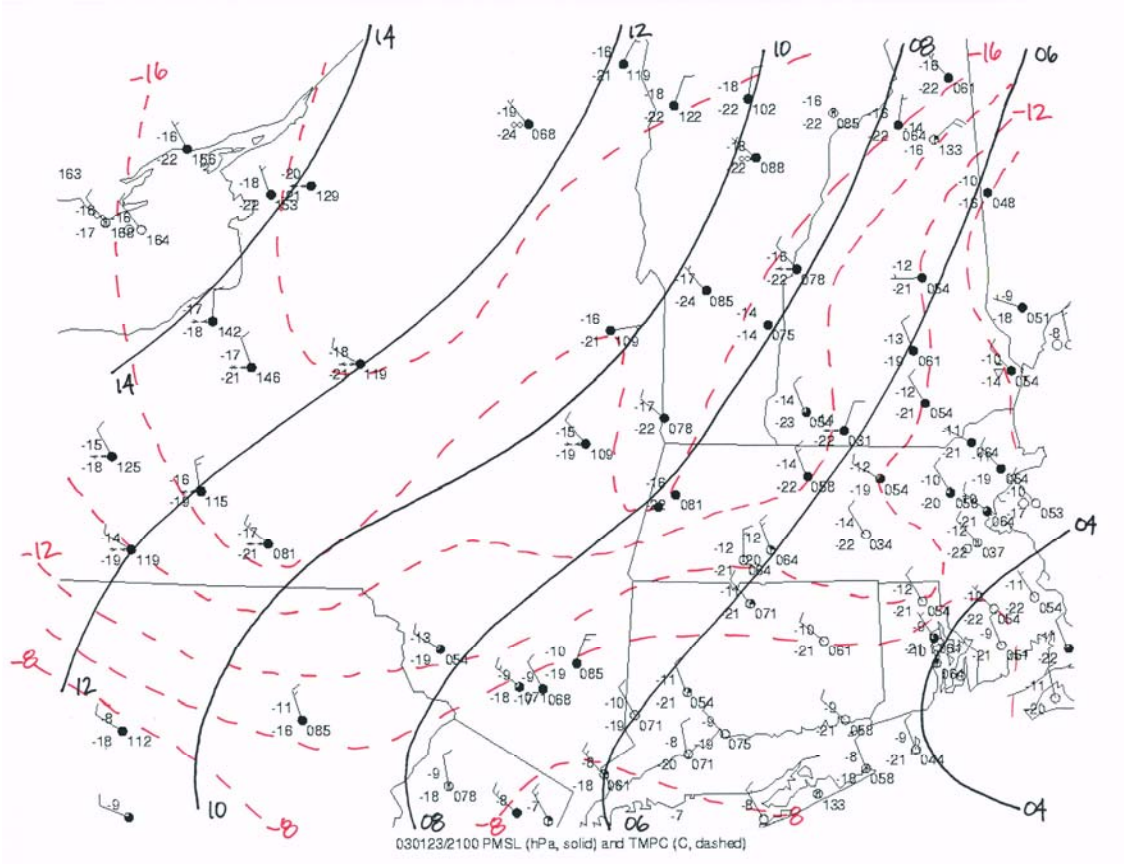

Figure 3.53: As in Fig. 3.16, except for 2100 UTC 23 January 2003.

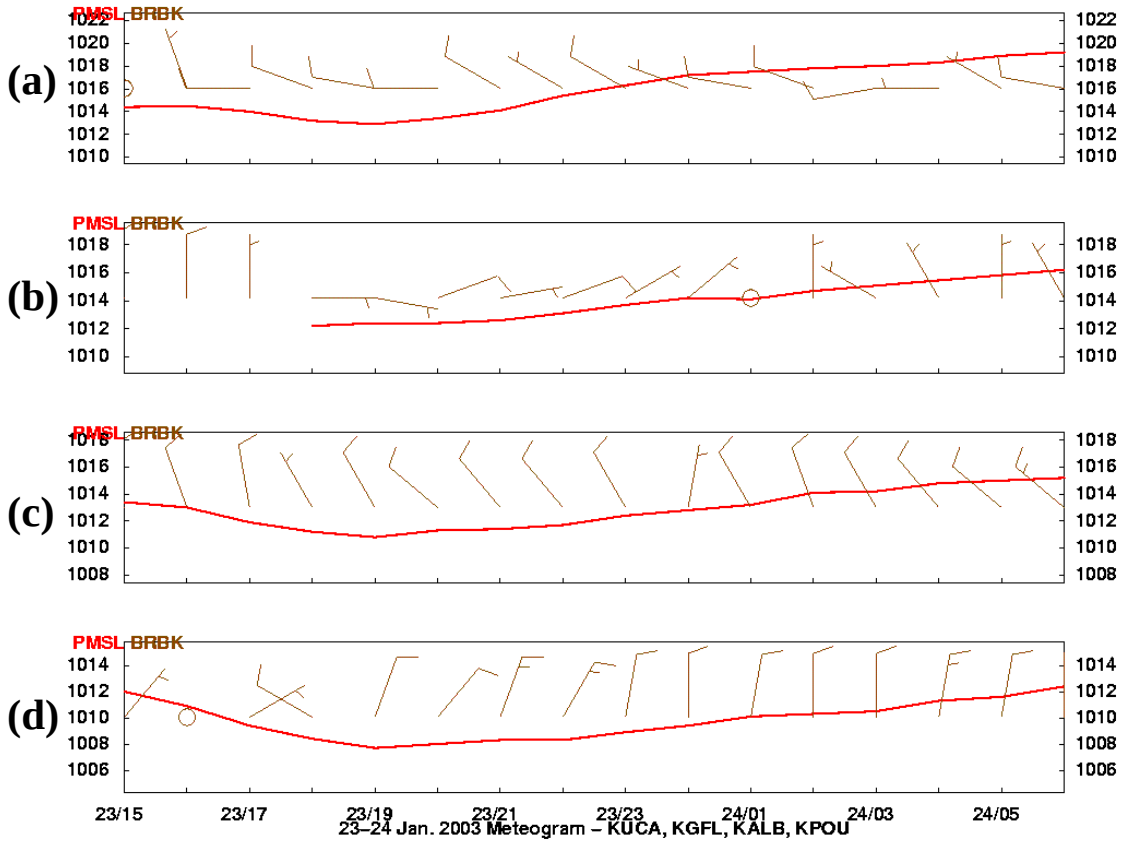

Figure 3.54: As in Fig. 3.17, except from 1500 UTC 23 January to 0600 UTC 24 January 2003. (Data source: the University at Albany DEAS archives, with supplemental data provided by the Historical Weather Data Archives of NSSL).

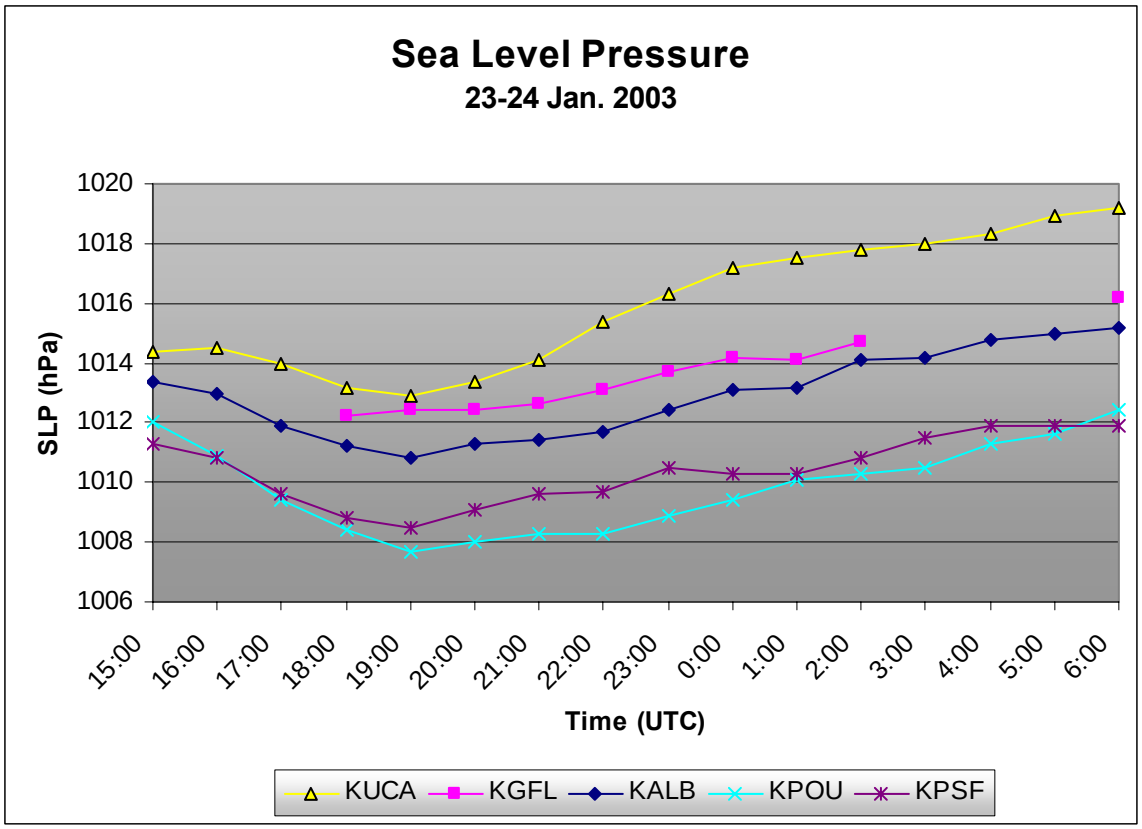

Figure 3.55: As in Fig. 3.18, except from 1500 UTC 23 January to 0600 UTC 24 January 2002. (Data source: the University at Albany DEAS archives, with supplemental data provided by the Historical Weather Data Archives of NSSL).

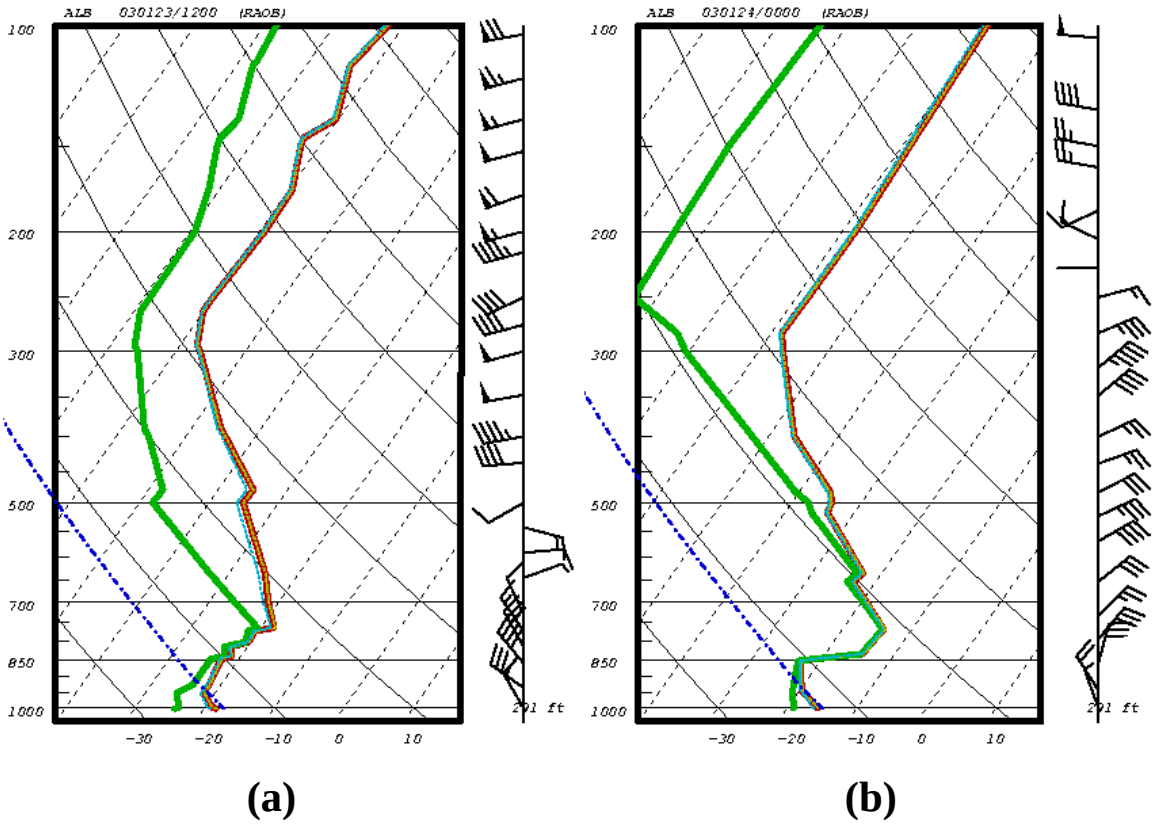

(a) **(b)**

Figure 3.56: As in Fig. 3.19, except for (a) 1200 UTC 23 January 2003 and (b) 0000 UTC 24 January 2003.

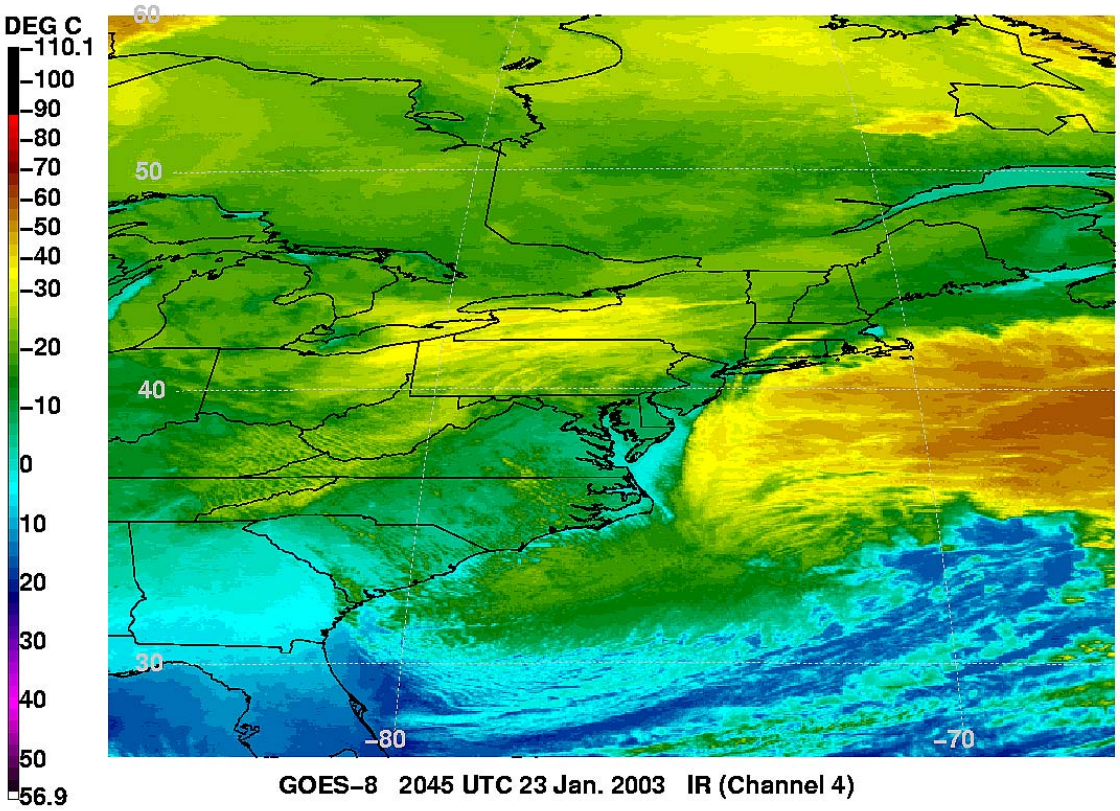

Figure 3.57: As in Fig. 3.23, except for 2045 UTC 23 January 2003.

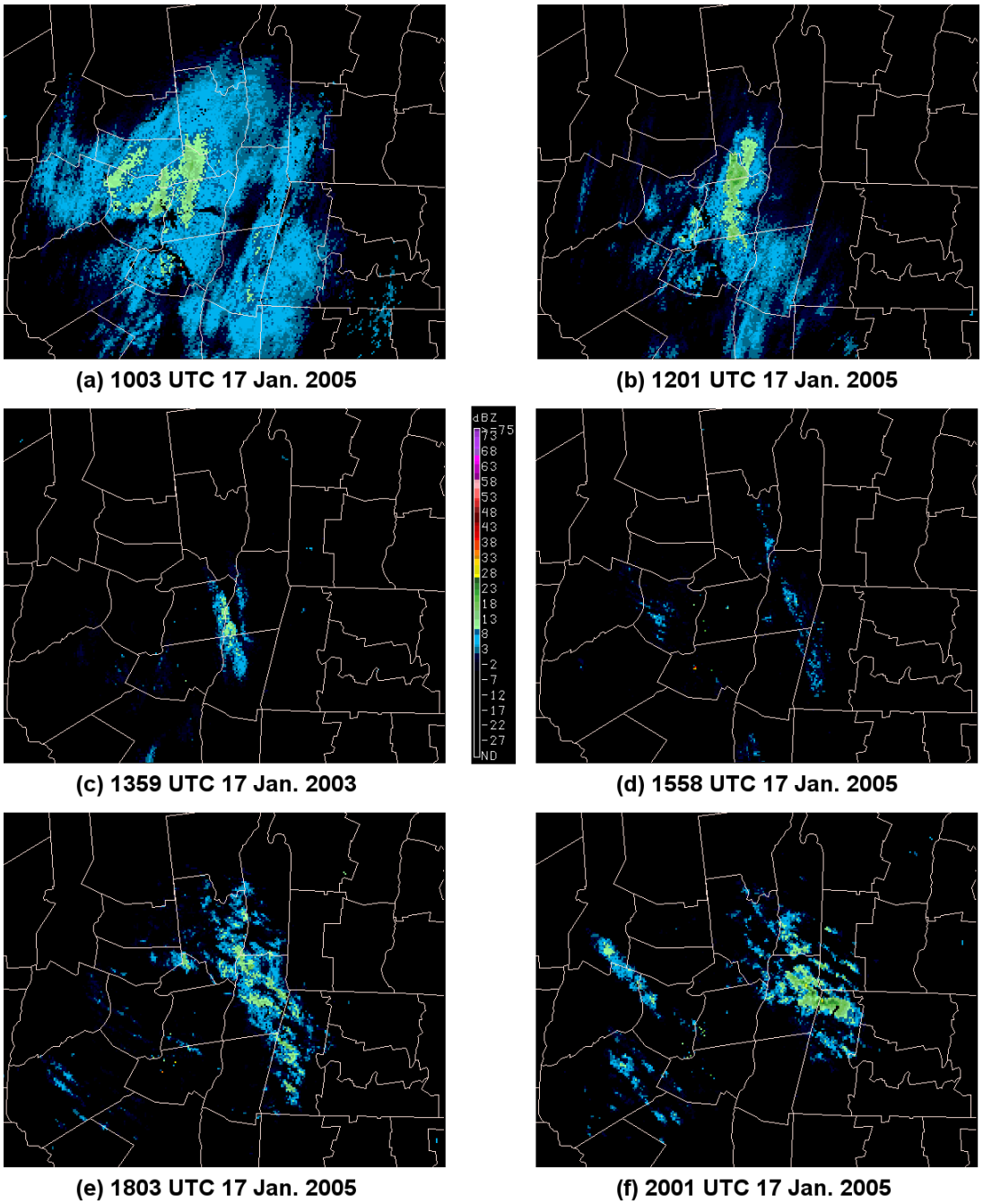

Figure 3.58: As in Fig. 3.15, except for (a) 1003, (b) 1201, (c) 1359, (d) 1558, (e) 1803, and (f) 2001 17 January 2005.

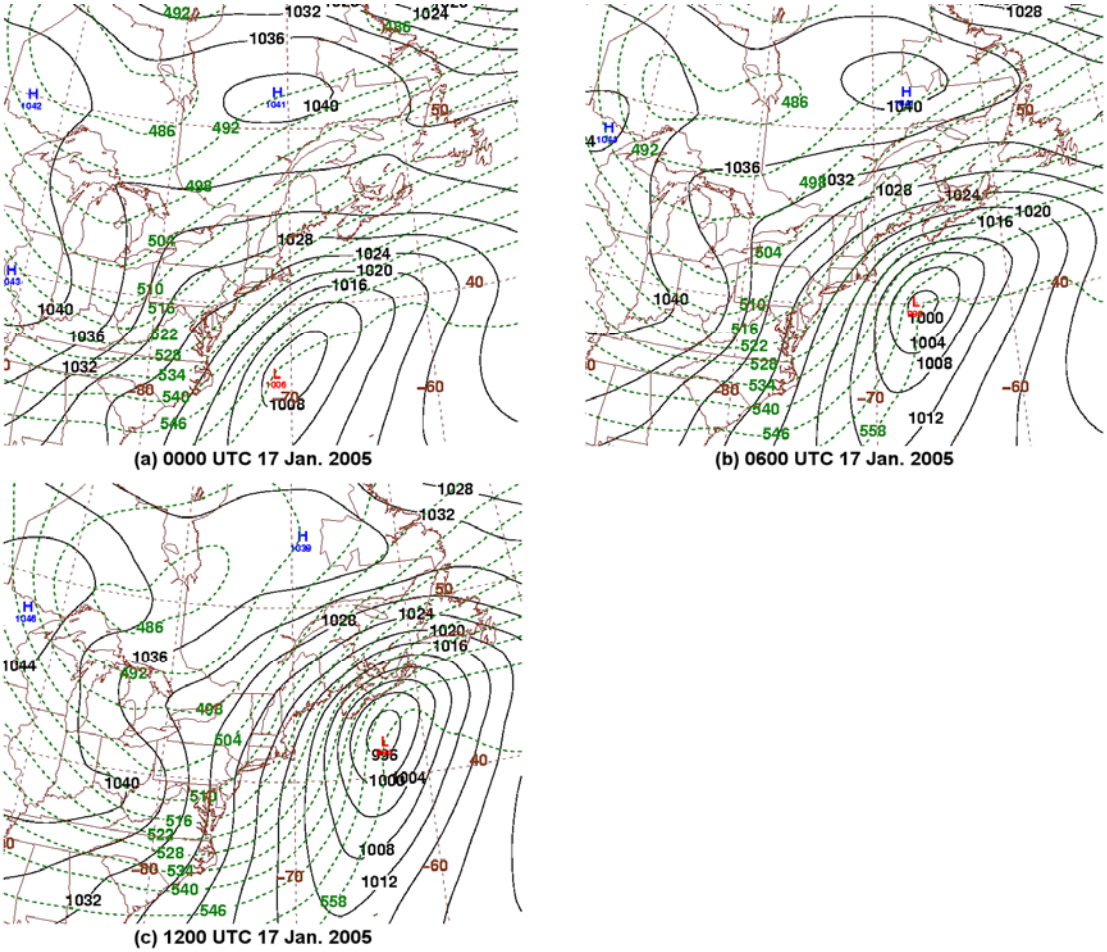

Figure 3.59: As in Fig. 3.7, except for (a) 0000, (b) 0600, and (c) 1200 UTC 17 January 2005.

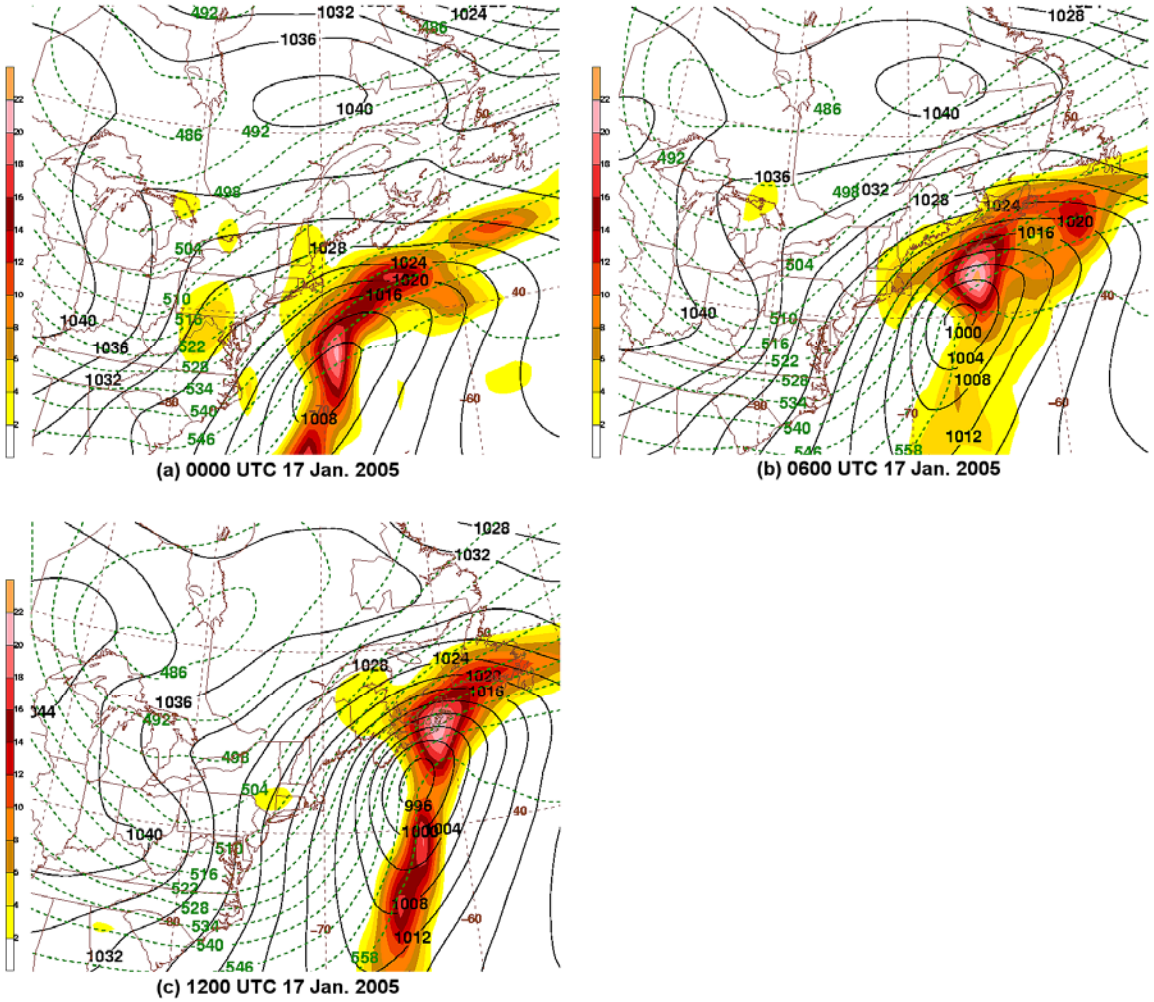

Figure 3.60: As in Fig. 3.10, except for (a) 0000, (b) 0600, and (c) 1200 UTC 17 January 2005.

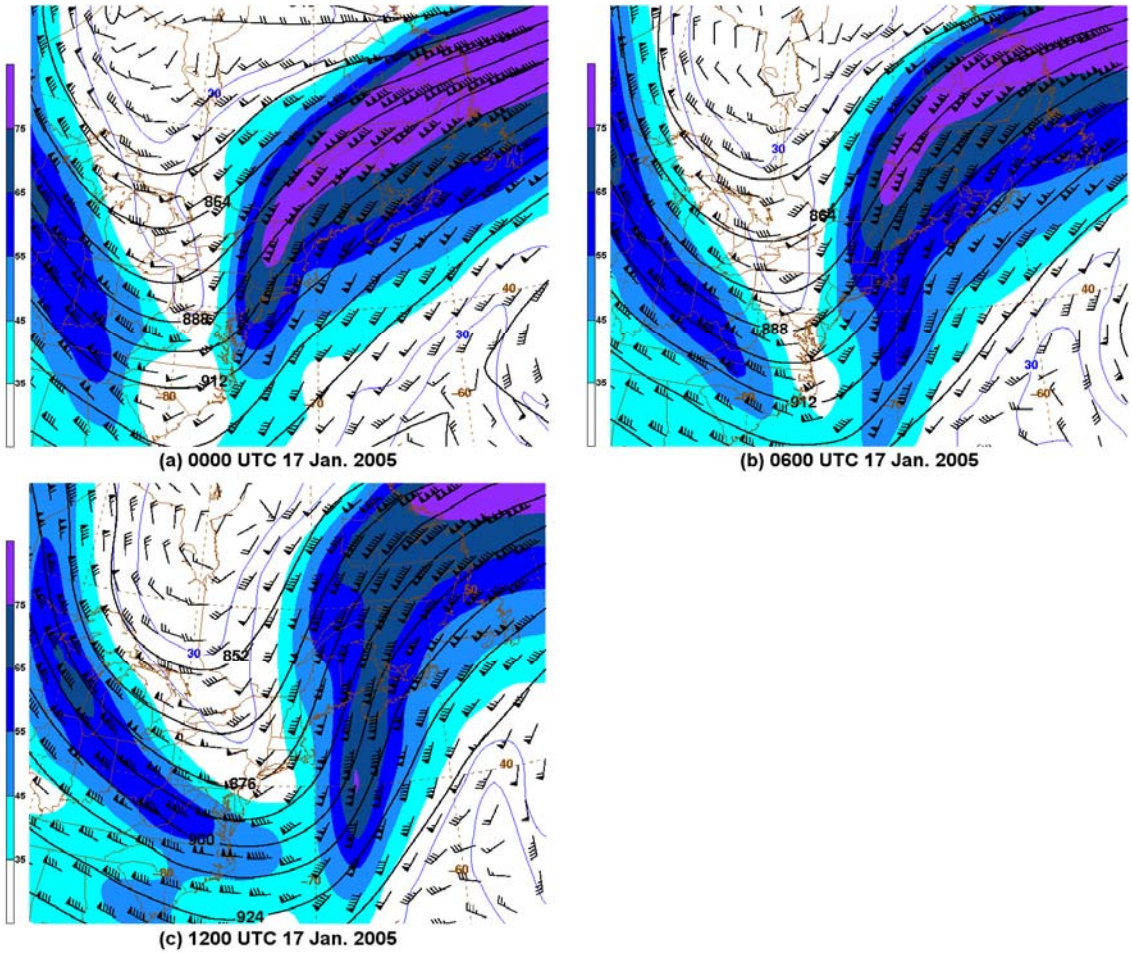

Figure 3.61: As in Fig. 3.13, except for (a) 0000, (b) 0600, and (c) 1200 UTC 17 January 2005.

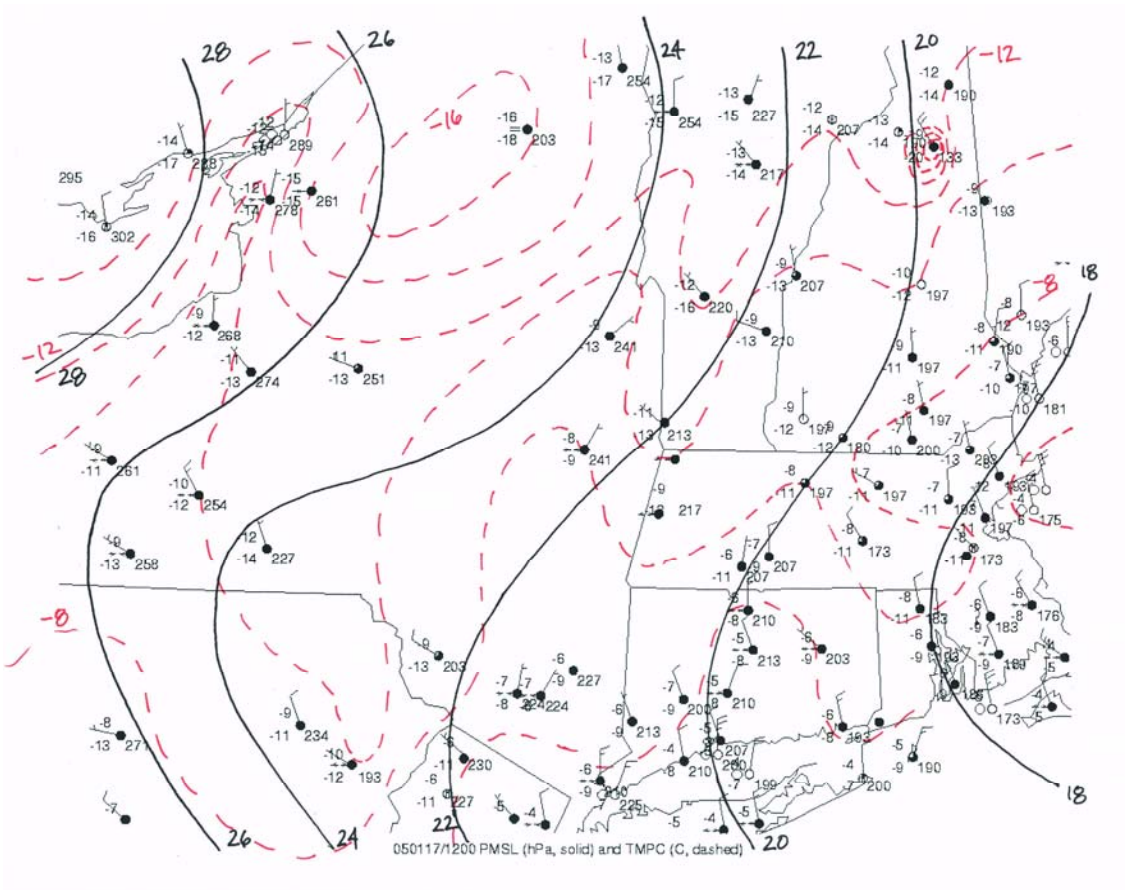

Figure 3.62: As in Fig. 3.16, except for 1200 UTC 17 January 2005.

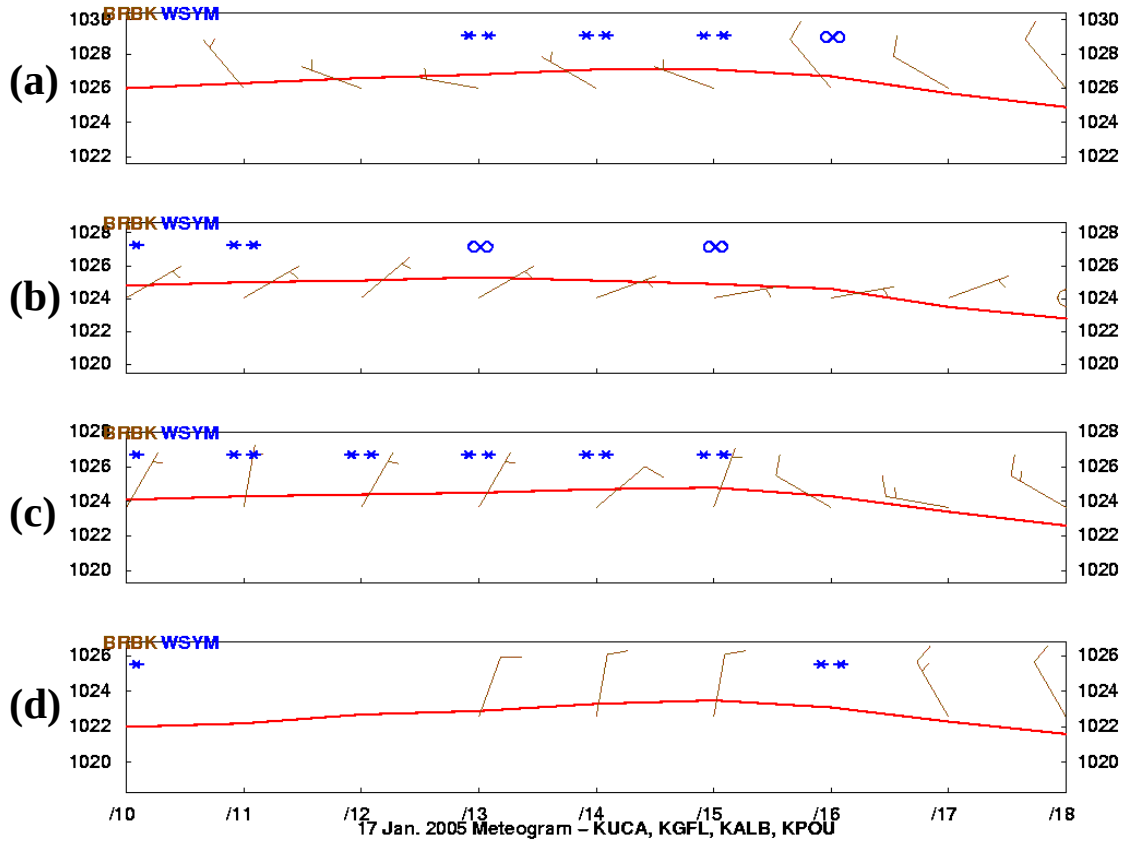

Figure 3.63: As in Fig. 3.17, except from 1000 to 1800 UTC 17 January 2005.

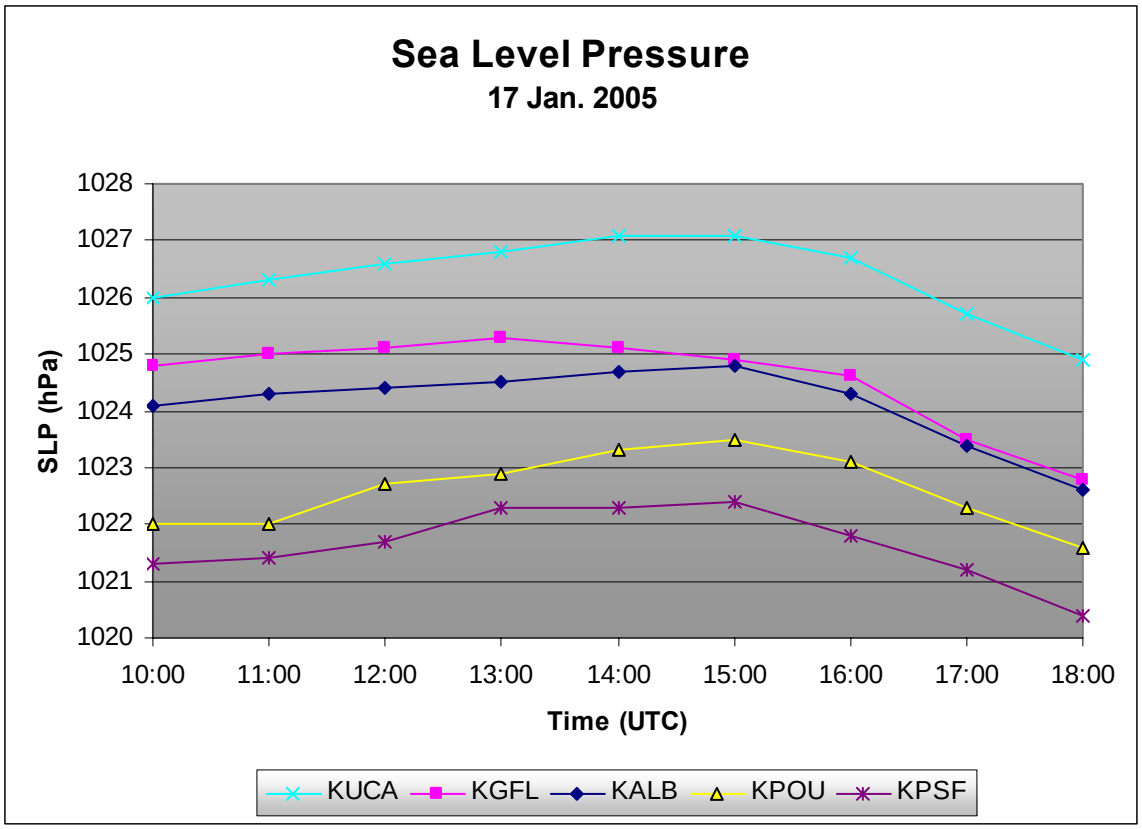

Figure 3.64: As in Fig. 3.18, except from 1000 to 1800 UTC 17 January 2005. (Data source: University at Albany DEAS archives).

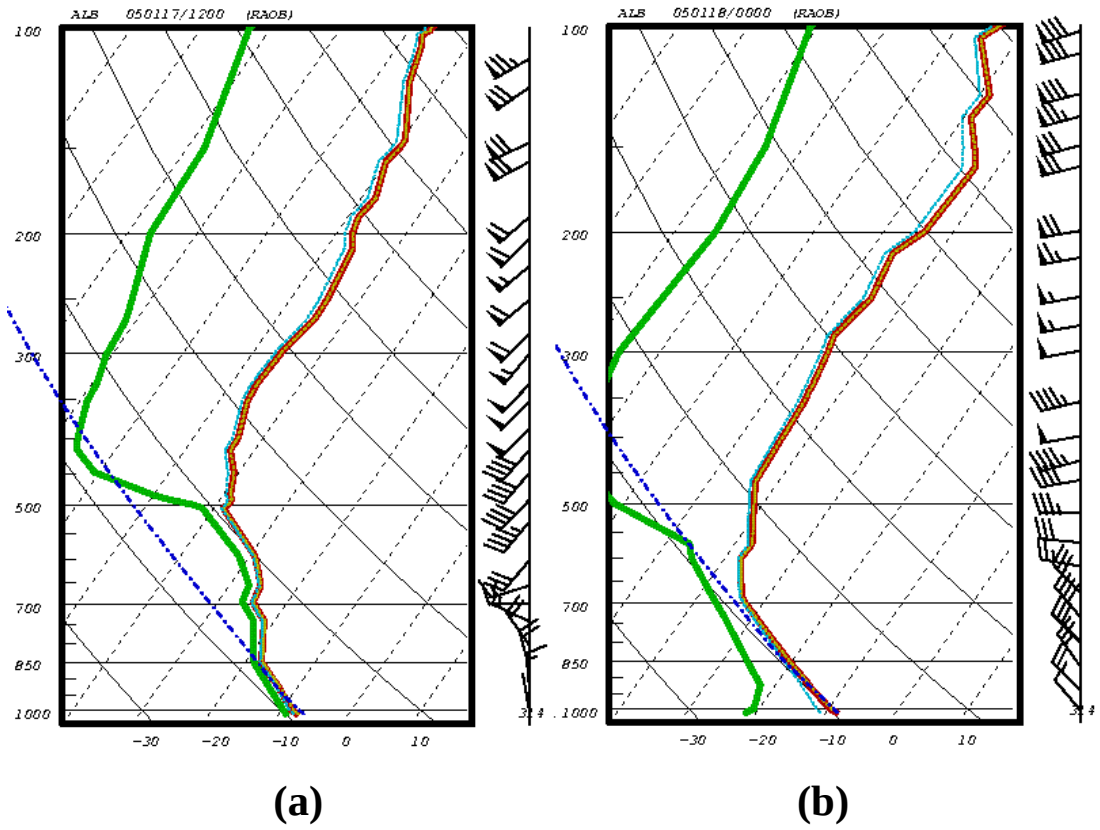

Figure 3.65: As in Fig. 3.19, except for (a) 1200 UTC 17 January 2005 and (b) 0000 UTC 18 January 2005.

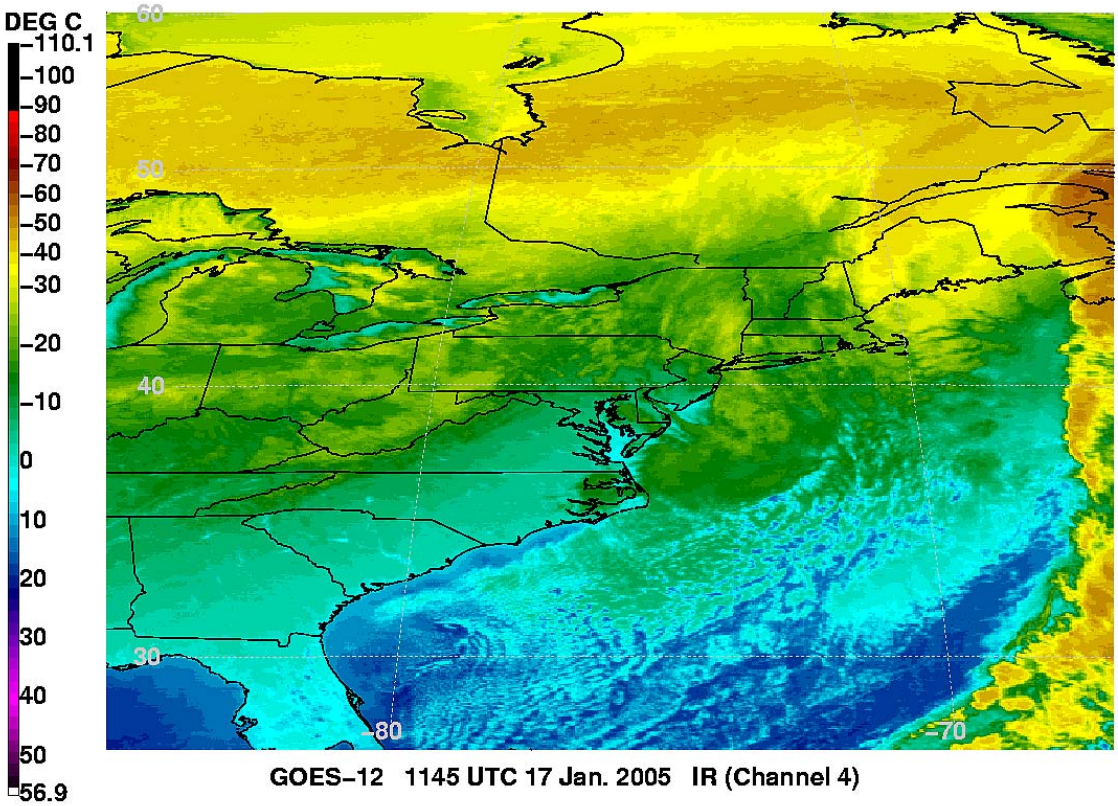

Figure 3.66: As in Fig. 3.23, except from GOES-12 at 1145 UTC 17 January 2005.

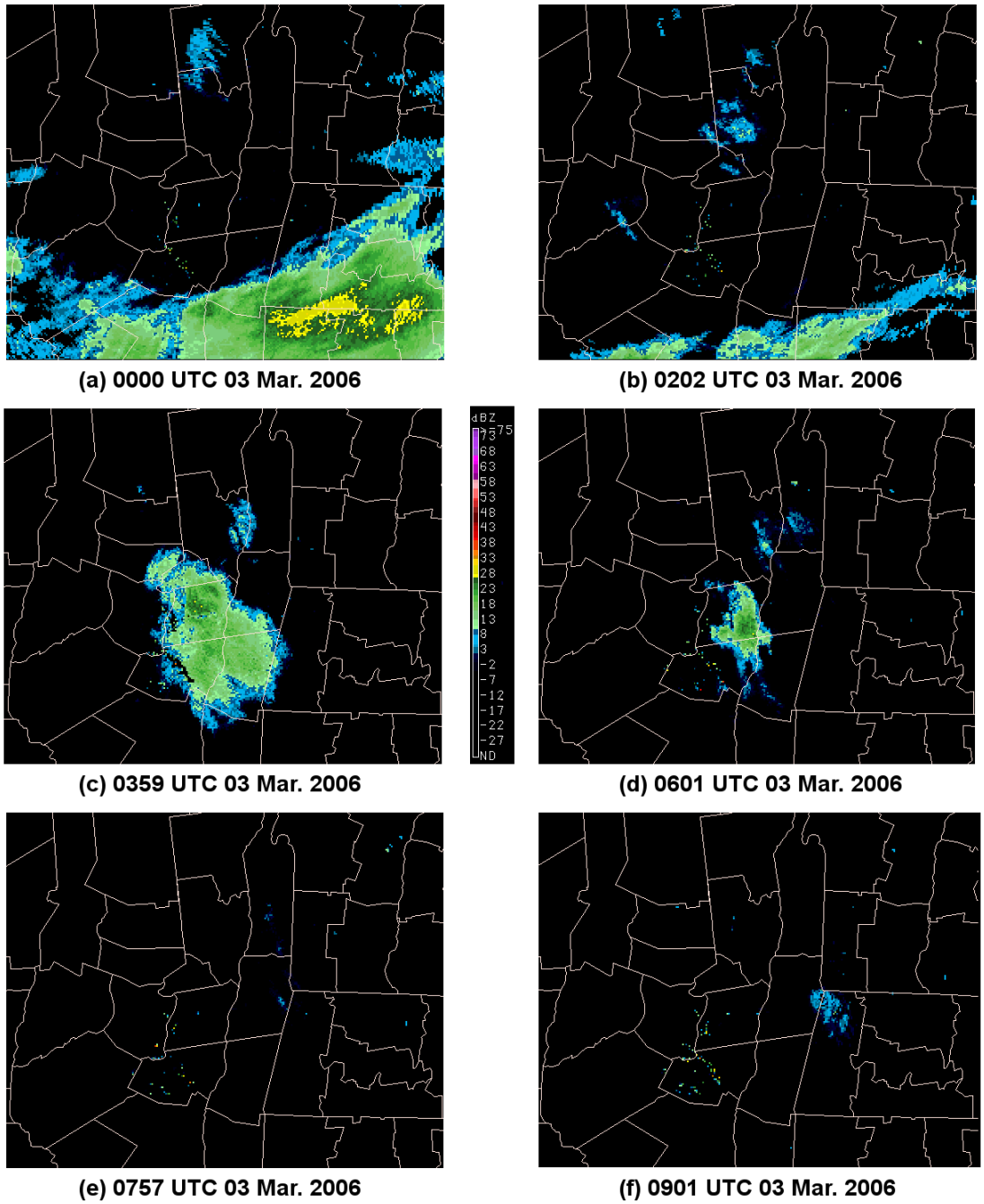

Figure 3.67: As in Fig. 3.15, except for (a) 0000, (b) 0202, (c) 0359, (d) 0601, (e) 0757, and (f) 0901 UTC 3 March 2006.

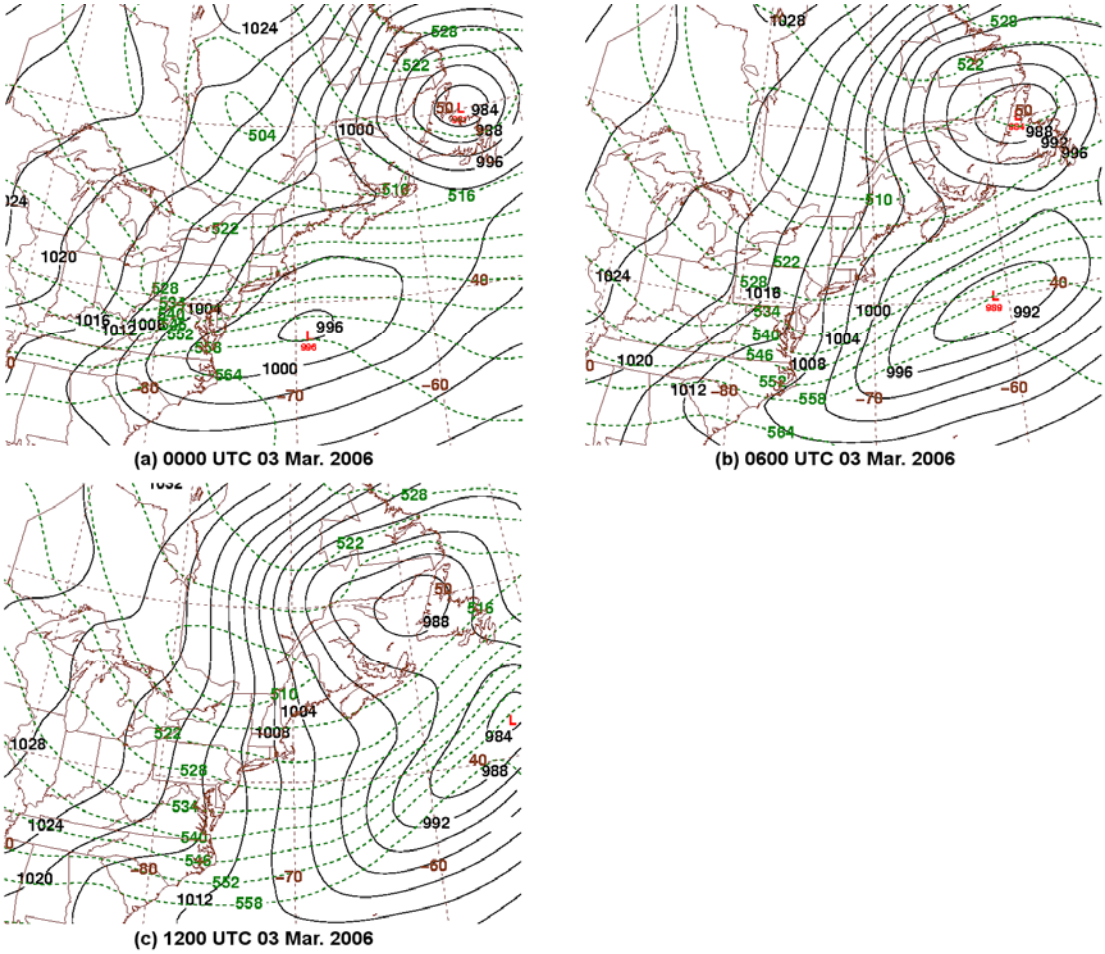

Figure 3.68: As in Fig. 3.7, except for (a) 0000, (b) 0600, and (c) 1200 UTC 3 March 2006.

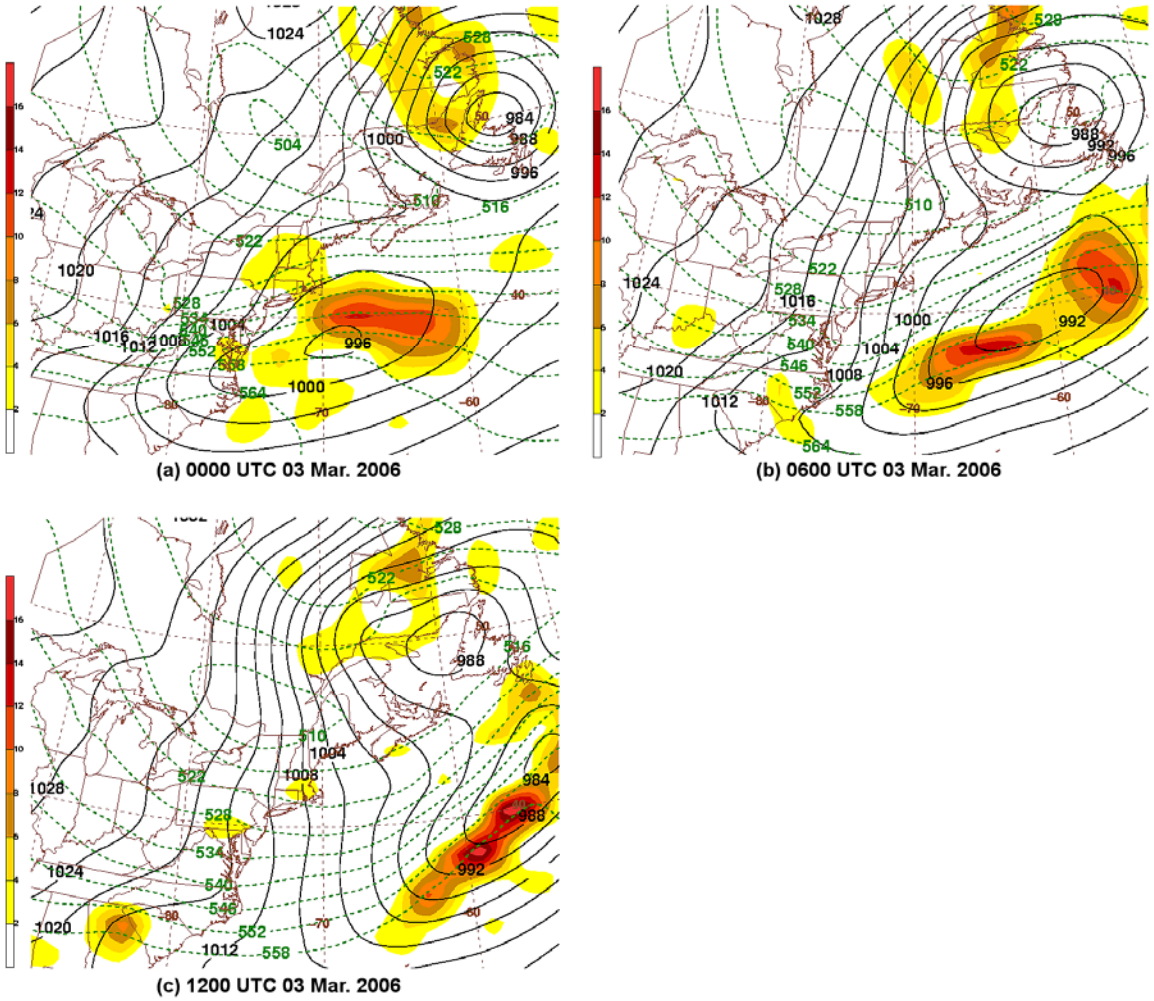

Figure 3.69: As in Fig. 3.10, except for (a) 0000, (b) 0600, and (c) 1200 UTC 3 March 2006.

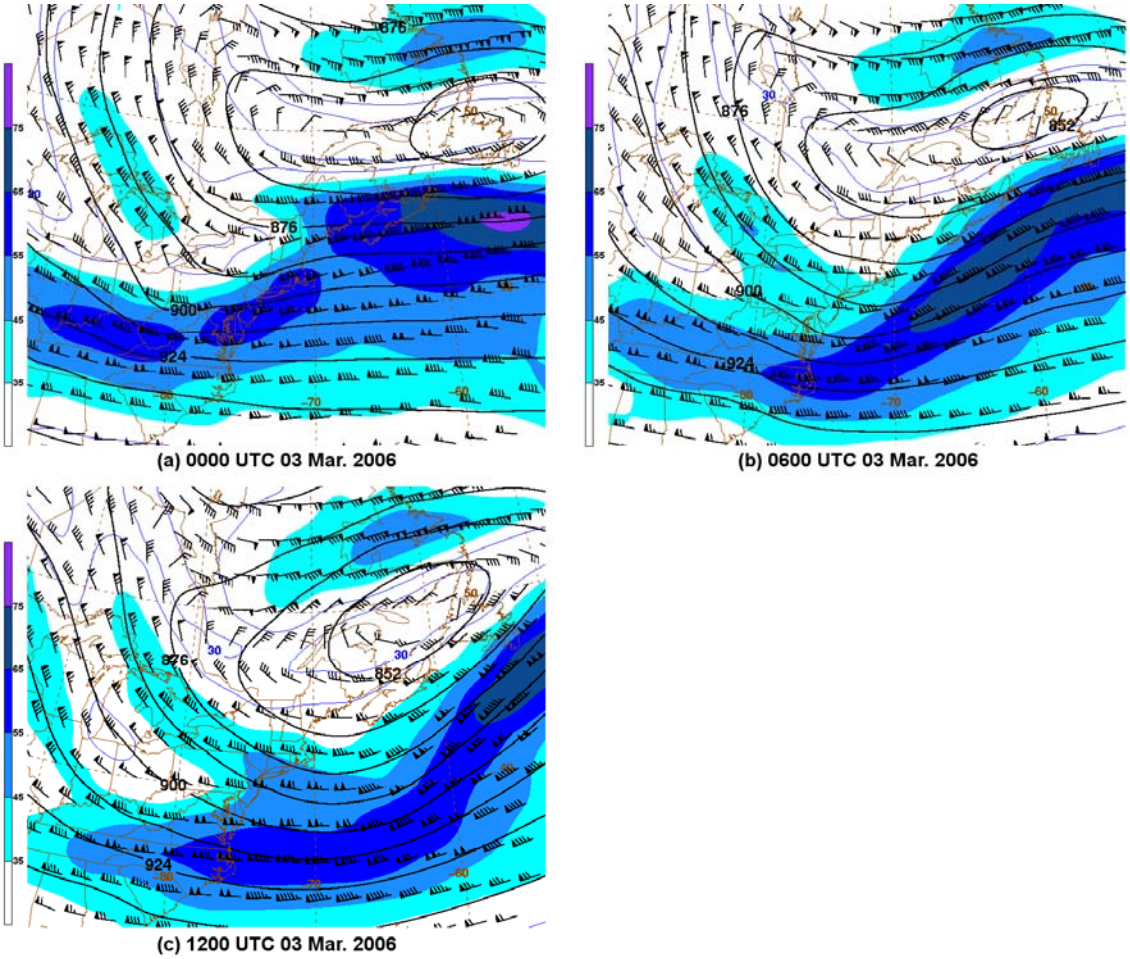

Figure 3.70: As in Fig. 3.13, except for (a) 0000, (b) 0600, and (c) 1200 UTC 3 March 2006.

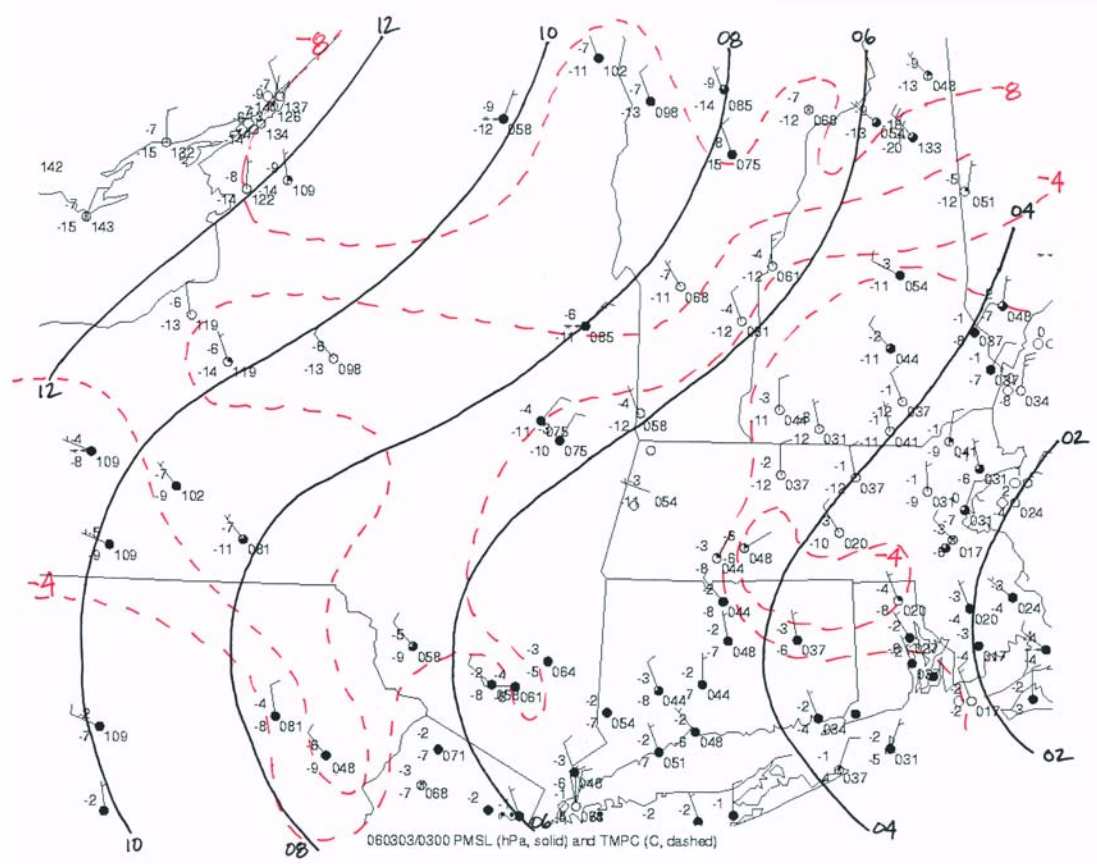

Figure 3.71: As in Fig. 3.16, except for 0300 UTC 3 March 2006.

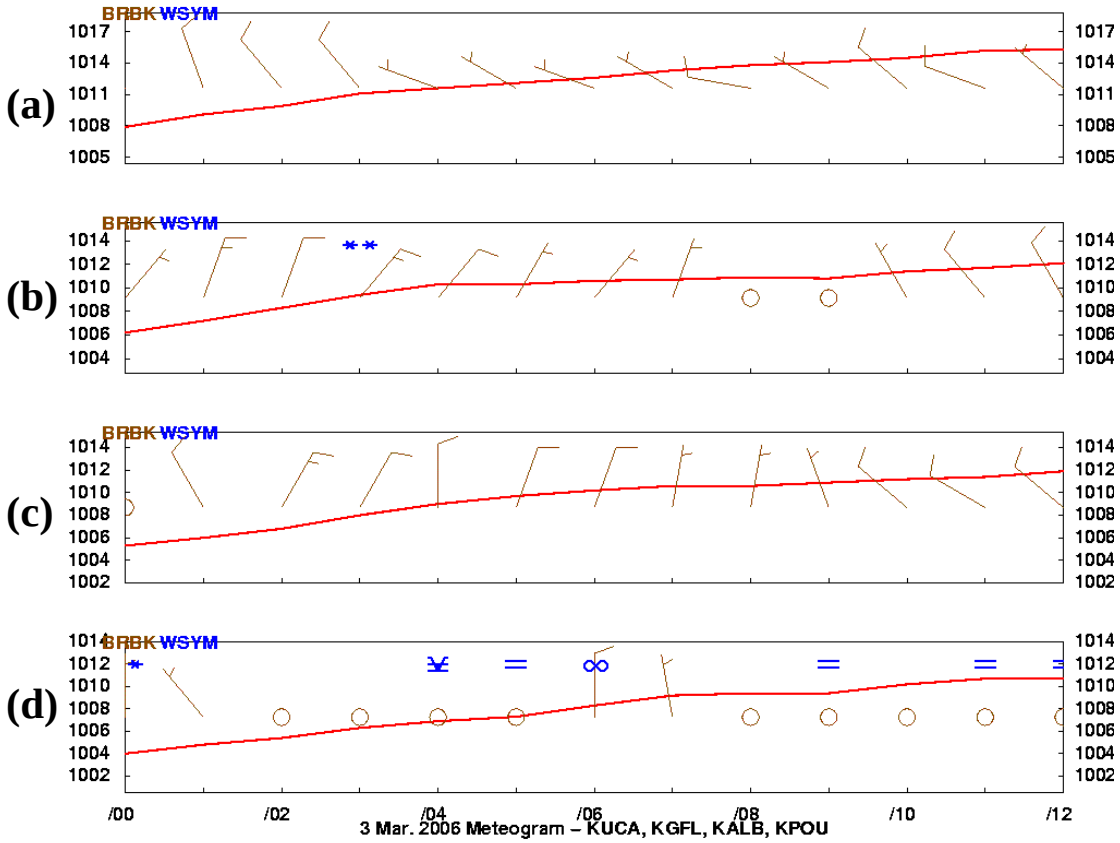

Figure 3.72: As in Fig. 3.17, except from 0000 to 1200 UTC 3 March 2006.

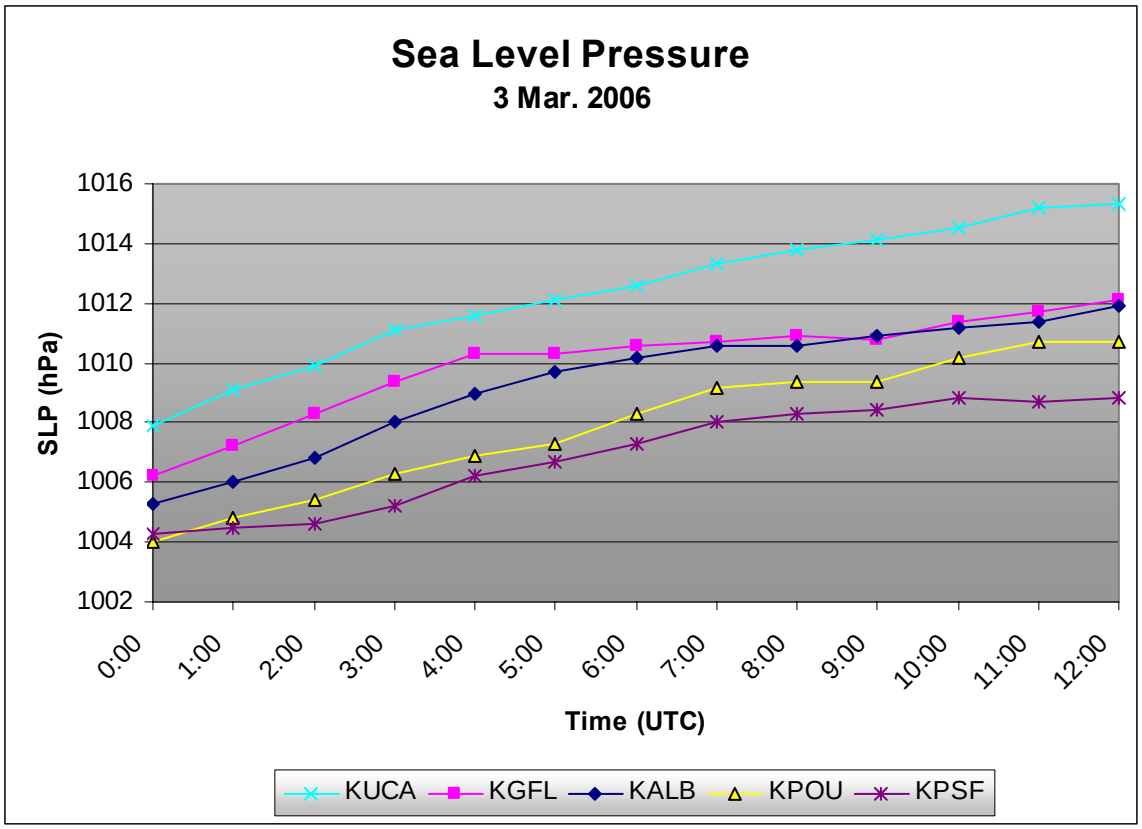

Figure 3.73: As in Fig. 3.18, except from 0000 to 1200 UTC 3 March 2006. (Data source: University at Albany DEAS archives).

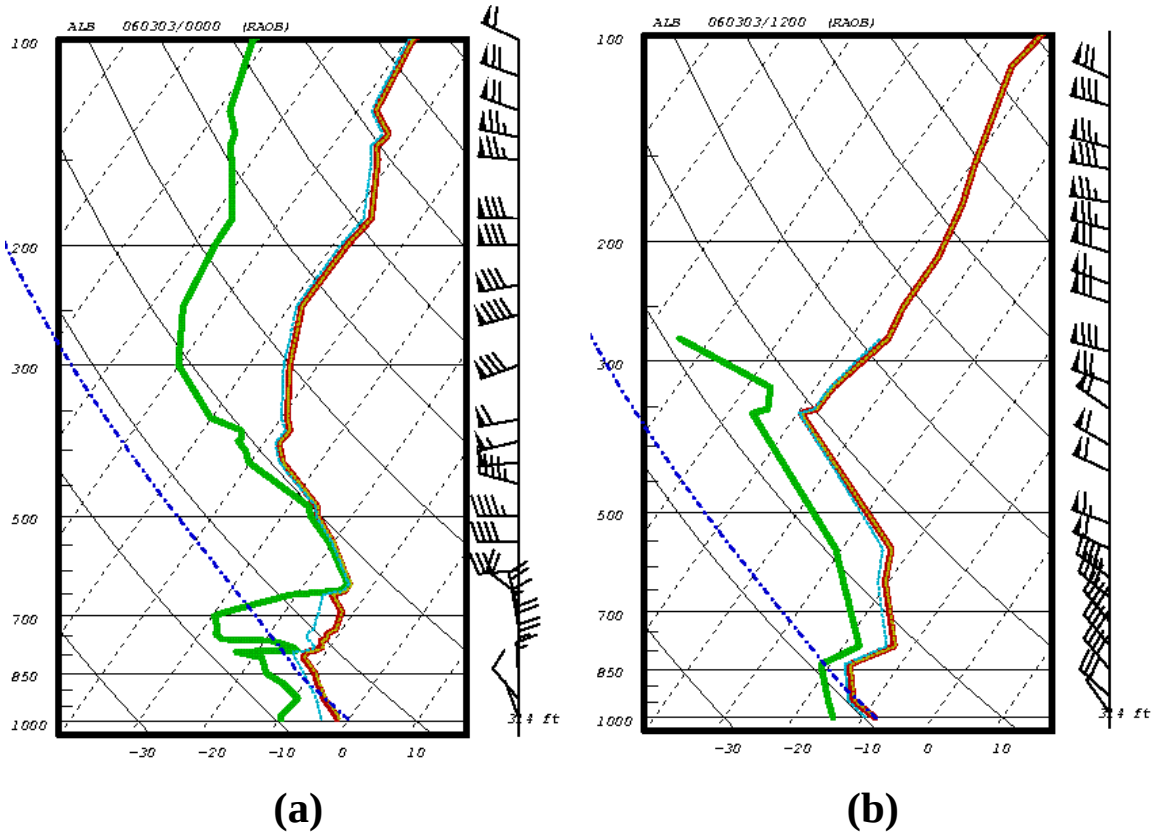

(a) **(b)**

Figure 3.74: As in Fig. 3.19, except for (a) 0000 UTC 3 March 2006 and (b) 1200 UTC 3 March 2006.

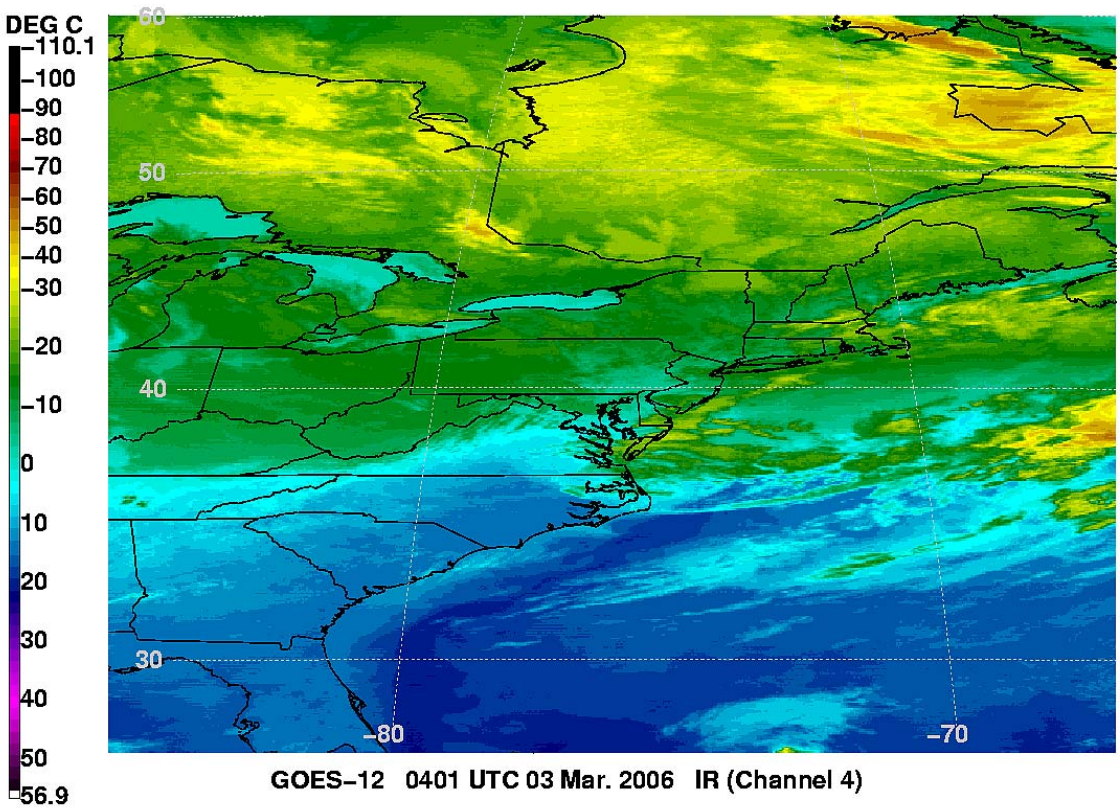

Figure 3.75: As in Fig. 3.23, except from GOES-12 at 0401 UTC 3 March 2006.

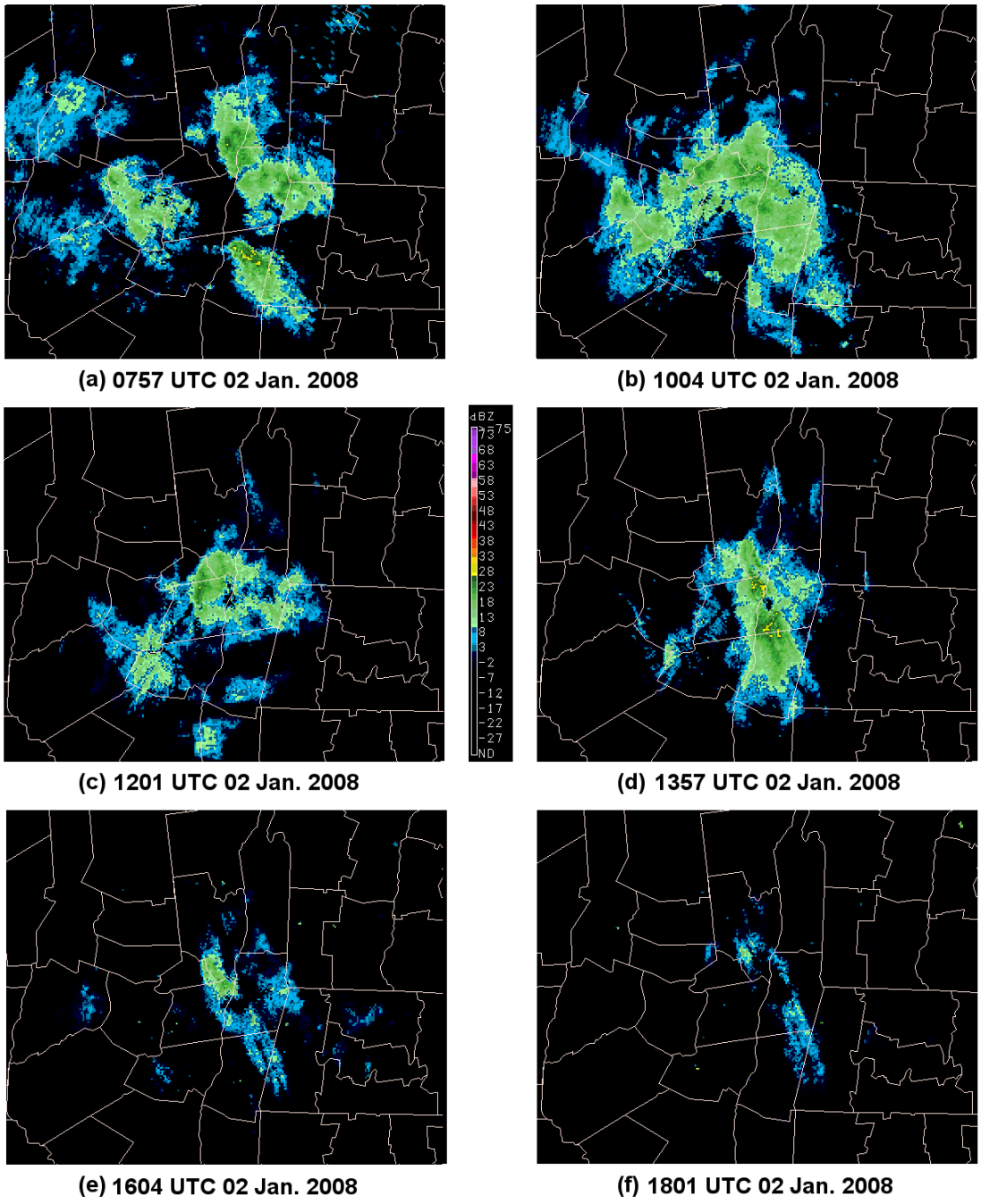

Figure 3.76: As in Fig. 3.15, except for (a) 0757, (b) 1004, (c) 1201, (d) 1357, (e) 1604, and (f) 1801 UTC 2 January 2008.

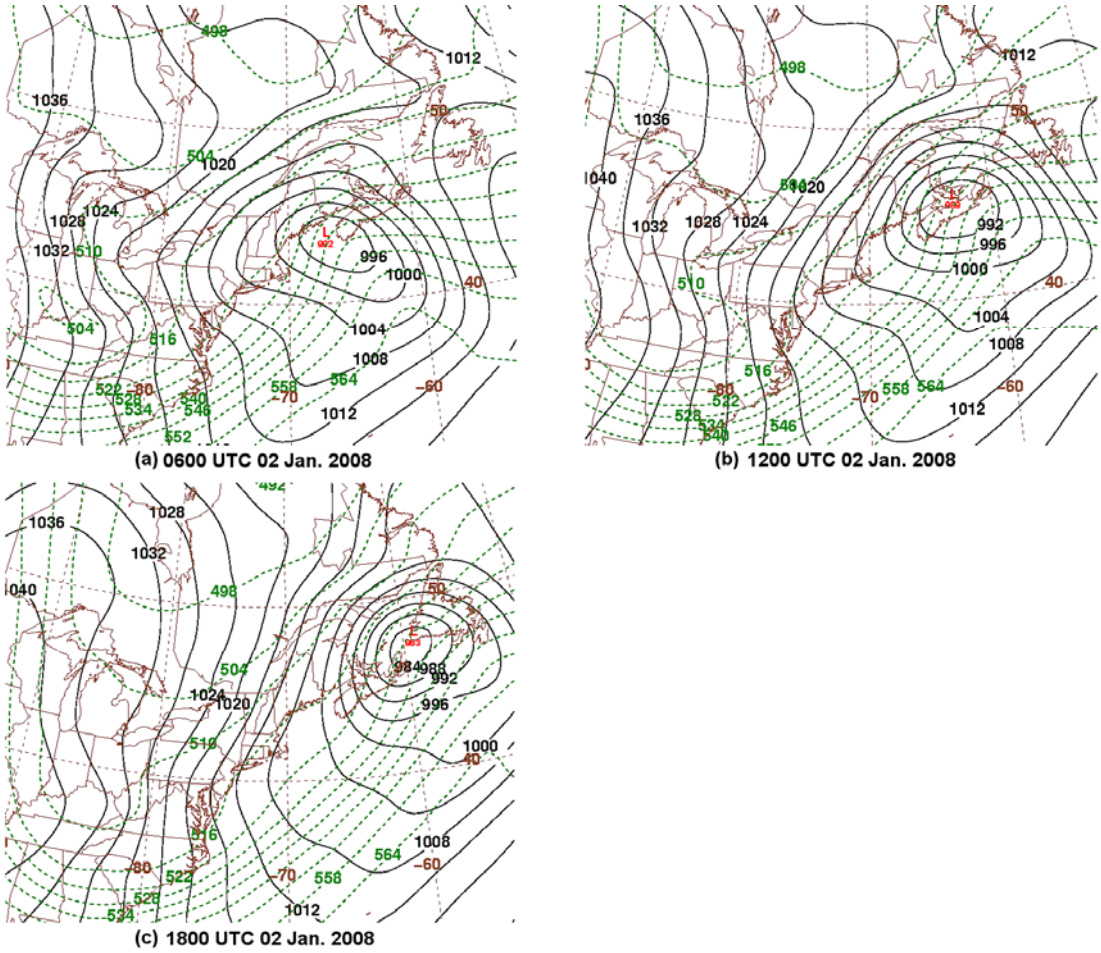

Figure 3.77: As in Fig. 3.7, except for (a) 0600, (b) 1200, and (c) 1800 UTC 2 January 2008.

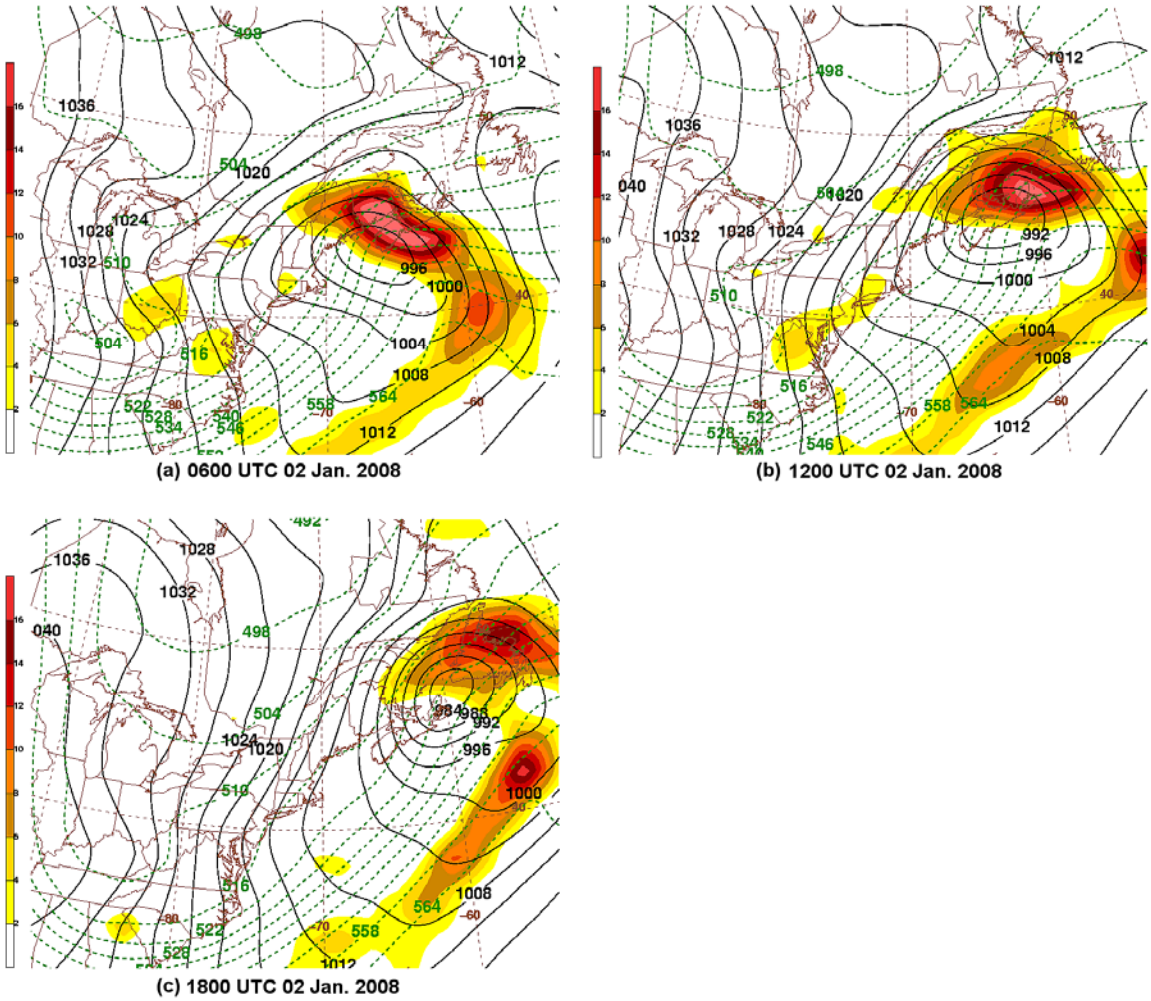

Figure 3.78: As in Fig. 3.10, except for (a) 0600, (b) 1200, and (c) 1800 UTC 2 January 2008.

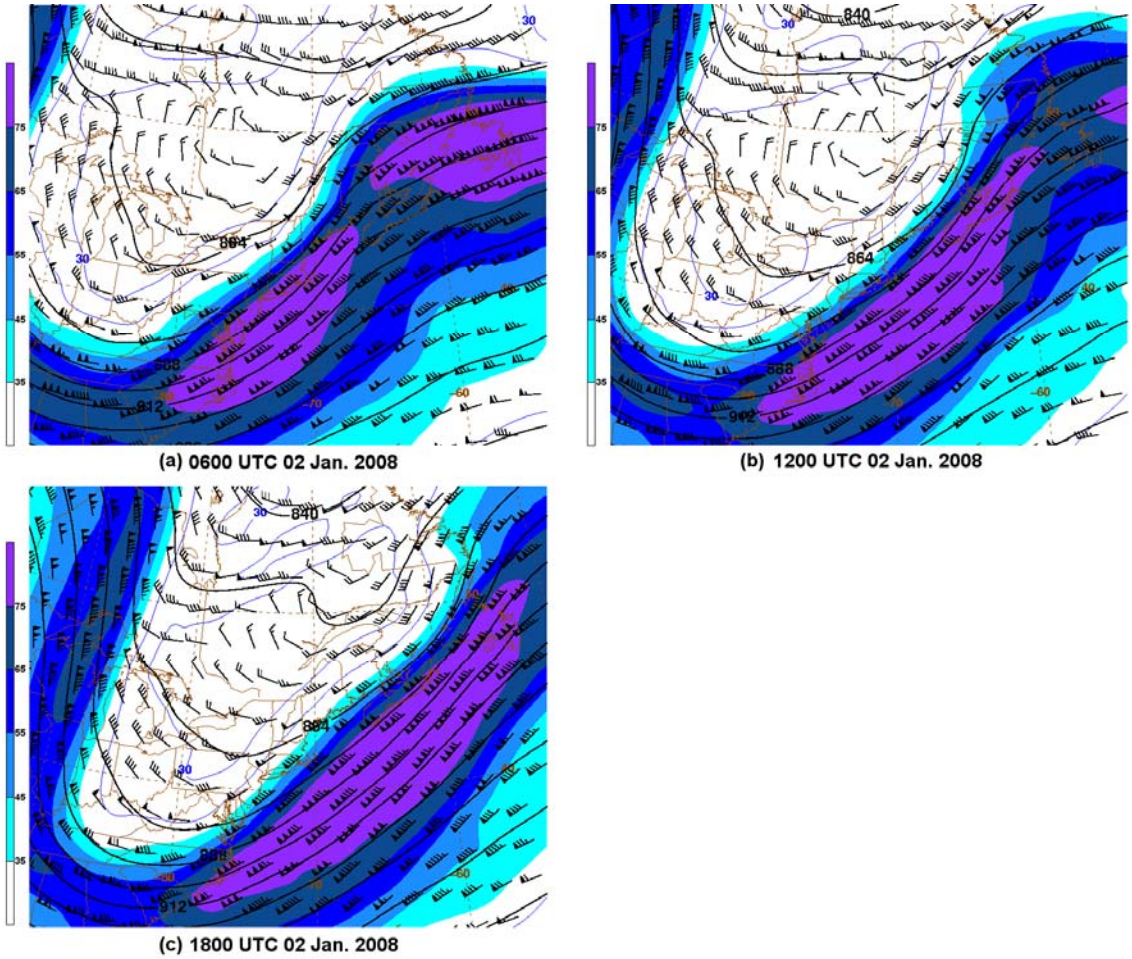

Figure 3.79: As in Fig. 3.13, except for (a) 0600, (b) 1200, and (c) 1800 UTC 2 January 2008.

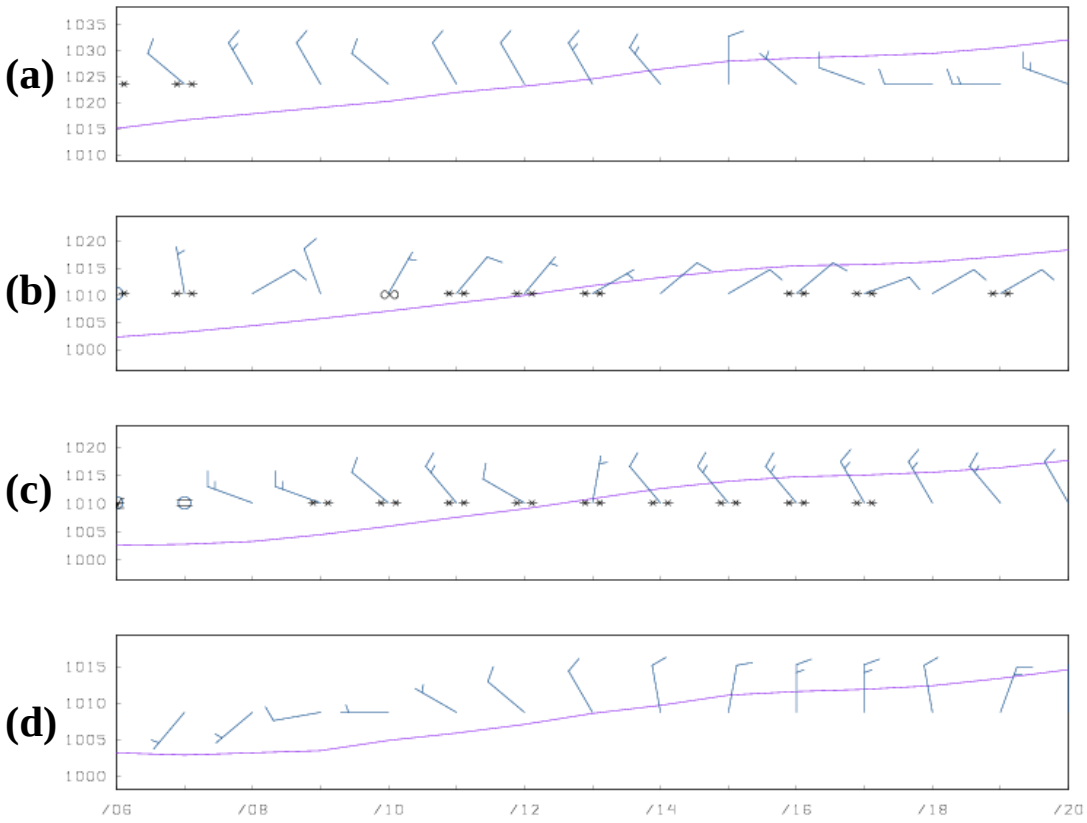

Figure 3.80: As in Fig. 3.17, except from 0600 to 2000 UTC 2 January 2008. (Data source: the Historical Weather Data Archives of NSSL).

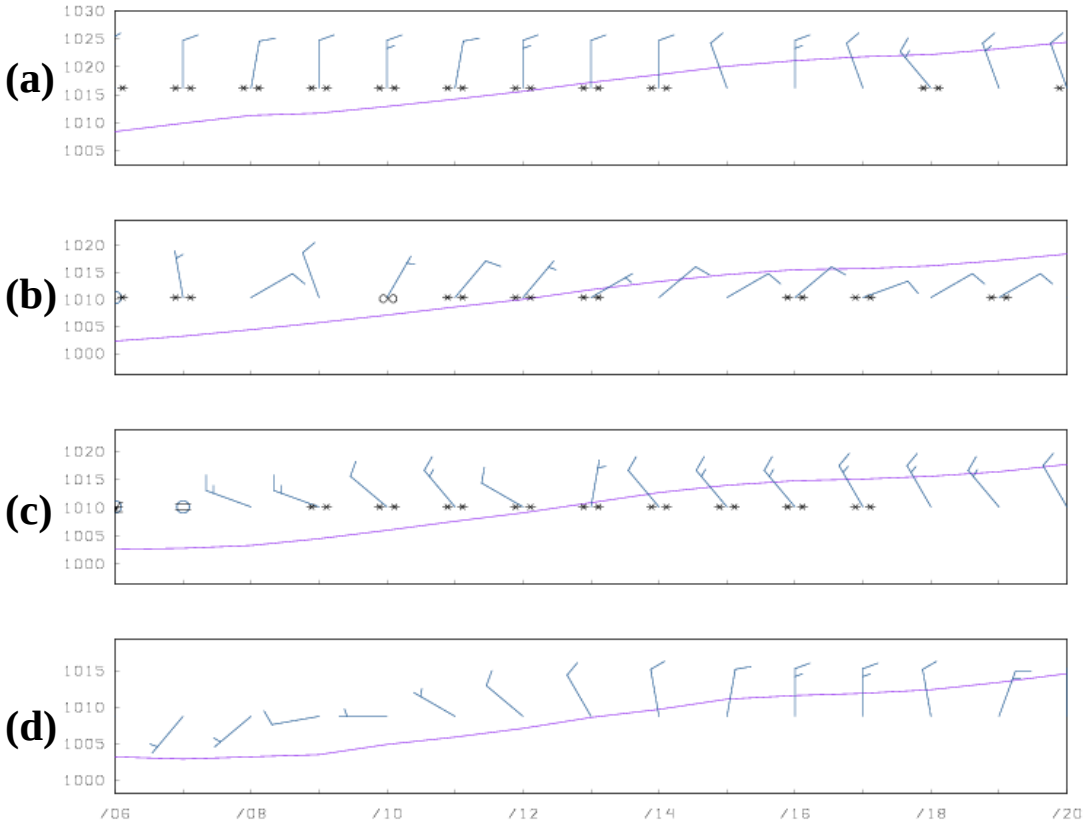

Figure 3.81: As in Fig. 3.80, except for (a) KSYR, (b) KGFL, (c) KALB, and (d) KPOU.

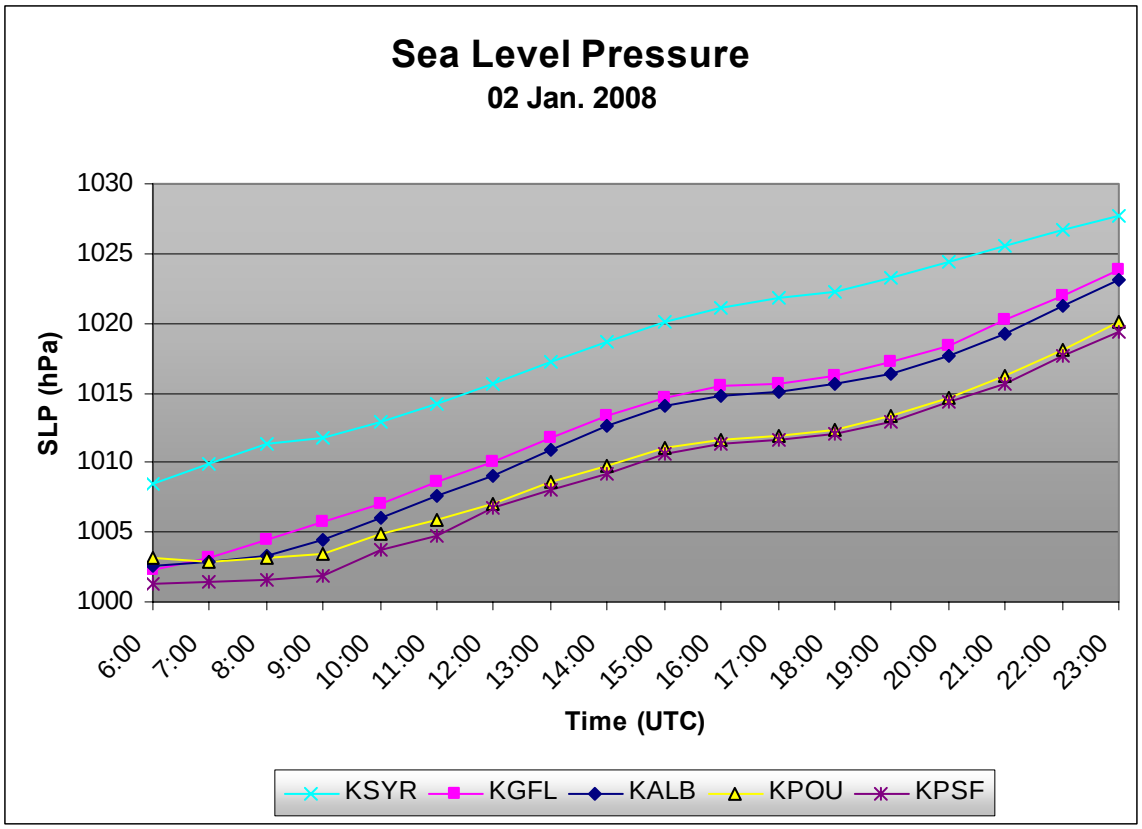

Figure 3.82: Sea level pressure time series (hPa) from 0600 to 2300 UTC 2 January 2008 for KSYR, KGFL, KALB, KPOU, and KPSF (trace and data point markers according to the legend). (Data source: the University at Albany DEAS archives).

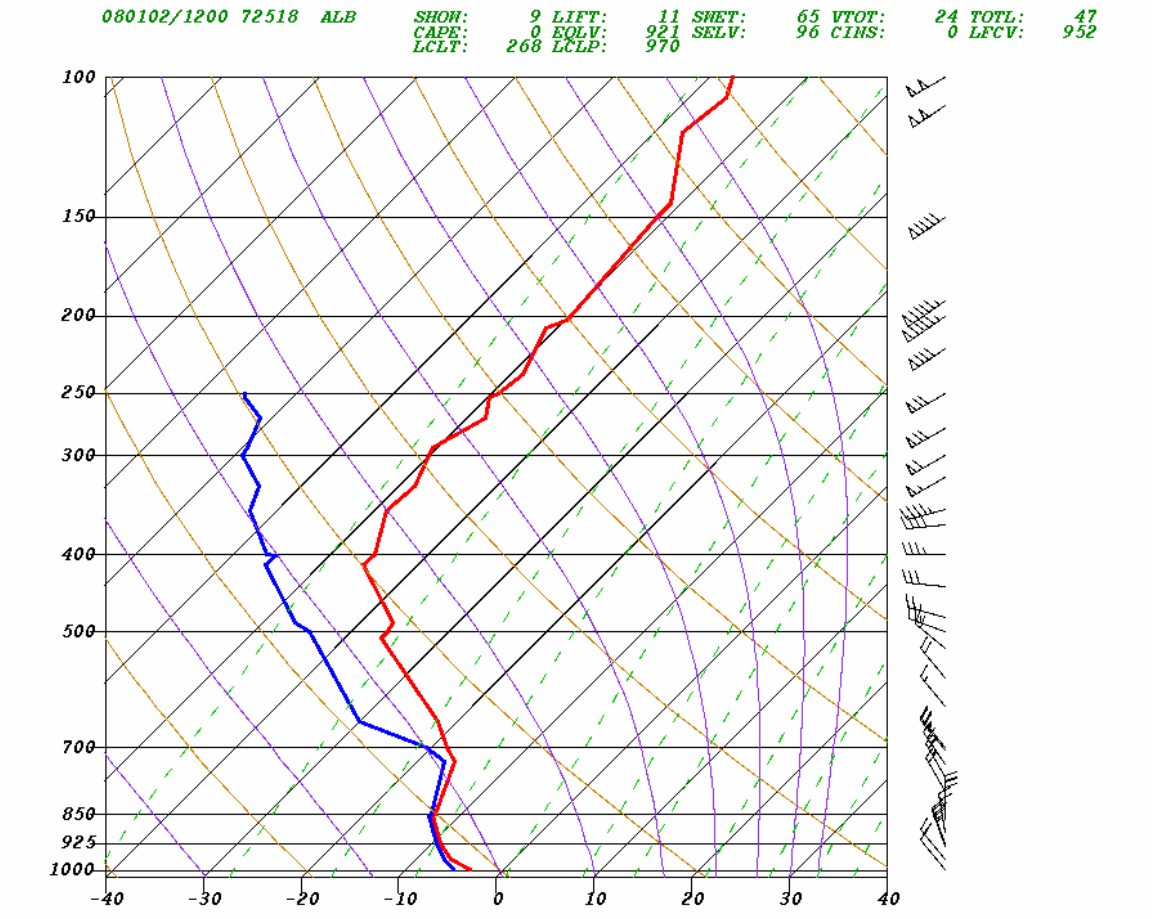

Figure 3.83: Skew *T*–log *p* radiosonde observations at KALY (72518) of air temperature (red line, in °C), dewpoint (blue line, in °C), and wind (to the right of the sounding; m s^{-1}, with pennant, full barb, and half barb denoting 25, 5, and 2.5 m s^{-1}, respectively) for 1200 UTC 2 January 2008. Various thermodynamic parameters are reported in green text at the top of the sounding. (Data source: Ohio State University weather archives).

4. Discussion

This thesis contains data collected from case studies of seven MHC events, all of which occurred between November 2002 and January 2008. The synoptic and mesoscale weather features present during each case were examined, and statistical analyses of wind speed and SLP were carried out for seven case studies. Observational findings and results from the statistical analyses were presented in sections 3.1 and 3.2, respectively, were summarized in section 3.3, and are discussed in section 4.1. A discussion of the findings in this thesis in relation to preexisting research on low-level flow channeling follows in section 4.2. Finally, section 4.3 contains a proposed methodology to aid in the operational forecasting of MHC events.

4.1 Composite Results of Case Studies

Weak mid- and upper-level forcing (i.e., from the 700-hPa level and above) is present during the seven MHC case studies presented in this thesis. The case studies, analyses, and the observational data instead indicate that surface and lower-tropospheric weather features exert the greatest influence on MHC development. Particularly important is a positive west–east (north–south) pressure difference along the Mohawk (Hudson) valley, which is the key to driving the low-level confluent flow observed during all seven cases. This setup is illustrated vividly during the January 2008 event. In this event, MHC-related precipitation began to appear on radar (Figs. 3.76a–f) after a positive SLP difference between KGFL and KPOU developed at 0700 UTC 2 January 2008 (Fig. 3.82). The SLP differences involved in any case must be great enough to promote air

motion down the valleys and ascent where the confluent airstreams meet, but not so large that the orographic effects are overwhelmed and damped out by the synoptic-scale flow.

Measurements of SLP across the MHC domain (see Fig. 1.2) show that higher values were present along the northern and western sides of the domain, as compared to the southern and eastern sides, during all seven case studies. A statistical analysis shows that SLP differences between two pairs of bellwether sites (KGFL and KPOU in the north–south direction; KUCA and KPSF in the west–east direction), recorded hourly during ongoing MHC events, fell within a consistent range for the five case studies between November 2002 and March 2006 (Fig. 3.5a). In these cases, the west–east (north–south) SLP difference measured from 4 to 7 hPa (1 to 5 hPa).

Similar calculations were made for the January 2007 case study (Fig. 3.6); during this study, SLP-difference values in the north–south direction also fell within the 1–5-hPa range. Unfortunately, due to the cessation of reports from KUCA and the slow implementation of a reliable replacement site, it is impossible to draw a parallel conclusion regarding SLP differences in the west–east direction. The pattern of higher SLP values to the west is, however, observed in both the January 2007 and January 2008 cases (Figs. 3.35 and 3.82). It is proposed that, in future studies, SLP differences calculated between KRME and KPSF be used to develop a set of values to indicate the likelihood of an MHC event.

At any given hour during the case studies, the SLP difference seen in the west–east direction was always greater than that in the north–south direction; however no strong correlation was found between the magnitude of west–east versus north–south SLP differences (Fig. 3.5a). When SLP-difference measurements were grouped and

analyzed as a function MHC event maturity (i.e., those taken at the beginning, middle, or end of an event; see Figs. 3.5b–d), no clear-cut signals emerged. Nevertheless, SLP differences in the north–south direction tend to be larger at the beginning of events than at the end of events.

The aforementioned SLP differences present across the Mohawk and Hudson Valleys promote a confluent low-level wind signature within these valleys, as revealed in the wind climatology of MHC events. Winds at KGFL regularly blew from the northeast or east-northeast during MHC events (Fig. 3.1a), consistent with well-channeled winds within the upper Hudson valley. Likewise, west-northwest winds occurred frequently at KUCA (and KSYR) during MHC events (Fig. 3.2a), consistent with well-channeled winds within the Mohawk valley. The low-level airflows in each of these valleys converged in the vicinity of KALB, which shows a bimodal wind climatology during MHC events (Fig. 3.3a) owing to the intersection of both valleys. Northwest winds were experienced at KALB with nearly the same frequency as northeast winds, with a slight preference for north or northeast winds to occur at the beginning of events (Fig. 3.4a), and a slight preference for northwest winds to occur at the end of events (Fig. 3.4b).

Several distinctive synoptic weather features gave rise to the aforementioned SLP and wind patterns. At the surface, during all MHC events, SLP isobars over eastern New York and western New England exhibited a "reverse-S" shape, with a weak ridge of high pressure frequently located over northern New York, and a weak trough of low pressure located south of the Mohawk Valley. This trough commonly originated from an offshore surface low and extended westward or west-northwestward approximately along the border between New York and Pennsylvania. In all cases, this surface low center was

intensifying as it tracked offshore, commonly south and east (i.e., "outside") of a reference point at 40°N, 70°W. All MHC events occur in the wake of a coastal cyclone, and following the passage of its synoptic-scale precipitation shield. The presence of such a cyclone appears to be a dominant influence on the formation and duration of MHC, as illustrated on 29 January 2007 during a particularly long-lived MHC event. In this case, MHC-related precipitation began as one intensifying surface low tracked from off the North Carolina coast to well southeast of Nova Scotia (Figs. 3.24a–d), and continued as a second low intensified and followed a similar track (Figs. 3.24d–f).

On the other hand, surface low centers which pass over or just north or west (i.e., "inside") of the reference point located at 40°N, 70°W should not be ignored. Some surface lows that track slightly inside of this reference point, such as the low in the January 2008 case study, are also capable of producing MHC-related precipitation. Likewise, the passage of an 850-hPa warm front from north to south across the region, as seen in the 23–24 January 2003 case, can generate winds with a westerly (northerly) component in the Mohawk (Hudson) valley, and is a potential mechanism for creating MHC.

It is important to note that strong forcing for vertical motion (ascent or descent) can act to upset the delicate balance of conditions that can lead to MHC events. Strong CAA, for example, could lead to the downward mixing of higher momentum from aloft to the surface. The pressure-driven channeled wind flows at the surface could be disrupted or damped out by such downward momentum mixing. Moreover, the subsidence associated with strong CAA could lead to drying of the PBL, whereas a moist PBL is necessary for MHC-generated precipitation. At the same time, CAA at middle

levels led in several case studies to the development and lowering of a subsidence inversion, which acted to lower atmospheric mixing heights and reduce the downward transfer of horizontal momentum. This effect is shown nicely in the KSCH profiler data from 1800 to 2100 UTC 27 November 2002 (Fig. 3.20), during the period when MHC-forced precipitation had reached its peak intensity. At that time wind speeds were 5 m s^{-1} or less from the surface to 950 hPa, with wind speeds ranging from 5 to 10 m s^{-1} in the 950–800-hPa layer. Inversions seen on the radiosonde soundings of other MHC case studies have a similar "shielding" effect on low-level winds, and also indicate an atmosphere that is stable with respect to surface-based convection.

Strong vertical motions are lacking at any level in all of the case studies examined in this thesis, even during the warm-front case of January 2003 which featured a maximum vertical motion of −5.0 μb s^{-1} at 550 hPa (not shown). The ascent attributed to MHC itself was shown in all case studies to maximize at a height of 925 hPa or below, generally at a value of −1.0 μb s^{-1}. In cases where the dendritic snow-growth region lies near or below 925 hPa, forecasters should be aware of the potential for enhanced snowfall rates and totals.

Upper-air forcing for vertical motions also must be weak so as not to damp out the more subtle SLP-driven channeling effects present at the surface. At jet-stream level (300 hPa), forcing for ascent is lacking in all case studies. The MHC domain is consistently under confluent flow at 300 hPa or the downward motion associated with the circulation around jet streaks, or both. At 500 hPa, cyclonic curvature of geopotential height contours is present in all MHC case studies. Horizontal advection of both cyclonic

and anticyclonic absolute vorticity is present at 500 hPa during the MHC events, but in all cases these advection regimes are weak.

It appears that MHC is far more common during the cold season than the warm season simply because the necessary antecedent weather conditions and synoptic regimes are more common at that time of year. Aside from the lower likelihood of these ingredients coming together, there seems to be no reason why MHC could not occur during the warm season.

4.2 Relationships to Preexisting Research on Low-Level Flow Channeling

The thrust of this research is to gain an understanding of the physical processes which drive MHC, and to synthesize from these findings a forecast methodology aimed at increasing its predictability. Criteria developed by Gross and Wippermann (1987) through their study of the flow-channeling effectiveness of Germany's upper Rhine Valley show that the Mohawk and Hudson River valleys are also effective flow-channeling features. The Mohawk and Hudson valleys, like the Tennessee valley, were also shown to susceptible to pressure-driven flow channeling, one of the four processes presented by Whiteman and Doran (1993) that produce in-valley winds which differ from ambient winds. Wasula et al. (2002) found that the Mohawk and Hudson valleys strongly modulate the surface wind climatology of the region, showing that surface winds frequently align with the valley axes. Severe weather reports were also found to occur preferentially south of the Mohawk valley into the Catskills and Berkshires (from the Mohawk valley west of KALB extending northward into the southern Adirondacks) on northwest-flow (southwest-flow) severe weather days, indicating that the valleys act to

channel the ambient flow. LaPenta et al. (2005) and Bosart et al. (2006) found that channeling of near-surface southerly flow contributed to an increase in directional and speed shear (compared to surrounding areas) by producing more clockwise-turned hodographs, and by lengthening these hodographs. Given a day favorable for severe weather over the Northeast, such resulting shear changes might contribute to areas of increased numbers of tornadoes. Wasula et al. (2002), LaPenta et al. (2005), and Bosart et al. (2006), however, do not mention the presence of a topographically forced low-level convergence zone in eastern New York and western New England, such as that present during MHC.

There is a strong resemblance between MHC and the PSCZ, a phenomenon that has been studied extensively. The frequency with which each phenomenon occurs varies seasonally [shown for the PSCZ by Mass (1981)]. The PSCZ is shown by Mass (1981) and Chien and Mass (1997) to form as a narrow range of surface wind directions along the coast of western Washington develop in a post cold-frontal environment. This environment is similar to the one in which MHC typically forms; i.e., following the departure of a surface low pressure system and in the presence of weak CAA. Weak synoptic-scale forcing is present during MHC and the PSCZ (Mass 1981; Chien and Mass 1997), with a specific SLP pattern giving rise to light-to-moderate surface winds (generally 2.5–7.5 m s^{-1}). Chien and Mass (1997) showed, using computer modeling, that if the unique orographic features of the Puget Sound did not exist, the confluent flow seen during these events also would not develop. This thesis has shown that the topography of eastern New York and western New England is likewise critical to the formation of MHC. Both phenomena generate low-levels ascent, with Mass (1981) and

Chien and Mass (1997) showing that ascent is maximized at ~850 hPa (~1.2 km AGL) in the case of the PSCZ, while maximum ascent in MHC cases is shown to occur at ~925 hPa (~0.5 km AGL). Whitney et al. (1993) formulated a decision tree, employed by the Seattle, Washington (SEW), National Weather Service Forecast Office to aid in the medium-range prediction of PSCZ events. This decision tree is the basis for a similar scheme developed to aid in the prediction of MHC, as discussed in section 4.3.

Several differences between MHC and the PSCZ are also noted. Chien and Mass (1997) show, through the use of computer modeling, that latent heat release is important in the formation and strength of the PSCZ. The low precipitable-water values in MHC cases (generally less than 10 mm; see Table V), however, argue that the effects of latent heat release on MHC are negligible. The PSCZ also significantly modifies the precipitation climatology for the Puget Sound region, while the MHC does not appear to affect the climatology of eastern New York and western New England. The reasons for this difference are straightforward: MHC occurs much less frequently than, and is not as strong as, the PSCZ. Reasons for these differences may include: (1) the presence of more-subtle terrain features in eastern New York and western New England than in the Puget Sound region, and (2) the lower overall moisture content of air involved during MHC events (of the continental-polar classification) versus during PSCZ (of the maritime-polar classification).

The environment of the Longmont anticyclone (LA), studied by Wesley et al. (1995), also bears a clear resemblance to MHC. In both cases, significant advections of temperature or absolute geostrophic vorticity are noticeably lacking. Both phenomena also feature light, and sometimes calm, surface winds in the vicinity of the center of

convergence, and generally light precipitation amounts. The ability of the LA to enhance preexisting precipitation is documented by Wesley et al. (1995), an effect which is seen during the MHC event of 23–24 January 2003 as well.

4.3 A Proposed Methodology for Forecasting MHC

Much the same as Mass (1981) and Whitney et al. (1993) deemed that accurate forecasts of the PSCZ could be made, MHC is also inherently predictable. A consistent set of weather features and conditions have been identified (in section 4.1) to be present each time MHC occurs, and schematics of the idealized synoptic-scale and mesoscale weather features associated with MHC events are shown in Figs. 4.1a,b, respectively. The intent is that these schematic diagrams be used in conjunction with a decision tree (shown in Fig. 4.2) to improve the accuracy of operational forecasts of MHC.

The SLP pattern across the Mohawk and Hudson valleys is the driving force behind MHC, and this ingredient is addressed at very beginning (top) of the decision tree. Of primary importance is that higher SLP values be located north and west of KALB in order to drive airflow simultaneously down the Mohawk and Hudson valleys. Empirical evidence suggests that the SLP difference in the north–south direction (between KGFL and KPOU) must fall in the 1–5-hPa range.

Specific values of west–east SLP difference have not yet been established, owing to the recent location changes and reliability issues of surface observation sites in the western Mohawk Valley. However, for the five case studies occurring from November 2002 to March 2006, the SLP difference between KUCA and KPSF consistently falls in the 4–7-hPa range. As the synoptic-scale pressure pattern during MHC events has higher

pressures located to the west, it is safe to reason that the lower bound in the zonal direction is 4 hPa, if KRME or KSYR are used in place of KUCA.

Of secondary importance to the formation of MHC is the orientation of surface features, such that pressure-driven airflow is directed into and along the Mohawk and Hudson valleys simultaneously. The "reverse-S" sea level isobar pattern that is present over eastern New York and western New England during every case arises when an intensifying surface low tracks off the East Coast. In most instances, this low center passes "outside" (i.e., to the east or south) of a benchmark point at 40°N, 70°W. This benchmark rule should only be considered a guideline, however, and storms tracking over or just "inside" of 40°N, 70°W should also be monitored closely.

Most MHC cases occur in a post-storm environment that remains moist at low levels, contains a low- or mid-level "cap," and features weak synoptic-scale forcing. If all of the preceding conditions are met, MHC is likely. However, a second (if less common) set of circumstances can also trigger MHC. This scenario, which involves the passage of an equatorward-moving 850-hPa warm front across the region, is accounted for on the right hand side of the decision tree (Fig. 4.2).

If an MHC event is deemed likely, traditional rules governing snowfall forecasting apply. The location of the dendritic snow-growth layer, where air temperatures are between approximately −12° and −18°C, should be considered. If the dendritic snow-growth layer extends through 925 hPa, forecast snowfall accumulations should be increased accordingly. Particularly strong convergence events can produce snowfall rates to 2.5 cm h^{-1} or more.

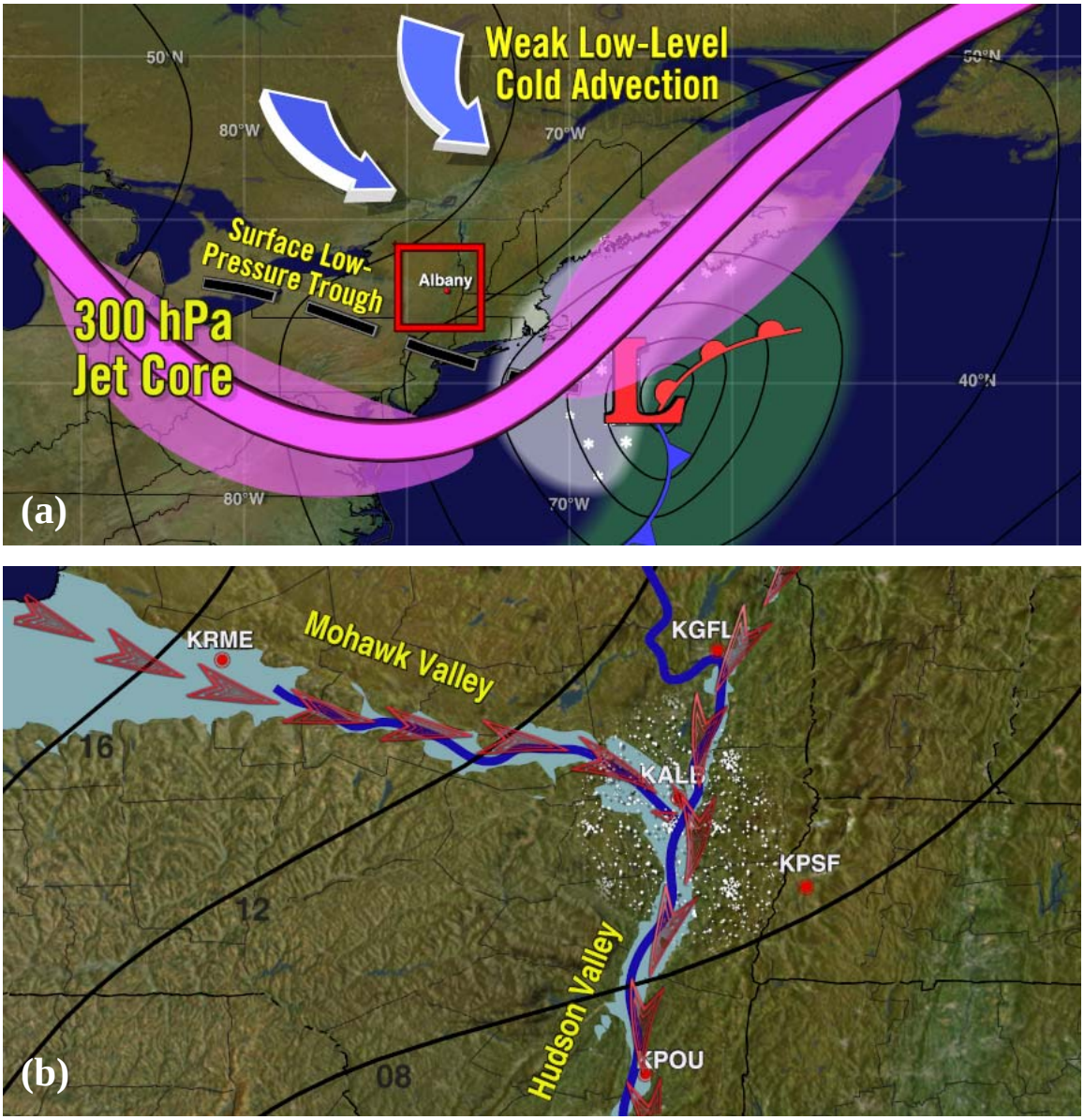

Figure 4.1: Schematic of the key features observed during a prototypical MHC event on the (a) synoptic-scale and (b) mesoscale. Shown in (a) are: an intensifying area of surface low pressure located southeast of 40°N, 70°W, and moving northeastward (red "L"); sea level isobars (solid black lines); a trough of surface low pressure; the attendant areas of synoptic-scale snow (white shading) and rain (green shading); the axis of 300-hPa maximum winds (heavy pink line) and jet streaks (pink shading); weak low-level cold advec-tion from the north; the area which bounds the MHC domain (red box). Shown in (b) are: the Mohawk and Hudson Rivers (royal blue line) and their associated valleys (light blue shading); low-level channeled flow (red arrows); sea level isobars with higher pressures indicated to the north and west (solid black lines); the approximate location of mesoscale snow forced by MHC effects (stippled shading); the locations of bellwether surface observation sites used in seven case studies (red circles and corresponding station codes.

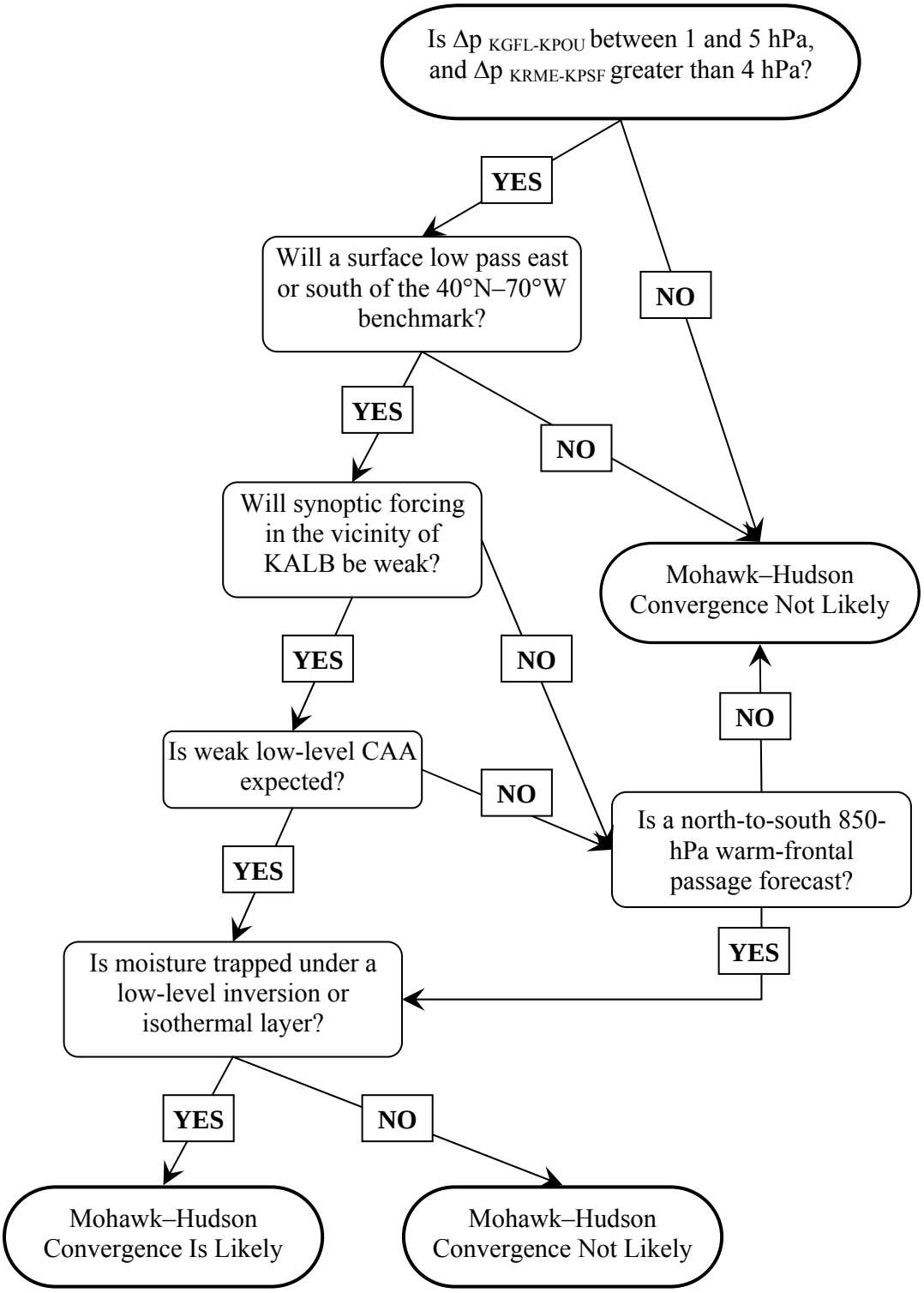

Figure 4.2: A decision tree for forecasting MHC. Adapted from Fig. 2 of Whitney et al. (1993).

5. Conclusions and Future Work

This thesis investigated the formation and evolution of low-level flow channeling in the Mohawk and Hudson River valleys of New York, which produces confluent low-level flow in the vicinity of KALB. This confluent flow creates a zone of near-surface convergence, resulting in a phenomenon called Mohawk–Hudson convergence (MHC) by local forecasters. From time to time, this phenomenon has been known to generate a mesoscale area of snow, the formation and behavior of which has been difficult to forecast accurately.

A concise definition of the weather features which comprise MHC events was developed in order to systematically distinguish instances of MHC from other precipitation-producing processes. This definition, based principally on radar presentation, helped to identify seven occurrences of MHC which spanned November 2002–January 2008. Each case was investigated through various means including radar, satellite, radiosonde, and surface data. A synoptic overview of upper-air weather features present during each case study was constructed using the initialized 0-hour analyses from the 1.0° gridded NCEP GFS, and the 32-km NCEP NARR.

A positive SLP difference was found from west-to-east (north-to-south) across the Mohawk (Hudson) River valley during all of the MHC cases studied. The Mohawk and Hudson valleys were found to be inherently susceptible to pressure-driven channeling, one of the four mechanisms shown by Whiteman and Doran (1993) to produce in-valley winds which differ in speed and direction from ambient winds. Thus, the aforementioned positive SLP difference across the Mohawk and Hudson valleys was deemed to be the principal physical factor which drives the confluent flow and the formation of the

resultant zone of low-level convergence. Other key aspects of the typical environment present during MHC events include: (1) an absence of strong forcing for vertical motions, which could overpower the weaker vertical motions generated by terrain and convergence effects; (2) an absence of strong CAA, which precludes strong subsidence and drying of the boundary layer; and (3) a statically stable atmospheric stratification, which prevents downward momentum transfer and the elimination of mesoscale terrain-induced wind patterns. The synoptic pattern which typically gives rise to this type of environment includes the presence of an intensifying area of surface low pressure, passing off the east coast on a track that is south of 40°N and/or east of 70°W, and the presence of a weak area of surface high pressure located over the Great Lakes. Several composite maps of the idealized weather conditions present during MHC events, and a decision tree aimed at increasing the accuracy of forecasting MHC, were presented in Figs. 4.1 and 4.2, respectively.

The ability of the Mohawk and Hudson valleys to influence the local warm-season severe weather climatology was previously documented by Wasula et al. (2002), LaPenta et al. (2005), and Bosart et al. (2006); however, this thesis represents the first systematic effort to date addressing the MHC. In reality, the seven events studied likely represent a fraction of the total number of MHC events that occurred over the six-year research period. As a real-time evaluation of potential cases for study was employed for this thesis, fleeting occurrences of MHC and events that had a negligible impact on the general public were likely overlooked. Future research would certainly benefit from the development of a larger repertoire of cases, including those which occur during the warm season, if such cases exist.

Additional cases would increase the total number of hourly observations on which to perform statistical analyses of parameters such as SLP, and wind direction. A larger sample size may lead to new correlations of these parameters, such as whether the magnitude of the SLP gradient across the Mohawk and Hudson valleys alone can influence precipitation intensity, or what factors influence the specific location over which the initial precipitation echoes form. Within the case studies themselves, the incorporation of surface observations from a consistent and reliable bellwether site in the western Mohawk Valley (perhaps KRME or KSYR) would allow for a more rigorous definition of the range in which west–east SLP-difference values must fall in order for MHC to occur.

An assessment of the forecast skill shown by the decision tree (see Fig. 4.2) would be helpful in updating the current methodology to generate more accurate forecasts. Investigating scenarios in which MHC is favored by the synoptic-scale pattern but none occurs ("null cases") could lead to further understanding and refinements in the forecasting methodology. Mesoscale modeling of MHC cases might facilitate determining the sensitivity of this phenomenon to SLP gradient, wind speed and direction, static stability, or topography.

TABLE I: Low- and Mid-Level Wind Speeds Over Albany, NY, For Selected Times During Mohawk–Hudson Convergence Events

Date/Time (UTC)	850-hPa Wind Speed ($m\ s^{-1}$)	925-hPa Wind Speed ($m\ s^{-1}$)
021127/21	7.5	5.0
021217/00	12.5	10.0
030123/21	7.5	7.5
050117/12	10.0	5.0
060303/03	10.0	7.5
070129/06	7.5	5.0

TABLE II: Dates and Times of Six Original Mohawk–Hudson Convergence Case Studies, and Relative Observation Time Classification Scheme for Each

Storm	Date	Time	Relative Observation Time Classifications
Nov. 2002	27	1500 UTC–2300 UTC	Beginning: 1500 UTC–1600 UTC
			Middle: 1700 UTC–2000 UTC
			End: 2100 UTC–2300 UTC
Dec. 2002	16–17	2000 UTC–0600 UTC	Beginning: 2000 UTC–2200 UTC
			Middle: 2300 UTC–0300 UTC
			End: 0400 UTC–0600 UTC
Jan. 2003	23	1900 UTC–2300 UTC	Beginning: 1900 UTC–1900 UTC
			Middle: 2000 UTC–2200 UTC
			End: 2300 UTC–2300 UTC
Jan. 2005	17	1100 UTC–1500 UTC	Beginning: 1100 UTC–1100 UTC
			Middle: 1200 UTC–1400 UTC
			End: 1500 UTC–1500 UTC
Mar. 2006	3	0200 UTC–0700 UTC	Beginning: 0200 UTC–0200 UTC
			Middle: 0300 UTC–0500 UTC
			End: 0600 UTC–0700 UTC
Jan. 2007	29	0300 UTC–1200 UTC	Beginning: 0300 UTC–0400 UTC
			Middle: 0500 UTC–1100 UTC
			End: 1200 UTC–1200 UTC

TABLE III: Number of Surface Wind Direction Reports During Six Original Mohawk–Hudson Convergence Events

Wind Direction	Observation Site		
	KALB	KUCA/KSYR	KGFL
000°	4	1	1
010°	4	2	0
020°	7	0	2
030°	7	0	2
040°	2	0	6
050°	1	0	7
060°	0	0	4
070°	0	0	4
080°	0	0	4
090°	0	0	0
100°	0	0	1
110°	0	0	0
120°	0	0	0
130°	0	0	0
140°	0	0	0
150°	0	0	0
160°	0	0	0
170°	0	0	0
180°	0	0	0
190°	0	0	0
200°	0	0	0
210°	0	0	0
220°	0	0	0
230°	0	0	0
240°	0	0	0
250°	0	0	0
260°	0	1	0
270°	0	2	0
280°	0	4	0
290°	0	11	1
300°	4	8	1
310°	7	1	1
320°	3	6	1
330°	3	1	2

Wind Direction	Observation Site		
	KALB	KUCA/KSYR	KGFL
340°	3	4	3
350°	1	2	1
Calm	0	2	6
TOTALS	46	45	47

TABLE IV: Number of Surface Wind Direction Reports at KALB During Six Original Mohawk–Hudson Convergence Events, Classified by Relative Observation Time (Event Maturity)

Wind Direction	Relative Observation Time		
	Beginning	Middle	End
000°	3	1	0
010°	1	2	1
020°	1	4	2
030°	2	5	0
040°	0	2	0
050°	0	1	0
060°	0	0	0
070°	0	0	0
080°	0	0	0
090°	0	0	0
100°	0	0	0
110°	0	0	0
120°	0	0	0
130°	0	0	0
140°	0	0	0
150°	0	0	0
160°	0	0	0
170°	0	0	0
180°	0	0	0
190°	0	0	0
200°	0	0	0
210°	0	0	0
220°	0	0	0
230°	0	0	0
240°	0	0	0
250°	0	0	0
260°	0	0	0
270°	0	0	0
280°	0	0	0
290°	0	0	0
300°	0	1	3
310°	1	5	1
320°	1	2	0

Wind Direction	Relative Observation Time		
	Beginning	Middle	End
330°	1	0	2
340°	0	1	2
350°	0	1	0
Calm	0	0	0
TOTALS	10	25	11

TABLE V: Summary of Important Parameters For Mohawk–Hudson Convergence Case Studies

PARAMETERS		**2100 UTC** ***27 Nov. 02***	**0000 UTC** ***17 Dec. 02***	**2100 UTC** ***23 Jan. 03***
Temperature Advection	925 hPa	−10.0	−17.9	−7.0
(10^{-5} °C s^{-1})	850 hPa	−14.5	−7.1	52.2
	700 hPa	−10.0	0.1	13.8
Ascent	925 hPa	−1.5	0.0	−0.3
(μb s^{-1})	850 hPa	−0.8	0.5	−2.8
	700 hPa	0.8	2.6	−4.0
500-hPa Abs. Vort. Advection		AVA	AVA	AVA
(Classification)		(Weak)	(Weak)	(Weak)
700-hPa Rel. Vort. Advection By Thermal Wind		0	0	AVA
(Classification)		---	---	(Weak)
Cloud Top Temperature		−14°C	−18°C	−22°C
(Inferred Pressure Level)		840 hPa	650 hPa	675 hPa
Top of Moist Layer		825 hPa	700 hPa	650 hPa
Precipitable Water		3.8 mm	7.1 mm	3.8 mm
(% of Normal)		60%	90%	60%
MLCAPE (J kg^{-1}) **(* denotes MUCAPE)**		0	0*	0
Lifted Index **(* denotes MULI)**		+10°C	+4°C*	+26°C
Surface–2km Shear		3 m s^{-1}	3 m s^{-1}	10 m s^{-1}

PARAMETERS	**1200 UTC** *17 Jan. 05*	**0300 UTC** *3 Mar. 06*	**0600 UTC** *29 Jan. 07*
Temperature Advection	−8.7	−13.5	−12.5
(1 x 10^{-5} °C s^{-1})	−14.1	−20.7	−10.2
	−20.5	−7.6	−11.0
Ascent	−0.7	−1.4	−2.2
(μb s^{-1})	−0.2	−0.6	−1.6
	−0.3	0.4	−1.0
500-hPa Abs. Vort. Advection	CVA	AVA	CVA
(Classification)	(Weak)	(Weak)	(Weak)
700-hPa Rel. Vort. Advection By Thermal Wind	0	AVA	0
(Classification)	---	(Weak)	---
Cloud Top Temperature	−28°C	−20°C	−20°C
(Inferred Pressure Level)	600 hPa	525 hPa	775 hPa
Top of Moist Layer	500 hPa	500 hPa	750 hPa
Precipitable Water	4.6 mm	6.4 mm	3.8 mm
(% of Normal)	72%	65%	60%
MLCAPE (J kg^{-1}) (* denotes MUCAPE)	0	0	0
Lifted Index (* denotes MULI)	+14°C	+20°C	+16°C
Surface–2km Shear	6 m s^{-1}	6 m s^{-1}	5 m s^{-1}

Abs. = Absolute Rel. = Relative Vort. = Vorticity

AVA = Anticyclonic Vorticity Advection CVA = Cyclonic Vorticity Advection

MLCAPE = Mixed-Layer Convective Available Potential Energy

MUCAPE = Most-Unstable Convective Available Potential Energy

MULI = Most-Unstable Lifted Index

References

Andretta, Thomas A., and Dean S. Hazen, 1998: Doppler radar analysis of a Snake River Plain convergence event. *Wea. and Forecasting,* **13,** 482–491.

Bell, Gerald D., and Lance F. Bosart, 1988: Appalachian cold-air damming. *Mon. Wea. Rev.,* **116,** 137–161.

Bosart, Lance F., Anton Seimon, Kenneth D. LaPenta, and Michael J. Dickinson, 2006: Supercell tornadogenesis over complex terrain: the Great Barrington, Massachusetts, tornado on 29 May 1995. *Wea. and Forecasting,* **21,** 897–922.

Chien, Fang-Ching, and Clifford F. Mass, 1997: Interaction of a warm-season frontal system with the coastal mountains of the western United States, Part II: evolution of a Puget Sound convergence zone. *Mon. Wea. Rev.,* **125,** 1730–1752.

Kossmann M., and A. P. Sturman, 2003: Pressure-driven channeling effects in bent valleys. *J. Appl. Meteor.,* **42,** 151–158.

LaPenta, Kenneth D., Lance F. Bosart, Thomas J. Galarneau Jr., and Michael J. Dickinson, 2005: A multiscale examination of the 31 May 1998 Mechanicville, New York, tornado. *Wea. and Forecasting,* **20,** 494–516.

Mass, Clifford, 1981: Topographically forced convergence in western Washington State. *Mon. Wea. Rev.,* **109,** 1335–1347.

Mesinger, F., and Coauthors, 2006: North American Regional Reanalysis. *Bull. Amer. Meteor. Soc.,* **87,** 343–360.

Richwein, B. A., 1980: The damming effect of the southern Appalachians. *Natl. Wea. Dig.,* **5**(1)**,** 2–12.

Roebber, Paul J., and John R. Gyakum, 2003: Orographic influences on the mesoscale structure of the 1998 ice storm. *Mon. Wea. Rev.,* **131,** 27–50.

Steenburgh, W. James, and Thomas R. Blazek, 2001: Topographic distortion of a cold front over the Snake River Plain and central Idaho mountains. *Wea. and Forecasting,* **16,** 301–314.

Szoke, E. J., M. L. Weisman, J. M. Brown, F. Caracena, and T. W. Schlatter, 1984: A subsynoptic analysis of the Denver tornadoes of 3 June 1981. *Mon. Wea. Rev.,* **112,** 790–808.

Wasula, Alicia C., Lance F. Bosart, and Kenneth D. LaPenta, 2002: The influence of terrain on the severe weather distribution across interior eastern New York and western New England. *Wea. and Forecasting,* **17,** 1277–1289.

Wesley, Douglas A., Roy M. Rasmussen, and Ben C. Bernstein, 1995: Snowfall associated with a terrain-generated convergence zone during the Winter Icing and Storms Project. *Mon. Wea. Rev.,* **123,** 2957–2977.

Whiteman, C. David, and J. Christopher Doran, 1993: The relationship between overlying synoptic-scale flows and winds within a valley. *J. Appl. Meteor.*, **32,** 1669–1682.

Whitney, William M., Robert L. Doherty, and Bradley R. Colman, 1993: A methodology for predicting the Puget Sound convergence zone and its associated weather. *Wea. and Forecasting,* **8,** 214–222.

Wilczak, J. M., and J. W. Glendening, 1988: Observations and mixed-layer modeling of a terrain-induced mesoscale gyre: the Denver Cyclone. *Mon. Wea. Rev.,* **116,** 1599–1622.

-----, and T. W. Christian, 1990: Case study of an orographically induced mesoscale vortex (Denver Cyclone). *Mon. Wea. Rev.,* **118,** 1082–1102.

Wippermann, F., and G. Gross, 1987: Channeling and countercurrent in the upper Rhine valley: numerical simulations. *J. Climate Appl. Meteor.*, **26,** 1293–1304.

WRGB-TV, cited 2008: Albany, NY climate data. [Available online at http://www.cbs6albany.com/sections/weather/historical/.]